

NMR Spectroscopic Investigations on Flavin Catalyzed Photooxidations



Dissertation

zur Erlangung des Doktorgrades
der Naturwissenschaften (Dr. rer. nat.)
an der Fakultät für Chemie und Pharmazie
der Universität Regensburg

vorgelegt von
Christian Feldmeier
aus Wörth a. d. Donau

2014

Die vorliegende Dissertation beruht auf Arbeiten, die im Zeitraum von Juni 2010 bis April 2014 am Institut für Organische Chemie der Universität Regensburg unter der Leitung von Prof. Dr. Ruth M. Gschwind durchgeführt wurden.

Promotionsgesuch eingereicht am 09.04.2014

Prüfungsausschuss: Prof. Dr. Alkwin Slenczka
Prof. Dr. Ruth M. Gschwind
Prof. Dr. Werner Kremer
Prof. Dr. Ingo Morgenstern

Vorsitzender
1. Gutachter
2. Gutachter
3. Prüfer

Ich erkläre hiermit, dass ich die vorliegende Arbeit ohne unzulässige Hilfe Dritter und ohne Benutzung anderer als der angegebenen Hilfsmittel angefertigt habe. Die aus anderen Quellen direkt oder indirekt übernommenen Daten und Konzepte sind unter Angabe des Literaturzitats gekennzeichnet.

Diese Arbeit wurde bisher weder im In- noch im Ausland in gleicher oder ähnlicher Form einer anderen Prüfungsbehörde vorgelegt.

Regensburg, April 2014

NMR Spectroscopic Investigations on Flavin Catalyzed Photooxidations

Contents

1	Introduction and Outline	1
2	Aggregation Effects in Visible-Light Flavin Photocatalysts: Synthesis, Structure, and Catalytic Activity of 10-Arylflavins	3
2.1	Abstract.....	4
2.2	Introduction	5
2.3	Results and Discussion	8
2.3.1	Synthesis	8
2.3.2	Crystal Structures.....	9
2.3.3	Aggregation Properties Determined by ¹ H-DOSY NMR Spectroscopy	11
2.3.4	Spectral and Electrochemical Properties.....	13
2.3.5	Photooxidation of 4-Methoxybenzyl Alcohol	15
2.4	Conclusion	18
2.5	Experimental Details	19
2.6	Supporting Information.....	25
2.6.1	Experimental Data for Aggregation Numbers	25
2.6.2	¹ H and ¹³ C Assignments.....	27
2.7	Additional Experimental Findings	28
2.7.1	Self-Aggregation of Flavins	28
2.7.2	Aggregation between RFT and MBA.....	32
2.7.3	Experimental Details	39
2.8	References.....	40
3	LED based NMR Illumination Device for Mechanistic Studies on Photochemical Reactions - Versatile and Simple, yet Surprisingly Powerful.....	47
3.1	Abstract.....	48
3.2	Introduction	49
3.3	Materials and Methods.....	51

3.3.1	Circuit – Light Source.....	51
3.3.2	Light Source – Optical Fiber.....	52
3.3.3	Optical Fiber – Sample	53
3.3.4	Sample Preparation – Measurement.....	54
3.4	Results and Discussion.....	56
3.5	Conclusion.....	58
3.6	Additional Experimental Findings	60
3.6.1	Different Types of LEDs.....	60
3.6.2	LED Performance at Different Light Pulse Lengths	61
3.6.3	Photo-CIDNP Pulse Sequences	62
3.6.4	Modification of the Pulse Programs.....	64
3.6.5	Photo-CIDNP Build Up and Relaxation	64
3.6.6	Photo-CIDNP Cross Polarization	66
3.6.7	Experimental Details	67
3.6.8	¹ H and ¹³ C Chemical Shift Assignment.....	68
3.7	References	69
4	Photo-CIDNP Patterns of Free Flavins in Solution: Solvent, Structural and Heavy Atom Effects	73
4.1	Abstract	74
4.2	Introduction.....	75
4.3	Results and Discussion.....	77
4.3.1	Separation of Singlet and Triplet Pathway	77
4.3.2	Photo-CIDNP Polarization – Singlet vs. Triplet Pathway	79
4.3.3	Solvent Dependent Photo-CIDNP Cancelation	83
4.3.4	Photo-CIDNP Effects of Heavy Atom Flavins	88
4.3.5	Calculations	91
4.3.6	Photo-CIDNP Polarizations - Kaptein’s Sign Rules	98
4.4	Conclusion and Outlook.....	105
4.5	Additional Experimental Findings.....	107

4.5.1	Heavy Atom Flavins - Quantum Yields and Chemical Conversions.....	107
4.5.2	Temperature Dependent Photo-CIDNP Polarizations.....	108
4.6	Experimental Details	111
4.7	References.....	113
5	Solvent Stabilized Radical Intermediates in Flavin Catalyzed Reactions: One- vs. Two-Electron Oxidations	117
5.1	Abstract.....	118
5.2	Introduction	119
5.3	Results and Discussion	120
5.3.1	Model System	120
5.3.2	Reduced Flavin Species - Characterization and Stabilization	121
5.3.3	Kinetics	129
5.3.4	Mechanistic Proposal	131
5.3.5	Reoxidation of Flavin.....	132
5.4	Conclusion and Outlook	136
5.5	Supporting Information	139
5.5.1	¹ H and ¹³ C Chemical Shift Assignment.....	139
5.6	Additional Experimental Findings	141
5.6.1	EPR Spectra of the Semiquinone Radical	141
5.6.2	Spin Density Dependent Line Broadening	142
5.6.3	Semiquinone Radical Stability	143
5.6.4	Oxidative Side of the Catalytic Cycle - Oxygen Concentration	145
5.6.5	H ₂ O ₂ as the Second Reaction Product	149
5.6.6	Protonation of the Flavin Species.....	151
5.6.7	Amount of Semiquinone Radical	156
5.7	Experimental Details	159
5.8	References.....	162
6	Summary.....	167
7	Zusammenfassung.....	171

1 Introduction and Outline

The use of sunlight as an energy source for chemical conversions is a principle well known from nature where numerous processes in organisms are initiated and catalyzed by the absorption of photons in photoreceptors. In recent years the use of light as a driving force for chemical conversions has gained much attention in synthetic chemistry and the area of photocatalysis has seen a rapid development. However, detailed studies of the underlying reaction mechanisms lack behind these fast advances of visible light photocatalysis in synthetic applications despite the huge importance of mechanistic information for exploiting the full potential of photocatalysis and designing photocatalytic systems rationally.

The method of choice for mechanistic investigations on photocatalytic reactions is UV/Vis spectroscopy and in particular transient absorption spectroscopy as it provides access to the transient excited intermediates of the absorbing chromophore. Despite the manifold possibilities and techniques NMR provides for mechanistic studies, far too little attention has been paid to the application of NMR spectroscopy to investigations on photocatalytic reactions. Valuable information accessible directly by NMR is therefore often omitted in mechanistic studies. The objective of this thesis is therefore the application of modern NMR techniques to mechanistic studies of photocatalytic reactions. To enable the investigation of photochemical systems by means of NMR a device for *in situ* illumination of NMR samples was developed. With the help of this illumination device various NMR techniques were applied for the investigation of flavin catalyzed photooxidations as a central model system to get insights in the mechanism of the particular reaction, to test the possibilities of the NMR approach for the study of photochemical reactions and to reveal general underlying principles in photocatalysis. For a comprehensive approach considering also species invisible for NMR spectroscopy the NMR techniques were supplemented by Photo-CIDNP spectroscopy, UV/Vis spectroscopy and EPR spectroscopy.

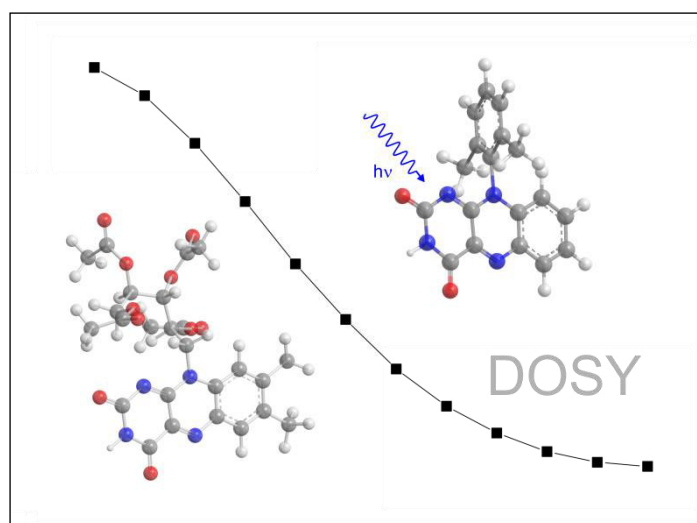
The importance of flavin self-aggregation for its reactivity is shown in chapter 2. By means of ¹H-DOSY solution NMR and crystal structures solvent dependent catalyst aggregates are revealed and the role of hydrogen bonds and π - π interactions are discussed. It is described how the catalyst aggregation, its photophysical properties and reactivity can be tuned by synthetically modifying the steric demand of the flavin side chain. Additionally, pre-associated flavin-substrate complexes are investigated by NMR-titration and ¹H-DOSY NMR techniques.

In chapter 3, a new illumination device for NMR spectrometers is presented. Based on LEDs switched directly by the NMR spectrometer and an optical fiber with a roughened tip the light is guided directly into the NMR sample to illuminate it enabling the application of well-established NMR techniques to mechanistic investigations of all kinds of photochemical reactions. Pulsed operation of the LEDs at high powers in low duty cycles enables exceptional high optical powers and makes the setup suitable even for applications in Photo-CIDNP spectroscopy.

A comprehensive study of Photo-CIDNP effects of flavins is presented in chapter 4. The effect of the solvent on Photo-CIDNP polarization of flavins is discussed. Detailed investigations of the Photo-CIDNP effect in different flavin derivatives are conducted on a small molecule model system using acetonitrile as a solvent to enable the detection of Photo-CIDNP effects in flavins. The implications of different substituents at the isoalloxazine moiety on the Photo-CIDNP spectroscopic properties and the radical pair mechanism are addressed in terms of Kaptein's sign rules and supplemented by DFT calculations of electron spin densities.

Finally, chapter 5 assesses solvent effects on the stabilization of the flavin semiquinone radical intermediate in flavin catalyzed photooxidations of benzyl alcohols. It is shown by a combination of NMR, Photo-CIDNP and UV/Vis spectroscopy that the semiquinone radical intermediate can be stabilized by the solvent water and that the stabilization makes flavin act as a one-electron oxidation agent for the photooxidation. The influence of solvent variation on the radical stabilization and the implications for the reaction mechanism and the efficiency of the photoreactions are discussed.

2 Aggregation Effects in Visible-Light Flavin Photocatalysts: Synthesis, Structure, and Catalytic Activity of 10-Arylflavins



Jitka Daďová and Susanne Kümmel did the synthesis and performed the photocatalytic reactions. Jana Cibulková did the crystallizations. Christian Feldmeier did the NMR spectroscopic aggregation studies.

J. Daďová, S. Kümmel, C. Feldmeier, J. Cibulková, R. Pažout, J. Maixner, R. M. Gschwind, B. König, R. Cibulka, *Chem. – A Eur. J.* **2013**, *19*, 1066–1075.

Reproduced with permission of John Wiley and Sons

2.1 Abstract

A series of 10-arylflavins (10-phenyl-, 10-(2',6'-dimethylphenyl)-, 10-(2',6'-diethylphenyl)-, 10-(2',6'-diisopropylphenyl)-, 10-(2'-tert-butylphenyl)-, and 10-(2',6'-dimethylphenyl)-3-methyl-isoalloxazine (**2a–f**)) was prepared as potentially nonaggregating flavin photocatalysts. The investigation of their structures in the crystalline phase combined with ¹H-DOSY NMR spectroscopic experiments in CD₃CN, CD₃CN/D₂O (1:1), and D₂O confirm the decreased ability of 10-arylflavins **2** to form aggregates relative to tetra-*O*-acetyl riboflavin (**1**). 10-Arylflavins **2a–d** do not interact by π–π interactions, which are restricted by the 10-phenyl ring oriented perpendicularly to the isoalloxazine skeleton. On the other hand, N3-H···O hydrogen bonds were detected in their crystal structures. In the structure of 10-aryl-3-methylflavin (**2f**) with a substituted N3 position, weak C-H···O bonds and weak π–π interactions were found. 10-arylflavins **2** were tested as photoredox catalysts for the aerial oxidation of 4-methoxybenzyl alcohol to the corresponding aldehyde (model reaction), thus showing higher efficiency relative to **1**. The quantum yields of 4-methoxybenzyl alcohol oxidation reactions mediated by arylflavins **2** were higher by almost one order of magnitude relative to values in the presence of **1**.

2.2 Introduction

Flavins (isoalloxazines) are biologically active compounds that are responsible for redox processes in many types of enzymes, mostly in the form of flavin mononucleotide or flavin adenine dinucleotide cofactors.^[1–4] Besides, synthetic flavin analogues are the subject of intensive research as organocatalysts of oxidation and reduction reactions.^[5–25] The redox activity of flavin derivatives is dramatically enhanced by absorption of visible light; the longest wavelength absorption maximum is at around $\lambda_{\text{max}} = 450 \text{ nm}$.^[26] Thus, the photoexcitation of flavins enables the oxidation of substrates that cannot be oxidized thermally.^[27–47] Until now, flavins have been applied to the photooxidation of benzyl alcohols,^[27–37] benzyl amines,^[38] and methylbenzenes^[39] to benzaldehydes; the photooxidation of benzyl methyl ethers to methyl benzoates;^[39] the photooxidation of dopamine,^[40] amino acids,^[41] indols,^[42] unsaturated lipids and fatty acids,^[43,44] glucose,^[45] and phenols;^[46] and the selective photocatalytic removal of benzylic protecting groups.^[47] The photooxidation reactions mentioned are usually performed in the presence of air, thus allowing the regeneration of the flavin catalyst **FI** from its dihydro form **FI-H₂**, which is formed from flavin in the excited state **FI*** in the presence of a substrate (quencher) by a subsequent two-electron reduction and protonation process. Therefore, only a catalytic amount of flavin is required (Figure 2-1). Flavins are also known to sensitize singlet oxygen production.^[48,49] Until now, flavin-mediated sulfoxidation reactions^[50] and oxidation reactions of unsaturated lipids^[36,51] that are proceeded by a singlet oxygen mechanism have been reported.

In almost all studies, the photooxidation of benzyl alcohols to benzaldehydes in acetonitrile was studied as a typical procedure to elucidate the efficiency of the flavin photocatalyst. The activity of simple flavins, for example, tetra-*O*-acetyl riboflavin (**1**) and lumiflavin (see Figure 2-2 for the structures), in the oxidation of 4-methoxybenzyl alcohol in acetonitrile is very low, with quantum yields of up to 0.03 %.^[27,29] Several attempts to improve the efficiency of flavins have recently been reported. Substantially higher quantum yields of the oxidation of benzyl alcohol were achieved if the flavin photocatalyst was protonated or coordinated to rare-earth metal ions, with the highest value of 17 % in the case of a scandium(III) complex.^[13–15,19] Also, thiourea accelerated the photooxidation of benzyl alcohol mediated by flavins and reached a high turnover number (TON) of up to 580.^[29] A remarkable improvement in the catalytic efficiency of the flavin moiety was achieved by its covalent attachment to Zn^{II}-cyclen or a β -cyclodextrin substrate binding site.^[30,32] The reaction medium enhances the photooxidation if performed in sodium dodecyl sulfate (SDS) micelles.^[31] A positive effect

of water on the rate of photooxidation reactions mediated by flavins has also been described.^[27,30,52] Immobilization of flavins on fluorinated silica gel stabilizes the chromophore.^[28]

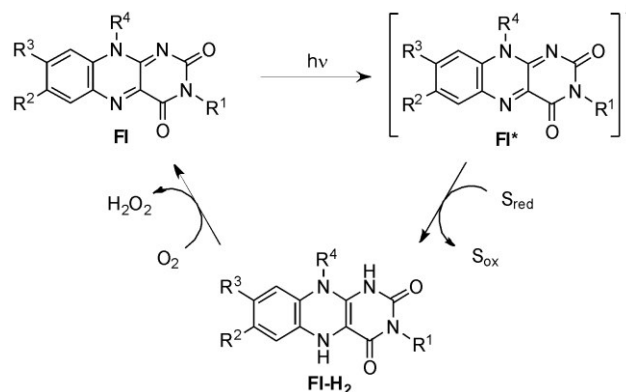


Figure 2-1 Catalytic cycle for the aerobic photooxidation of a substrate S mediated by flavin FI.

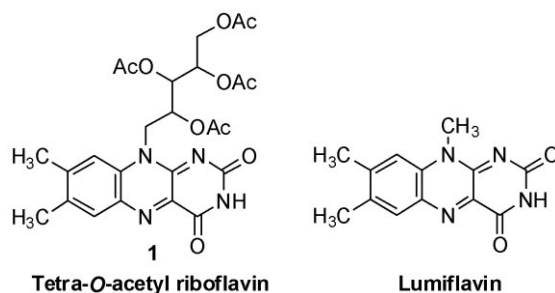


Figure 2-2 Structures of the flavin compounds typically used in photocatalysis.

Besides hydrogen bonding, flavins are known to interact with several molecules by π - π stacking,^[53–60] donor- π interactions,^[61] and cation or anion- π interactions.^[62,63] These interactions are essential not only for the binding of flavin cofactors in proteins, but also to modulate their redox properties and, consequently, the reactivity of flavin moieties in biological systems.^[58,62,63] The effect of noncovalent interactions on the properties of flavins in artificial systems is also well documented.^[53–61] There is evidence for flavin dimer formation, even in dilute solutions,^[64] and such intermolecular aggregation may decrease the photocatalytic efficiency of flavins by quenching excited states or alter their redox properties.^[27] With the aim of minimizing the ability of flavins to aggregate, we prepared a series of derivatives **2b–e**, with an *ortho*-substituted phenyl ring in position 10 (Figure 2-3). The aryl ring should be oriented perpendicular to the flavin skeleton due to *ortho* substitution, thus making π - π interactions between flavins less possible. Compound **2a**, without substitution on the phenyl ring, and the 3-methyl derivative **2f** were prepared for comparison. The photochemical, electrochemical, and aggregation properties, crystal structures and ability to mediate the photooxidation of

4-methoxybenzyl alcohol (model reaction) of arylflavins **2** were studied and compared with those of **1**.

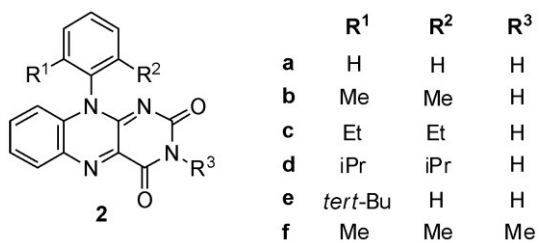


Figure 2-3 Structure of 10-arylflavins synthesized and investigated as photocatalysts.

2.3 Results and Discussion

2.3.1 Synthesis

The synthesis of 10-arylisalloxazines **2** (Figure 2-4) was started by converting commercially available substituted anilines **3a–e** with 6-chlorouracil (**4a**) into 6-arylamino-uracils **5a–e**. It is evident from the reaction conditions and yields (Table 2-1) that the substitution becomes more difficult with increasing steric hindrance of the substituents on C2 and C6 of the phenyl ring. Although the nonsubstituted phenyl derivative **5a** was obtained almost quantitatively, sterically hindered aminouracils were isolated only in moderate yields (i.e., **5c** and **5e**) or after a substantially longer reaction time (i.e. **5d**).

Table 2-1 Reaction conditions and yields for the preparation of 6-aminouracils **5** by the reaction of 6-chlorouracil (**4a**) with substituted anilines **3**.^[a]

6-aminouracil	T [°C]	Reaction time [h]	Yield [%]
5a	150	1	98
5b	180	1	74
5c	180	7	58
5d	200	24	75
5e	180	10	57

[a] A mixture of **4a** and **3** was heated in a nitrogen atmosphere (see supporting information for further details).

The prepared aminouracils **5a–e** were converted into the target flavins **2a–e** by reaction with nitrosobenzene in acetic acid/acetic anhydride (1:1). Although this synthetic approach was effective for the synthesis of other sterically hindered flavins,^[9,65] derivatives **2** were obtained in relatively low yields (13–25 %). Unfortunately, the yield did not increase even when acetic acid and acetic anhydride in other ratios were used as solvent. The 3-methyl derivative **2f** was prepared in an analogous process by using 6-chloro-3-methylaminouracil (**4b**; Figure 2-4). Interestingly, the conversion of 6-arylamino-3-methyluracil (**5f**) into 3-methylflavin (**2f**) proceeded in a substantially higher yield relative to the formation of **2b** (44 versus 23 %, respectively), which possesses a nonsubstituted N3 position.

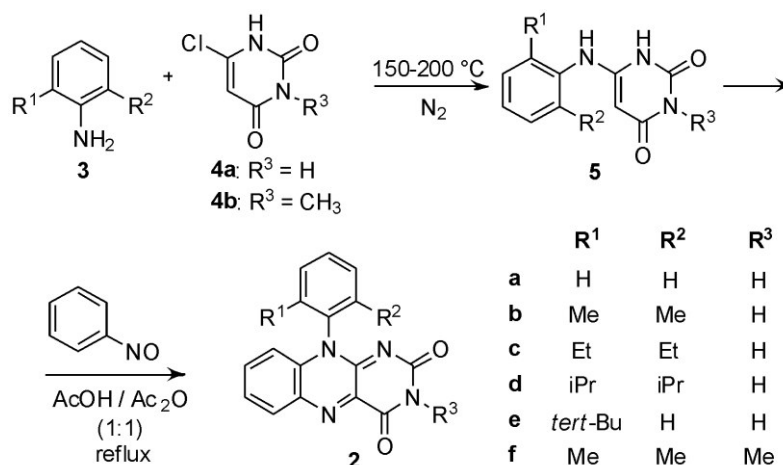


Figure 2-4 Synthesis of 10-arylflavins **2**.

2.3.2 Crystal Structures

The interaction of flavin molecules in the crystal can provide information about the aggregation behavior in solution. For this purpose, crystals for single-crystal analysis were prepared of **2a–d** and **2f**. Interestingly, of the five structures only two **2b** and **2d** exhibited one molecule in the asymmetric unit, as could be expected. Three structures **2a**, **2c**, and **2f** possessed two different molecules A and B in the asymmetric unit. A close inspection of the structures with A and B molecules showed that a significant difference between the two molecules was displayed only by **2c**, in which one ethyl group of the *ortho*-substituted phenyl ring of the molecule B was rotated around the C(phenyl)-CH₂ bond by 83.9(1)° (Figure 2-5 C). In the structure of **2f**, molecules A and B differed only by a slightly different rotation of the phenyl ring (Table 2-2). In the case of the structure **2a**, no marked difference between molecules A and B was observed.

Table 2-2 Dihedral angles between the aryl and isoalloxazine planes in the crystal structures.

Flavin	Angle [°]
2a	79.73(5), ^[a] 78.43(4) ^[b]
2b	83.25(4)
2c	86.48(4), ^[a] 83.48(4) ^[b]
2d	85.69(5)
2f	79.49(5), ^[a] 82.02(5) ^[b]

[a] Molecule A. [b] Molecule B.

Structures of several simple flavin derivatives have already been investigated by X-ray diffraction.^[66–71] In most cases, π -stacking interactions between the isoalloxazine moieties were recognized, which results in the packing of flavin molecules with distances

of between 3.3 and 3.6 Å. In such stacked systems, flavin molecules adopt an alternating orientation, and the benzene ring of one flavin moiety overlaps with the pyrimidine ring of the adjacent one (and vice versa). Tetra-*O*-acetyl riboflavin (**1**),^[69] 3-methyl-tetra-*O*-acetyl riboflavin,^[66] 3-benzylflavin,^[67] and 10-methylisoalloxazine^[70] are examples of such stacked structures in the crystal phase. As expected, no π - π interactions between flavin moieties were found in the structures of 10-arylflavins **2b-d**, even in the case of **2a** with the unsubstituted phenyl ring, in which a coplanar orientation of the phenyl and isoalloxazine subunits was still allowed. In the structures of flavins **2a-d**, the aryl ring is almost perpendicular to the mean plane of the isoalloxazine fragment, with a dihedral angle that ranges from 78.4 to 86.5°, thus preventing the stacking of flavins (see Table 2-2, Figure 2-5, and supporting information). A similar value of the dihedral angle of 79.7° was reported for 10-(2-hydroxyphenyl)-3-methylisoalloxazine.^[72] The analysis of the X-ray crystallographic data showed pairs of symmetrical hydrogen N-H \cdots O bonds between the pyrimidine rings of two adjacent molecules of flavins **2a-d** (Figure 2-5 A-D). Additionally, a relatively short N3B-H \cdots O12A hydrogen bond in the structure of **2c** and weak C-H \cdots O interactions in **2a-d** contribute to the aggregation. Hydrogen bonds C16-H \cdots O11 in **2b** (Figure 2-5 B) and C22-H \cdots O12 in **2d** (Figure 2-5 D), with participation of the hydrogen atoms on the (alkyl)phenyl ring on one hand, and hydrogen bond C7B-H \cdots O11B in **2a** (Figure 2-5 A), with participation of the hydrogen atoms on the isoalloxazine skeleton on the other hand, can be given as examples (see supporting information for all the hydrogen-bonding data). In contrast to flavins with a free N3-H bond (**2a-d**), compound **2f** cannot form N-H \cdots O bonds, and thus relatively weak C-H \cdots O interactions dominate in the crystal structure of **2f** (Figure 2-5 E). Methyl groups on both the N3 atom and the aryl ring participate in these C-H \cdots O bonds. However, despite the presence of the *ortho,ortho*-disubstituted phenyl ring with perpendicular orientation toward the isoalloxazine skeleton (Table 2-2), little overlap of the flavin subunits that results in a weak π - π interaction was found in the structure of **2f** (Figure 2-5 F). The distance between the neighboring planes in the stack is about 3.5 Å.

The investigation of the structure in the crystalline phase confirms that 10-arylflavins **2** have no structural prerequisites to interact by mean of strong π - π interactions and to form stacks in a similar manner to simple flavin molecules.^[66-71] One could speculate about the situation in solution due to the conformational flexibility of the molecules. Flavin **2a** may show rotation of the phenyl ring; however, this behavior is strongly limited by the *ortho* substituents in **2b-f**. Therefore, only partial overlap of the isoalloxazine skeletons (e.g., by one ring) that results in a weak π - π interaction could be expected in solution. As was shown in flavoenzyme models, the binding constants based on the overlap of

one or three rings of the flavin skeleton with an aromatic compound can differ by a factor of 30.^[59]

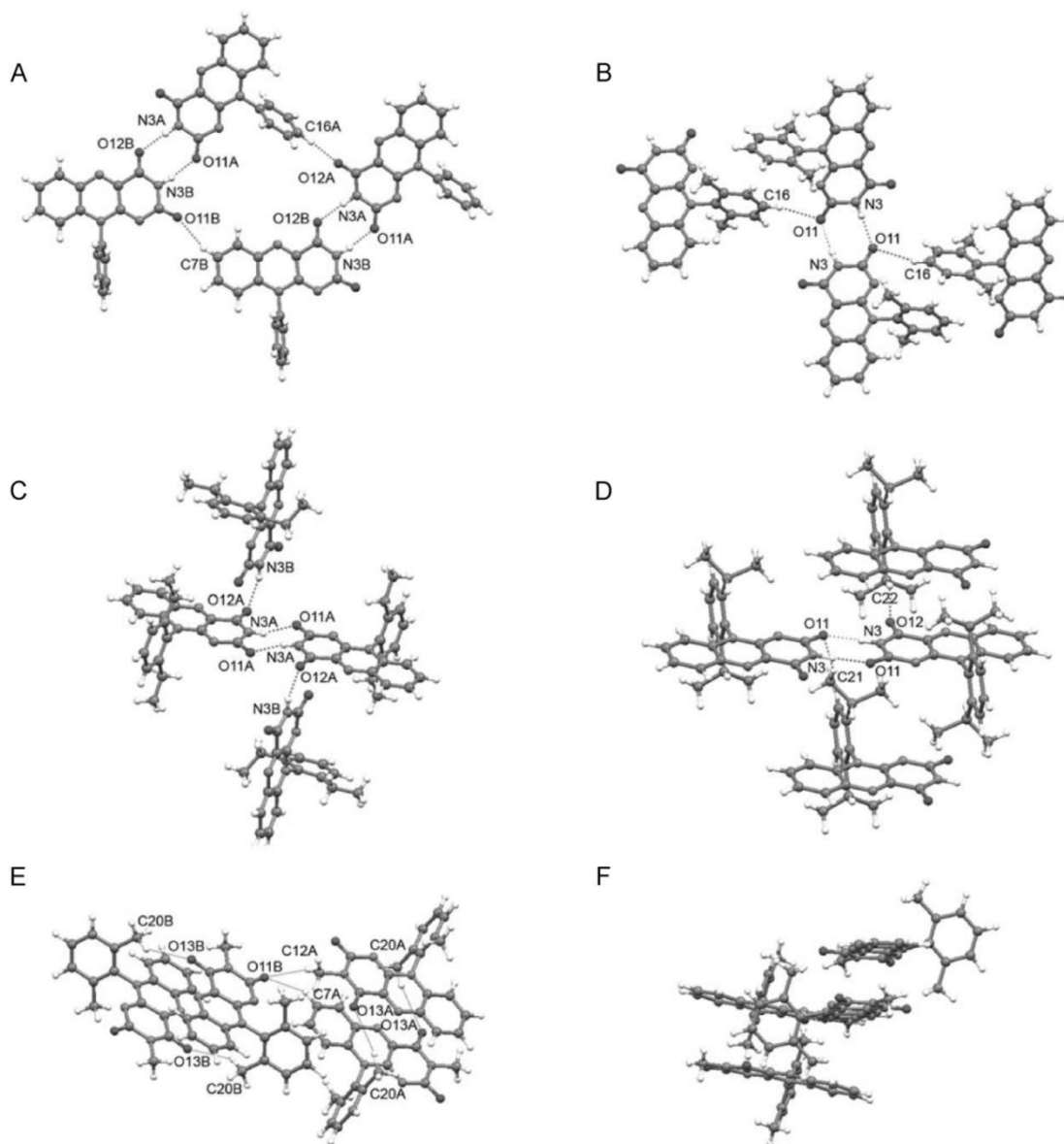


Figure 2-5 Hydrogen bonding in the crystal structures of 10-arylflavins A) **2a**, B) **2b**, C) **2c**, D) **2d**, and E) **2e** and F) a fragment that shows π stacking of the molecules **2f**. The hydrogen bonds are shown as dashed lines, and the non-hydrogen atoms that participate in the hydrogen bonds are labeled. See supporting information for hydrogen-bonding data and more images.

2.3.3 Aggregation Properties Determined by ¹H-DOSY NMR Spectroscopy

¹H-DOSY NMR experiments^[73] were used to measure the diffusion coefficients of **1** and arylflavins **2** in CD₃CN, D₂O, and CD₃CN/D₂O (1:1). The resulting aggregation numbers calculated from the experimental diffusion coefficients (see experimental section and supporting information) are presented in Table 2-3.

Table 2-3 Aggregation numbers of **1** and 10-arylflavins **2** in different solvents.^[a]

Flavin	aggregation number		
	CD ₃ CN	CD ₃ CN / D ₂ O (1:1)	D ₂ O
1	3.0	1.7	1.0
2a	2.4	1.2	1.0
2b	2.6	1.4	1.0
2c	1.9	1.0	1.0
2d	2.1	1.2	1.0
2e	2.2	1.0	1.0
2f	2.4	1.3	1.0

[a] Conditions: T=300 K, c=5×10⁻⁵ molL⁻¹ of flavins **1** and **2** in solution with CD₃CN and CD₃CN/D₂O (1:1) or a saturated solution in D₂O.

A significant aggregation for **1** was detected in CD₃CN, with an average aggregation number of 3.0, which decreased upon the addition of water down to monomers in pure D₂O. Next, the aggregation trends for arylflavins **2a–f** were investigated. For all the compounds, a significantly decreased aggregation number was found in CD₃CN relative to **1**. Again, the addition of water led to disaggregation for arylflavins **2a–f**. These data show that the basic idea to decrease π–π interactions in the aggregates by the introduction of an aryl ring with sterically demanding substituents works. However, there was no direct correlation between the steric demand of the substituents in **2a–f** and the aggregation number detected experimentally. For example, **2c** shows decreased aggregation relative to **2b**, as expected for ethyl groups relative to methyl groups as substituents; however, a further increase in the steric demand in **2d** and **2e** did not lead to decreased aggregation numbers. This finding suggests that not only π–π interactions between the isoalloxazine moieties contribute to the aggregation, but also additional stabilizing dispersion forces between the bulkier substituents^[74] and other noncovalent interactions play an important role. Interestingly, analysis of the crystal structures of **2a–d** revealed N–H···O hydrogen bonding as the dominant noncovalent interaction for these arylflavins and not π–π interactions, as found for **1**. In the 3-methyl derivative **2f**, hydrogen bonding through the N3–H bond is blocked. However, the diffusion measurements showed only a slightly decreased aggregation number relative to **2b**. This outcome is in accordance with the crystal structure of **2f**, which shows π–π interactions again besides weaker C–H···O interactions. The solvent-dependent disaggregation of arylflavins **2a–e** going from CD₃CN to CD₃CN/D₂O (1:1) and D₂O correlates with the relative hydrogen-bond acceptor properties of these solvents in terms of better solute/solvent interactions

toward pure D₂O.^[75,76] Interestingly, the aggregates driven by π - π -interactions show a similar solvent dependence, thus demonstrating that the solvent dependence in flavins cannot be used as an indicator of the intermolecular interaction mode. Thus, the combination of aggregation numbers and crystal-structure analysis reveals that both π - π interactions and hydrogen bonding play a decisive role in the aggregation of the flavins, and their relative contribution can be tuned by the structure of the synthesized flavins.

2.3.4 Spectral and Electrochemical Properties

The spectral and electrochemical properties of the newly prepared 10-arylflavins **2** in acetonitrile were studied and compared to those of **1** (see Table 2-4 and supporting information).

Table 2-4 Spectroscopic data for flavins **1** and **2** in acetonitrile.

Flavin	λ_2 [nm] (ϵ [mol ⁻¹ dm ³ cm ⁻¹]) ^[a]	λ_1 [nm] (ϵ [mol ⁻¹ dm ³ cm ⁻¹]) ^[a]	λ_F [nm] ^[b]	Φ_F ^[c]
1	343 (8500)	440 (12000)	505	0.499
2a	335 (6200)	436 (8900)	517	0.244
2b	330 (7000)	437 (10000)	498	0.447
2c	331 (7000)	434 (10000)	500	0.537
2d	330 (6200)	436 (8900)	501	0.434
2e	332 (7000)	437 (9900)	502	0.328
2f	321 (5500)	427 (6500)	498	0.282

[a] λ_1 and λ_2 are the positions of the two lowest-energy bands in the absorption spectra; [b] The maximum of the fluorescence emission spectrum, $\lambda_{ex} = \lambda_1$; [c] The fluorescence quantum yield determined using quinidine sulphate as a standard.

The aryl substituent in position 10 of the isoalloxazine causes a small blue shift of the absorption maxima and a decrease in the absorption intensity in the UV/Vis spectra. Substitution at the N3 position of the 10-arylisoalloxazine ring effects the position of the absorption maxima more significantly (cf. flavins **2b** and **2f**), than it was observed in the case of lumiflavin and 10-methylisoalloxazine.^[77,78] All flavins **2** show intensive fluorescence with a maximum at around $\lambda_{max} = 500$ nm. A small effect of the aryl substitution on the fluorescence maxima was only observed in the case of **2a**, which bears a nonsubstituted phenyl ring. However, the fluorescence quantum yield of **2a** is significantly decreased by half relative to **1** and **2b-d**. Similarly, substitution at N3 decreases the fluorescence quantum yield of arylflavins, which corresponds to the

observed effect of N3 substitution in **1**^[79] and 10-methylisoalloxazine.^[78] On the other hand, the fluorescence quantum yields reported for lumiflavin and 3-methyllumiflavin are almost the same.^[77]

The reduction potentials of the synthesized flavin derivatives in acetonitrile that correspond to one-electron reduction ($\text{Fl} \rightarrow \text{Fl}^{\cdot-}$)^[79] were determined by cyclic voltammetry (CV) relative to ferrocene/ferrocenium. Moreover, the change in the Gibbs free energy ΔG_{ET} of the electron transfer from the substrate 4-methoxybenzyl alcohol to the excited flavins in the singlet state (Table 2-5) were calculated from the observed reduction potentials by using the Rehm-Weller equation (1).^[80,81]

$$\Delta G_{\text{ET}} = 96.4(E_{1/2}^{\text{ox}} - E_{1/2}^{\text{red}}) - e^2 / \epsilon a - E^{0-0}$$

where $E_{1/2}^{\text{ox}}$ and $E_{1/2}^{\text{red}}$ are the oxidation potentials of the substrate ($E_{1/2}^{\text{ox}} = +1.19$ V for 4-methoxybenzyl alcohol)^[30] and the reduction potential of the flavin (Table 2-5); $e^2 / \epsilon a$ is the Coulomb term (5.4 kJmol^{-1});^[79] E^{0-0} is the flavin excitation energy (given in kJmol^{-1}), which was estimated as the average of absorption (hc/λ_1) and emission (hc/λ_F) energies with λ_1 and λ_F values derived from the flavin absorption and fluorescence spectra (Table 2-4); h is the Planck constant ($6.63 \times 10^{-34} \text{ m}^2\text{kg s}^{-1}$); and c is the velocity of light ($2.99 \times 10^8 \text{ ms}^{-1}$). The redox potential of arylflavins **2** shifts to more positive values, but by only 60 mV relative to **1**, which did not seem to be enough to influence the oxidation power of the flavin significantly. According to Gibbs free energy changes, electron transfer between 4-methoxybenzyl alcohol and flavins **1** and **2** in their singlet excited state is exergonic, and thus favorable ($\Delta G_{\text{ET}} < 0$). The ΔG_{ET} values are less negative for **1** and 10-phenylisoalloxazine (**2a**) by about 10 kJmol^{-1} relative to **2b-f**.

Fluorescence quenching for the newly synthesized derivatives **2** with 4-methoxybenzyl alcohol was studied in acetonitrile. Stern–Volmer plots constructed from the results are linear in all the cases (see supporting information). The values of Stern–Volmer constants K_S ($K_S = k_Q \tau_F$, where k_Q is the apparent rate constant and τ_F is the fluorescence lifetime) were calculated as the slope of Stern–Volmer dependence ($I_0/I = 1 + K_S[Q]$), that is, as the slope of the ratio of the fluorescence intensities I_0/I in the absence and presence of 4-methoxybenzyl alcohol (quencher Q) plotted against concentration [Q]. Interestingly, for almost all the newly prepared flavins bearing substituted phenyl rings **2b-f**, higher quenching K_S constants were measured relative to **1**. Only the value for 10-phenylisoalloxazine (**2a**) is equal to that of **1**. The observed decreased values of Stern–Volmer K_S constants for **1** and **2a** probably result from the decreased rate of

electron transfer k_Q , which corresponds to the decreased Gibbs free energy changes ΔG_{ET} (Table 2-5).

Table 2-5 Redox potentials of flavins **1** and **2**, estimated free energy changes ΔG_{ET} and Stern-Volmer constants K_S for the electron transfer from 4-methoxybenzyl alcohol to flavins **1** and **2** in acetonitrile.

Flavin	E^{red} [V] ^[a]	ΔG_{ET} [kJ mol ⁻¹] ^[b]	K_S [L mol ⁻¹]
1	-1.18	-24	26
2a	-1.12	-24	25
2b	-1.11	-34	42
2c	-1.10	-34	44
2d	-1.11	-33	35
2e	-1.10	-33	36
2f	-1.11	-34	33

[a] Values obtained in acetonitrile at a scan rate of 50 mVs⁻¹ in 0.001 molL⁻¹ solutions of the flavins with 0.01 molL⁻¹ Bu₄NPF₆ at 20 °C versus ferrocene / ferrocenium. [b] Free energy changes calculated from equation (1) using $E_{1/2}^{\text{ox}}$ (4-methoxybenzyl alcohol) = 1.19 V versus ferrocene / ferrocenium.^[30]

2.3.5 Photooxidation of 4-Methoxybenzyl Alcohol

The ability of the prepared flavins **2** to mediate the photooxidation of 4-methoxybenzyl alcohol with oxygen to the corresponding aldehyde was investigated under standard conditions, namely, 10 mol% of photocatalyst in deuterated acetonitrile at 25 °C under the atmospheric pressure of air (Figure 2-6). A high power light-emitting diode was used for the irradiation of the reaction mixture. A comparison of the efficiencies of flavins in the photooxidation reactions was made by determining 1) conversion after 90 minutes determined by ¹H NMR spectroscopic analysis of the reaction mixture and 2) quantum yield of the photooxidation reactions determined independently. Importantly, the oxidation reaction does not proceed in the absence of flavin or light.

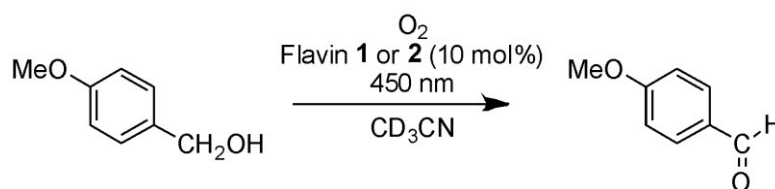


Figure 2-6 Model photooxidation reaction.

With **1** as a photocatalyst, only 5 % conversion was achieved after 90 minutes of irradiation (Table 2-6, entry 1). The use of **2a** without substitution on the phenyl ring led to only a small improvement of the conversion (Table 2-6, entry 2). On the other hand, the introduction of an phenyl ring with substituents in *ortho* positions resulted in a

substantial increase in flavin efficiency to mediate photooxidation, thus reaching conversions of up to 37 % after 90 minutes of irradiation in the presence of **2b** (Table 2-6, entry 3). The character of the alkyl substituents on the aryl ring seems to be important for the efficiency of the flavin photocatalysts. The diethyl derivative **2c** showed nearly the same activity as **2b** (compare entries 3 and 4 in Table 2-6), whereas the activity of **2d** and **2e** with branched isopropyl and *tert*-butyl substituents is slightly decreased (Table 2-6, entries 5 and 6). Interestingly, the alkylation of the N3 atom also decreases the efficiency of the flavin chromophore in the photooxidation reactions (Table 2-6, entry 7). The conversion of the photooxidation reactions in the presence of **2b–f** are relatively high after 1.5 hours of irradiation, but they are not remarkably increased during the next irradiation period. This behavior is caused by degradation of the flavin photocatalysts during photooxidation reactions, which was evidenced from bleaching of the reaction mixtures (see Table 2-6 and supporting Information). Nevertheless, the photo stability is not the most important factor that influences the activity of flavin photocatalysts. The least stable flavin **2c** showed relatively high efficiency. Interestingly, all the synthesized catalysts **2** are less photostable than flavin **1**.

Table 2-6 Photooxidation of 4-methoxybenzyl alcohol to 4-methoxybenzaldehyde in CD₃CN catalyzed by **1** and 10-arylflavins **2a–f**.

Entry	Flavin	Conversion [%] ^[a]	Rel. absorbance [%] ^[b]	Quantum yield ^[c] Φ [%] of aldehyde formation
1	1	5	94	0.0034 (0.0041 ^[d])
2	2a	9	74	0.0045 (0.0042 ^[d])
3	2b	37	83	0.0204 (0.0210 ^[d])
4	2c	36	27	0.0179 (0.0149 ^[d])
5	2d	29	72	0.0126 (0.0125 ^[d])
6	2e	28	56	0.0102 (0.0086 ^[d])
7	2f	25	87	0.0118 (0.0113 ^[d])

[a] After irradiation for 90 min. Conditions: $c_{\text{alcohol}}=4 \times 10^{-3} \text{ molL}^{-1}$, $c_{\text{flavin}}=4 \times 10^{-4} \text{ molL}^{-1}$, irradiation with 1W LED ($\lambda_{\text{max}}=450 \text{ nm}$), $T=25 \text{ }^{\circ}\text{C}$, monitoring by ¹H NMR. [b] Relative absorbance of the reaction mixture at $\lambda=443 \text{ nm}$ after irradiation for 60 min relative to the absorbance at the beginning of the experiment. [c] Determined by independent experiments with monitoring by GC. [d] Determined in CH₃CN.

The results of quantum-yield measurements are in accordance with the observed conversions (Table 2-6). The introduction of disubstituted aryl rings at position 10 of the isoalloxazine ring causes a substantial increase in the quantum yield of the oxidation of 4-methoxybenzyl alcohol, which is, in the case of **2b**, by almost one order of magnitude higher than the photooxidation in the presence of **1**. However, the increase in the quantum yield of the flavin photocatalyst is approximately half with bulky isopropyl or

tert-butyl substituents or if the N3 position of isoalloxazine is substituted by a methyl group. As expected, the quantum yields of the oxidation reactions are not affected by deuteration of the solvent, thus indicating that a singlet-oxygen pathway is not involved.^[82–84]

One could speculate that the lower efficiency of **2a** relative to **2b–f** is a result of its smaller oxidation power, but the differences in reduction potentials and in estimated ΔG_{ET} values are not sufficient to explain the observed significant differences in reactivity. The low activity of **2a** can also be attributed to the possible free rotation of the non-substituted aryl ring, thus allowing its coplanar arrangement relative to the isoalloxazine plane. This effect may increase the ability of **2a** to aggregate in solution with flavins or substrates, thus supporting fast unproductive charge recombination.^[27] Interestingly, the N3-H \cdots O hydrogen bonds that dominate among the intermolecular interactions of flavins **2b–e** seem to have no negative effect on the catalytic activity of flavin photocatalysts, as evidenced by the comparison of **2b** and **2f** (compare entries 3 and 7 in Table 2-6).

Table 2-7 Photooxidation of 4-methoxybenzyl alcohol to 4-methoxybenzaldehyde in CD₃CN/D₂O (1:1) catalyzed by **1** and 10-arylflavin **2b**.

Flavin	Conversion after irradiation [%] ^[a]		Relative absorbance [%] ^[b]	$\Phi/\Phi_{\text{CD}_3\text{CN}}$ ^[c]
	5 min	15 min		
1	17	51	94	80
2b	58	quant.	49	220

[a] Conditions: $c_{\text{alcohol}}=4\times 10^{-3}\text{ molL}^{-1}$, $c_{\text{flavin}}=4\times 10^{-4}\text{ molL}^{-1}$, irradiation with 1 W LED ($\lambda_{\text{max}}=450\text{ nm}$), $T=25\text{ }^{\circ}\text{C}$, monitoring by ¹H NMR. [b] Relative absorbance of the reaction mixture at $\lambda=443\text{ nm}$ after irradiation for 10 min relative to the absorbance at the beginning of the experiment. [c] Relative values of the quantum yields in CD₃CN/D₂O (1:1) relative to the quantum yields in pure CD₃CN (Table 6).

Significantly enhanced quantum yields (by a factor of 80) were reported for the oxidation of 4-methoxybenzyl alcohol catalyzed by **1** by changing the solvent from pure acetonitrile to acetonitrile/water (1:1).^[27,52] In the case of arylflavin **2b**, the effect of water content on the quantum yield is even higher and a factor of 220 was reached (Table 2-7). Consequently, quantitative conversion was observed after only 15 minutes of photooxidation catalyzed by **2b**, whereas only 37 % conversion was achieved in pure CD₃CN after 90 minutes (compare Table 2-7 with Table 2-6, entry 3). Unfortunately, the decomposition of **2b** was also relatively fast in CD₃CN/D₂O (1:1; see Table 7 and supporting information).

2.4 Conclusion

10-Arylisoalloxazines **2a–f** were prepared as potentially nonaggregating flavin photocatalysts by condensation of the appropriately substituted aminouracils **5a–f** with nitrosobenzene. The investigation of their structures in the crystalline phase confirms that 10-arylflavins **2** have no structural prerequisites to interact by means of strong π - π interactions and to form stacks in a similar manner to simple flavin molecules, which is caused by steric hindrance of the substituted phenyl ring oriented perpendicularly to the flavin skeleton. X-ray diffraction studies also revealed that N-H \cdots O hydrogen bonding dominates in the crystals of **2a–d**. Blocking the N3 position with a methyl group in **2f** inhibits the formation of N-H \cdots O bonds; instead, C-H \cdots O hydrogen bonds and weak π - π interactions shape the structure of the molecules in the solid state. The significantly lower tendency of flavins **2a–f** to aggregate in acetonitrile was confirmed by ^1H -DOSY NMR spectroscopic experiments. Nevertheless, it was shown that there is no direct correlation between the steric demand of the substituents in **2a–f** and the aggregation numbers, which is probably due to the contributions of other noncovalent interactions; for example, the N-H \cdots O hydrogen bonds in the case of **2a–e** or dispersion forces between the bulkier substituents in the case of **2d** and **2e**.

Flavins **2b–f** are far more effective photocatalysts for the photooxidation of 4-methoxybenzyl alcohol than tetra-*O*-acetyl riboflavin (**1**). The observed quantum yield of this oxidation in the presence of **2b** (the best photocatalyst among 10-arylflavins **2**) exceeds that of **1** by almost one order of magnitude. Unfortunately, the increased reactivity of **2** is accompanied by their lower photostability. Although the conversions of the photooxidation reactions of 4-methoxybenzyl alcohol in acetonitrile catalyzed by flavins **2b–f** are not quantitative, they are among the most active flavins tested so far in the photooxidation reactions of benzyl alcohols. The efficiency of flavins **2** can be significantly enhanced by water as reported for **1**.^[27,52]

The results show that the efficiency of a flavin photocatalyst can be altered and improved by changing the structural elements that influence aggregation properties. However, there is no simple correlation as to how intermolecular interactions affect the ability of flavins to mediate the photooxidation of 4-methoxybenzyl alcohol. Although π - π interactions decrease the activity of flavin photocatalysts, the effect of hydrogen bonding seems to be positive. Therefore π - π interactions and hydrogen bonding should both be taken into account in the design of the structure of new flavins for photocatalysis. Additionally, photophysical properties (e.g., the quantum yields of singlet and triplet flavin excited state formation) are influenced by substitution.

2.5 Experimental Details

NMR spectra were recorded on a Varian Mercury Plus 300 (299.97 and 75.44 MHz for ^1H and ^{13}C , respectively), Bruker Avance 300 (300.13 and 75.03 MHz for ^1H and ^{13}C , respectively), Bruker Avance 400 (400.13 and 100.03 MHz for ^1H and ^{13}C , respectively), and Bruker Avance 600 (600.13 and 150.03 MHz for ^1H and ^{13}C , respectively) spectrometers. Chemical shifts δ are given in ppm with the residual solvent or tetramethylsilane (TMS) as an internal standard. Coupling constants are reported in Hz. UV/Vis spectra were recorded on a Varian Cary 50 spectrophotometer and fluorescence spectra on a Varian Cary Eclipse fluorescence spectrophotometer. TLC analyses were carried out on DC Alufolien Kieselgel 60 F254 and on DC Silicagel 60 RP-18 F254s (Merck). Preparative column chromatography separations were performed on silica gel Kieselgel 60 0.040–0.063 mm (Merck). Melting points were measured on a Boetius melting point apparatus or SRS MPA100 OptiMelt and are uncorrected. Elemental analyses (C, H, N) were performed on a Perkin–Elmer 240 analyzer. MS spectra were recorded on a ThermoQuest Finnigan TSQ 7000 mass spectrometer in tandem with a Janeiro LC system. HPLC analyses were carried out on an Ingos HPLC System (column: Phenomenex Luna 5u Silica, 150-4.6 mm) with a UV/Vis spectrophotometric detector. The starting materials and reagents were purchased from Sigma–Aldrich, Eurorad (deuterated solvents: CDCl_3 , $[\text{D}_6]\text{DMSO}$, CD_3CN), and Lach-Ner (acetonitrile, propan-2-ol, and n-heptane for HPLC). The solvents were purified and dried by using standard procedures.^[85]

Tetra-*O*-acetyl riboflavin (**1**),^[86] 6-chlorouracil (**4a**),^[87,88] 6-chloro-3-methyluracil,^[9] and nitrosobenzene^[89] were prepared according to the reported procedures. The experimental details about the synthesis and characterization of 6-aminouracils **5a–f** are provided in the supporting information.

Synthesis of 10-arylisalloxazines **2a–f**: Nitrosobenzene and the substituted 6-arylaminouracil **5** were dissolved in acetic acid/acetic anhydride (1:1, 10 mL). The reaction mixture was heated under reflux and stirred for 1.5 h (monitoring by TLC analysis with dichloromethane/methanol (10:1) as the mobile phase). The solvent was evaporated under reduced pressure and the crude product was purified by column chromatography with dichloromethane/methanol as the eluent (10:1 for **2a–c** and **2f**; 8:1 for **2d** and **2e**) or/and by recrystallization from ethanol. The resulting isalloxazine derivative was dried in vacuo.

10-Phenylisalloxazine (**2a**): Following the general procedure, aminouracil **5a** (0.68 g, 3.35 mmol) and nitrosobenzene (1.00 g, 10.4 mmol) were heated to reflux to yield

10-phenylisoalloxazine (**2a**) as a green-yellow powder (0.32 g, 33 %). M.p. 215 °C; ¹H NMR (400 MHz, [D₆]DMSO, 25 °C, TMS): δ=6.75 (dd, *J*(H,H)=8.5, 0.8 Hz, 1H; Ar-*H*), 7.44 (dd, *J*(H,H)=5.2, 3.2 Hz, 2H; Ar-*H*), 7.85–7.54 (m, 5H; Ar-*H*), 8.19 (dd, *J*(H,H)=8.1, 1.3 Hz, 1H; Ar-*H*), 11.43 ppm (s, 1H; NH); ¹³C NMR (100 MHz, [D₆]DMSO, 25 °C, TMS): δ=116.71, 125.93, 127.78, 129.75, 130.26, 131.33, 134.00, 134.69, 136.05, 139.46, 151.68, 155.46, 159.47 ppm; UV/Vis (CH₃CN): λ_{max}(ε)=335 (6200), 436 nm (8900 mol⁻¹dm³cm⁻¹); MS (ESI): *m/z* (%): 291 (100) [M+H]⁺; 581 (32) [2M+H]⁺; HRMS (ESI): *m/z* calcd for C₁₆H₁₀N₄O₂ [M+H]⁺: 291.08765; found: 291.08764; elemental analysis calcd (%) for C₁₆H₁₀N₄O₂: C 66.20, H 3.47, N 19.30; found: C 66.24, H 3.15, N 18.86.

10-(2',6'-Dimethylphenyl)isoalloxazine (**2b**): Following the general procedure, aminouracil **5b** (360 mg, 1.56 mmol) and nitrosobenzene (500 mg, 4.67 mmol) were heated to reflux to yield 10-(2',6'-dimethylphenyl)isoalloxazine (**2b**). The pure product was obtained after recrystallization from ethanol as an orange powder (115 mg, 23 %). M.p. 350 °C (decomp); ¹H NMR (400 MHz, CDCl₃, 25 °C, TMS): δ=1.93 (s, 6H; CH₃), 6.80 (dd, *J*(H,H)=8.5, 1.0 Hz, 1H; Ar-*H*), 7.29 (d, *J*(H,H)=7.7 Hz, 2H; Ar-*H*), 7.40 (dd, *J*(H,H)=8.1, 7.1 Hz, 1H; Ar-*H*), 7.67–7.57 (m, 1H; Ar-*H*), 7.71 (ddd, *J*(H,H)=8.6, 7.2, 1.6 Hz, 1H; Ar-*H*), 8.38 (dd, *J*(H,H)=8.1, 1.5 Hz, 1H; Ar-*H*), 8.83 ppm (s, 1H; NH); ¹³C NMR (100 MHz, CDCl₃, 25 °C, TMS): δ=17.81, 116.19, 127.26, 129.79, 130.57, 133.09, 133.58, 134.38, 135.98, 136.47, 138.64, 150.46, 155.15, 159.18 ppm; UV/Vis (CH₃CN): λ_{max}(ε)=330 (7000), 437 nm (10 000 mol⁻¹dm³cm⁻¹); MS (ESI): *m/z* (%): 319 (100) [M+H]⁺; 637 (82) [2M+H]⁺; HRMS (ESI): *m/z* calcd for C₁₈H₁₄N₄O₂ [M+Na]⁺: 341.10090; found: 341.10087; elemental analysis calcd (%) for C₁₈H₁₄N₄O₂: C 67.91, H 4.43, N 17.60; found: C 67.91, H 4.29, N 17.72.

10-(2',6'-Diethylphenyl)isoalloxazine (**2c**): Following the general procedure, aminouracil **5c** (405 mg, 1.56 mmol) and nitrosobenzene (500 mg, 4.67 mmol) were heated to reflux to yield 10-(2',6'-diethylphenyl)isoalloxazine (**2c**). The pure product was obtained after recrystallization from ethanol as an orange powder (110 mg, 20 %). M.p. 350 °C (decomp); ¹H NMR (400 MHz, CDCl₃, 25 °C, TMS): δ=1.06 (t, *J*(H,H)=7.6 Hz, 6H; CH₃), 2.07 (dq, *J*(H,H)=15.1, 7.5 Hz, 2H; CH₂), 2.24 (dq, *J*(H,H)=15.2, 7.6 Hz, 2H; CH₂), 6.78 (dd, *J*(H,H)=8.5, 1.1 Hz, 1H; Ar-*H*), 7.36 (d, *J*(H,H)=7.7 Hz, 2H; Ar-*H*), 7.52 (t, *J*(H,H)=7.7 Hz, 1H; Ar-*H*), 7.65–7.59 (m, 1H; Ar-*H*), 7.69 (ddd, *J*(H,H)=8.6, 7.3, 1.5 Hz, 1H; Ar-*H*), 8.37 (dd, *J*(H,H)=8.1, 1.5 Hz, 1H; Ar-*H*), 8.96 ppm (s, 1H; NH); ¹³C NMR (100 MHz, CDCl₃, 25 °C, TMS): δ=13.41, 23.85, 116.76, 127.21, 127.46, 130.87, 132.55, 132.97, 133.84, 135.91, 136.17, 138.59, 139.49, 151.05, 155.14, 159.24 ppm; UV/Vis

(CH₃CN): $\lambda_{\max}(\epsilon)=331$ (7000), 434 nm (10 100 mol⁻¹dm³cm⁻¹); MS (ESI): *m/z* (%): 347 (100) [M+H]⁺; 693 (70) [2M+H]⁺; HRMS (ESI): *m/z* calcd for C₂₀H₁₈N₄O₂ [M+Na]⁺: 369.13220; found: 369.13216; elemental analysis calcd (%) for C₂₀H₁₈N₄O₂: C 69.35, H 5.24, N 16.17; found: C 69.20, H 5.20, N 16.55.

10-(2',6'-Diisopropylphenyl)isoalloxazine (**2d**): Following the general procedure, aminouracil **5d** (200 mg, 0.70 mmol) and nitrosobenzene (224 mg, 2.09 mmol) were reacted to yield 10-(2',6'-diisopropylphenyl)isoalloxazine (**2d**). The pure product was obtained after recrystallization from ethanol as an orange powder (50 mg, 19 %). M.p. 350 °C (decomp); ¹H NMR (400 MHz, CDCl₃, 25 °C, TMS): $\delta=0.97$ (d, *J*(H,H)=6.8 Hz, 6H; CH₃), 1.15 (d, *J*(H,H)=6.8 Hz, 6H; CH₃), 2.16 (m, 2H; CH), 6.82 (dd, *J*(H,H)=8.5, 1.0 Hz, 1H; Ar-H), 7.40 (d, *J*(H,H)=7.8 Hz, 2H; Ar-H), 7.75–7.50 (m, 3H; Ar-H), 8.37 (dd, *J*(H,H)=8.1, 1.3 Hz, 1H; Ar-H), 8.79 ppm (s, 1H; NH); ¹³C NMR (100 MHz, CDCl₃, 25 °C, TMS): $\delta=23.84, 24.09, 29.18, 117.20, 125.54, 127.22, 130.65, 131.34, 132.97, 134.44, 135.87, 138.47, 144.52$ ppm; UV/Vis (CH₃CN): $\lambda_{\max}(\epsilon)=330$ (6200), 436 nm (8900 mol⁻¹dm³cm⁻¹); MS (ESI): *m/z* (%): 375 (100) [M+H]⁺; 749 (24) [2M+H]⁺; HRMS (ESI): *m/z* calcd for C₂₂H₂₂N₄O₂ [M+Na]⁺: 397.16350; found: 397.16345; elemental analysis calcd (%) for C₂₂H₂₂N₄O₂: C 69.57, H 5.92, N 14.96; found: C 69.86, H 6.06, N 15.25.

10-(2'-*tert*-Butylphenyl)isoalloxazine (**2e**): Following the general procedure, aminouracil **5e** (390 mg, 1.50 mmol) and nitrosobenzene (483 mg, 4.50 mmol) were heated to reflux to yield 10-(2'-*tert*-butylphenyl)isoalloxazine (**2e**). The pure product was obtained after recrystallization from ethanol as an orange powder (65 mg, 13 %). M.p. 300 °C (decomp); ¹H NMR (400 MHz, CDCl₃, 25 °C, TMS): $\delta=1.12$ (s, 9H; CH₃), 6.83 (dd, *J*(H,H)=8.6 and 0.9 Hz, 1H; Ar-H), 6.91 (dd, *J*(H,H)=7.9 and 1.4 Hz, 1H; Ar-H), 7.42 (m, 1H; Ar-H), 7.58–7.51 (m, 1H; Ar-H), 7.61 (m, 1H; Ar-H), 7.71 (m, 1H; Ar-H), 7.76 (dd, *J*(H,H)=8.2 and 1.3 Hz, 1H; Ar-H), 8.34 (dd, *J*(H,H)=8.2 and 1.3 Hz, 1H; Ar-H), 8.80 ppm (s, 1H; NH); ¹³C NMR (100 MHz, CDCl₃, 25 °C, TMS): $\delta=31.75, 36.70, 118.24, 127.03, 128.73, 129.34, 130.76, 131.15, 132.81, 135.49, 135.62, 135.77, 138.16, 146.29, 152.66, 154.80, 159.11$ ppm; UV/Vis (CH₃CN): $\lambda_{\max}(\epsilon)=332$ (7000), 437 nm (9900 mol⁻¹dm³cm⁻¹); MS (ESI): *m/z* (%): 347 (100) [M+H]⁺; 693 (60) [2M+H]⁺; HRMS (ESI): *m/z* calcd for C₂₀H₁₈N₄O₂ [M+Na]⁺: 369.13220; found: 369.13213; elemental analysis calcd (%) for C₂₀H₁₈N₄O₂: calcd C 69.35, H 5.24, N 16.17; found: C 68.93, H 5.62, N 16.42.

10-(2',6'-Dimethylphenyl)-3-methylisoalloxazine (**2f**): Following the general procedure, aminouracil **5f** (100 mg, 0.41 mmol) and nitrosobenzene (200 mg, 1.87 mmol) were reacted to yield isoalloxazine **2f**. The pure product was obtained after recrystallization

from ethanol as an orange powder (60 mg, 44 %). M.p. 350 °C (decomp); ^1H NMR (400 MHz, CDCl_3 , 25 °C, TMS): δ =1.92 (s, 6H; CH_3), 3.52 (s, 3H; CH_3), 6.86–6.73 (m, 1H; Ar-H), 7.30 (d, $J(\text{H,H})=7.6$ Hz, 2H; Ar-H), 7.40 (d, $J(\text{H,H})=7.4$ Hz, 1H; Ar-H), 7.64–7.56 (m, 1H; Ar-H), 7.68 (dd, $J(\text{H,H})=8.5$ and 1.4 Hz, 1H; Ar-H), 8.39 ppm (dd, $J(\text{H,H})=8.1$ and 1.4 Hz, 1H; Ar-H); ^{13}C NMR (100 MHz, CDCl_3 , 25 °C, TMS): δ =17.66, 28.87, 115.84, 126.79, 129.60, 130.38, 132.81, 132.85, 133.30, 134.42, 135.87, 135.94, 137.93, 148.73, 155.81, 159.70 ppm; UV/Vis (CH_3CN): $\lambda_{\text{max}}(\epsilon)=321$ (5500), 427 nm ($6500 \text{ mol}^{-1}\text{dm}^3\text{cm}^{-1}$); MS (ESI): m/z (%): 333 (100) $[\text{M}+\text{H}]^+$; 665 (86) $[2\text{M}+\text{H}]^+$; HRMS (ESI): m/z calcd for $\text{C}_{19}\text{H}_{16}\text{N}_4\text{O}_2$ $[\text{M}+\text{H}]^+$: 333.13460; found: 333.13457; elemental analysis calcd (%) for $\text{C}_{19}\text{H}_{16}\text{N}_4\text{O}_2$: C 69.35, H 5.24, N 16.17; found: C 69.20, H 5.20, N 16.55.

X-ray diffraction studies: Single crystals of **2a**, **2b**, **2d**, and **2f** suitable for X-ray analysis were prepared by slow evaporation of the solvent from solutions of **2a** (2.6 mg, 0.009 mmol), **2b** (1.6 mg, 0.005 mmol), **2d** (4.4 mg, 0.012 mmol), and **2f** (1.0 mg, 0.003 mmol) in ethanol (1.46, 1.00, 0.50, and 0.20 mL, respectively). A single crystal of **2c** was prepared by slow cooling of a solution of **2c** (3.2 mg, 0.009 mmol) in ethanol (0.50 mL) from 60 °C to ambient temperature. X-ray diffraction data for yellow-to-ruby crystals of flavin derivatives **2a–d** and **2f** were measured at 170 K on a four-circle CCD diffractometer Gemini of Oxford Diffraction Ltd. with graphite monochromated $\text{Cu}_{\text{K}\alpha}$ radiation ($\lambda = 1.5418 \text{ \AA}$). Data reduction including empirical absorption correction by using spherical harmonics were performed with CrysAlis-Pro (Oxford Diffraction). The crystal structure was solved by the charge-flipping method using the program Superflip^[90] and refined with the Jana2006 program package by full-matrix least-squares technique on F . The non-hydrogen atoms were refined anisotropically and the hydrogen atoms were positioned geometrically and refined by using the riding model. The molecular-structure plots were prepared by using ORTEP III, and the intermolecular interactions were viewed in Mercury.^[91] Selected data for **2a–d** and **2f** are collected in the supporting information.

CCDC-887842 (**2c**), CCDC-887843 (**2a**), CCDC-887844 (**2b**), CCDC-887845 (**2d**), and CCDC-887846 (**2f**) contain the supplementary crystallographic data for this paper. These data can be obtained free of charge from The Cambridge Crystallographic Data Centre via www.ccdc.cam.ac.uk/data-request/cif.

^1H -DOSY NMR: The ^1H -DOSY NMR spectroscopic measurements were conducted on a Bruker Avance 600 spectrometer (600.13 Hz) equipped with a triple-resonance broadband inverse (TBI) $^{31}\text{P}/^{13}\text{C}$ selective probe. Temperature stability was ensured by a

BVT 3000 unit. The data were processed and evaluated with Bruker Topspin 2.1 with the software package t1/t2. The measurements were conducted at 300 K with solutions of $c_{\text{flavin}} = 5 \times 10^{-3} \text{ molL}^{-1}$ in CD_3CN and $\text{CD}_3\text{CN}/\text{D}_2\text{O}$ (1:1) and saturated solutions in D_2O ($c_{\text{flavin}} \leq 5 \times 10^{-3} \text{ molL}^{-1}$). The aggregation numbers are based on diffusion coefficients measured by ^1H -DOSY NMR experiments by using a convection-compensating pulse sequence developed by Jerschow and Müller.^[92] Diffusion coefficients of TMS served as a viscosity reference. By assuming a spherical shape of the molecules and considering a microfriction factor, calculation of the hydrodynamic volumes from experimental diffusion coefficients was carried out according to the reported procedure.^[73,93] The comparison of this experimentally determined hydrodynamic volumes with theoretical volumes calculated according to Zhao *et al.*^[94] show that all the experimental hydrodynamic volumes for the flavins in water are smaller than the theoretically expected values with a factor of 0.7–0.8. This factor is in accordance with previous studies on experimental diffusion coefficients of aromatic systems^[95,96] and shows that the flavins appear as monomers in D_2O . The aggregation numbers were calculated as the ratio between the experimentally determined hydrodynamic volumes of the flavins in the respective solvent and the experimentally determined hydrodynamic volumes of their monomers in D_2O . An experimental hydrodynamic volume of flavin **2f** in D_2O was not accessible due to its poor solubility. Therefore, this value was calculated by adding the theoretical volume of a methyl group^[94] to the experimental hydrodynamic volume of flavin **2b** (see supporting information for data).

Cyclic voltammetry: Cyclic voltammetry measurements were carried out on an Autolab PGSTAT 302N setup at 20 °C in acetonitrile and acetonitrile/water (1:1) solutions containing flavin ($c = 1 \times 10^{-3} \text{ molL}^{-1}$) in an argon atmosphere with the use of a conventional undivided electrochemical cell, a glassy carbon working electrode, platinum wire as the counter electrode, and silver wire as the reference electrode. The redox potentials were referenced against ferrocenium/ferrocene. In all the experiments, the scan rate was 50 mVs^{-1} and tetrabutylammonium tetrafluoroborate was the supporting electrolyte ($c = 0.1 \text{ molL}^{-1}$).

Fluorescence quantum yields and quenching: The relative fluorescence intensities were measured on a Varian Eclipse spectrometer ($\lambda_{\text{ex}} = 427\text{--}440 \text{ nm}$, according to the flavin derivative). Fluorescence quantum yields Φ_F of flavins **1** and **2a–f** were determined by a standard procedure at $c = 3 \times 10^{-6} \text{ molL}^{-1}$ in acetonitrile and ethanol with quinidine sulfate ($c = 1 \times 10^{-7} \text{ molL}^{-1}$) in sulfuric acid (0.5 molL^{-1}) as a standard.^[97] Fluorescence quenching by 4-methoxybenzyl alcohol was measured in acetonitrile and ethanolic solutions

containing **1** or **2a-f** ($c = 3 \times 10^{-6} \text{ molL}^{-1}$) and 4-methoxybenzyl alcohol ($c = 0.9 \times 10^{-3} \text{ molL}^{-1}$) at 25 °C. Stern–Volmer plots ($I_0/I = 1 + K_S[Q]$) were constructed, and the constant K_S was evaluated as the slope of the dependence by using Origin 6.1 software.^[98]

Photooxidation reactions: The photooxidation of 4-methoxybenzyl alcohol (MBA; $c_{\text{MBA}} = 4 \times 10^{-3} \text{ molL}^{-1}$, $c_{\text{flavin}} = 4 \times 10^{-4} \text{ molL}^{-1}$) was performed in quartz cuvettes ($d = 1 \text{ cm}$). Deuterated acetonitrile or $\text{CD}_3\text{CN}/\text{D}_2\text{O}$ (1:1) was used as the solvent. The mixture was purged with oxygen for 2 min before the reaction was started. The reaction mixture was stirred, tempered to 25 °C, and irradiated with a diode (LED Luxeon Star; 1 W, 220 mW, 350 mA, 2.8–4 V, 440–460 nm, $\Delta\lambda_{1/2} = 20 \text{ nm}$). The conversion was monitored by ^1H NMR spectroscopic analysis by using the ratio of integral intensities of the Ar-H signals. The quantum yields of the photooxidation reactions were measured with a simple apparatus based on the absorption of light from an LED focused with a lens in a common quartz cuvette and measured by a calibrated solar cell as described before.^[52] The concentration of the 4-methoxybenzyl alcohol was $c = 4 \times 10^{-3} \text{ molL}^{-1}$ with 10 mol% of the flavin catalyst in acetonitrile, deuterated acetonitrile, or $\text{CD}_3\text{CN}/\text{D}_2\text{O}$ (1:1). The yield of 4-methoxybenzaldehyde was determined after 20, 30, 60, 120, 180, and 240 min by mean of GC analysis with chlorobenzene as an internal standard, and the quantum yield was determined as an average from all these measurements.

2.6 Supporting Information

Here only the experimental data for aggregation numbers and the ^1H and ^{13}C chemical shift assignment of the flavins are presented. The supporting information for the contributions of the collaborators can be found along with the publication.^[99]

2.6.1 Experimental Data for Aggregation Numbers

Diffusion coefficients of flavins **1** and **2**, TMS diffusion coefficient based viscosity values of the solutions, hydrodynamic volumes and aggregation numbers of flavins **1** and **2** determined by ^1H -DOSY NMR and calculated theoretical volumes.

Table 2-8 Experimental data for the calculation of the aggregation numbers of **1** and **2a-f**

flavin	solvent	diffusion coefficient [$10^{-9}\text{m}^2\text{s}^{-1}$] ^[a]	viscosity [mPa·s] ^[b]	hydrodynamic volume [\AA^3] ^[c]	theoretical monomer volume [\AA^3] ^[d]	aggregation number
1	CD ₃ CN	1.23	0.31	950.8		3.0
	CD ₃ CN/D ₂ O	0.49	0.96	523.6	485.0	1.7
	D ₂ O	0.43	1.23	314.8		1.0
2a	CD ₃ CN	1.62	0.31	470.8		2.4
	CD ₃ CN/D ₂ O	0.65	1.01	228.0	238.4	1.2
	D ₂ O	0.54	1.25	198.0		1.0
2b	CD ₃ CN	1.55	0.32	501.3		2.6
	CD ₃ CN/D ₂ O	0.56	1.13	256.6	273.0	1.4
	D ₂ O	0.52	1.32	189.8		1.0
2c	CD ₃ CN	1.58	0.32	473.2		1.9
	CD ₃ CN/D ₂ O	0.57	1.11	250.6	307.6	1.0
	D ₂ O	0.49	1.25	251.2		1.0

2d	CD ₃ CN	1.53	0.32	519.2	342.1	2.1
	CD ₃ CN/D ₂ O	0.54	1.12	287.2		1.2
	D ₂ O	0.50	1.24	242.6		1.0
2e	CD ₃ CN	1.57	0.32	488.9	307.6	2.2
	CD ₃ CN/D ₂ O	0.59	1.11	235.0		1.0
	D ₂ O	0.51	1.25	225.0		1.0
2f	CD ₃ CN	1.56	0.32	495.8	290.2	2.4
	CD ₃ CN/D ₂ O	0.57	1.09	263.1		1.3
	D ₂ O	----	----	207.1		1.0

[a] Experimental diffusion coefficient of the corresponding flavin as measured by ¹H-DOSY NMR^[92]. [b] Viscosity based on the experimental diffusion coefficient and the volume of TMS. [c] Hydrodynamic volume calculated as described in Chen.^[93] [d] Theoretical volume of a monomer of the respective flavin calculated according to Zhao.^[94]

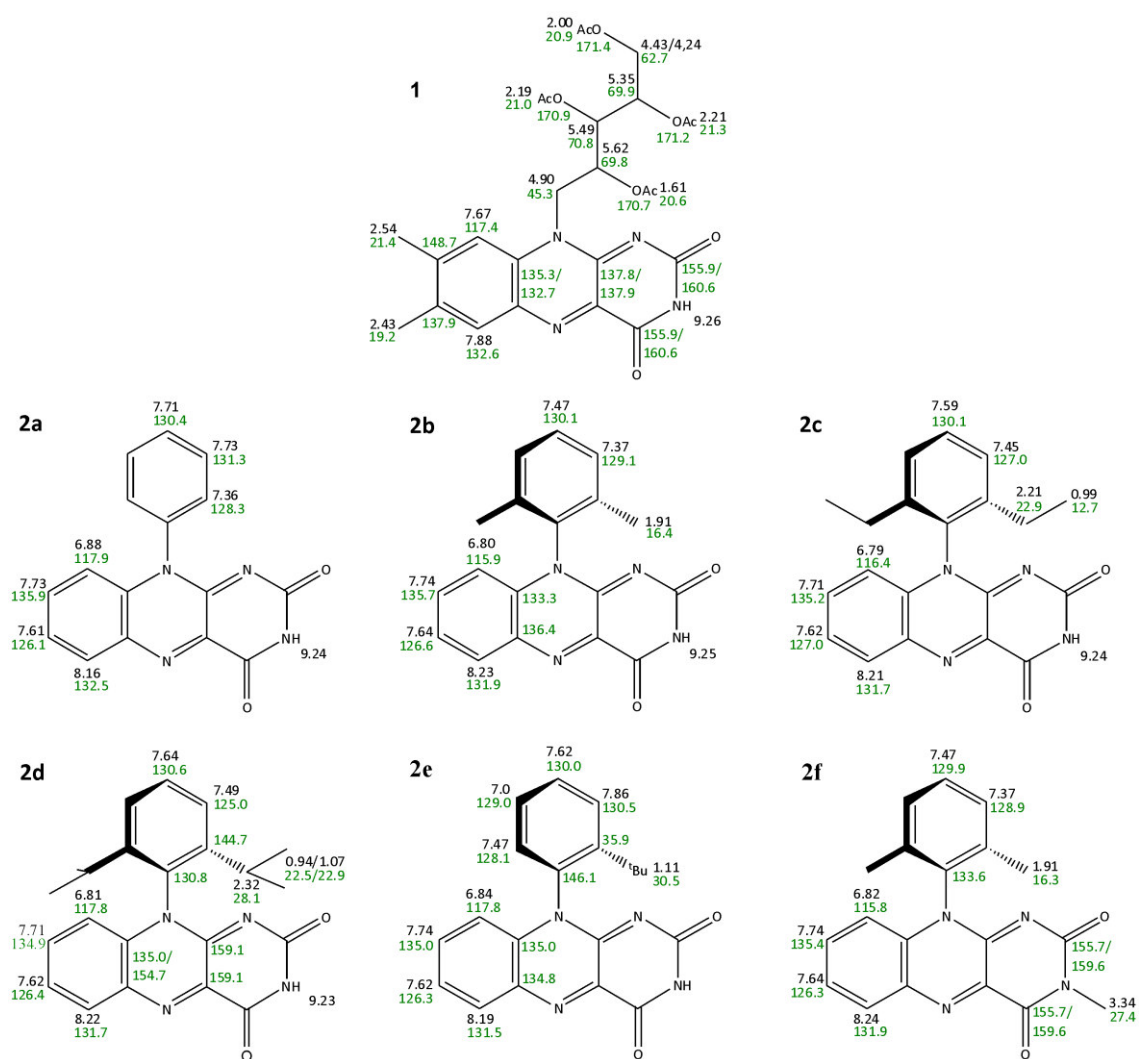
2.6.2 ^1H and ^{13}C Assignments

Figure 2-7 Overview of the ^1H (black) and ^{13}C (green) chemical shift assignments for tetra-*O*-acetyl riboflavin (**1**) and the 10-arylflavins (**2a-f**) in CD_3CN at 300 K referenced to the chemical shift of TMS.

2.7 Additional Experimental Findings

2.7.1 Self-Aggregation of Flavins

2.7.1.1 Solvent Dependence

It was shown by ¹H-DOSY experiments that RFT forms aggregates in CD₃CN and that these aggregates break up through the addition of water to the reaction mixture. The aggregation numbers of differently substituted flavins and their crystal structures revealed that both hydrogen bonds and π-π interactions contribute to the self-aggregation of the different flavins (chapter 2.3.3).

To gain further insight into the self-aggregation mode of RFT its aggregation in other solvents was studied. Apart from CD₃CN, CD₃CN/D₂O (1:1) and D₂O these investigations were performed for RFT solved in CD₂Cl₂, CDCl₃ and deuterated DMF and chlorobenzene. For this purpose the diffusion coefficients of RFT in the different solvents were measured by ¹H-DOSY NMR. To consider the different viscosities of the solutions TMS was added as a viscosity reference. In this way the diffusion coefficients were corrected relative to 20 mM RFT in CD₃CN at 300 K as temperature and viscosity standard. Table 2-9 shows the experimental data for the diffusion coefficients, viscosity and the resulting hydrodynamic volumes and aggregation numbers for RFT in the different solvents. Figure 2-8 shows the viscosity corrected diffusion coefficients of RFT in the respective solvents (relative to the solution of 20 mM RFT in CD₃CN).

After the viscosity correction the diffusion coefficients are referenced to one basic viscosity and thus directly comparable. It is obvious that water is the only solvent among the tested ones that leads to a complete disaggregation of the flavins. In water RFT shows the highest diffusion coefficient which corresponds to a RFT monomer (compare chapter 2.3.3). Changing the solvent from pure water to CD₃CN/ D₂O mixture (1:1) leads to a smaller diffusion coefficient and thus to RFT self-aggregation corresponding to an average aggregation number of 1.7 (compare chapter 2.3.3 and Table 2-9). For the case of all other investigated solvents significantly smaller diffusion coefficients were detected which shows that in all these solvents RFT forms aggregates. The corresponding aggregation numbers are 2.5 for CD₂Cl₂, 2.8 for DMF and CDCl₃ and 3.0 for CD₃CN (Table 2-9) for 5 mM of RFT. The lowest diffusion coefficient for RFT and thus the highest aggregation is found when RFT is solved in chlorobenzene with an aggregation number of 3.5. The comparison of the aggregation numbers of RFT in CD₂Cl₂ and in chlorobenzene gives hints on the aggregation mode of RFT. CD₂Cl₂ and chlorobenzene have similar Kamelt and Taft's parameters π* (0.73 for dichloromethane and 0.68 for

chlorobenzene) which describe the dipolarity and polarizability of the respective solvents^[100]. However, the solvents differ in the Kamelt and Taft's parameters α and β describing their hydrogen-bond donor and acceptor abilities^[100] (dichloromethane: $\alpha = 0.13$, $\beta = 0.10$; chlorobenzene: $\alpha = 0.00$, $\beta = 0.07$). CD_2Cl_2 is much more prone to form hydrogen bonds with the solute in particular acting as a hydrogen bond donor. In contrast chlorobenzene tends to interact via π - π interactions with the solute due to its aromatic ring. The observation that RFT disaggregates from an aggregation number of 3.5 for chlorobenzene to an aggregation number of 2.5 in CD_2Cl_2 thus suggests that for aggregations higher than a dimer hydrogen bonds are the prevalent interaction causing aggregation of RFT.

Table 2-9 Diffusion coefficients of RFT, viscosity values of the respective solutions based on TMS diffusion coefficients, hydrodynamic volumes and aggregation numbers of 5 mM RFT in different solvents and the data of RFT as a saturated solution in D_2O determined by ^1H -DOSY NMR and calculated theoretical volumes.

Solvent	diffusion coefficient [$10^{-9}\text{m}^2\text{s}^{-1}$] ^[a]	viscosity [mPa·s] ^[b]	corrected diffusion coefficient [$10^{-9}\text{m}^2\text{s}^{-1}$] ^[c]	hydrodyn. volume [\AA^3] ^[d]	theoretical monomer volume [\AA^3] ^[e]	aggregation number
D_2O	0.43	1.23	1.69	314.8	485.0	1.0
$\text{CD}_3\text{CN}/\text{D}_2\text{O}$	0.49	0.96	1.45	523.6	485.0	1.7
CD_2Cl_2	1.05	0.41	1.30	773.6	485.0	2.5
CDCl_3	7.77	0.53	1.20	889.9	485.0	2.8
DMF	5.10	0.82	1.26	891.1	485.0	2.8
CD_3CN	1.23	0.31	1.18	950.8	485.0	3.0
chlorobenzene	5.94	0.64	1.12	1099.3	485.0	3.5

[a] Experimental diffusion coefficient of RFT as measured by ^1H -DOSY NMR^[92]. [b] Viscosity based on the experimental diffusion coefficient of TMS. [c] Diffusion coefficient corrected with respect to different viscosities of the solutions. [d] Hydrodynamic volume calculated as described by Chen.^[93] [e] Theoretical volume of a monomer calculated according to Zhao.^[94]

The concentration dependence of the detected self-aggregation was studied for CD_3CN and $\text{CD}_3\text{CN}/\text{D}_2\text{O}$ (1:1) mixture for concentrations from 0.2 mM up to 30 mM (Figure 2-8). Surprisingly, there is no evident increase in the diffusion coefficients even for the lowest tested concentration of 0.2 mM in pure CD_3CN and in $\text{CD}_3\text{CN}/\text{D}_2\text{O}$ (1:1) mixture as it could be expected for disaggregation of the aggregates at lower concentrations. This shows that the aggregation constant is quite high so that the diffusion constants show no concentration dependence in the investigated concentration range. Even dilution of the solution down to concentrations of 0.2 mM in pure CD_3CN and in $\text{CD}_3\text{CN}/\text{D}_2\text{O}$ (1:1) mixture does not cause an evident reduction of the RFT aggregation. This shows that in the observed concentration range the self-aggregation of RFT does either not change at

all or changes only slightly with the changes lying below the detection limit of DOSY measurements. A much more sensitive tool for the investigation of aggregation is the study of concentration dependent change of NMR chemical shifts.

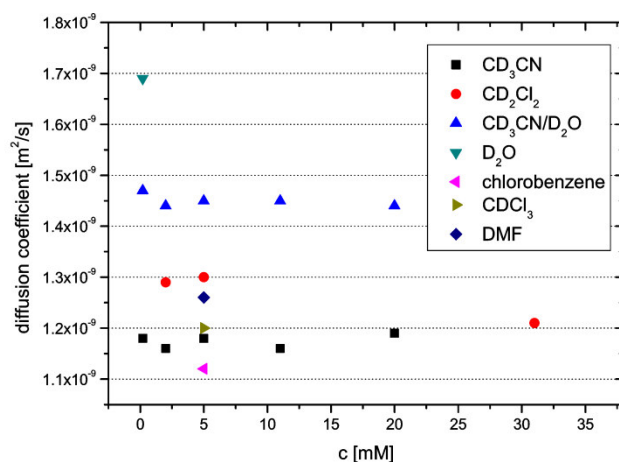


Figure 2-8 Viscosity corrected diffusion coefficients of RFT in the solvents CD₃CN, CD₃CN/D₂O (1:1), D₂O, CD₂Cl₂, CDCl₃, deuterated chlorobenzene and DMF for different RFT concentrations.

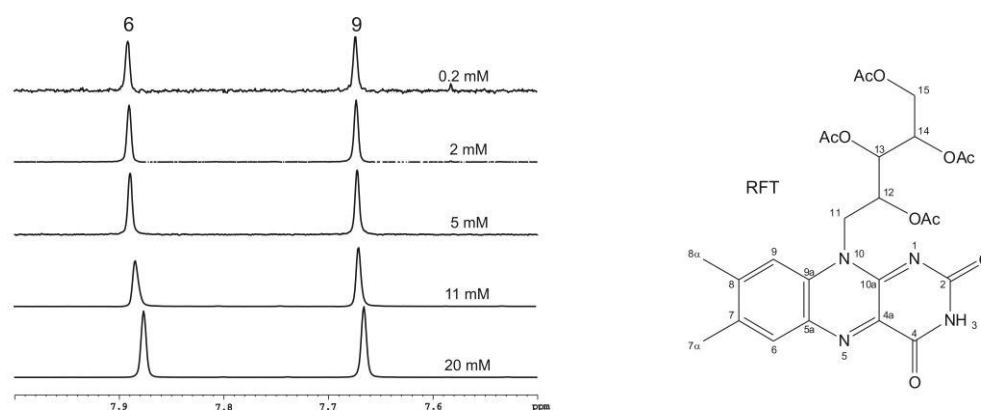


Figure 2-9 Upfield shift of the resonances of the aromatic protons FI(6) and FI(9) in CD₃CN with increasing RFT concentration.

For this reason the change of the chemical shifts with increasing RFT concentration was studied in the same concentration range as the ¹H-DOSY experiments. A small but clear change of the chemical shifts of all proton resonances is observed with varying concentrations. Figure 2-9 exemplarily shows the behavior of the aromatic flavin protons FI(6) and FI(9). The exact chemical shifts of the proton resonances of the isoalloxazine moiety FI(6), FI(9), FI(11), FI(7 α), FI(8 α) and FI(3) are listed in Table 2-10 for RFT solved in pure CD₃CN and for RFT solved in CD₃CN/D₂O (1:1) mixture in Table 2-11. In both pure CD₃CN and CD₃CN/D₂O (1:1) mixture a small but clear highfield shift of all proton resonances is observed with increasing RFT concentrations. The only exception from this trend, the NH proton at position FI(3), cannot be considered as an indicator for RFT self-aggregation as it exchanges with water and the MBA OH group. The downfield shift

with decreasing concentrations is caused by deshielding of the respective nuclei and shows that the RFT aggregates slightly disaggregate in the investigated concentration range. However, the disaggregation is rather weak in this range and the aggregation constant accordingly high, so that the disaggregation is too small to be observed by the DOSY experiments.

Table 2-10 Change of the proton chemical shifts of RFT with increasing RFT concentrations c_{RFT} in CD_3CN . The blue numbers show the absolute ^1H chemical shifts of RFT of 0.2 mM, the black numbers show the chemical shift changes at higher concentrations relative to the ^1H chemical shift of 0.2 mM RFT. To describe the small chemical shift changes the ^1H proton chemical shifts are listed with three decimal places.

	chemical shift [ppm] / chemical shift change $\Delta\delta$				
c_{RFT} [mM]:	0.2	2	5	11	22
Peak					
Fl(6)	7.891	0.001	0.002	0.008	0.015
Fl(9)	7.674	0.000	0.001	0.004	0.008
Fl(11)	4.902	-0.001	0.000	-0.067	0.004
Fl(7 α)	2.430	0.000	0.001	0.003	0.006
Fl(8 α)	2.543	0.000	0.000	0.002	0.003
Fl(3)	9.166	-0.009	-0.003	-0.065	-0.088

Table 2-11 Change of the proton chemical shifts of RFT with increasing RFT concentrations in $\text{CD}_3\text{CN}/\text{D}_2\text{O}$ (1:1). The blue numbers show the absolute ^1H chemical shifts of RFT of 0.2 mM, the black numbers show the chemical shift changes at higher concentrations relative to the ^1H chemical shift of 0.2 mM RFT. To describe the small chemical shift changes the ^1H proton chemical shifts are listed with three decimal places.

	chemical shift [ppm] / chemical shift change $\Delta\delta$				
c_{RFT} [mM]:	0.2	2	5	11	22
Peak					
Fl(6)	7.9786	0.003	0.005	0.023	0.040
Fl(9)	7.7551	0.001	0.002	0.013	0.023
Fl(11)	5.0144	-0.002	-0.001	0.009	0.018
Fl(7 α)	2.4558	0.001	0.001	0.007	0.011
Fl(8 α)	2.5739	0.000	0.001	0.005	0.007

In summary the aggregation of RFT in different solvents was shown by means of ^1H -DOSY NMR. The aggregation of RFT shows a very strong dependence on the solvent. Among the tested solvents D_2O is the only one that causes a complete disaggregation of the RFT aggregates. ^1H -DOSY measurements revealed that in CD_2Cl_2 ,

CDCl₃, DMF, CD₃CN and chlorobenzene RFT appears as dimers or trimers. For CD₃CN and CD₃CN/D₂O (1:1) mixture no disaggregation of the aggregates was detected by ¹H-DOSY NMR for the concentration range from 0.2 mM to 20 mM. However, the proton resonances show a small but clear upfield shift with increasing RFT concentrations. This shows that the influence of the RFT concentration on its aggregation is rather weak and the self-aggregation constant respectively high.

2.7.2 Aggregation between RFT and MBA

2.7.2.1 Limits of Aggregation Studies by ¹H-DOSY NMR

The interaction between the photocatalyst RFT and the substrate MBA was studied to elucidate if any pre-aggregated complexes are formed and have an effect on the mechanism as it was suggested by Megerle *et al.*^[27] from transient absorption spectroscopy measurements. For this purpose the diffusion coefficients of RFT and MBA were measured by ¹H-DOSY experiments for a fixed concentration of RFT of 2 mM and varying concentrations of MBA from 2 mM up to 1600 mM in CD₃CN/D₂O (1:1). The experimental data are presented in Table 2-12.

Table 2-12 MBA concentrations, viscosities of the respective solutions, experimental diffusion coefficients and viscosity corrected diffusion coefficients of RFT and MBA at RFT concentrations of 2 mM and varying MBA concentrations as determined by ¹H-DOSY measurements.

MBA concentration [mM]	viscosity [mPa·s] ^[a]	RFT		MBA	
		diffusion coefficient [10 ⁻⁹ m ² s ⁻¹] ^[b]	corrected diffusion coefficient [10 ⁻⁹ m ² s ⁻¹] ^[c]	diffusion coefficient [10 ⁻⁹ m ² s ⁻¹] ^[b]	corrected diffusion coefficient [10 ⁻⁹ m ² s ⁻¹] ^[c]
2	0.963	0.48	0.48	0.99	0.99
50	1.013	0.47	0.50	0.98	1.03
100	1.015	0.46	0.48	0.96	1.02
200	0.987	0.46	0.47	0.96	0.99
400	1.145	0.43	0.51	0.89	1.06
800	1.215	0.38	0.48	0.82	1.04
1600	1.342	0.32	0.45	0.70	0.98

[a] Viscosity based on the experimental diffusion coefficient of TMS. [b] Experimental diffusion coefficient of the corresponding molecule as measured by ¹H-DOSY NMR^[92]. [c] Diffusion coefficient corrected with respect to different viscosities of the solutions.

The dependence of the diffusion coefficients of both RFT and MBA on the MBA concentrations is shown in Figure 2-10 A. The diffusion coefficients of both RFT and MBA show a significant decrease with increasing MBA concentrations. To consider the viscosity changes caused by the addition of the comparatively high viscous MBA the

diffusion coefficients were corrected relative to the viscosity of 2 mM RFT and 2 mM MBA in CD₃CN/D₂O (1:1). Figure 2-10 B shows the viscosity corrected diffusion coefficients that are now directly comparable. The data reveal that the decrease of the diffusion coefficients at higher MBA concentrations observed in Figure 2-10 is mainly caused by the changed overall viscosity of the solution. After viscosity correction the strong decrease of the diffusion coefficients is not that prominent anymore and easy to confuse with measurement accuracy. Also, if only RFT or MBA alone are present in the solution the diffusion coefficients do not change compared to the cases where both molecules are present in the mixture. The absence of significant changes in diffusion coefficients at different RFT/MBA ratio suggests that RFT and MBA interact rather weakly or not at all.

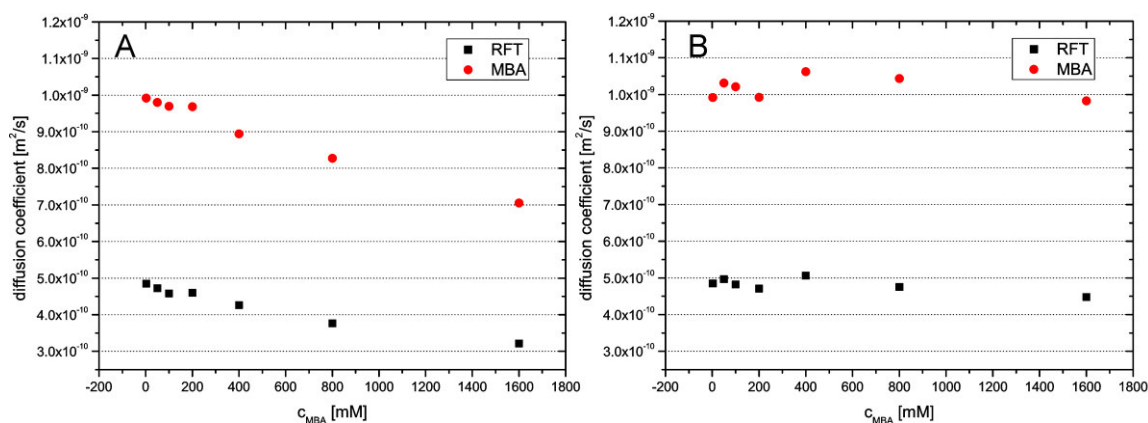


Figure 2-10 A) Experimental diffusion coefficient of RFT in CD₃CN/D₂O (1:1) at different MBA concentrations and constant RFT concentration of 2 mM. B) Viscosity corrected diffusion coefficient of RFT in CD₃CN/D₂O (1:1) at different MBA concentrations and a constant RFT concentration of 2 mM.

2.7.2.2 Aggregation between MBA and RFT Revealed by Chemical Shift Changes

As seen before DOSY measurements provide a rather rough tool for studying the aggregations between molecules. For finer measurements chemical shifts can be used as an indicator for aggregations between molecules. For this reason titration experiments were conducted. In these experiments the concentration of one analyte is kept constant while the one of the other is increased. Changes in respective spectra reveal interactions between the molecules. Common spectroscopic techniques employed for titration experiments are UV/Vis or NMR spectroscopy. UV/Vis spectroscopy is reliable for aggregations in the orders of magnitude of K_a from 10 M⁻¹ to 1000 M⁻¹ and NMR is suitable for aggregations in the range of $K_a = 0.1$ M⁻¹ to 10 M⁻¹ [101].

The aggregation constant is determined by an NMR-titration and the fitting of the chemical shift changes of the averaged signals with fast exchange on the NMR time scale. A model for a 1:1 complex formation as described in a considerable amount of

literature^[102–106] was used for aggregation of one single RFT molecule with one single MBA molecule.

The aggregation constant K_a of a complex of one RFT and one MBA molecule can be calculated from the concentration of the complex c_c , the concentration of the free RFT $c_{RFT\ free}$ and the concentration of free MBA $c_{MBA\ free}$ by:

$$K_a = \frac{c_{RFT\ free} c_{MBA\ free}}{c_c}$$

For the case that the complex and free RFT exchange fast on the NMR time scale the observed chemical shifts of RFT δ caused by complexation with MBA can be expressed as the weighted average of the chemical shift δ_{RFT} of the free not complexed RFT and the chemical shift δ_c of the RFT in the complex δ_c . The chemical shifts are weighted by the respective relative proportion of free RFT and complexed RFT:

$$\delta = \frac{c_c}{c_{RFT}} \delta_c + \frac{c_{RFT\ free}}{c_{RFT}} \delta_{RFT}$$

where c_{RFT} is the total concentration of flavin in solution and c_{MBA} is the total concentration of MBA in the solution. With

$$c_{RFT} = c_{RFT\ free} + c_c \quad c_{MBA} = c_{MBA\ free} + c_c$$

The change in chemical shift of RFT $\Delta\delta_{obs}$ in the presence of MBA can be expressed by

$$\Delta\delta_{obs} = \Delta\delta_{max} \frac{(c_{RFT} + c_{MBA} + K_a) - \sqrt{(c_{RFT} + c_{MBA} + K_a)^2 - 4 c_{RFT} c_{MBA}}}{2 c_{RFT}} \quad (1)$$

with

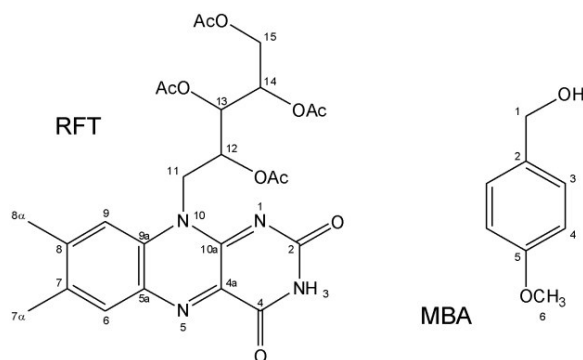
$$\Delta\delta_{obs} = \delta - \delta_{RFT} \quad \Delta\delta_{max} = \delta_c - \delta_{RFT}$$

This equation provides a relation between the aggregation constant K_a and the observed RFT chemical shift change for a complex of one RFT molecule and one MBA molecule at fast exchange on the NMR time scale.

Based on this relation a titration experiment was performed with a constant concentration of RFT of 2 mM and varying concentrations of MBA from 0 mM up to 1600 mM. The chemical shifts of RFT and MBA were assigned for each MBA concentration. The results obtained from this analysis are presented in Table 2-13. The chemical shifts were measured in reference to TMS with a chemical shift of 0.00 ppm and the signal of the residual not deuterated acetonitrile at 2.00 ppm. The signals of the protons FI(15a) and

FI(15b) were only partially observable as they disappear with increasing amounts of MBA under the MBA(1) signal.

Table 2-13 Chemical shifts of all visible proton resonances of RFT in CD₃CN/D₂O (1:1) at varying MBA concentrations and a constant RFT concentration of 2 mM. The blue numbers show the absolute ¹H chemical shifts of RFT without MBA, the black numbers show the chemical shift changes with the addition of MBA relative to the ¹H chemical shift of RFT without MBA. To describe the small chemical shift changes the ¹H proton chemical shifts are listed with three decimal places.



	chemical shift [ppm] / chemical shift change $\Delta\delta$								
C_{MBA} [mM]:	0	2	50	100	200	400	800	1600	
Peak									
FI(6)	7.977	0.001	0.006	0.010	0.019	0.029	0.038	0.044	
FI(7 α)	2.456	0.000	0.002	0.004	0.008	0.015	0.025	0.041	
FI(8 α)	2.575	0.000	0.002	0.004	0.007	0.012	0.018	0.025	
FI(9)	7.757	0.001	0.011	0.021	0.037	0.058	0.073	0.081	
FI(11)	5.044	-0.004	0.014	0.028	0.047	0.071	0.092	-	
FI(12)	5.621	-0.001	0.004	0.009	0.012	0.013	0.007	-0.013	
FI(13)	5.506	-0.001	-0.001	-0.004	-0.008	-0.019	-0.035	-0.068	
FI(14)	5.405	0.000	-0.001	-0.002	-0.004	-0.013	-0.026	-0.050	
FI(15)	4.463	0.000	0.000	-0.003	-0.006	-	-	-	
FI(15)	4.511	-	-	-	-	-	-	-	
FI(12 OAc)	1.679	0.000	0.002	0.003	0.004	0.003	0.001	-0.010	
FI(13 OAc)	2.199	-0.001	-0.002	-0.004	-0.010	-0.023	-0.038	-0.059	
FI(14 OAc)	2.192	0.000	-0.004	-0.009	-0.016	-0.026	-0.034	-0.048	
FI(15 OAc)	2.033	0.000	-0.001	-0.003	-0.005	-0.009	-0.012	-0.015	

Table 2-14 Chemical shifts of all visible proton resonances of MBA in CD₃CN/D₂O (1:1) at varying MBA concentrations and a constant RFT concentration of 2 mM. The blue numbers show the absolute ¹H chemical shifts of MBA at 2 mM, the black numbers show the MBA ¹H chemical shift changes at higher MBA concentrations relative to the ¹H chemical shift of MBA at 2 mM. To describe the small chemical shift changes the ¹H proton chemical shifts are listed with three decimal places.

<i>c</i> _{MBA} [mM]:	chemical shift [ppm] / chemical shift change Δδ							
	0	2	50	100	200	400	800	1600
Peak								
MBA(1)	-	4.511	-0.001	-0.003	-0.006	-0.011	-0.016	0.006
MBA(3)	-	7.295	0.000	-0.001	-0.001	-0.001	0.001	0.148
MBA(4)	-	6.941	0.001	0.002	0.004	0.009	0.018	0.175
MBA(6)	-	3.795	0.001	0.003	0.005	0.010	0.020	0.186

All values in equation 1 are known from the measurements except K_a and $\Delta\delta_{max}$ which is only directly measurable if saturation is reached by the performed titration and all RFT molecules would be complexed with MBA. These two missing parameters can be determined by fitting the measured data of $\Delta\delta$ in dependence of c_{MBA} with equation 1. For the calculation of the aggregation constant of a RFT-MBA complex the data rows of the proton signals of the isoalloxazine moiety FI(6), FI(9), FI(11), FI(8 α) and FI(7 α) were used (see Figure 2-11 A). They show dependencies consistent with the model described above, i.e. chemical shifts change with addition of MBA and converge to a maximum at high MBA concentrations. Most chemical shifts of the protons in the RFT side chain (FI(12) – FI(15)) showed behavior other than the one used for the model above. Three examples for the behavior of the chemical shifts of protons in the RFT side chain are shown in Figure 2-11 B. FI(12) shows an upfield shift at low MBA concentrations which reaches a minimum at an MBA concentration of 400 mM and then shifts back downfield. The chemical shifts of FI(13) and FI(14) start with a comparably small downfield shift which increases stronger with rising MBA concentrations. This surprising behavior can be due to the RFT-MBA complex formation with a concomitant conformational change of the flexible RFT side chain which additionally changes the electron densities and thus the chemical shifts of the protons in the RFT side chain. Another explanation for this surprising behavior is the additional formation of complexes consisting of one RFT and two MBA molecules.

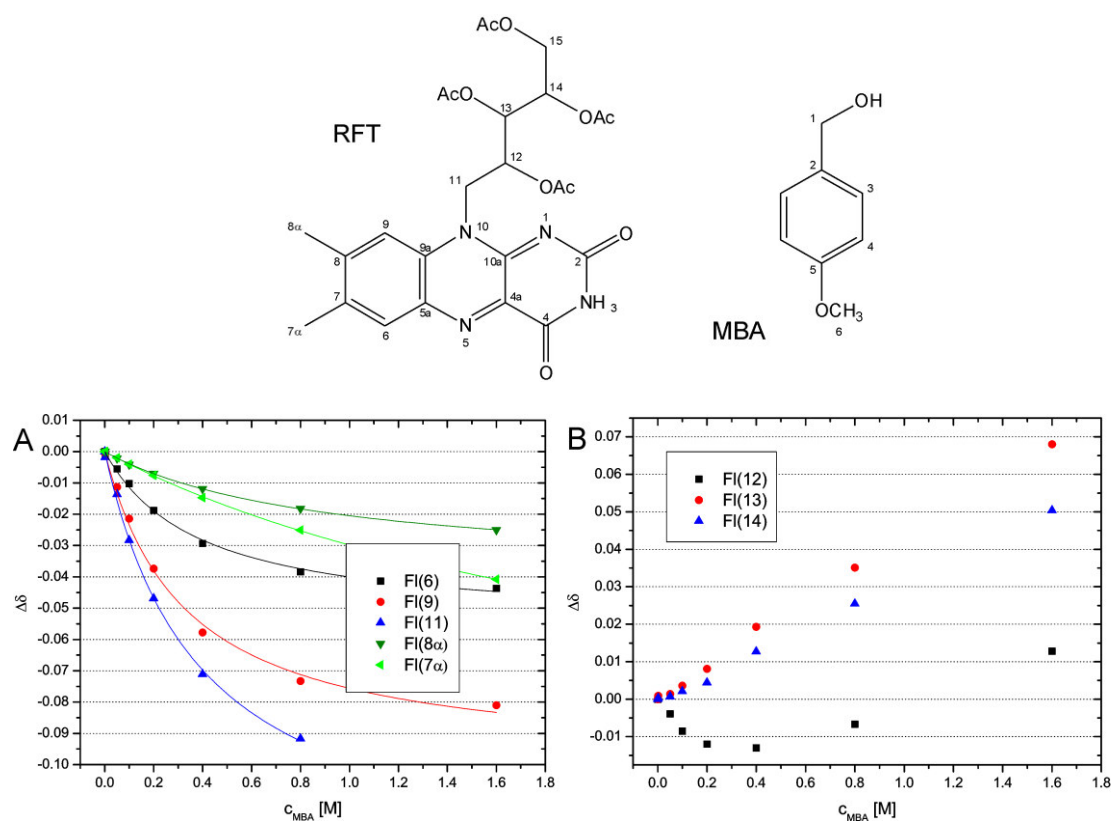


Figure 2-11 The graphs show the change of the chemical shifts $\Delta\delta$ of different RFT ^1H resonances at a constant RFT concentration of 2 mM and different concentrations of MBA. A) shows the data of protons FI(6), FI(9), FI(11), FI(7 α) and FI(8 α) of the isoalloxazine moiety and the corresponding dimer model fits. B) shows RFT ^1H resonances of the RFT side chain.

The values for $\Delta\delta_{\text{max}}$ and K_{a} resulting from the dataset fits of FI(6), FI(9), FI(11), FI(8 α) and FI(7 α) are compared in Table 2-15. The signals of all protons in Table 2-13 shift upfield with the strongest shift change for proton FI(11). Surprisingly, the aggregation constants derived from the fitting of the titration curves of the protons FI(6), FI(9) and FI(11) are in accordance with each other, whereas the aggregation constant derived from FI(8 α) is about double as big as the one from the protons FI(9), FI(6) and FI(11) and the aggregation constant of FI(7 α) is about six times as big. This deviation from the values of FI(9), FI(6) and FI(11) could be explained by an additional aggregation of the MBA to the methyl groups FI(8 α) and FI(7 α) so that the model used for the fitting is only valid for the central protons. However, the values give a good assessment of the order of magnitude of the aggregation between RFT and MBA in $\text{CD}_3\text{CN}/\text{D}_2\text{O}$ (1:1) and is in accordance with a value for the aggregation constant of $K = 0.6 \text{ M}^{-1}$ in $\text{CD}_3\text{CN}/\text{D}_2\text{O}$ (1:1) that was calculated for transient absorption measurements.^[27]

Table 2-15 The maximal chemical shift change $\Delta\delta_{\max}$ and the aggregation constant K_a for RFT-MBA dimers for the proton resonances FI(6), FI(9), FI(11), FI(8 α) and FI(7 α) calculated from fitting the dependence of the chemical shift change of the MBA concentration.

	$\Delta\delta_{\max}$ [ppm]		K_a [M^{-1}]	
	value	standard error	value	standard error
FI(6)	-0.055	0.002	0.383	0.031
FI(9)	-0.100	0.003	0.326	0.030
FI(11)	-0.137	0.004	0.383	0.025
FI(8 α)	-0.039	0.001	0.911	0.025
FI(7 α)	-0.105	0.003	2.507	0.092

The upfield shift of the 1H resonances of the protons of the isoalloxazine moiety suggest a face-to-face stacking of the isoalloxazine ring system and the benzyl ring of the alcohol. The strongest upfield shift is observed for protons FI(9) and FI(11), less pronounced changes for 1H resonances of FI(6), FI(7 α) and FI(8 α). This suggests that MBA is coordinated over the isoalloxazine moiety in a way that MBA is in close contact with protons FI(9) and FI(11) of the isoalloxazine ring system causing the pronounced chemical shift change of these 1H resonances. Most probably the MBA molecule lies over the heteroaromatic rings and the protons FI(9) and FI(11). A clearer picture of the interaction pattern and the coordination of the molecules to each other could be achieved by studying the carbon or nitrogen chemical shifts of the isoalloxazine ring system as in this way the whole ring system is accessible.

In summary the aggregation between the photocatalyst RFT and the substrate MBA was shown by the change of the chemical shifts at different RFT/MBA ratios. The fit of the chemical shift changes with a dimer model yields an aggregation constant of about $0.4 M^{-1}$. To gain further insight in the aggregation mode the same experiments can be performed in other solvents, e.g. in chlorobenzene to elucidate if and to what extent the aggregation between RFT and MBA is caused by π - π interactions.

2.7.3 Experimental Details

¹H-DOSY NMR experiments were performed on a Bruker Avance 600 spectrometer (600.13 Hz) with a ¹H, BB, ³¹P or ¹H, BB, ¹³C probe and a BVT 3000 unit to set the required temperature and on a Bruker Avance III 600 (600.25 MHz) spectrometer with a TCI cryoprobe with z-gradient (53.5 G/cm). A convection compensating pulse sequence developed by A. Jerschow and N. Müller^[92] was used for the ¹H-DOSY experiments. Bruker TOPSPIN 2.1 and Bruker TOPSPIN 3.0 were used for the procession and evaluation of the acquired NMR data. The experimental diffusion coefficients were determined from the DOSY diffusion plots with the included software package t1/t2. Tetramethylsilane (TMS) was added to all solutions as a viscosity reference. For comparability viscosity and temperature correction was performed with the diffusion coefficient of TMS in CD₃CN at 300 K as a reference using the Stokes-Einstein law describing the diffusion coefficient of a spherical particle in solution by its diffusion coefficient D:

$$D = \frac{k_B T}{6\pi\eta R_0}$$

k_B is the Boltzmann constant, T the temperature of the solution, η the viscosity of the solution and R_0 is the Stokes radius of the diffusing molecule. The hydrodynamic radii and volumes of the molecules were calculated from the experimental diffusion coefficients with a spherical shape approximation and considering a microfriction factor according to the reported procedure.^[93,107] The theoretical values for the hydrodynamic volumes of monomers of the molecules were calculated according to Zhao *et al.*^[94] For the case of D₂O as the solvent the experimentally determined hydrodynamic volumes of all flavins are much smaller than the calculated ones. This observation was reported earlier for aromatic flat systems^[96,108] and shows that the flavins appear as monomers in D₂O. Owing to this the aggregation numbers were calculated as the ratio between the experimental hydrodynamic volume of the flavin in the respective solvents and its respective experimental hydrodynamic volume of the monomers in D₂O.

¹H spectra were recorded on a Bruker Avance 600 spectrometer (600.13 Hz) with a ¹H, BB, ³¹P or ¹H, BB, ¹³C probe and a BVT 3000 unit and on a Bruker Avance III 600 (600.25 MHz) spectrometer with a TCI cryoprobe with z-gradient. Chemical shifts were determined from ¹H spectra and referenced relative to the chemical shift of TMS at 0.00 ppm.

2.8 References

- [1] F. Müller, Ed., *Chemistry and Biochemistry of Flavoenzymes*, CRC, Boca Raton, **1991**.
- [2] B. Palfey, V. Massey, *Comprehensive Biological Catalysis*, Academic Press, London, **1998**.
- [3] V. Massey, *Biochem. Soc. Trans.* **2000**, *28*, 283–296.
- [4] S. Ghisla, V. Massey, *Eur. J. Biochem.* **1989**, *181*, 1–17.
- [5] F. G. Gelalcha, *Chem. Rev.* **2007**, *107*, 3338–3361.
- [6] Y. Imada, T. Naota, *Chem. Rec.* **2007**, *7*, 354–361.
- [7] V. Mojz, M. Budesinsky, R. Cibulka, T. Kraus, *Org. Biomol. Chem.* **2011**, *9*, 7318–7326.
- [8] Y. Imada, T. Kitagawa, T. Ohno, H. Iida, T. Naota, *Org. Lett.* **2009**, *12*, 32–35.
- [9] R. Jurok, R. Cibulka, H. Dvořáková, F. Hampl, J. Hodačová, *European J. Org. Chem.* **2010**, *2010*, 5217–5224.
- [10] V. Mojz, V. Herzig, M. Budesinsky, R. Cibulka, T. Kraus, *Chem. Commun.* **2010**, *46*, 7599–7601.
- [11] J. Žurek, R. Cibulka, H. Dvořáková, J. Svoboda, *Tetrahedron Lett.* **2010**, *51*, 1083–1086.
- [12] C. Smit, M. W. Fraaije, A. J. Minnaard, *J. Org. Chem.* **2008**, *73*, 9482–9485.
- [13] J. Piera, J.-E. Bäckvall, *Angew. Chemie* **2008**, *120*, 3558–3576.
- [14] J. Piera, J.-E. Bäckvall, *Angew. Chemie Int. Ed.* **2008**, *47*, 3506–3523.
- [15] L. Baxová, R. Cibulka, F. Hampl, *J. Mol. Catal. A Chem.* **2007**, *277*, 53–60.
- [16] A. A. Lindén, M. Johansson, N. Hermanns, J.-E. Bäckvall, *J. Org. Chem.* **2006**, *71*, 3849–3853.
- [17] Y. Imada, H. Iida, S. Ono, Y. Masui, S.-I. Murahashi, *Chem. – An Asian J.* **2006**, *1*, 136–147.
- [18] Y. Imada, H. Iida, T. Naota, *J. Am. Chem. Soc.* **2005**, *127*, 14544–14545.
- [19] Y. Imada, H. Iida, S.-I. Murahashi, T. Naota, *Angew. Chemie* **2005**, *117*, 1732–1734.
- [20] A. A. Lindén, N. Hermanns, S. Ott, L. Krüger, J.-E. Bäckvall, *Chem. – A Eur. J.* **2005**, *11*, 112–119.

- [21] Y. Imada, H. Iida, S. Ono, S.-I. Murahashi, *J. Am. Chem. Soc.* **2003**, *125*, 2868–2869.
- [22] S.-I. Murahashi, S. Ono, Y. Imada, *Angew. Chemie* **2002**, *114*, 2472–2474.
- [23] A. B. E. Minidis, J.-E. Bäckvall, *Chem. – A Eur. J.* **2001**, *7*, 297–302.
- [24] C. Mazzini, J. Lebreton, R. Furstoss, *J. Org. Chem.* **1996**, *61*, 8–9.
- [25] S. Murahashi, T. Oda, Y. Masui, *J. Am. Chem. Soc.* **1989**, *111*, 5002–5003.
- [26] E. Silva, A. M. Edwards, Eds., *Comprehensive Series in Photochemical & Photobiological Sciences*, RSC Publishing, Cambridge, **2006**.
- [27] U. Megerle, M. Wenninger, R.-J. Kutta, R. Lechner, B. König, B. Dick, E. Riedle, *Phys. Chem. Chem. Phys.* **2011**, *13*, 8869–8880.
- [28] H. Schmaderer, P. Hilgers, R. Lechner, B. König, *Adv. Synth. Catal.* **2009**, *351*, 163–174.
- [29] J. Svoboda, H. Schmaderer, B. König, *Chem. – A Eur. J.* **2008**, *14*, 1854–1865.
- [30] R. Cibulka, R. Vasold, B. König, *Chem. – A Eur. J.* **2004**, *10*, 6223–6231.
- [31] M. Yasuda, T. Nakai, Y. Kawahito, T. Shiragami, *Bull. Chem. Soc. Jpn.* **2003**, *76*, 601–605.
- [32] V. T. D'Souza, *Supramol. Chem.* **2003**, *15*, 221–229.
- [33] S. Fukuzumi, K. Yasui, T. Suenobu, K. Ohkubo, M. Fujitsuka, O. Ito, *J. Phys. Chem. A* **2001**, *105*, 10501–10510.
- [34] S. Fukuzumi, S. Kuroda, *Res. Chem. Intermed.* **1999**, *25*, 789–811.
- [35] W. Tong, H. Ye, H. Zhu, V. T. D'Souza, *J. Mol. Struct.* **1995**, *333*, 19–27.
- [36] S. Fukuzumi, K. Tanii, T. Tanaka, *J. Chem. Soc. Chem. Commun.* **1989**, 816–818.
- [37] S. Fukuzumi, S. Kuroda, T. Tanaka, *J. Am. Chem. Soc.* **1985**, *107*, 3020–3027.
- [38] J. M. Kim, M. A. Bogdan, P. S. Mariano, *J. Am. Chem. Soc.* **1993**, *115*, 10591–10595.
- [39] R. Lechner, S. Kümmel, B. König, *Photochem. Photobiol. Sci.* **2010**, *9*, 1367–1377.
- [40] W. A. Massad, Y. Barbieri, M. Romero, N. A. García, *Photochem. Photobiol.* **2008**, *84*, 1201–1208.
- [41] J. García, E. Silva, *J. Nutr. Biochem.* **1997**, *8*, 341–345.

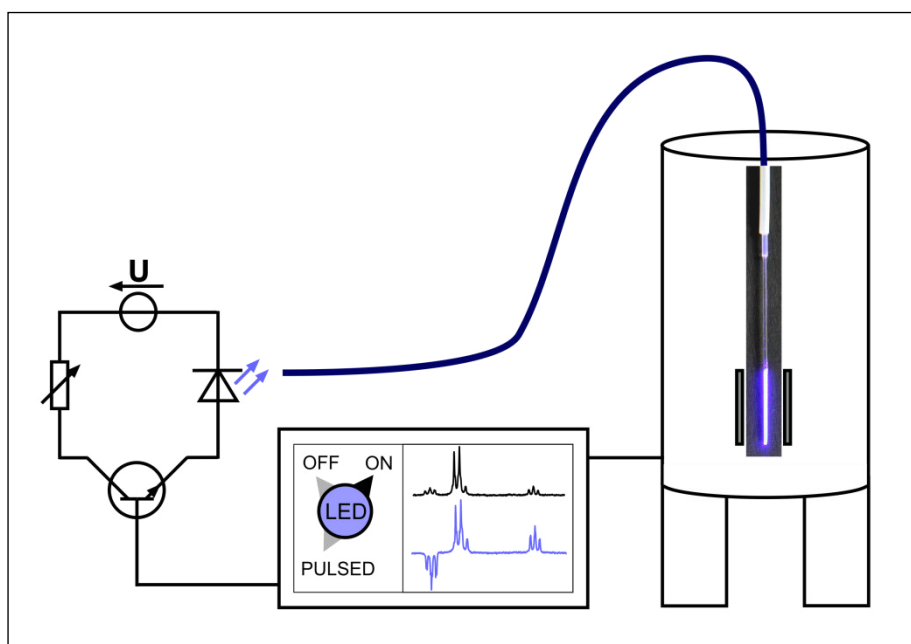
- [42] C. B. Martin, M.-L. Tsao, C. M. Hadad, M. S. Platz, *J. Am. Chem. Soc.* **2002**, *124*, 7226–7234.
- [43] K. Huvaere, D. R. Cardoso, P. Homem-de-Mello, S. Westermann, L. H. Skibsted, *J. Phys. Chem. B* **2010**, *114*, 5583–5593.
- [44] C. Lu, G. Bucher, W. Sander, *ChemPhysChem* **2004**, *5*, 47–56.
- [45] E. Silva, A. M. Edwards, D. Pacheco, *J. Nutr. Biochem.* **1999**, *10*, 181–185.
- [46] K. Tatsumi, H. Ichikawa, S. Wada, *J. Contam. Hydrol.* **1992**, *9*, 207–219.
- [47] R. Lechner, B. König, *Synthesis* **2010**, *9*, 1712–1718.
- [48] E. Sikorska, M. Sikorski, R. P. Steer, F. Wilkinson, D. R. Worrall, *J. Chem. Soc., Faraday Trans.* **1998**, *94*, 2347–2353.
- [49] E. Sikorska, I. Khmelinskii, A. Komasa, J. Koput, L. F. V Ferreira, J. R. Herance, J. L. Bourdelande, S. L. Williams, D. R. Worrall, M. Insińska-Rak, et al., *Chem. Phys.* **2005**, *314*, 239–247.
- [50] J. Dad'ová, E. Svobodová, M. Sikorski, B. König, R. Cibulka, *ChemCatChem* **2012**, *4*, 620–623.
- [51] J. N. Chaon, G. R. Jamieson, R. S. Sinclair, *Chem. Phys. Lipids* **1987**, *43*, 81–99.
- [52] U. Megerle, R. Lechner, B. König, E. Riedle, *Photochem. Photobiol. Sci.* **2010**, *9*, 1400–1406.
- [53] N. A. McDonald, C. Subramani, S. T. Caldwell, N. Y. Zainalabdeen, G. Cooke, V. M. Rotello, *Tetrahedron Lett.* **2011**, *52*, 2107–2110.
- [54] S. T. Caldwell, G. Cooke, S. G. Hewage, S. Mabruk, G. Rabani, V. Rotello, B. O. Smith, C. Subramani, P. Woisel, *Chem. Commun.* **2008**, 4126–4128.
- [55] S.-Y. Ju, F. Papadimitrakopoulos, *J. Am. Chem. Soc.* **2007**, *130*, 655–664.
- [56] S. M. Butterfield, C. M. Goodman, V. M. Rotello, M. L. Waters, *Angew. Chemie Int. Ed.* **2004**, *116*, 742–745.
- [57] M. Gray, A. J. Goodman, J. B. Carroll, K. Bardon, M. Markey, G. Cooke, V. M. Rotello, *Org. Lett.* **2004**, *6*, 385–388.
- [58] J. D. Pellett, D. F. Becker, A. K. Saenger, J. A. Fuchs, M. T. Stankovich, *Biochemistry* **2001**, *40*, 7720–7728.
- [59] A. Niemz, V. M. Rotello, *Acc. Chem. Res.* **1998**, *32*, 44–52.
- [60] H. A. Staab, J. Kanellakopoulos, P. Kirsch, C. Krieger, *Liebigs Ann.* **1995**, *1995*, 1827–1836.

- [61] E. C. Breinlinger, C. J. Keenan, V. M. Rotello, *J. Am. Chem. Soc.* **1998**, *120*, 8606–8609.
- [62] F. Collard, R. L. Fagan, J. Zhang, I. Nemet, B. A. Palfey, V. M. Monnier, *Biochemistry* **2011**, *50*, 7977–7986.
- [63] C. Estarellas, A. Frontera, D. Quiñonero, P. M. Deyà, *Chem. – An Asian J.* **2011**, *6*, 2316–2318.
- [64] R. Drabent, H. Grajek, *Biochim. Biophys. Acta - Gen. Subj.* **1983**, *758*, 98–103.
- [65] F. Yoneda, K. Shinozuka, K. Tsukuda, A. Koshiro, *J. Heterocycl. Chem.* **1979**, *16*, 1365–1367.
- [66] M. Insińska-Rak, E. Sikorska, J. L. Bourdelande, I. V Khmelinskii, W. Prukala, K. Dobek, J. Karolczak, I. F. Machado, L. F. V Ferreira, E. Dulewicz, et al., *J. Photochem. Photobiol. A Chem.* **2007**, *186*, 14–23.
- [67] M. Á. Farrán, R. M. Claramunt, C. López, E. Pinilla, M. R. Torres, J. Elguero, *Ark. (Gainesville, FL, U.S.)* **2007**, *4*, 20–38.
- [68] M. Insinska-Rak, E. Sikorska, J. R. Herance, J. L. Bourdelande, I. V Khmelinskii, M. Kubicki, W. Prukala, I. F. Machado, A. Komasa, L. F. V Ferreira, et al., *Photochem. Photobiol. Sci.* **2005**, *4*, 463–468.
- [69] M. Ebitani, Y. In, T. Ishida, K. -i. Sakaguchi, J. L. Flippen-Anderson, I. L. Karle, *Acta Crystallogr. Sect. B* **1993**, *49*, 136–144.
- [70] M. Wang, C. J. Fritchie Jnr, *Acta Crystallogr. Sect. B* **1973**, *29*, 2040–2045.
- [71] M. von Glehn, R. Norrestam, *Acta Chem. Scand. 1947 - 1999* **1972**, *26*, 1490–1502.
- [72] S. Shinkai, S. Kawanabe, A. Kawase, T. Yamaguchi, O. Manabe, S. Harada, H. Nakamura, N. Kasai, *Bull. Chem. Soc. Jpn.* **1988**, *61*, 2095–2102.
- [73] A. Macchioni, G. Ciancaleoni, C. Zuccaccia, D. Zuccaccia, *Chem. Soc. Rev.* **2008**, *37*, 479–489.
- [74] P. R. Schreiner, L. V Chernish, P. A. Gunchenko, E. Y. Tikhonchuk, H. Hausmann, M. Serafin, S. Schlecht, J. E. P. Dahl, R. M. K. Carlson, A. A. Fokin, *Nature* **2011**, *477*, 308–311.
- [75] C. A. Hunter, *Angew. Chemie Int. Ed.* **2004**, *43*, 5310–5324.
- [76] C. A. Hunter, *Angew. Chemie* **2004**, *116*, 5424–5439.
- [77] E. Sikorska, I. V Khmelinskii, W. Prukala, S. L. Williams, M. Patel, D. R. Worrall, J. L. Bourdelande, J. Koput, M. Sikorski, *J. Phys. Chem. A* **2004**, *108*, 1501–1508.
- [78] E. Sikorska, I. V Khmelinskii, J. Koput, J. L. Bourdelande, M. Sikorski, *J. Mol. Struct.* **2004**, *697*, 137–141.

- [79] B. König, M. Pelka, H. Zieg, T. Ritter, H. Bouas-Laurent, R. Bonneau, J.-P. Desvergne, *J. Am. Chem. Soc.* **1999**, *121*, 1681–1687.
- [80] D. Rehm, A. Weller, *Berichte der Bunsen-Gesellschaft* **1969**, *73*.
- [81] F. Scandola, V. Balzani, G. B. Schuster, *J. Am. Chem. Soc.* **1981**, *103*, 2519–2523.
- [82] P. R. Ogilby, C. S. Foote, *J. Am. Chem. Soc.* **1983**, *105*, 3423–3430.
- [83] R. S. Davidson, J. E. Pratt, *Photochem. Photobiol.* **1984**, *40*, 23–28.
- [84] R. L. Jensen, J. Arnbjerg, P. R. Ogilby, *J. Am. Chem. Soc.* **2010**, *132*, 8098–8105.
- [85] D. D. Perrin, W. L. F. Armarego, *Purification of Laboratory Chemicals, 4th Ed.*, Elsevier Science Ltd., Oxford, **1996**.
- [86] D. B. McCormick, *J. Heterocycl. Chem.* **1970**, *7*, 447–450.
- [87] M. Mansurova, M. S. Koay, W. Gärtner, *European J. Org. Chem.* **2008**, *2008*, 5401–5406.
- [88] J. M. Wilson, G. Henderson, F. Black, A. Sutherland, R. L. Ludwig, K. H. Vousden, D. J. Robins, *Bioorg. Med. Chem.* **2007**, *15*, 77–86.
- [89] B. Priewisch, K. Rück-Braun, *J. Org. Chem.* **2005**, *70*, 2350–2352.
- [90] L. Palatinus, G. Chapuis, *J. Appl. Crystallogr.* **2007**, *40*, 786–790.
- [91] C. F. Macrae, P. R. Edgington, P. McCabe, E. Pidcock, G. P. Shields, R. Taylor, M. Towler, J. van de Streek, *J. Appl. Crystallogr.* **2006**, *39*, 453–457.
- [92] A. Jerschow, N. Müller, *J. Magn. Reson.* **1997**, *125*, 372–375.
- [93] H. C. Chen, S. H. Chen, *J. Phys. Chem.* **1984**, *88*, 5118–5121.
- [94] Y. H. Zhao, M. H. Abraham, A. M. Zissimos, *J. Org. Chem.* **2003**, *68*, 7368–7373.
- [95] K. Schober, E. Hartmann, H. Zhang, R. M. Gschwind, *Angew. Chemie* **2010**, *122*, 2855–2859.
- [96] K. Schober, E. Hartmann, H. Zhang, R. M. Gschwind, *Angew. Chemie Int. Ed.* **2010**, *49*, 2794–2797.
- [97] S. L. Murov, I. Carmichael, G. L. Hug, *Handbook of Photochemistry, 2nd Edition*, CRC Press, New York, **1993**.
- [98] Origin 6.1. Origin Lab Corporation, Northampton, **2000**.
- [99] J. Dađová, S. Kümmel, C. Feldmeier, J. Cibulková, R. Pažout, J. Maixner, R. M. Gschwind, B. König, R. Cibulka, *Chem. – A Eur. J.* **2013**, *19*, 1066–1075.

- [100] C. Reichardt, T. Welton, *Solvents and Solvent Effects in Organic Chemistry*, Wiley-VCH Verlag, **2010**.
- [101] K. Hirose, *J. Incl. Phenom. Macrocycl. Chem.* **2001**, *39*, 193–209 LA – English.
- [102] M. P. Williamson, *Prog. Nucl. Magn. Reson. Spectrosc.* **2013**, *73*, 1–16.
- [103] N. Kachel, K. S. Erdmann, W. Kremer, P. Wolff, W. Gronwald, R. Heumann, H. R. Kalbitzer, *J. Mol. Biol.* **2003**, *334*, 143–155.
- [104] R. S. Macomber, *J. Chem. Educ.* **1992**, *69*, 375.
- [105] H. J. Schneider, R. Kramer, S. Simova, U. Schneider, *J. Am. Chem. Soc.*, **1988**, *110*, 6442–6448.
- [106] K. A. Connors, *Binding Constants: The Measurement of Molecular Complex Stability*, Wiley-Interscience, **1987**.
- [107] D. Zuccaccia, A. Macchioni, *Organometallics* **2005**, *24*, 3476–3486.
- [108] H. Zhang, R. M. Gschwind, *Angew. Chemie Int. Ed.* **2006**, *45*, 6391–6394.

3 LED based NMR Illumination Device for Mechanistic Studies on Photochemical Reactions - Versatile and Simple, yet Surprisingly Powerful



The setup was developed in close collaboration with Hanna Bartling. She did the preparation of the fiber tip and the measurements concerning the fiber tip (Figure 3-3).

C. Feldmeier, H. Bartling, E. Riedle, R. M. Gschwind, *J. Magn. Reson.* **2013**, 232, 39–44.

Reproduced with permission of Elsevier

3.1 Abstract

An LED based illumination device for mechanistic studies on photochemical reactions by means of NMR spectroscopy is presented. The LEDs are directly switched by the NMR spectrometer with the help of a one-stage electronic circuit. This allows for continuous or alternatively pulsed operation of the LEDs. Continuous operation provides direct comparability with conditions in synthetic chemistry, in pulsed operation the short time light power can be enhanced nine-fold. The LEDs are efficiently coupled to a 1000 μm core optical fiber guiding the light into the spectrometer by simply bringing it in close contact to the fiber. The tip of the fiber is roughened by sandblasting and thus emits light in a uniform and efficient way over the full length of the receiver coil. The combination of these techniques tremendously increases the amount of light brought into the NMR sample and makes LEDs an easy, versatile and handy light source for the *in situ* illumination of NMR samples allowing even for single millisecond time resolved Photo-CIDNP spectroscopy.

3.2 Introduction

A detailed understanding of the mechanisms of chemical reactions is essential for their application and further development. In classical catalytic reactions such as applied in organocatalysis and transition metal catalysis, NMR has proven to be a very powerful tool for revealing diamagnetic intermediate species and for mechanistic investigations. For example, recently the elusive enamine intermediates,^[1] the Breslow intermediate,^[2] the key intermediate in enantioselective palladium catalyzed allylic substitution^[3] or Brønsted acid catalysis intermediates^[4] were detected and characterized by means of NMR. However, to apply the whole variety of NMR methods to photochemical reactions it is essential to be able to run the reaction inside the spectrometer, which implies that the NMR sample has to be illuminated inside the spectrometer. This not only allows the *in situ* detection of diamagnetic intermediates in photoreactions but also the analysis of the kinetics and reaction mechanisms. *In situ* illumination of NMR samples is applied in various different fields such as organometallic photochemistry^[5] or monitoring the kinetics of protein folding.^[6,7]

In addition to the standard NMR spectroscopic approaches feasible for reactions in the dark, there is a special hyperpolarization technique applicable exclusively to photoreactions, the Photo-CIDNP spectroscopy.^[8-10] Caused by the influence of the nuclear spin state on the intersystem crossing in radical pairs the Photo-CIDNP effect results in anomalous NMR signal intensities. The power of the CIDNP effect is that even extremely short-lived precursor radicals, not detectable in ESR, leave traces in the signal intensity pattern of their diamagnetic products detectable by NMR.^[11,12] In this way not only standard NMR techniques can be used for mechanistic studies on photocatalytic systems but even paramagnetic radical intermediates can be detected and characterized by means of NMR. However, both the application of well-established NMR techniques to photochemical reactions and the Photo-CIDNP spectroscopy require the illumination of the samples inside the spectrometer.

Various approaches have been reported to illuminate the sample inside the spectrometer and to guide the light into the sample using lasers or various lamps as light sources.^[5,13] The illumination of the sample from the side or from below by selected types of light guides is an approach compatible with both continuous wave light sources and intense pulsed lasers, but requires modifications of the NMR probe and hampers uniform illumination of the NMR sample. By using an optical fiber to guide the light into the spectrometer the sample can be illuminated from the inside by placing the tip of the optical fiber into a coaxial insert.^[14] Illumination uniformity is improved by replacing the

coaxial insert by a coneshaped insert^[6,7] or by tapering the optical fiber stepwise^[13] making the tip of the fiber emit light over the whole range of the receiver coil, instead of just from above. A shutter placed in the optical path and synchronized with the NMR spectrometer controls the illumination of the sample and allows the implementation of well-defined light pulses in NMR pulse sequences.^[14,15]

LEDs provide an extraordinarily inexpensive, energy saving and easy to handle light source available in a huge diversity of wavelengths in the infrared, visible and ultraviolet range. Among other reasons LEDs have therefore become the light source of choice in the recently rapidly expanding area of photocatalysis^[16-20]. Despite these indisputable advantages LEDs have so far not been used as light sources for systematic illumination of NMR samples to the best of our knowledge.

Here we present a notably versatile, easy and inexpensive setup for the illumination of NMR samples using LEDs as light source. To achieve maximal and uniform illumination of the sample (i) the LEDs are switched directly by the spectrometer, (ii) they are brought in direct contact with the optical fiber and (iii) the tip of the optical fiber inserted in the sample is roughened by sandblasting. This setup allows both, the investigation of photocatalytic reactions under synthetic conditions and by pulsed operation of the LEDs even millisecond time resolved Photo-CIDNP spectroscopy.

3.3 Materials and Methods

3.3.1 Circuit – Light Source

As light source different LEDs are used for the described setup. The high power LEDs are controlled by an electronic circuit, shown schematically in Figure 3-1 A. It consists of a power supply, the LED, a potentiometer to regulate the current through the LEDs and a transistor switched by a TTL signal from the time control unit of the spectrometer. With this circuit the LED can be switched on and off directly by the spectrometer. The potentiometer controls the current through the LEDs and so they can be operated as (i) continuous wave (cw) devices (at specified maximum cw operation currents or below) or (ii) in a pulsed manner at much higher currents. By pulsing the LEDs significantly higher short time powers for the duration of a short pulse in a low duty cycle can be achieved. The currents applied to the LEDs are usually limited by the heat the LEDs produce. However, if heating is minimized by a combination of short light pulses, proper heat dissipation methods realized by an aluminum heat sink, and low duty cycles currents higher by as much as a factor of 9 than those recommended for continuous operation can be used and significantly higher peak output light powers can be achieved. This technique is used in various different fields such as imaging flow velocimetry,^[21] high speed photography^[22] or laser-flash-photolysis.^[23]

Additionally, an opto-isolator is placed between the time control unit of the spectrometer and the LED circuit in order to isolate the two units galvanically and thus to protect the spectrometer time control unit from high and rapidly changing currents from the LED circuit.

In the described way the LED light can be controlled by a spare spectrometer time control unit output. However, to implement defined light pulses into pulse sequences for time resolved CIDNP-spectroscopy^[12] it is important to know how fast the LEDs respond with respect to the TTL signal from the spectrometer. Additionally to the intrinsic response time of the LEDs the circuit with the opto-isolator causes a delay between the TTL output signal of the spectrometer and the LED light. To determine the total delay between the TTL pulse and the response of the LED light a photo resistor was used. The total delay was determined by simultaneously measuring the voltage at the TTL signal input and the voltage across a photo resistor illuminated by the LED at the time when the LED was switched on and off, Figure 3-1 B. Graph B shows the LED response (LED output) for a 10 ms pulse of the spectrometer output on the millisecond time scale. Graph C reveals on the microsecond timescale that the response time of the LED in this

setup is about 3–8 μs . For millisecond time resolved experiments this delay is insignificant. However, for time resolved experiments on smaller time scales it has to be considered when the pulse sequences are implemented. The exponentially increasing light output in the first few μs is most likely due to heating of the LED that increases the efficiency. If this variation in illumination power is of concern, it can readily be compensated with an improved current control circuit that applies a slightly higher voltage and current initially and then decreases it over the next few μs .

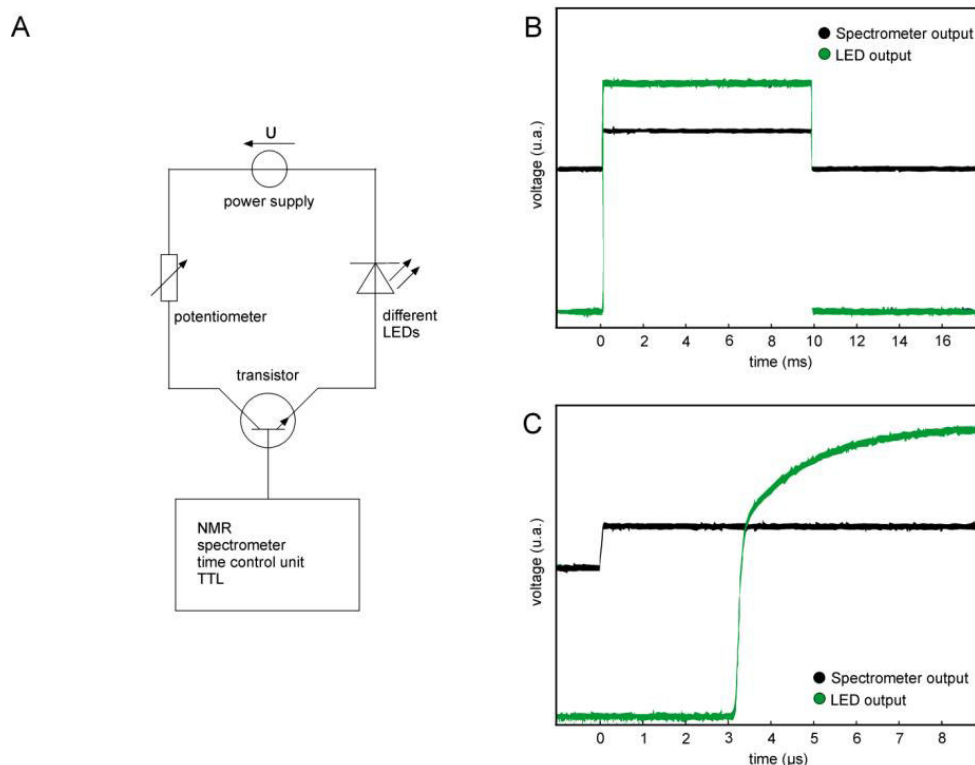


Figure 3-1 (A) Scheme of the circuit used to control and to pulse the LEDs, consisting of a power supply, a potentiometer to adjust the current through the LED and a transistor controlled by the spectrometer. Graph (B) shows the response of the LED to a 10 ms pulse from the spectrometer output on a millisecond time scale and graph (C) reveals at microsecond time resolution that the response time of the LED in this setup is about 3–8 μs .

3.3.2 Light Source – Optical Fiber

The light from the high power LEDs is guided into the sample by 14 m of a BFH optical fiber with 1000 μm diameter purchased from Thorlabs. Due to the direct switching of the LED by the spectrometer, a shutter in the light path as it is often described in the literature^[11,12,14] can be omitted. As a result it is possible to bring the LED in direct contact with the end of the optical fiber, enabling much higher light intensities by avoiding loss due to the strongly diverging LED output or due to additional optics. The light emitting area of the LED is about the same size as the cross section of the optical fiber core. The silicone lens of the LED is cut off and so the optically active part of the LED is brought in

even closer contact with the end of the fiber guaranteeing optimal coupling of the LED to the fiber. As LEDs we found the following models well suited for our applications, but others are likely equally suitable: Cree XP-E, Nichia SMD, LUXEON Rebel LXML, LUXEON K2 LXX2.

3.3.3 Optical Fiber – Sample

The light guided by the optical fiber from the LEDs into the spectrometer has to illuminate the NMR sample in a way that the whole sample inside the measurement coils is illuminated efficiently and uniformly.

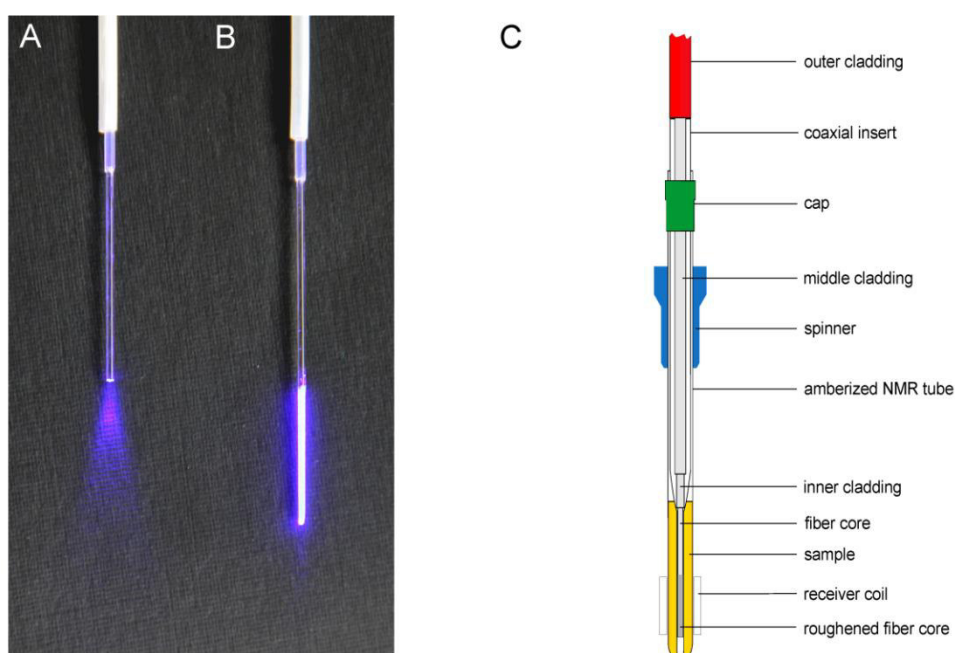


Figure 3-2 (A) Picture of an untreated fiber tip emitting light from just its tip in a cone-shaped manner. (B) Picture of the roughened fiber tip emitting light uniformly over the whole roughened range. (C) Scheme of the optical fiber inserted in a coaxial inlet inside the NMR tube. To guarantee uniform illumination along the z-axis the tip of the fiber is roughened over the whole range of the receiver coil.

For this the claddings of the optical fiber tip were stripped off, the main part of the fiber was masked and the 21 mm at the tip of the fiber were sandblasted to roughen its surface and thus make it emit light over this whole range instead of just from its tip. Siliconcarbide 180 was used as the abrasive mineral. Figure 3-2 A and B shows the light emission of the untreated fiber compared to the light emission of the roughened fiber. Whereas the untreated fiber emits light in a cone-shaped manner just from its tip, the roughened fiber emits light over the whole roughened area. Roughening the optical fiber is a remarkable easy, fast and hazard-free method to treat the tip of the optical fiber compared to other reported techniques as the etching with hydrofluoric acid.^[13]

Optimal and uniform illumination of the NMR sample in the measuring coils of the spectrometer is ensured by aligning the light emitting area of the fiber to the coils, schematically shown in Figure 3-2 C. For this the optical fiber is inserted in a standard Rototec-Spintec stem coaxial insert which is retained in a Rototec-Spintec 5 mm NMR-Tube 7 in. 535-PP-7 similar as in the setup presented by Scheffler *et al.*^[14] The coaxial insert centers the optical fiber in the NMR tube and the shim coils. Moreover the insert prevents direct contact of the fiber with the sample and thus makes it very easy to handle.

3.3.4 Sample Preparation – Measurement

With the described setup all photochemical reactions tested so far can be followed by NMR spectroscopy. In addition, with this setup the identical light sources can be used for synthetic applications and NMR investigations allowing for direct comparisons. No deviations in the products, reactivities, yields or trends found by the synthetically working chemists were found in the reactions tested so far, like in the flavin catalyzed photo oxidations,^[24–26] the arylation of heteroarenes with diazonium salts,^[27] the photocatalytic coupling of N-arylamines with nucleophiles^[28,29] or in spiropyran photochromism.^[30]

The most demanding test for the scope and limitations of LEDs used for the illumination of NMR samples and connected mechanistic studies are Photo-CIDNP and especially time resolved Photo-CIDNP experiments, because there, short light pulses of high intensities are required.^[11] The intensity of the CIDNP signals is directly proportional to the photochemical turnover.^[12] Therefore the intensity of a Photo-CIDNP signal is used as a direct measure for the amount of light brought into the NMR sample and to test the effect of the three innovations.

As a test reaction the flavin catalyzed photo oxidation of benzyl alcohols to the corresponding aldehydes was used.^[24–26,31] The reduced flavin is reoxidized by oxygen. Flavins in general are a common model system for CIDNP studies, because flavin radicals have suitable magnetic properties and are prone to show CIDNP signals. For this reason flavins are often employed as photosensitizers for CIDNP-studies on proteins.^[11,32]

For the measurements 2 mM riboflavin tetraacetate (RFT) and 20 mM methoxybenzyl alcohol (MBA) were dissolved in CD₃CN and the sample was purged with argon for 1 h. NMR spectra were recorded on a Bruker Avance 600 spectrometer with a 5 mm broadband triple resonance z-gradient probe. The temperature of 300 K was controlled by a Bruker BVTE 3000 unit. As a light source a Cree XP-E high power LED with a

center wavelength of 455 nm and 500 mW optical output power was used, according to the absorption maximum of RFT.^[26] To determine the current through the LED the voltage on a resistance in series with the LED was measured. As a measure for the light intensity in the sample the Photo-CIDNP signal intensity of the aromatic proton of RFT at 7.89 ppm was chosen (Figure 3-3 A) because this proton shows a well baseline separated and emissive Photo-CIDNP signal. The CIDNP spectra were taken as the difference spectra between the ¹H spectra of the illuminated sample and the dark sample.

3.4 Results and Discussion

In the following the three innovations for the *in situ* illumination of NMR samples are tested. This was done by measuring the Photo-CIDNP polarization of the flavin aromatic proton with altered setups. First, the new easy and efficient way to roughen the fiber tip and thus to improve illumination uniformity over the whole sample is tested. Second, the effective coupling of the LED with the optical fiber possible through the direct switching of the LED by the spectrometer was investigated. Third, the pulsed operation of the LEDs to achieve higher short time powers was tested.

The effect of the roughened fiber tip was tested by measuring the Photo-CIDNP polarization of the flavin aromatic proton. For that the light ^1H spectra were measured with a 30° rf pulse and 16 scans, while illuminating the sample with a constant LED current of 1 A and with the LED directly coupled to the optical fiber. Alternating dark ^1H spectra with a 30° rf pulse and 16 scans were measured and subtracted from the illuminated spectra to yield the Photo-CIDNP spectra.

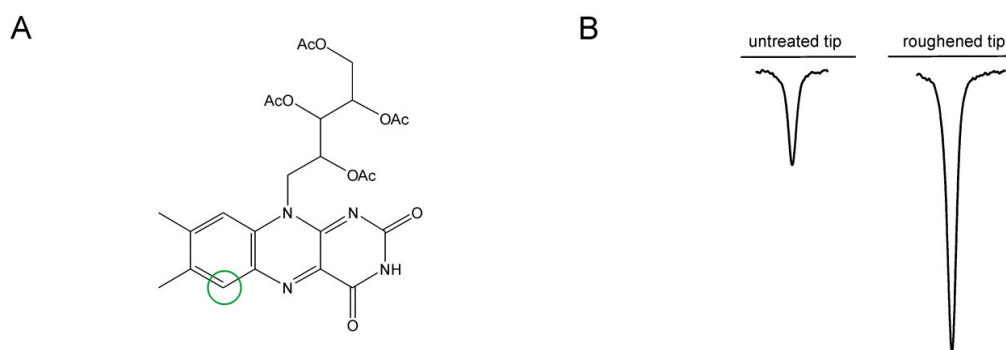


Figure 3-3 (A) Structure of riboflavin tetraacetate (RFT). The emissive Photo-CIDNP signal of the encircled aromatic proton appearing at a chemical shift of 7.89 ppm was observed for the Photo-CIDNP experiments. (B) ^1H Photo-CIDNP intensities of the aromatic RFT proton for the concentration of 2 mM RFT and 20 mM MBA in acetonitrile, measured with the untreated tip (left) and the roughened tip of the optical fiber (right).

The ^1H spectra with maximum CIDNP-intensity are shown in Figure 3-3 B. With the setup the difference in the CIDNP intensities between the two tips of the optical fiber is pleasantly large. Using the roughened fiber instead of the untreated one the maximal CIDNP polarization was increased by a factor of about 3. These results are due to the improved uniform illumination by the roughened tip. The untreated fiber emits light in a cone shaped manner just from its tip, whereas the roughened fiber emits light over the whole roughened range (see Figure 3-2 A and B).

So as a first achievement, roughening the optical fiber by sand blasting is a remarkable easy, fast and hazard-free method to treat the tip and make it emit light over the whole area of the receiver coil in a very efficient and uniform manner.

Next the effect of an optimized coupling of the glass fiber with the LEDs was tested. For that purpose (A) a setup leaving 0.5 cm space for a shutter, (B) a setup with direct attachment of the glass fiber to the LED and (C) a setup with direct attachment of the LED with a cut off silicone lens to the optical fiber were compared, see Figure 3-4. For that the Photo-CIDNP polarization of the aromatic proton of RFT are used as the difference spectra of illuminated and dark ^1H spectra with a 30° rf pulse and 16 scans each and illumination during the whole measurement. The reduction of the distance between diode and the end of the fiber core leads to a huge increase in light power and thus CIDNP polarization. The setup without the need of a shutter in the light path increases the signal intensity by a factor of about 20 (Figure 3-4 B). Further reduction of the distance between diode and fiber core by cutting off the LED silicone lens leads to a further increase in light intensity and CIDNP polarization (Figure 3-4 C). In total the signal intensity is increased by a factor of about 30 compared to the setup with space for a shutter. The output power of the optical fiber coupled in the described way was measured to be about 50 mW.

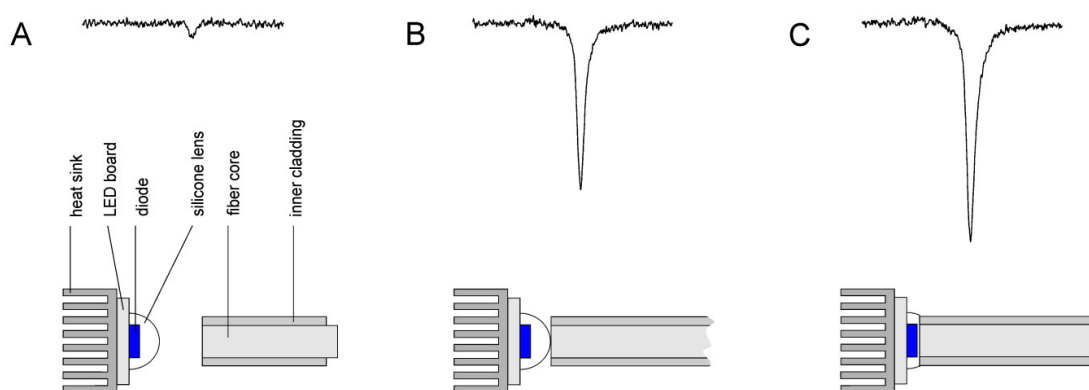


Figure 3-4 (A) Setup with 0.5 cm space for a shutter between the optical fiber and the LED and the corresponding Photo-CIDNP signal of the aromatic proton of RFT. (B) Setup with the LED in direct contact with the optical fiber and the effect on the Photo-CIDNP signal. (C) Setup with the silicone lens of the LED cut off and direct contact to the optical fiber and the effect on the Photo-CIDNP signal.

The described setup provides an extraordinarily easy and efficient way to couple the LEDs to the optical fiber without the need of specially designed and cumbersome optics.

Finally the gain in CIDNP-intensity and thus in light intensity by the pulsed operation of the LEDs was investigated. For this purpose the sample was illuminated by a short light pulse of only 1 ms length after a relaxation delay D1 of 120 s. The relaxation delay ensures the complete relaxation of all polarization and a sufficiently low duty cycle of the LED. The light pulse was directly followed by a 30° rf pulse on the proton channel and acquisition. Then the same pulse sequence was applied without the light pulse to record the dark spectrum which was then subtracted from the light spectrum to yield the Photo-CIDNP spectrum. Both the light and the dark spectrum were recorded with one single

scan only. In this way five different Photo-CIDNP spectra were acquired with rising currents through the LED. Starting with the manufacturer recommended maximum current of 1 A the current was raised in steps of 2 A up to 9 A. Figure 3-5 shows the Photo-CIDNP intensity in dependence on the current through the LED. At a current of 1 A no Photo-CIDNP signal is detectable for the aromatic proton of RFT. A detectable signal with low signal to noise ratio appears at 3 A. Further increase of the current strongly enhances the Photo-CIDNP signal. Figure 3-5 B reveals that the increase of the Photo-CIDNP signal is proportional to the LED current which results in an increase of the signal by a factor of about 9 for the presented measurements. The LED used for the tests broke down at currents higher than 9 A. With shorter light pulses, with other LEDs or with additional cooling of the LEDs a further increase of the light intensities and thus the Photo-CIDNP signals can be expected. This shows that the pulsed operation of the LEDs enables light intensities much higher than at standard operation. Through these high light intensities Photo-CIDNP signals can be enhanced tremendously and otherwise not detectable signals become detectable even at the millisecond time scale. This paves the way to millisecond time resolved Photo-CIDNP spectroscopy even with this comparatively simple setup.

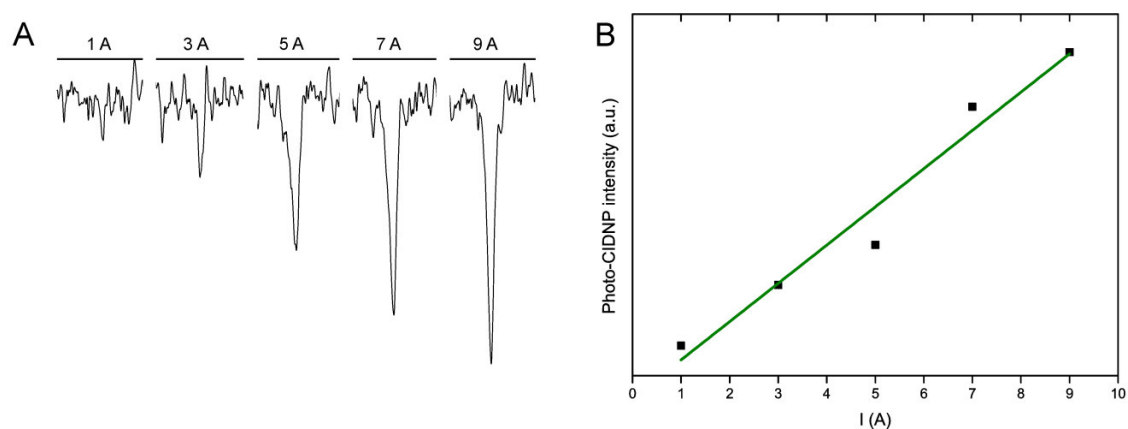


Figure 3-5 (A) The Photo-CIDNP signal of the RFT aromatic proton for light pulses of 1 ms length and for LED currents of 1 A (maximum current for continuous operation) up to 9 A. (B) The Photo-CIDNP intensity shows a linear dependency on the current through the LED.

3.5 Conclusion

Despite the clear benefits of LEDs compared to other light sources, such as easy handling, low cost, availability in a huge variety of wavelengths and direct comparability with conditions in synthetic chemistry LEDs have not been used as light sources for the systematic illumination of a NMR sample yet. Here an innovative LED based device for the *in situ* illumination of NMR samples is presented. The combination of an efficient coupling of the LEDs to the optical fiber, a specially prepared fiber tip and the high power

pulsed operation of the LEDs allows for tremendous increases in the amount of light brought into the NMR sample. The LEDs are directly switched by the NMR spectrometer. This allows for continuous LED operation at standard currents and for pulsed LED operation at much higher currents. By using the LEDs in continuous operation the whole variety of NMR methods can be applied directly to photochemical reactions and the use of LEDs provides direct comparability with conditions in synthetic chemistry. Pulsed operation of the LEDs allows for currents and light intensities well above the maximal currents of continuous operation. This makes time resolved Photo-CIDNP spectroscopy on a millisecond time scale possible even with this simple setup.

Switching the LED directly by the spectrometer makes a shutter that is commonly used to control the illumination redundant. Therefore the light emitting area of the LED can be brought in direct contact with the end of the optical fiber guiding the light from the LED into the NMR sample. This provides a remarkably easy, versatile and efficient coupling without the need of any further optical components.

To provide uniform and efficient illumination of the whole NMR sample along the measuring coils the tip of the optical fiber inserted in the sample was roughened by sandblasting which is an extraordinarily fast, simple and hazard-free preparation method.

3.6 Additional Experimental Findings

3.6.1 Different Types of LEDs

The presented setup for the *in situ* illumination of NMR samples is based on LEDs. LEDs have the great advantage that they are available in a huge amount of different emission wavelengths from the UV to the infrared and low priced compared to laser systems. When the absorption of the photosensitizer of interest is measured and compared to the emission spectra of the different available LEDs a perfect matching LED for each molecule of interest can be found, this means a LED with emission spectrum with maximal overlap with the absorption of the molecule.

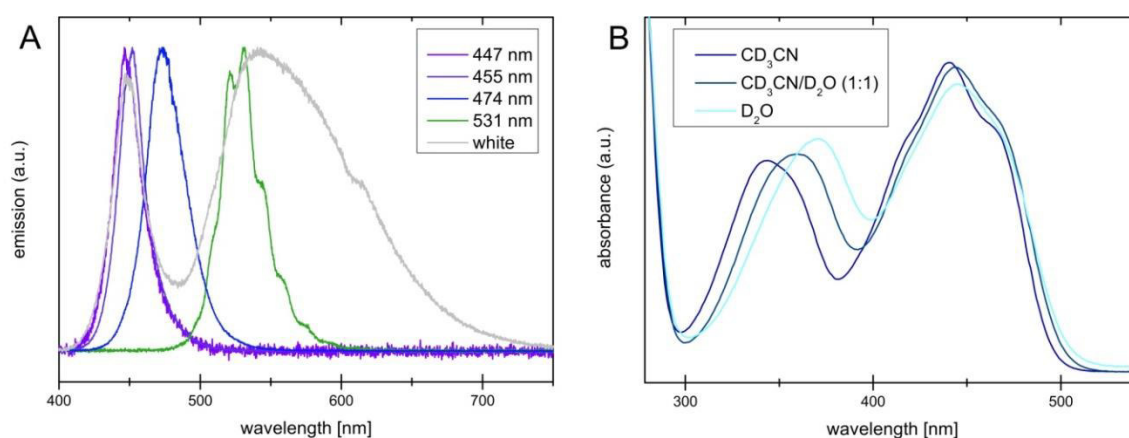


Figure 3-6 A) Emission spectra of the different LEDs tested for the presented setup with the characteristic peak-emission wavelengths B) Normalized absorption spectra of RFT in CD₃CN, CD₃CN/D₂O and D₂O

Figure 3-6 shows the emission spectra of the different LEDs selected for our applications. The LEDs shown are CREE XP-E royal blue with peak-emission wavelength of 455 nm and 500 mW optical output power, LUXEON Rebel LXML PRO1 0425 royal blue with peak-emission wavelength of 452 nm and 425 mW optical output power, CREE XP-E blue with peak-emission wavelength of 474 nm and a luminous flux of 76 lm, LUXEON K2 LXX2-PM14-U00 green with peak-emission wavelength of 531 nm and luminous flux of 130 lm and the white LED Seoul Z-LED P4 white with 240 lm luminous flux. The setup was additionally tested with different LEDs emitting in the UV range among others the Nichia SMD LED UV NCSU033B with central emission peak at 365 nm and optical output power of 325 mW (emission spectrum not shown). The absorption spectra were all recorded at ambient temperature and currents of 700 mA which is beyond the recommended maximal operation current for all LEDs used for the tests. The peak-emission peaks of the LEDs were determined from the emission spectra. Based on the absorption spectra shown in Figure 3-6 B the CREE XP-E royal blue with peak-emission wavelength of 447 nm was chosen for all our studies on the flavin catalyzed photo

oxidation of benzyl alcohols^[24,26,33] as the spectra show very similar maxima and maximal overlap.

3.6.2 LED Performance at Different Light Pulse Lengths

In chapter 3.4 it was demonstrated the gain in light power and Photo-CIDNP intensity can be increased considerably by operating the LEDs at high currents and at short light pulses. This was shown exemplarily for pulse lengths of 1 ms. Longer illumination times cause higher conversion and thus more sorting of the α and β spins and thus higher CIDNP-intensities. However, this is restricted by two factors. The first factor lies within the system itself. The prolonged spin sorting competes with relaxation of the created polarization. The second factor is of pure technical nature. To operate the LEDs at currents exceeding the recommended ones the pulses have to be short and the duty cycles correspondingly low. With longer pulses and currents the LEDs heat up and finally break.

To test the limits of the LED pulsing technique the LEDs were tested for longer pulse lengths by performing the same measurements as described above. The light pulse length was fixed to 1 ms, 10 ms, 100 ms or 1 s and the LED current increased continuously. For each measurement a new CREE XP-E royal blue was used. Figure 3-7 provides the results obtained for light pulses of 1 ms, 10 ms, 100 ms and 1 s length. At the shortest tested light pulse lengths of 1 ms and 10 ms the Photo-CIDNP intensity gradually increases with increasing currents showing an approximately proportional dependency up to a current of 9 A which is a factor of 9 bigger than the recommended one. At 10 A there is a further increase in Photo-CIDNP intensity for a light pulse length of 10 ms whereas for a pulse length of 1 ms the LED breaks and the Photo-CIDNP intensity drops. This is not that surprising keeping in mind that LEDs even being of exactly the same type can show different behavior especially when having different history.^[34] For significantly longer illumination periods the maximal applicable current decreases. For 100 ms light pulses the Photo-CIDNP intensity and thus the LED power reaches a maximum at a current of 7 A before it drops. For pulses of 1 s the maximal current that causes an increase in the Photo-CIDNP intensity is 5 A. As expected the LEDs break at lower currents at prolonged illumination periods. However, the steeper rise at lower currents compensates for the earlier failure of the LEDs and Photo-CIDNP intensities similar to the ones at short pulses and high currents can be achieved. The best operation pulse lengths however are the short ones due to the nonlinear behavior accompanied by the unnecessary stress the LED is exposed to. With additional cooling of the LEDs and shorter pulse lengths and duty cycles it can be expected that the short

time optical output power can be enhanced further considerably. At the same time it seems very likely that the light pulse length can be decreased as far as to enable time resolved Photo-CIDNP spectroscopy well below ms time resolution with the presented setup.

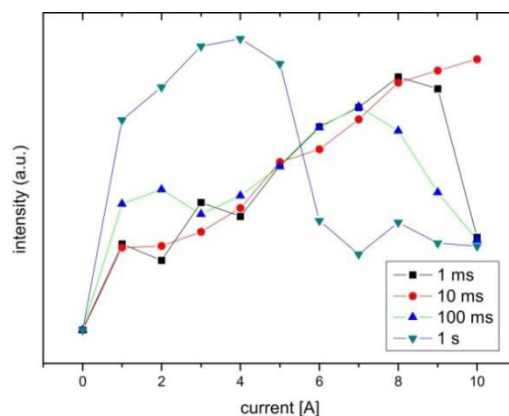


Figure 3-7 Photo-CIDNP intensity of the aromatic proton signal FI(6) of RFT at 7.88 ppm in dependence of the applied current through the LED for light pulse lengths of 1 ms, 10 ms, 100 ms and 1 s.

3.6.3 Photo-CIDNP Pulse Sequences

With the LED-transistor circuit the LEDs can be switched directly by the console of the NMR spectrometer and standard NMR pulse programs can be supplemented by light pulses. ^1H pulse programs were modified for continuous wave (cw) Photo-CIDNP studies as well as for time resolved experiments.

Photo-CIDNP experiments are termed continuous wave experiments if the sample is illuminated during the whole pulse sequence. The light source is switched on before the main pulse sequence is started. After acquisition the light source is switched off again so that the whole experiment is conducted while the sample was illuminated. This is done in a way that the created Photo-CIDNP polarization has reached saturation when the FID is acquired, i.e. the equilibrium of Photo-CIDNP polarization generation and its relaxation is reached.

The subtraction of the respective spectrum recorded in the dark and the spectrum of the illuminated spectrum yields the Photo-CIDNP spectrum. As the CIDNP-polarization is saturated in this method the difference Photo-CIDNP spectrum shows the maximal achievable Photo-CIDNP polarizations that is possible at the given sample conditions and light power. Continuous wave Photo-CIDNP spectroscopy already provides valuable information about the radical intermediates such as the prove for a mechanism involving radical pairs, the nature of the precursor or information about the exit channel multiplicity.^[12,35,36] However, caution must be taken when interpreting the signs and intensities of the Photo-CIDNP signals of continuous wave Photo-CIDNP experiments.

The reason for this is that the direct polarization arising from the Photo-CIDNP effect can relax via nuclear dipole-dipole interactions with nearby nuclei. Magnetization is thus transferred from the directly polarized nuclei to neighboring nuclei which are indirectly polarized.^[11] So the Photo-CIDNP polarization patterns as observed in the cw experiments consist of both the direct Photo-CIDNP polarization and the indirect cross-polarization from nuclear dipole-dipole interactions. In direct analogy to the nuclear Overhauser effect the phase and the extent of cross-polarization depends on the distance between the protons and the molecular motion.^[11,37]

The interpretation of the signs and intensities of the Photo-CIDNP signals can be used to determine the hyperfine coupling constants of the unpaired electrons with the nuclei of the radical and thus to further characterize the radicals involved in the reaction.^[12,38,39]

The intensities and signs of the Photo-CIDNP polarizations are proportional to the spin densities of the unpaired electrons of the radical precursors and thus to their hyperfine coupling constants to the respective nuclei.^[12,39,40] However, in order to separate the direct polarization caused by the Photo-CIDNP spin sorting from the indirect cross-polarization time resolved CIDNP-techniques have to be used. A typical pulse sequence for time resolved studies is depicted in Figure 3-8. An optional pre-saturation pulse program element is followed by a light pulse $h\nu$ of varying length T_L , a delay Δ and a 90° pulse and acquisition of the FID. The same sequence is repeated without the light pulse. The difference between light and dark spectrum yields the Photo-CIDNP spectrum which depends on the length T_L of the light pulse.^[36,41] The optional pre-saturation element can be applied to saturate the whole spectrum prior to Photo-CIDNP polarization generation and remove artefacts caused by heating of the illuminated sample. If the spectrum is presaturated only the Photo-CIDNP polarization without the thermal polarization is detected. In many cases it is first (light) part of the described pulse sequence is sufficient. This prevents the loss of $\sqrt{2}$ in sensitivity arising from difference spectroscopy.^[11]

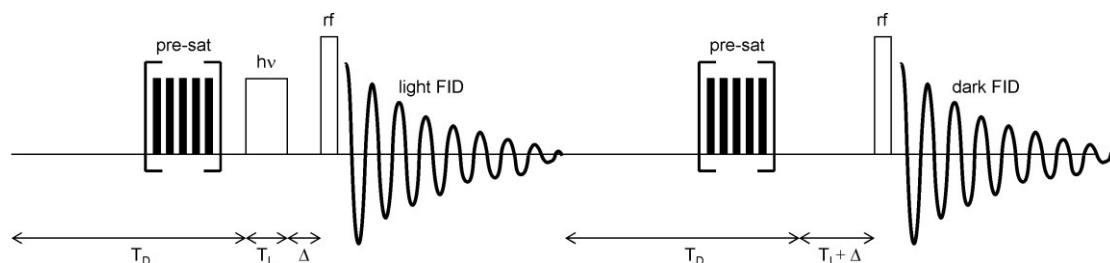


Figure 3-8 Pulse sequence used for the time resolved Photo-CIDNP studies^[12] consisting of an optional pre-saturation element, a light pulse $h\nu$ of length T_L , a delay Δ and a 90° pulse followed by acquisition of the FID. The same sequence is repeated without the light pulse. The difference between light and dark spectrum yields the Photo-CIDNP spectrum.^[36]

3.6.4 Modification of the Pulse Programs

To control the transistor the central time control unit TCU3 of the Bruker console Avance I of the Bruker Avance 600 MHz spectrometer is employed. The TCU3 synchronizes the timing of most operations in the spectrometer. Some of the outputs on the front panel, however, are not in use in standard operation and can thus be used to synchronize internal processes with external devices. In this way external processes can be embedded into pulse sequences and standard NMR pulses can be supplemented by light pulses.

The outputs of the TCU3 are 5V TTL signals and can be accessed directly by the pulse program commands

```
d11 setnmr4^3  
d11 setnmr4|3
```

In this example the first command sets the 3rd bit of NMR word 4 high (inactive), the second command sets the 3rd bit of NMR word 4 low (active). d11 is the delay in which the switching takes place and can be set to a minimum of 50 ns, the time needed of the switching process.^[42]

These commands are also defined in the directive 'avance.incl', that is usually included at the beginning of each pulse program. There they are identified by the commands

```
TTL1_LOW  TTL2_LOW  TTL3_LOW  TTL4_LOW  
TTL1_HIGH TTL2_HIGH TTL3_HIGH TTL4_HIGH
```

These set the bits 28-31 of NMR word 3 high or low, respectively. The advantage of addressing the TCU3 outputs indirectly via the define directive 'avance.incl' is that even if the wiring of the TCU3 is changed all pulse programs will still work by just changing the 'avance.incl' file.^[42]

3.6.5 Photo-CIDNP Build Up and Relaxation

In order to test the application opportunities and limitations of the LED based illumination device, Photo-CIDNP studies with time resolution were conducted. For this the built up and relaxation of the different nuclei were studied with the pulse sequence described in chapter 3.6.3 and depicted in Figure 3-8. The build-up of the Photo-CIDNP signals with increasing illumination time can be monitored by doing measurements with gradually increasing light pulse lengths T_L and setting the delay Δ between the light pulse and rf

pulse to $\Delta=0$ s. In this way the Photo-CIDNP intensities of the RFT proton resonances were measured for the case that 2 mM of RFT was solved in CD_3CN with 20 mM MBA as the substrate.

Figure 3-9 A shows the built up of the Photo-CIDNP polarization of four different proton resonances of RFT for light pulse lengths from 0 s up to 25 s. There is a steep increase in the Photo-CIDNP intensity with rising illumination times up to about 3 s. After about 10 s saturation is reached because the light induced Photo-CIDNP generation counteracts its relaxation and finally leads to equilibrium.

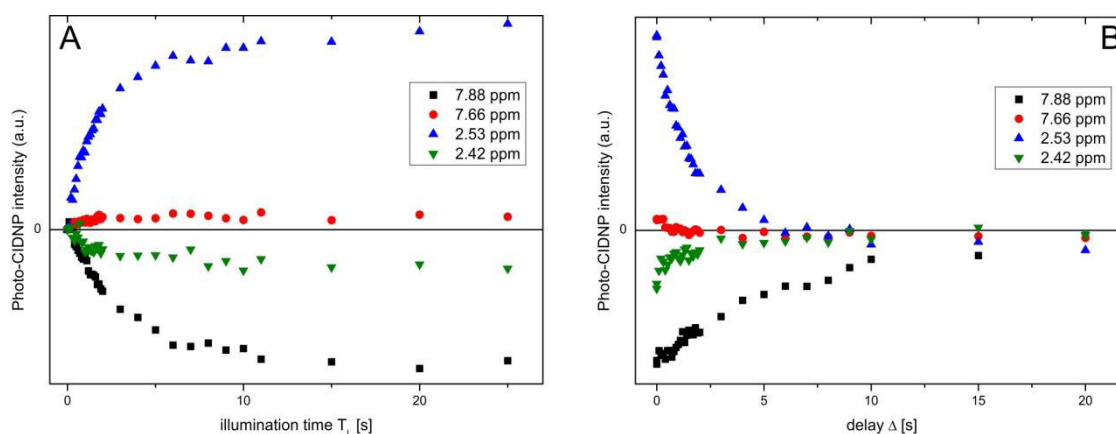


Figure 3-9 The built up (A) and relaxation (B) of the CIDNP polarizations of the flavin resonances of the aromatic protons at 7.88 ppm and 7.66 ppm and the methyl groups at 2.53 ppm and 2.42 ppm.

The relaxation of the spins can directly be observed in Figure 3-9 B where after an illumination period of 10 s when maximal Photo-CIDNP polarization was reached the delay between light pulse and 90° rf pulse was varied starting from 0 s up to 20 s. All the CIDNP-polarization is relaxed after about 10 s. In this way the relaxation time of the different Photo-CIDNP polarizations can be determined which is important to arrange optimal experimental timings. Too short delays cause artifacts arising from residual Photo-CIDNP polarization. Too long delays make the experiments unnecessarily long on the other hand. The same applies to the illumination times when equilibrium is established between generation of Photo-CIDNP polarization and its competing relaxation.

The Photo-CIDNP effect perturbs nuclear spins from its thermal equilibrium and thus increases or reduces the population difference. The following rf pulse generates the NMR signal which is either enhanced or decreased compared from the signal caused solely by the thermal population difference. With increasing delay between the light pulse and the rf pulse the perturbed thermal equilibrium reestablishes and the detected NMR signal intensity gradually draws closer to the thermal equilibrium value. The relaxation of the Photo-CIDNP polarization in dependence of the time after illumination was fitted with

an exponential function known from the spin-lattice relaxation of rf pulse perturbed thermal equilibrium.^[43]

$$M(t) = M_0(1 - e^{-t/T})$$

M_0 is the maximal generated Photo-CIDNP polarization and T the time constant for relaxation of the respective nucleus. The time constants for the relaxation T is determined from the fits of the curves depicted in Figure 3-9 B. The smallest time constant of 0.59 s is found for the aromatic proton with the chemical shift of 7.66 ppm, followed by T=1.13 s for the methyl group at 2.42 ppm and T=1.27 s for the methyl group with the chemical shift of 2.53 ppm. The longest time constant is found for the 7.99 ppm aromatic proton with T=5.34 s. These values were considered for all the Photo-CIDNP experiments to provide optimal experimental setups with maximal possible signal intensities whilst preventing artifacts caused by insufficient relaxation of the system.

3.6.6 Photo-CIDNP Cross Polarization

As the additional polarization created by nuclear spin dependent intersystem crossing can be transferred to nearby nuclei by cross polarization time resolved Photo-CIDNP techniques have to be employed to distinguish the direct Photo-CIDNP polarization from the indirect cross polarization.^[11,43] The new LED based setup was tested with the time resolved Photo-CIDNP pulse sequence described above at the model system of the flavin catalyzed photooxidation of benzyl alcohols. The illumination time was increased from 0 s up to 0.5 s in steps of 10 ms. Figure 3-10 provides the CIDNP intensities of the aromatic protons and the methyl groups in dependence of the illumination time. Both the Photo-CIDNP intensity of the aromatic proton FI(6) with a chemical shift of 7.88 ppm and the methyl protons FI(8 α) at 2.53 ppm increases right from the start with appreciable CIDNP polarizations even at comparatively short illumination periods under 0.2 s. The Photo-CIDNP polarization of the FI(7 α) becomes prominent with longer illumination times as described in the Photo-CIDNP review of Hore *et al.*^[11] The most likely cause for this is that the Photo-CIDNP polarization is generated at the protons FI(6) and FI(8 α) and then transferred to the neighboring proton FI(7 α) via cross polarization. Even though flavin is one of the most widely used photosensitizers for Photo-CIDNP studies of proteins^[11,32,44] there are hardly any studies on the Photo-CIDNP polarizations of flavins themselves. However it is known from theoretical and EPR studies^[11,32,45,46] that the flavin semiquinone radicals show appreciable hyperfine coupling to the aromatic proton FI(6) and the methyl protons at position FI(8 α). This is in agreement with the measurements for the differentiation between direct Photo-CIDNP and indirect cross polarization were

also protons FI(6) and FI(8 α) show direct polarization generated already at comparably short illumination periods.

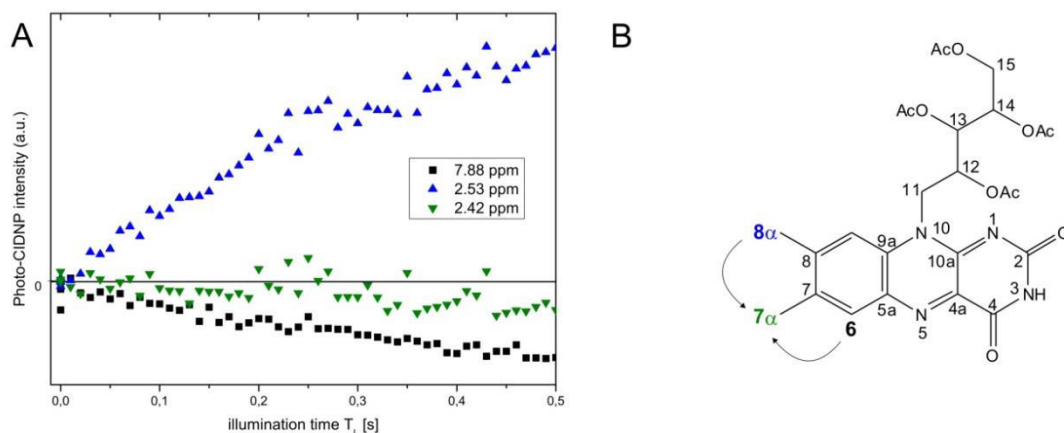


Figure 3-10 A) dependence of the Photo-CIDNP polarization intensities of four different riboflavintetraacetate (RFT) proton resonances on the length of the illumination period. B) Cross polarization pathways in RFT from proton FI(6) and proton FI(8 α) to proton FI(7 α).

3.6.7 Experimental Details

The RFT absorption spectra were measured on a Varian Cary 50 Bio UV/Vis-spectrometer. For the preparation of the RFT solutions in D₂O, CD₃CN/D₂O and CD₃CN UV-quartz cuvettes were used. The emission spectra of the LEDs were recorded with a Hamamatsu Photonic Multi Channel Analyzer C10027.

LED performance tests and the Photo-CIDNP build up and relaxation studies were measured with solutions of 2 mM riboflavin tetraacetate (RFT) and 20 mM methoxybenzyl alcohol (MBA) in CD₃CN. To minimize the Photo-CIDNP relaxation the sample was degassed by purging the solution with argon for 1 hour. NMR spectra were recorded on a Bruker Avance 600 spectrometer with a 5 mm broadband triple resonance z-gradient probe. The temperature of 300 K was controlled by a Bruker BVTE 3000 unit. T_D was chosen to guarantee a sufficient relaxation of the Photo-CIDNP polarization created before and to ensure sufficiently long duty cycles. Alternatingly measurements of ¹H spectra with and without illumination were conducted. The spectra recorded with the light pulse was subtracted from the one recorded without light pulse to yield the Photo-CIDNP spectra. NMR data were processed with Bruker TOPSPIN 3.0. As a light source a Cree XP-E high power LED with a center wavelength of 455 nm and 500 mW optical output power was used, according to the absorption maximum of RFT^[26] (compare Figure 3-6 B). To determine the current through the LED the voltage on a resistance in series to the LED was measured. The Photo-CIDNP build up and relaxation studies were performed at a constant LED current of 2.2 A.

3.6.8 ^1H and ^{13}C Chemical Shift Assignment

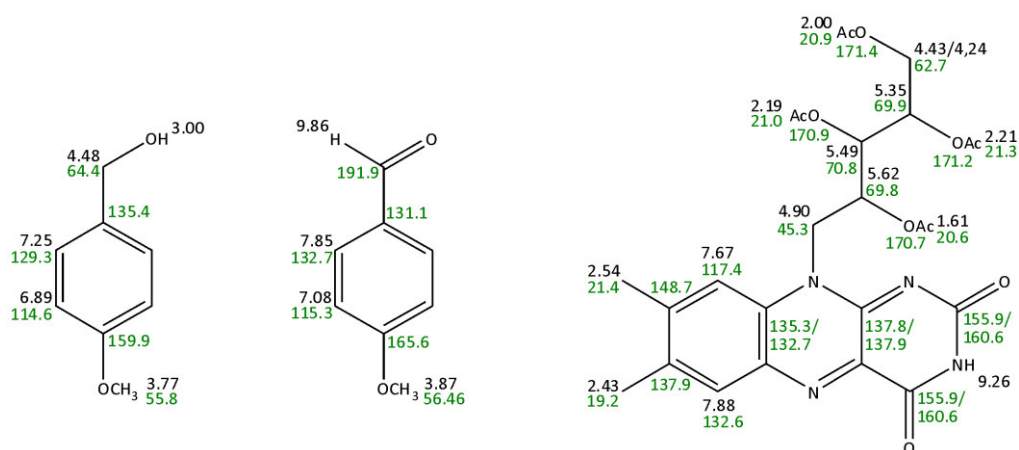


Figure 3-11 Overview of the ^1H (black) and ^{13}C (green) chemical shift assignments of the oxidized riboflavin tetraacetate, methoxybenzyl alcohol and methoxybenzyl aldehyde solved in CD_3CN .

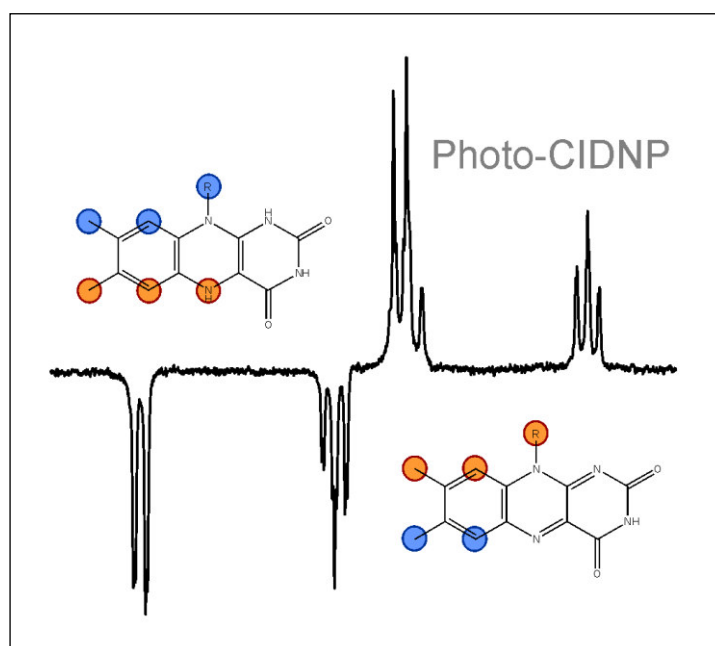
3.7 References

- [1] M. B. Schmid, K. Zeitler, R. M. Gschwind, *Angew. Chemie Int. Ed.* **2010**, *49*, 4997–5003.
- [2] A. Berkessel, S. Elfert, V. R. Yatham, J.-M. Neudörfl, N. E. Schlörer, J. H. Teles, *Angew. Chemie Int. Ed.* **2012**, *51*, 12370–12374.
- [3] B. Böttcher, V. Schmidts, J. A. Raskatov, C. M. Thiele, *Angew. Chemie Int. Ed.* **2010**, *49*, 205–209.
- [4] M. Fleischmann, D. Drettwan, E. Sugiono, M. Rueping, R. M. Gschwind, *Angew. Chemie Int. Ed.* **2011**, *50*, 6364–6369.
- [5] G. E. Ball, in *Spectrosc. Prop. Inorg. Organomet. Compd. Tech. Mater. Appl. Vol. 41*, The Royal Society Of Chemistry, **2010**, pp. 262–287.
- [6] T. Kühn, H. Schwalbe, *J. Am. Chem. Soc.* **2000**, *122*, 6169–6174.
- [7] J. Wirmer, T. Kühn, H. Schwalbe, *Angew. Chemie Int. Ed.* **2001**, *40*, 4248–4251.
- [8] H. R. Ward, R. G. Lawler, *J. Am. Chem. Soc.* **1967**, *89*, 5518–5519.
- [9] J. Bargon, H. Fischer, *Z Naturforsch A.* **1967**, *22*, 1556–1562.
- [10] J. Bargon, H. Fischer, *Z Naturforsch A.* **1967**, *22*, 1551–1555.
- [11] P. J. Hore, *Photo-CIDNP of Biopolymers*, Pergamon Press, Oxford, **1993**.
- [12] M. Goetz, in *Annu. Reports NMR Spectrosc.* (Ed.: A.W. Graham), Academic Press, **2009**, pp. 77–147.
- [13] I. Kuprov, P. J. Hore, *J. Magn. Reson.* **2004**, *171*, 171–175.
- [14] J. E. Scheffler, C. E. Cottrell, L. J. Berliner, *J. Magn. Reson.* **1985**, *63*, 199–201.
- [15] I. Kuprov, M. Goetz, P. A. Abbott, P. J. Hore, *Rev. Sci. Instrum.* **2005**, *76*, 84103.
- [16] J. W. Tucker, Y. Zhang, T. F. Jamison, C. R. J. Stephenson, *Angew. Chemie Int. Ed.* **2012**, *51*, 4144–4147.
- [17] M. Cherevatskaya, M. Neumann, S. Földner, C. Harlander, S. Kümmel, S. Dankesreiter, A. Pfitzner, K. Zeitler, B. König, *Angew. Chemie Int. Ed.* **2012**, *51*, 4062–4066.
- [18] R. Lechner, S. Kümmel, B. König, *Photochem. Photobiol. Sci.* **2010**, *9*, 1367–1377.
- [19] M. Neumann, S. Földner, B. König, K. Zeitler, *Angew. Chemie Int. Ed.* **2011**, *50*, 951–954.

- [20] U. Megerle, R. Lechner, B. König, E. Riedle, *Photochem. Photobiol. Sci.* **2010**, *9*, 1400–1406.
- [21] C. Willert, B. Stasicki, J. Klinner, S. Moessner, *Meas. Sci. Technol.* **2010**, *21*, 75402.
- [22] W. Hiller, H. M. Lent, G. E. A. Meier, B. Stasicki, *Exp. Fluids* **1987**, *5*, 141–144.
- [23] U. Schmidhammer, S. Roth, E. Riedle, A. A. Tishkovand, H. Mayr, *Rev. Sci. Instrum.* **2005**, *76*, 093111–1–093111–7.
- [24] H. Schmaderer, P. Hilgers, R. Lechner, B. König, *Adv. Synth. Catal.* **2009**, *351*, 163–174.
- [25] J. Svoboda, H. Schmaderer, B. König, *Chem. – A Eur. J.* **2008**, *14*, 1854–1865.
- [26] U. Megerle, M. Wenninger, R.-J. Kutta, R. Lechner, B. König, B. Dick, E. Riedle, *Phys. Chem. Chem. Phys.* **2011**, *13*, 8869–8880.
- [27] D. P. Hari, P. Schroll, B. König, *J. Am. Chem. Soc.* **2012**, *134*, 2958–2961.
- [28] D. P. Hari, B. König, *Org. Lett.* **2011**, *13*, 3852–3855.
- [29] A. G. Condie, J. C. González-Gómez, C. R. J. Stephenson, *J. Am. Chem. Soc.* **2010**, *132*, 1464–1465.
- [30] B. S. Lukyanov, M. B. Lukyanova, *Chem. Heterocycl. Compd.* **2005**, *41*, 281–311
LA – English.
- [31] J. Dařová, S. Kümmel, C. Feldmeier, J. Cibulková, R. Pařout, J. Maixner, R. M. Gschwind, B. König, R. Cibulka, *Chem. – A Eur. J.* **2013**, *19*, 1066–1075.
- [32] G. Richter, S. Weber, W. Römisch, A. Bacher, M. Fischer, W. Eisenreich, *J. Am. Chem. Soc.* **2005**, *127*, 17245–17252.
- [33] B. König, S. Kümmel, R. Cibulka, in *Chem. Photocatal.* (Ed.: B. König), De Gruyter, **2013**, pp. 45–66.
- [34] C. Feldmeier, M. Abiko, U. T. Schwarz, Y. Kawakami, R. Micheletto, *Opt. Express* **2009**, *17*, 22855–22860.
- [35] M. Goetz, in *Adv. Photochem.* (Eds.: D. Neckers, D. Volmann, G. Bünau), Wiley New York, **1997**.
- [36] M. Goetz, in *Adv. Photochem.*, John Wiley & Sons, Inc., **2007**, pp. 63–163.
- [37] D. Neuhaus, M. P. Williamson, *The Nuclear Overhauser Effect in Structural and Conformational Analysis, 2nd Edition*, **2000**.
- [38] H. D. Roth, M. L. Manion, *J. Am. Chem. Soc.* **1975**, *97*, 6886–6888.

- [39] O. B. Morozova, K. L. Ivanov, A. S. Kiryutin, R. Z. Sagdeev, T. Kochling, H.-M. Vieth, A. V Yurkovskaya, *Phys. Chem. Chem. Phys.* **2011**, *13*, 6619–6627.
- [40] A. S. Kiryutin, O. B. Morozova, L. T. Kuhn, A. V Yurkovskaya, P. J. Hore, *J. Phys. Chem. B* **2007**, *111*, 11221–11227.
- [41] M. Goetz, *ChemInform* **2010**, *41*, 19.
- [42] Bruker BioSpin, *Bruker Service Manual 9.0 Console Avance I*, **2008**.
- [43] T. D. W. Claridge, *High-Resolution NMR Techniques in Organic Chemistry, 2nd Edition*, Elsevier Science, Oxford, **2009**.
- [44] K. Maeda, C. E. Lyon, J. J. Lopez, M. Cemazar, C. M. Dobson, P. J. Hore, *J. Biomol. NMR* **2000**, *16*, 235–244.
- [45] H. M. Swartz, J. R. Bolton, D. C. Borg, *Biological Applications of Electron Spin Resonance*, **1972**.
- [46] O. Madelung, Ed., *Landolt-Börnstein - Numerical Data and Functional Relationships in Science and Technology II/17h Magnetic Properties of Free Radicals*, Springer, **1985**.

4 Photo-CIDNP Patterns of Free Flavins in Solution: Solvent, Structural and Heavy Atom Effects



4.1 Abstract

Despite the huge importance of flavins as photosensitizers for protein Photo-CIDNP studies and as cofactors in enzymatic reactions no comprehensive investigation of Photo-CIDNP polarizations of free flavin in solution was presented so far. This is due to the small or vanishing Photo-CIDNP effect detected in flavins when water is used as the solvent. It is shown that the vanishing Photo-CIDNP effects are caused by the solvent and that the change of the solvent from water to acetonitrile reveals clear Photo-CIDNP polarizations of free flavins. Comprehensive studies of Photo-CIDNP effects of flavins are presented on the model system of the flavin catalyzed photooxidation of benzyl alcohols. The characteristic Photo-CIDNP patterns of flavin were studied in detail with focus on the difference between singlet and triplet exit channel and the effect of different substituents at the isoalloxazine moiety. Spectroscopic and mechanistic implications of substitutions with methyl groups and heavy atoms enhancing spin-orbit coupling are discussed in terms of Kaptein's sign rule and supported by DFT calculations.

4.2 Introduction

Photocatalytic reactions are usually initiated by the excitation of a chromophore and a consecutive electron transfer forming a radical pair. The unpaired electron spins in the radical pair are still spin correlated. This radical pair itself can undergo singlet-triplet mixing due to the spin multiplicity of the spin correlated unpaired electrons. The radical pair reactivity depends on the multiplicity of the spin correlated unpaired electrons. Recombination of the radical pair by back electron transfer is allowed for radical pairs in the singlet state. In contrast, for radical pairs in the triplet state recombination is spin forbidden. This can result in a longer lifetime of the triplet channel and in a higher probability of the triplet radical pair to separate and form reaction products. In contrast, radical pairs in the singlet state are usually associated with recombination products after back electron transfer. The NMR hyperpolarization technique Photo-CIDNP (chemically induced dynamic nuclear polarization) examines exactly the primary radical pair in photochemical reactions.^[1-4] When the radical pair is formed the unpaired electrons of the radicals remain spin correlated with the same multiplicity as their precursor, i.e. they are still in the singlet or triplet state and thus can undergo intersystem crossing between the two different spin multiplicities.^[5] In a magnetic field the rate of intersystem crossing within the radical pair depends on the spin state of the nuclei with hyperfine coupling to the unpaired electron. This nuclear spin dependent intersystem crossing in the radical pair together with the electron spin multiplicity dependent reaction paths leads to a sorting of α and β spins in the diamagnetic precursors and products of the paramagnetic radical pair. This results in additional net polarization from the nuclear spin sorting. As a result anomalous signal intensities are observed in the product and precursor NMR spectra.^[2-4,6] As the Photo-CIDNP polarization is created on the reaction stage of the intersystem crossing within the spin correlated radical pair, Photo-CIDNP spectroscopy is an ideal technique for the study of this radical pair.

One of the most prominent molecules in Photo-CIDNP spectroscopy are flavins due to their suitable magnetic properties^[2] and huge importance as cofactors in enzymatic reactions.^[7-11] Most of the studies of Photo-CIDNP effects using flavins employ flavins as a photosensitizer and focus on the Photo-CIDNP polarizations of its reaction partner. Previous studies with free flavins in solution have only marginally or not at all dealt with the Photo-CIDNP polarizations of flavins themselves. This is to a great part due to the fact that flavins themselves show only weak or no Photo-CIDNP polarizations.^[2] Here the first systematic study of Photo-CIDNP effects of free flavins is presented. Clear Photo-CIDNP polarizations were achieved by using acetonitrile instead of water as the solvent

for the Photo-CIDNP. The mechanism canceling the Photo-CIDNP polarization of flavins in water is not effective in acetonitrile. Owing to that the Photo-CIDNP patterns of flavin itself could be studied in detail. The Photo-CIDNP patterns for both the singlet and triplet exit channel were detected and the effect of different substituents at the isoalloxazine moiety on the flavin Photo-CIDNP pattern was elucidated. Mechanistic implications of substitutions with methyl groups and heavy atoms enhancing spin-orbit coupling are discussed in terms of Kaptein's sign rule^[12] and supported by DFT calculations.

4.3 Results and Discussion

As a model system for this study the riboflavin tetraacetate (RFT) catalyzed photooxidation of methoxybenzyl alcohols (MBA)^[13–16] was chosen for the investigations. RFT is excited by blue light and oxidizes MBA to the corresponding aldehyde. The photocatalyst is subsequently reoxidized by oxygen forming H₂O₂ as the second reaction product.

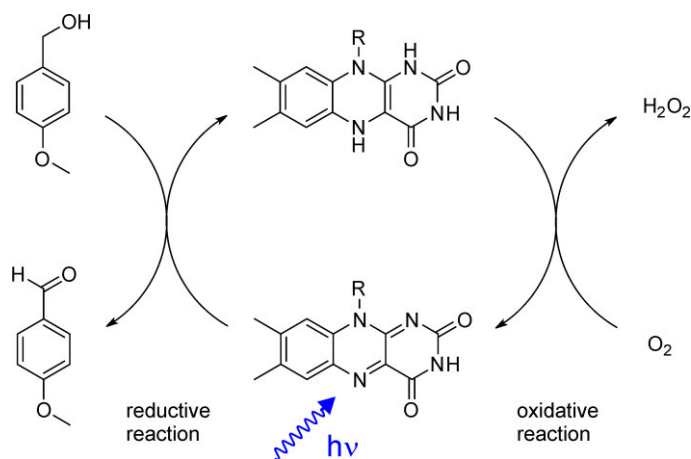


Figure 4-1 Reaction scheme of the model system. Flavin is excited by blue light ($\lambda = 455 \text{ nm}$) and oxidizes methoxybenzyl alcohol to the corresponding aldehyde. The photocatalyst is reoxidized by oxygen under production of hydrogen peroxide. To separate the singlet and triplet channel, to accumulate the reduced flavin species and to enable the detection of the corresponding characteristic Photo-CIDNP polarizations the experiments were conducted under anaerobic conditions.

4.3.1 Separation of Singlet and Triplet Pathway

By the Photo-CIDNP effect nuclear spins are sorted in the singlet exit channel (recombination products) and in the triplet exit channel (escape products).^[2,17] To distinguish between the singlet and triplet exit channel in NMR measurements the catalytic cycle was interrupted by deoxygenating the solvent and thus preventing the reduced flavin from reoxidizing. Without preventing the fully reduced flavin from reoxidizing the Photo-CIDNP nuclear spin sorting is undone and no Photo-CIDNP polarization is observed (chapter 5.3.2).^[2] When the reaction is performed in CD₃CN and *in situ* illuminated in the NMR spectrometer^[18] an additional signal set for the fully reduced flavin appears in the ¹H spectra. When the spectra are recorded with illumination of the sample the Photo-CIDNP effect causes anomalous signal intensities of the ¹H flavin resonances. Recording the same ¹H NMR spectrum without illumination yields the unaltered signals caused by Boltzmann polarization of the nuclear spins.

The generation of Photo-CIDNP polarization in the RFT sensitized photooxidation of methoxybenzyl alcohol is visualized in Figure 4-2. RFT in the ground state is excited to ¹RFT* in the singlet state and can undergo intersystem crossing yielding ³RFT* in the

triplet state. From both electron spin multiplicity states a radical pair $\text{RFT}^{\bullet-} \text{MBA}^{\bullet+}$ can be formed by electron transfer from MBA to RFT^* . It has been shown by means of transient absorption spectroscopy that this electron transfer is the initial step finally leading to the formation of methoxybenzyl alcohol.^[13] The electron spins of the unpaired electrons in the radicals stay spin correlated after the electron transfer forming the radical pair in the singlet state from the $^1\text{RFT}^*$ precursor and the triplet radical pair form the $^3\text{RFT}^*$ precursor. As the radicals in the radical pair $\text{RFT}^{\bullet-} \text{MBA}^{\bullet+}$ stay spin correlated intersystem crossing is still possible in the radical pair. For the triplet $\text{RFT}^{\bullet-} \text{MBA}^{\bullet+}$ radical pair recombination is spin forbidden so that this triplet exit channel (product formed from the triplet $\text{RFT}^{\bullet-} \text{MBA}^{\bullet+}$ radical pair) is usually associated with product formation,^[2,3,5,17] in this case yielding the product methoxybenzyl aldehyde and the fully reduced flavin. For the singlet exit channel (product formed from the singlet $\text{RFT}^{\bullet-} \text{MBA}^{\bullet+}$ radical pair by electron back transfer) recombination is allowed and it thus can yield the starting products being methoxybenzyl alcohol and the oxidized RFT after electron back transfer. The Photo-CIDNP polarizations detected in the diamagnetic products of the singlet and triplet exit channel (oxidized and fully reduced RFT respectively) are generated during the nuclear spin dependent intersystem crossing in the radical pairs. By this nuclear spin dependent intersystem crossing nuclei in different spin states (α and β) are sorted in the different reaction products of the singlet and triplet exit channel, i.e. in the fully reduced and the oxidized flavin where they appear in the form of additional polarizations in the NMR signals. However, if the catalytic cycle is closed and the fully reduced RFT is instantaneously reoxidized by molecular oxygen after it was formed both the fully reduced and the oxidized RFT end up in the same RFT NMR signal set, the signal set of the oxidized flavin. Owing to that the sorting of the nuclear spins of RFT molecules by the Photo-CIDNP effect is undone and no additional polarization is detectable in the NMR spectra.^[2]

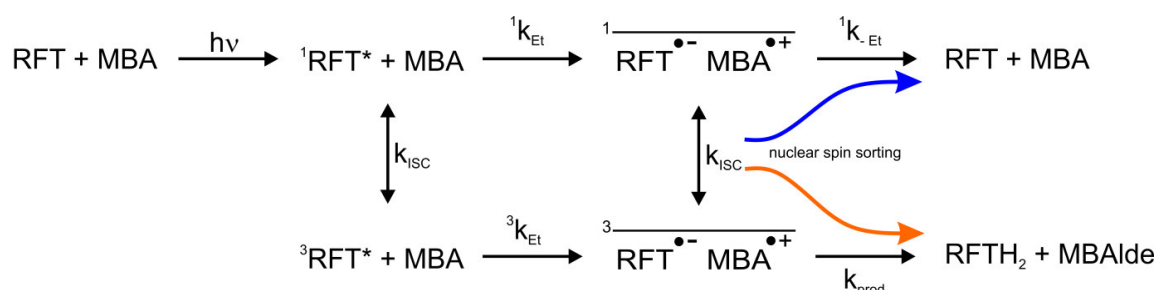


Figure 4-2 Scheme of the Photo-CIDNP generation in the flavin (RFT) catalyzed photooxidation of benzylic alcohols (MBA) to the corresponding aldehyde (MBAIde). RFT is excited to $^1\text{RFT}^*$ by light and undergoes intersystem crossing yielding $^3\text{RFT}^*$. Spin correlated radical pairs are generated after electron transfer. The intersystem crossing during the existence of the spin correlated radical pair is nuclear spin state dependent and causes nuclear spin sorting and generates the Photo-CIDNP effect.

To enable the detection of Photo-CIDNP polarizations of RFT the catalytic cycle was interrupted by the exclusion of oxygen from the reaction mixture. Thereby the reoxidation of the reduced RFT is inhibited and the fully reduced RFT is stabilized and appears as an additional signal set in the ^1H NMR spectrum (compare chapter 5.3.2). The oxidized and the reduced flavin species are detected simultaneously in the same ^1H spectrum as distinct signal sets. The products of the singlet and the triplet exit channel (Figure 4-2) are separated and the Photo-CIDNP spin sorting in the radical pairs is reflected in the oxidized flavin (recombination) and fully reduced flavin (escape products / productive pathway).

4.3.2 Photo-CIDNP Polarization – Singlet vs. Triplet Pathway

The Photo-CIDNP spectra arising from the singlet and the triplet exit channel were measured simultaneously in the same ^1H NMR spectra by alternately recording ^1H spectra of the not illuminated and the illuminated reaction mixture. The difference of the two spectra yields the Photo-CIDNP spectrum.

Figure 4-3 A shows sections of a ^1H spectrum of the not illuminated reaction mixture with the two separate signal sets for the oxidized and the fully reduced flavin after 1 h of illumination of a deoxygenated solution of 20 mM MBA and 2 mM RFT in CD_3CN . Figure 4-3 B shows the corresponding sections of the ^1H spectrum of the illuminated reaction mixture. The Photo-CIDNP spectrum resulting from the difference of the ^1H spectrum of the illuminated and the dark sample is depicted in Figure 4-3 C. The strongest Photo-CIDNP polarization is observed for the C(6)-H proton of the oxidized flavin (blue) as an emissive signal. The corresponding C(6)-H signal of the fully reduced flavin (green) shows an absorptive Photo-CIDNP signal. For the other aromatic proton of the isoalloxazine ring system C(9)-H the situation is inverted. The ^1H resonance of the oxidized form of the flavin shows an absorptive Photo-CIDNP polarization, whereas the ^1H signal of the corresponding reduced form is attenuated upon irradiation due to emissive Photo-CIDNP polarization. The other protons attached to the isoalloxazine that share an appreciable hyperfine coupling with unpaired electron of the semiquinone radical are the methyl groups C(8 α)-H₃ and C(7 α)-H₃. Compared to the dark ^1H spectrum C(7 α)-H₃ shows an enhanced absorptive signal upon illumination, this is again complemented by an emissive Photo-CIDNP signal of the C(7 α)-H₃ signal in the corresponding ^1H NMR signal set of the fully reduced flavin (data not shown). The same complementarity of the Photo-CIDNP phases in the signals of the oxidized and fully reduced flavin is observed for the C(8 α)-H₃ resonances with an absorptive signal for the oxidized RFT and an emissive signal for the fully reduced species (data not shown).

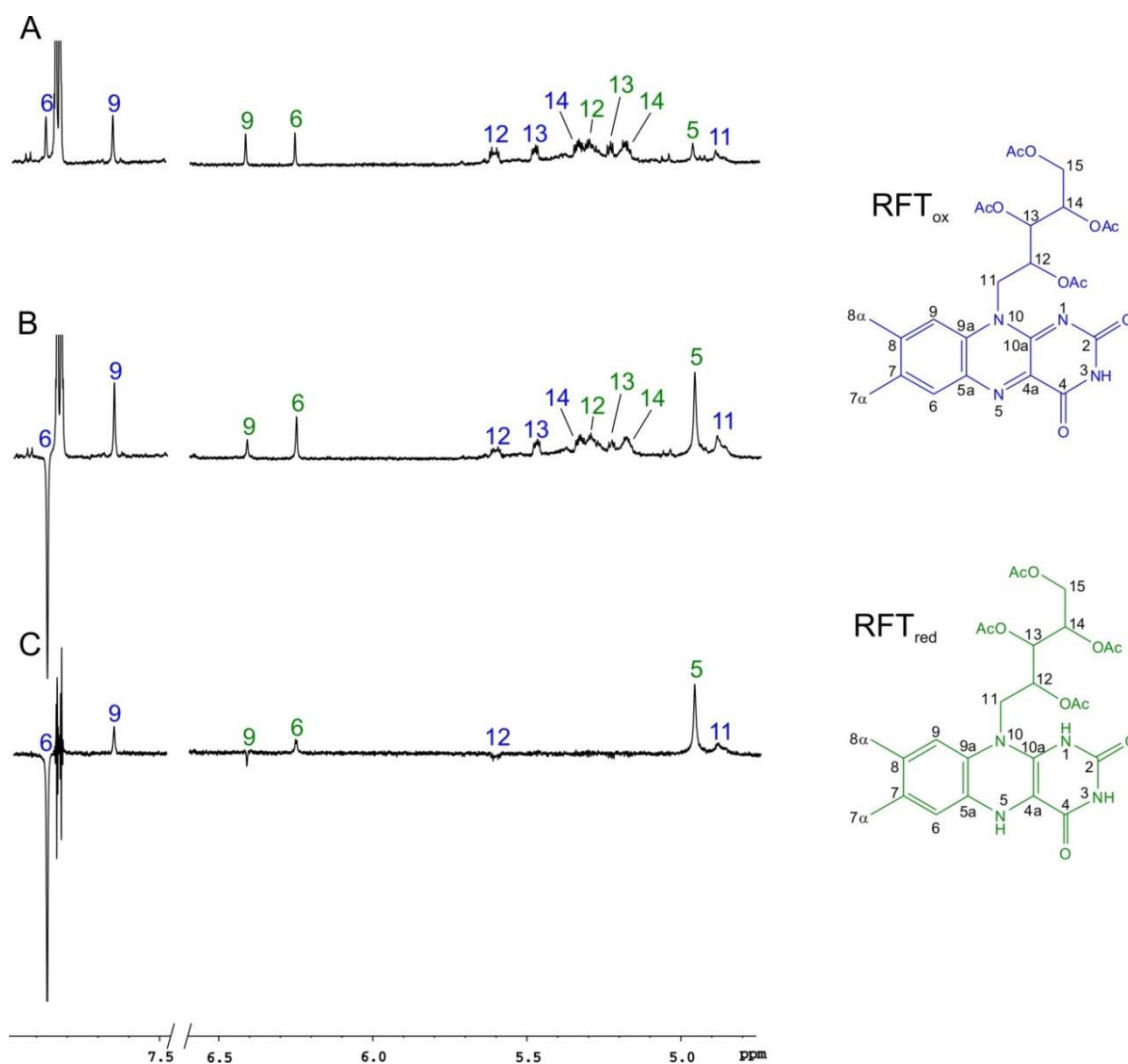


Figure 4-3 ^1H spectra of the reaction mixture of 2 mM RFT and 20 mM MBA in deoxygenated CD_3CN at 300 K after one hour of *in situ* illumination with 455 nm light. A) shows the spectrum of the not illuminated sample, B) the spectrum of the illuminated sample, C) the Photo-CIDNP spectrum as the difference spectrum of B) and A).

The dependency of the intersystem crossing on the nuclear spin state causing Photo-CIDNP polarizations is mediated by the hyperfine coupling of the respective nuclei to the unpaired electron of the radical. Thus the strength of the Photo-CIDNP effect depends on the distance of the nuclei from the radical center. This dependence is reflected in the Photo-CIDNP spectra depicted in Figure 4-3. Whereas the NMR resonances of the protons attached directly to the isoalloxazine moiety C(6)-H, C(9)-H, C(7 α)-H₃, C(8 α)-H₃ all exhibit appreciable Photo-CIDNP polarizations the proton resonances of the ribityl side chain show only very small or no Photo-CIDNP polarizations. For the C(11)-H₂ signal of the oxidized RFT a small absorptive polarization is detected, for C(12)-H a small emissive polarization. All other ^1H of the side chain that have a larger distance from the isoalloxazine moiety do not show a difference of the signal intensity between the spectra of the illuminated and the not illuminated sample. This dependence on the distance of

the nucleus from the isoalloxazine ring system is also observed for the line broadening of the signals of the oxidized flavin when the semiquinone is stabilized in deoxygenated CD₃CN/D₂O (1:1) (compare chapter 5) and is easily explained by the electron spin density in the semiquinone radical located mainly in the isoalloxazine ring system and having only minor contributions in the side chain.

It is obvious from Figure 4-3 that all Photo-CIDNP polarizations of the oxidized flavin exhibit significantly higher intensities than the corresponding ones of the fully reduced flavin. A very likely reason for these observations is the difference in lifetimes of the singlet and triplet radical pair. The radical pair in the singlet state recombines rapidly by back electron transfer. The lifetime of the triplet radical pair is longer and therefore the polarized nuclear spins are affected more by relaxation within the lifetime of the radical pair. The Photo-CIDNP polarizations are detected in the diamagnetic recombination and escape products and are thus differently affected by relaxation within the radical pair. This causes smaller Photo-CIDNP polarizations of the ¹H resonances of the reduced flavin compared to those of the oxidized flavin species.

The alcohol and aldehyde show signals in the Photo-CIDNP spectra even if a direct comparison of the ¹H spectra of the illuminated and of the dark reaction mixture does not show any obvious changes in signal intensities. A closer look reveals that their signals in the Photo-CIDNP spectra are caused by slight changes in the chemical shifts of these proton resonances upon illumination and not by signal intensity changes due to nuclear spin sorting by the Photo-CIDNP effect. This is confirmed by the vanishing integrals over the alcohol and aldehyde signals in the Photo-CIDNP spectra. Among the N-H proton resonances only the N(5)-H has been considered. The corresponding ¹H NMR signal shows a strong absorptive Photo-CIDNP polarization. The line widths reflecting the chemical exchange of protons of N(3)-H and N(1)-H are big compared to the line width of N(5)-H (compare chapter 5.6.6.3). For this reason the protons N(3)-H and N(1)-H can be expected to exchange chemically with other exchangeable protons carrying the Photo-CIDNP polarization. Therefore the Photo-CIDNP polarizations of these protons are prone to distortion and thus not considered further.

The detected Photo-CIDNP polarization phases are summarized and visualized as Photo-CIDNP polarization phase patterns in Figure 4-4. Blue circles symbolize emissive Photo-CIDNP polarizations, orange circles highlight protons that exhibit absorptive Photo-CIDNP polarizations. The comparison of the polarization patterns clearly shows that the polarization phases complement each other. For each emissive or absorptive polarization detected in the signal set of the oxidized flavin the corresponding proton

resonance in ^1H NMR signal set of the fully reduced RFT shows the opposite polarization. The same experiments were conducted with the sterically demanding flavin **2b**^[15] (Photo-CIDNP spectra not shown). Also in this case the Photo-CIDNP polarization patterns complement each other showing that the spin sorting in the radical pair directly leads to the oxidized and the fully reduced RFT (Figure 4-4).

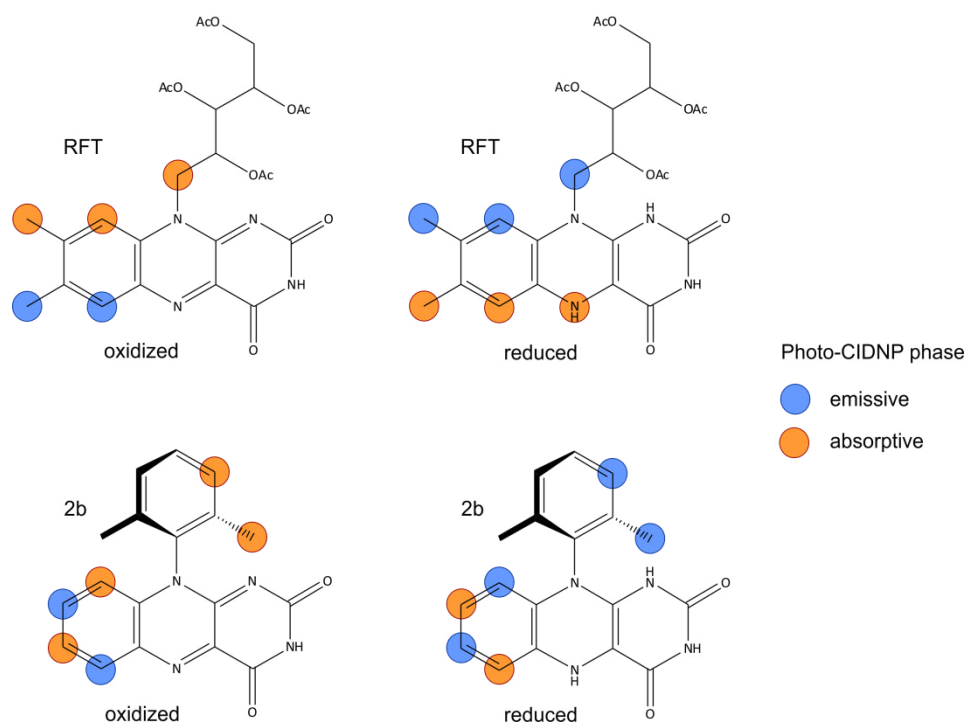


Figure 4-4 Photo-CIDNP patterns of the reduced and oxidized RFT and sterically demanding flavin **2b**. Blue circles depict emissive ^1H Photo-CIDNP signals, orange circles absorptive ^1H Photo-CIDNP signals.

The Photo-CIDNP patterns of the oxidized flavins result from back electron transfer to the recombination products and are thus assigned to the singlet exit channel of the radical pair. The Photo-CIDNP polarization patterns of the reduced flavins are thus the polarizations of the productive exit channel which is the triplet one as the recombination of the radicals in the triplet state is spin forbidden. As the Photo-CIDNP polarizations arise from spin sorting on the radical pair stage the patterns complement each other in terms of polarization phases. This can be seen in Figure 4-4 for RFT and the sterically demanding flavin **2b**. The radical electrons show appreciable hyperfine coupling with the protons of the isoalloxazine ring system, in particular with proton 6 and proton 8 α . The polarization of proton N-H(3) is not shown as it is modified by chemical exchange with other mobile and potentially polarized protons.

According to Kaptein's sign rule^[12] for the radical pair theory of Photo-CIDNP polarizations the inverted Photo-CIDNP polarization patterns arise from the different signs representing the different exit channels of the radical pair (+ for the escape product

from the triplet channel, - for the recombination products from the singlet channel). All other signs incorporated in Kaptein's sign rule are the same. The radicals forming the initial radical pair are the same and thus their difference in g-factors and their hyperfine coupling constants A are also equal. Thus the signs for the hyperfine coupling constants and the sign for the g-factor difference are the same whereas the signs for the exit channels are inverted. According to Kaptein's sign rule^[12] this shows that the radical pair precursor spin multiplicity has to be the same for both the escape type and recombination type reaction. This means that the radical pairs causing Photo-CIDNP polarizations of the ^1H resonances of the oxidized and the fully reduced RFT are both generated from RFT* of the same spin multiplicity. From probability and lifetime considerations it is most likely that they are formed from $^3\text{RFT}^*$, when the initial radical pair is formed from the excited triplet RFT as the lifetime of this radical pair is longer than the one of the radical pair in the singlet state.^[13] The radicals that do not perform a second electron oxidation or reduction before intersystem crossing within the radical pair recombine by back electron transfer and end up as recombination products.

4.3.3 Solvent Dependent Photo-CIDNP Cancellation

The Photo-CIDNP polarizations are created during the existence of the electron spin correlated radical pair due to the nuclear spin dependent intersystem crossing of this radical pair and the electron spin selective reaction paths associated with the singlet and triplet exit channel (compare Figure 4-2). The solvent can be expected to have a large impact on the Photo-CIDNP spectra. In the case of the studied solvents CD_3CN and $\text{CD}_3\text{CN}/\text{D}_2\text{O}$ (1:1) mixture the addition of water can facilitate the charge separation and thus the formation of the primary $\text{RFT}^{\cdot-} \text{MBA}^{\cdot+}$ radical pair by the polarity of water and in general stabilize the separated charges. On the other hand water could be expected to separate the primary radical pair and hinder back electron transfer or the addition of water could lead to faster protonation and deprotonation of the involved species. Solvents can also be expected to have a huge influence on radical pair substitutions. This kind of solvent dependence of Photo-CIDNP effects was reported by Goez *et al.*^[19,20] for the sensitized photolysis of iodine salts and to the variation of the radical pair substitution rate by the solvent polarity.

To study the influence of the solvent on the intersystem crossing in the radical pair $\text{RFT}^{\cdot-} \text{MBA}^{\cdot+}$ water was added to the reaction mixture, i.e. the reaction was performed in $\text{CD}_3\text{CN}/\text{D}_2\text{O}$ (1:1) and Photo-CIDNP experiments were conducted. Investigations in synthetic chemistry showed that the photooxidation of MBA catalyzed by RFT is strongly dependent on the solvent. Whereas in CD_3CN after 1 h of illumination only 7 % of the

substrate is oxidized, in the mixture $\text{CD}_3\text{CN}/\text{D}_2\text{O}$ (1:1) complete conversion of 100 % is achieved in the same time.^[14,16] As in the previous Photo-CIDNP studies of the reaction mixture in CD_3CN 2 mM of RFT were used with 20 mM of MBA and the solution was deoxygenated to prevent the reduced RFT from reoxidizing and thus to separate the singlet and triplet channel reaction products in the ^1H NMR spectra. Additionally, deoxygenation of the reaction mixture prolongs Photo-CIDNP polarization relaxation times and thus enhances the detected Photo-CIDNP signals.^[2] By illumination of the sample directly inside the NMR spectrometer with a LED based illumination device^[18] ^1H spectra of the illuminated and the not illuminated sample were recorded alternately to yield the Photo-CIDNP spectra as the difference spectra. Sections of the respective ^1H spectra are shown in Figure 4-5.

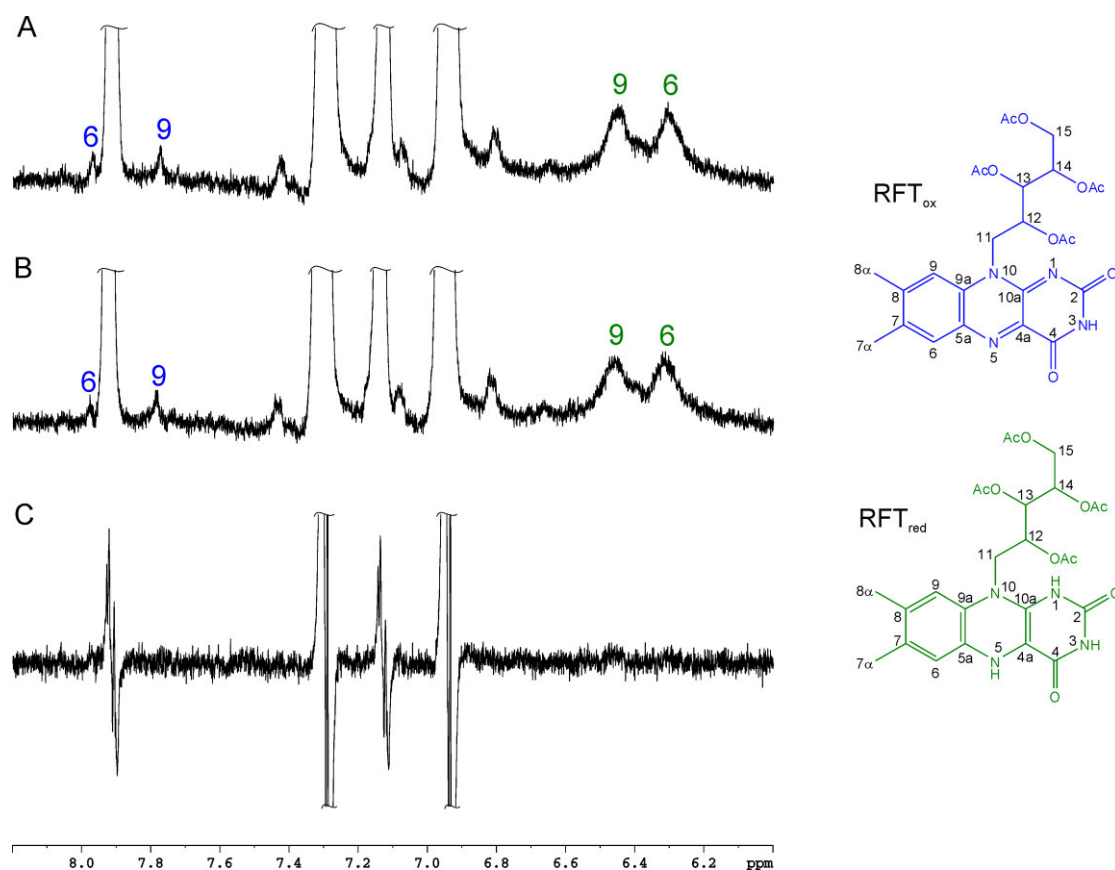


Figure 4-5 Sections of ^1H spectra of the reaction mixture of 2 mM RFT and 20 mM MBA in deoxygenated $\text{CD}_3\text{CN}/\text{D}_2\text{O}$ (1:1) at 280 K after *in situ* illumination with 455 nm light. A) shows the spectrum of the not illuminated sample, B) the spectrum of the illuminated sample C) the difference Photo-CIDNP spectrum.

Due to the stabilization of the semiquinone radical in deoxygenated $\text{CD}_3\text{CN}/\text{D}_2\text{O}$ (1:1) solution, the associated additional relaxation source and the chemical exchange between the different flavin oxidation states the lines of all proton resonances in the isoalloxazine moiety are broadened. The broadening is dependent of the distance from the radical center (compare chapter 5.6.2). Even though the lines of the aromatic protons

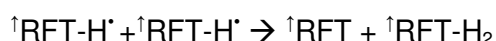
C(6)-H and C(9)-H of the fully reduced flavin species are affected by broadening they are well detectable and thus should show an increase or decrease of the signal intensity upon irradiation if they are affected by Photo-CIDNP effects. Figure 4-5 shows sections of the ^1H spectra with the C(6)-H and C(9)-H resonances of the oxidized and the fully reduced flavin species without illumination of the sample (Figure 4-5 A) and with illumination of the sample (Figure 4-5 B). It is obvious from the difference of the two spectra and the Photo-CIDNP spectrum (Figure 4-5 C) that the signal intensities of the aromatic proton signals of the fully reduced flavin species do not change upon illumination and that thus no Photo-CIDNP polarization is observable. The signals of the alcohol and aldehyde in the Photo-CIDNP spectrum shown in Figure 4-5 C are caused by slight changes in the chemical shifts of these proton resonances upon illumination and not by signal intensity changes due to nuclear spin sorting by the Photo-CIDNP effect. Overall, no Photo-CIDNP polarizations are detected when the model reaction is performed in $\text{CD}_3\text{CN}/\text{D}_2\text{O}$ (1:1) mixture. This is quite surprising keeping in mind that the photooxidation of MBA catalyzed by RFT is much faster in the mixture $\text{CD}_3\text{CN}/\text{D}_2\text{O}$ (1:1) where complete conversion of 100 % is achieved within 1 h, whereas in CD_3CN only 7 % of the substrate is oxidized in the same time as known from synthetic studies^[14,16] and the comparison of the reaction kinetics in the different solvents in chapter 5.3.3. One could assume that with this faster conversion more nuclear spins are sorted in the same time (Figure 4-2) and that thus stronger Photo-CIDNP effects should be detected for the case of $\text{CD}_3\text{CN}/\text{D}_2\text{O}$ (1:1) as the solvent. However, it is evident from the Photo-CIDNP measurements performed in the $\text{CD}_3\text{CN}/\text{D}_2\text{O}$ (1:1) reaction mixture that the addition of water does not enhance the Photo-CIDNP signals, on the contrary, the addition of water leads to the total deletion of Photo-CIDNP polarizations.

Both the g-factor and the hyperfine coupling constants of the RFT and MBA radicals can be expected not to change significantly with changing solvents. Therefore the cancelation of the Photo-CIDNP effects upon the addition of water must have mechanistic reasons. The difference between solvent separated and contact ion pairs plays an important role in photoinduced electron transfer reactions. As the products of these reactions result from the formation of free radicals, often polar solvents are used to promote the separation of the ionic radical pairs and thus hinder back electron transfer.^[21,22] As water is a more polar solvent than acetonitrile^[23] one could speculate that cancelation of the Photo-CIDNP polarization observed when the reaction is investigated in $\text{CD}_3\text{CN}/\text{D}_2\text{O}$ (1:1) is due to the better and faster separation of the initial ionic radical pair $\text{RFT}^- \text{MBA}^{+\bullet}$. The back electron transfer is hampered by the solvent

separated radical pair and thus the sorting of nuclear spins by the Photo-CIDNP effect in the recombination product (oxidized RFT) diminished.

Two other likely reasons for the cancelation of Photo-CIDNP signals upon the addition of water are disproportionation reactions of the involved radicals and degenerate electron and hydrogen atom transfer of the radicals to their diamagnetic species. These Photo-CIDNP cancelation mechanisms were described by Hore *et al.*^[2] and applied to flavin Photo-CIDNP systems by Kaptein *et al.*^[24] and Hore *et al.*^[25]

If two semiquinone radicals RFT-H[•] disproportionate they yield the oxidized RFT and the fully reduced RFT-H₂. The two disproportionating semiquinone radicals result from the separation of the RFT^{•-} MBA^{•+} radical pair and thus did not undergo back electron transfer to MBA and recombination. The semiquinone radicals therefore carry the escape type Photo-CIDNP polarization before disproportionation. Consequently after disproportionation only half of the escape type polarization ends up in the fully reduced flavin. The other half of this polarization, however, ends up in the starting material, the oxidized flavin. In this way the recombination type polarization in the oxidized RFT is diminished by escape type polarization originating from disproportionated semiquinone radicals. On the side of the fully reduced flavin the escape type Photo-CIDNP polarization is diminished by losing half of the sorted nuclear spins that end up in the oxidized flavin species. The mechanism leading to Photo-CIDNP cancelation via disproportionation of the RFT radicals to the diamagnetic counterparts is recapitulated in the following reaction equation. The arrows depict escape type polarization.^[2,24,25]



From these considerations it is evident that the disproportionation of the flavin radicals to their associated diamagnetic species can only diminish the Photo-CIDNP polarizations in the oxidized and the fully reduced flavin species if a recombination of the RFT^{•-} MBA^{•+} radical pair is possible. This has been shown by transient absorption measurements performed by Megerle *et al.*^[13] However, disproportionation of the semiquinone radicals can only diminish the Photo-CIDNP intensities but not cancel the polarizations completely.

The full cancelation of the Photo-CIDNP polarization in the RFT resonances observed in this study demands for an additional reason. In chapter 5 it is described that upon illumination of the reaction mixture of 2 mM RFT and 20 mM MBA solved in deoxygenated CD₃CN/D₂O (1:1) an equilibrium between the flavin radical and its diamagnetic counterparts is observed in the line broadening of the ¹H resonances of both

the oxidized and the fully reduced flavin. The stabilization of the semiquinone radical was shown by means of UV/Vis spectroscopy. The equilibrium between the three oxidation states is only observed for the solvent mixture of CD₃CN/D₂O (1:1) but not for the case of pure CD₃CN as the solvent. For pure CD₃CN as the solvent the ¹H resonances are sharp and no stable semiquinone radical could be detected in the reaction mixture. The observation of the equilibrium between the three RFT oxidation states and their exchange with each other resulting in the broadening of the ¹H resonances makes it very likely that the Photo-CIDNP cancelation observed for CD₃CN/D₂O as the solvent is caused by degenerate electron or hydrogen atom exchange. The cancelation mechanism is depicted in Figure 4-6.

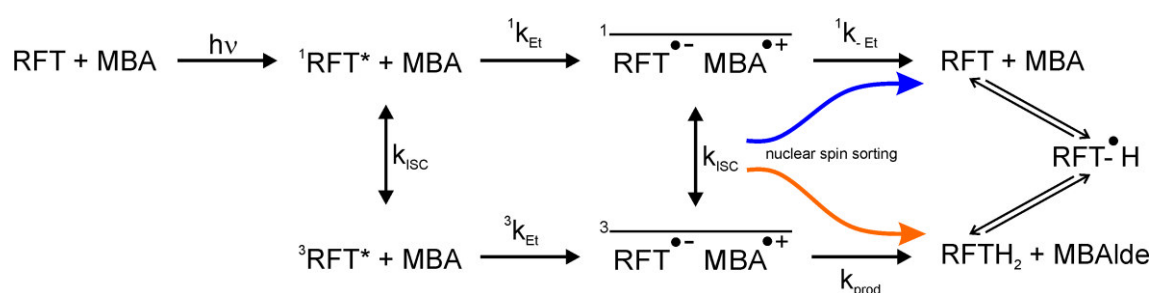


Figure 4-6 Scheme of the Photo-CIDNP generation in the flavin (RFT) catalyzed photooxidation of benzylic alcohols (MBA). RFT is excited to ¹RFT* by light and undergoes intersystem crossing yielding ³RFT*. Spin correlated radical pairs are generated after electron transfer. The intersystem crossing during the existence of the spin correlated radical pair is nuclear spin state dependent causing nuclear spin sorting and leading to the Photo-CIDNP effect. The oxidized and the fully reduced flavin species are in fast chemical exchange with the semiquinone radical mixing the previously sorted nuclear spins.

The primary steps until the creation of escape type and recombination type Photo-CIDNP polarization are analog to the generation of the Photo-CIDNP polarizations observed for pure CD₃CN as the solvent. RFT is excited to ¹RFT* by light and undergoes intersystem crossing yielding ³RFT*. Spin correlated radical pairs are generated after electron transfer from MBA to RFT. The intersystem crossing during the existence of the spin correlated radical pair is nuclear spin state dependent and causes nuclear spin sorting. The escape product RFTH₂ carries escape type Photo-CIDNP polarization. The recombination product RFT carries recombination type Photo-CIDNP polarization. As both RFT and RFTH₂ exhibit chemical exchange with the semiquinone radical the polarization generated at the stage of the electron spin correlated radical pair is diminished by the chemical exchange. Initially sorted nuclear spins are mixed again by the degenerate electron and hydrogen atom exchange between the oxidized RFT, the semiquinone radical and the fully reduced RFT species. In agreement with these considerations Hore *et al.* proposed exchange or disproportionation cancelations ³RFT to be the possible reasons for the observations that flavins used for protein Photo-CIDNP studies often show only very small or no Photo-CIDNP polarizations.^[2]

4.3.4 Photo-CIDNP Effects of Heavy Atom Flavins

In general the term “heavy atom effect” describes an effect heavy atoms have on various properties of molecules such as fluorescence,^[26,27] phosphorescence,^[28] NMR chemical shifts^[29,30] or intersystem crossing.^[31] The heavy atom effect can be external or internal depending on whether the heavy atom is part of or outside of a molecule. Here the heavy atom effect on the NMR chemical shift and the intersystem crossing are of importance.

The heavy atom effect in NMR describes the effect that a substitution by a heavy atom has on the chemical shift of the neighboring nuclei. Nuclei next to heavy halogen atom substituents are usually shifted upfield with higher atomic number (normal halogen dependence). Inverse halogen dependence describes the opposing effect with higher chemical shifts for nuclei neighboring halogen substituents with rising atomic number.^[29,30] This effect is often explained by diamagnetic shielding by the number of electrons around the halogens or electronegativity effects.^[30] In many studies the heavy atom effect on NMR chemical shifts is attributed to varying spin-orbit coupling induced electronic spin polarization.^[30,32]

In photochemistry the term heavy atom effect describes the increased rate of spin forbidden intersystem crossing through increased spin-orbit coupling caused by internal or external heavy atoms.^[31,33,34] To exploit this effect for flavin photocatalysis new flavin derivatives were synthesized by Susanne Kümmel.^[35] The ribityl side chain of RFT was substituted by a propyl side chain and the isoalloxazine ring system was substituted by bromine and iodine in position 7, the flavin with hydrogen in position 7 serves as a reference. The structures of the flavins are shown in Figure 4-7 together with their ¹H and ¹³C chemical shift assignments in CD₃CN. The heavy atom effect on the chemical shifts of the nuclei next to heavy halogen atom substituents is evident from the atomic number dependent upfield shift of the respective resonances.

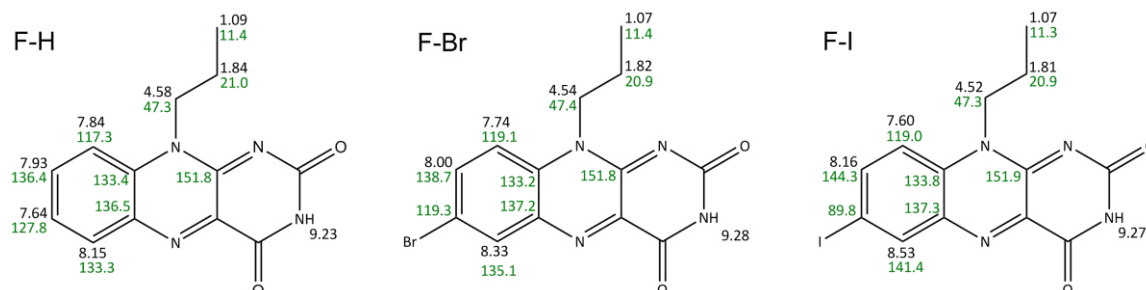


Figure 4-7 Assignment of the ¹H chemical shifts (black) and ¹³C chemical shifts (green) of the unsubstituted flavin F-H and the bromine and iodine substituted heavy atom flavin derivatives F-Br and F-I.

The first reaction steps of the flavin catalyzed oxidation of methoxybenzyl alcohol to the corresponding aldehyde were investigated by Megerle *et al.*^[13] The excited flavin in the triplet state was found to initiate the productive reaction path with an electron transfer from the alcohol to the flavin and a subsequent proton transfer. The excited flavin in the singlet state also forms a radical pair but in this case the fast back electron transfer inhibits further reaction. Substitution by heavy halogen atoms can enhance spin-orbit coupling and thus increase intersystem crossing rates. With faster population of the triplet state the reactive triplet channel is promoted and the reaction can be expected to be more efficient.

To elucidate the effect of heavy atom substitution on the Photo-CIDNP effects Photo-CIDNP experiments were performed with the three different flavins F-H, F-Br and F-I (2 mM) and MBA (20 mM) as a substrate in CD₃CN solution. The approach to separate the singlet from the triplet channel by deoxygenation and inhibiting the reoxidation of the reduced flavin species was not applied for the Photo-CIDNP studies of the heavy atom flavins F-Br and F-I and the reference F-H. Instead, the Photo-CIDNP polarizations detected in the ¹H NMR signal set of the oxidized flavin species were studied. The Photo-CIDNP phases detected for the heavy atom flavins do not change phases over the course of the reaction. For this reason the strongest Photo-CIDNP polarizations appearing during the reaction in the ¹H signal set of the oxidized flavin were analyzed. The Photo-CIDNP polarizations are revealed after oxygen is consumed due to the diminished relaxation of the polarizations and the hindered reoxidation of the escaped products (reduced flavin). For the heavy atom flavins no clear signal set for the reduced flavin species was detected probably caused by low photostability of the compounds. Therefore only the Photo-CIDNP effects detected in the recombination products (oxidized flavin) were studied.

Figure 4-8 shows the dark, the illuminated and the Photo-CIDNP difference ¹H spectra of the reference flavin F-H without substitution by a heavy atom in position 7 and of the heavy atom substituted flavin F-Br. The dark spectrum results from Boltzmann distribution, the illuminated spectrum from Boltzmann distribution and additional polarization caused by Photo-CIDNP spin sorting, the difference spectrum between the illuminated and the dark spectrum shows the pure Photo-CIDNP polarization caused by nuclear spin dependent intersystem crossing. The substitution by the heavy atom bromine in position 7 causes a change in the Photo-CIDNP polarization phases (position 6 and 8: emissive → absorptive, position 9: absorptive → emissive). Furthermore the

overall polarization of the protons at positions 6 and 8 increases after substitution with bromine, whereas the overall polarization of the proton in position 9 decreases.

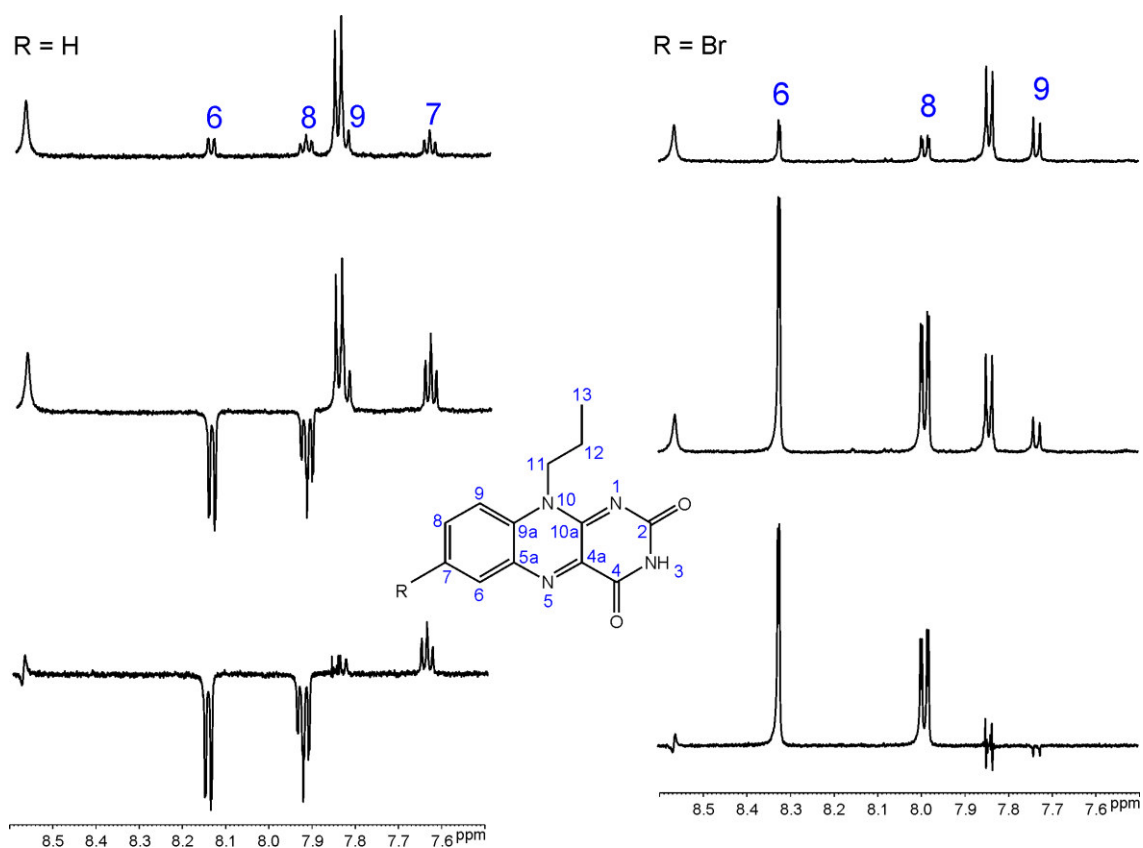


Figure 4-8 ^1H spectra of the dark sample (top), illuminated sample (middle) and ^1H Photo-CIDNP difference spectra (bottom) of flavin without (left) and with substitution by a heavy atom (right).

Figure 4-9 shows the Photo-CIDNP polarization patterns of the flavins with propyl side chain and different substituents at position 7 caused by the transient formation of the semiquinone radical. The polarization patterns reflect the spin density of the unpaired electrons in the paramagnetic precursors of the diamagnetic products detected by NMR. In this case the products are the products after the back electron transfer, i.e. the starting material. Flavin **2b** shows the characteristic polarization pattern for the singlet channel as detected for all other flavins without methyl groups in positions 7 and 8 like the sterically demanding flavin **2b** (chapter 4.3.2). The protons in position 7 and 9 show absorptive Photo-CIDNP signals, the protons in positions 6 and 8 emissive polarizations. When C(7)-H is substituted by heavy atoms the Photo-CIDNP phases change, the proton in position 9 shows emissive, the protons in position 6 and 8 show absorptive Photo-CIDNP polarization. The inversion of the Photo-CIDNP pattern upon substitution by heavy atoms is further discussed in chapter 4.3.6.3.

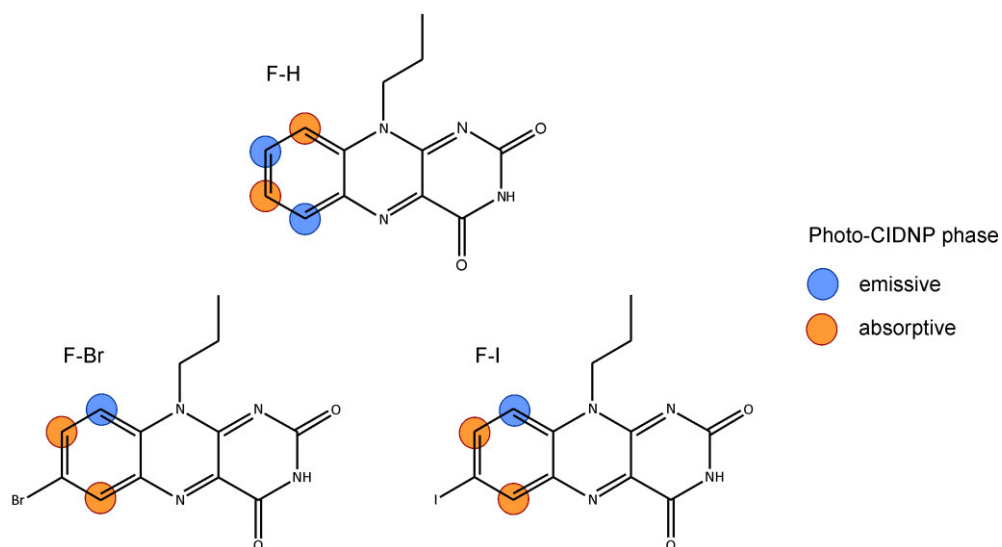


Figure 4-9 The Photo-CIDNP polarization phases of the aromatic proton signals of the reference flavin F-H and the heavy atom substituted flavin derivatives F-Br and F-I. Blue circles mark emissive Photo-CIDNP signals, orange circles mark absorptive Photo-CIDNP signals.

4.3.5 Calculations

For the interpretation of Photo-CIDNP spectra calculations of the spin densities of the unpaired radical electrons are essential. The hyperfine coupling constants are proportional to the Photo-CIDNP polarization they cause in the corresponding nuclei for geminate radicals with large $|\Delta g\mu_B B|$ (large difference in g-factors) and large number of magnetic nuclei. This was shown by Morozova *et al.* by means of theoretical considerations and experimental data.^[36] With Photo-CIDNP spectroscopy the hyperfine coupling constants are readily assigned to the corresponding nuclei. Furthermore the signs of the hyperfine coupling constants are easily accessible from the phases of the Photo-CIDNP signals and Kaptein's multiplicative sign rule.^[12] The Photo-CIDNP polarizations are proportional to the hyperfine couplings of the unpaired electrons to the corresponding nuclei and these to the spin densities of the unpaired radical electrons at the nuclei.^[17,36–38] For this reason the calculations of the magnetic properties of radicals like the hyperfine coupling constants or g-values can be employed to draw conclusions on the nature of the radicals causing the Photo-CIDNP effects. In this way for example the neutral and anionic form of the flavin semiquinone can be distinguished by means of their Photo-CIDNP phases.^[39]

For the comprehension and interpretation of the Photo-CIDNP effects observed in this study the Mulliken atomic spin densities of the unpaired electrons of different radicals of 10-propyl isoalloxazine F-H and 7,8,10-trimethyl isoalloxazine (lumiflavin) were calculated. Further calculations of the atomic spin densities were performed for the radicals associated with methoxybenzyl alcohol.

For the following discussion only the signs of the electron spin densities are considered as the Photo-CIDNP signal intensities are significantly affected by many factors such as solvent effects, aggregations, cross-polarizations and relaxation mechanisms.

4.3.5.1 Atomic Spin Densities of Flavin Radicals

Mulliken atomic spin densities of 10-propyl isoalloxazine F-H are listed in Table 4-1 for the F-H neutral biradical, for the F-H anion radical and for the F-H neutral radical. The Photo-CIDNP intensities and polarization phases correlate with the hyperfine coupling constants of the unpaired electron spins of the radical with the respective nuclei.^[36] For flavins the Photo-CIDNP polarization phases can be employed to distinguish between different radical species. The flavin anion radical can be distinguished from the neutral flavin radical by the sign of the Photo-CIDNP polarization of C(10a).^[39] Richter *et al.* reported on the ¹³C Photo-CIDNP effects.^[39] In Table 4-1 and Table 4-2 calculations of the Mulliken atomic spin densities of the neutral and anion radicals of two different flavin derivatives are presented. For better comparability positive values are presented in blue whereas negative values are presented in black. Different signs of the electron spin densities at corresponding nuclei in different radicals correspond to different Photo-CIDNP phases caused by these radicals and makes the radicals distinguishable by means of the Photo-CIDNP patterns. The calculations for 10-propyl isoalloxazine F-H and 7,8,10-trimethyl isoalloxazine (lumiflavin) are presented in Table 4-1 and Table 4-2. The anion radicals and the neutral radicals (protonated in position 5) show the same sign of the atomic spin densities for almost all nuclei. Only the signs of spin densities at the nuclei C(2), N(3) and C(10a) are affected after the protonation of the flavin radicals in position 5. C(2) and C(10a) both show a positive sign for the anion radical and a negative sign for the neutral radical. N(3) shows a negative sign for the anion radical and a positive one for the neutral radical. These difference in the sign of spin densities clearly shows that the neutral and anionic flavin radicals are only distinguishable by the Photo-CIDNP polarization pattern if one of the nuclei C(2), N(3) or C(10a) is considered and ¹³C Photo-CIDNP studies are conducted. The calculations show no difference between the signs of spin densities at any hydrogen atom between the flavin anion and flavin neutral radicals. This shows that the neutral and the anion radical are not distinguishable by means of ¹H Photo-CIDNP spectroscopy. For differentiation between the radicals the NMR resonances of the nuclei C(2), N(3) or C(10a) have to be employed.

With regard to the different Photo-CIDNP patterns detected for the different flavin derivatives, especially for RFT and F-H compared to the heavy atom substituted flavins the calculations were performed for 10-propyl isoalloxazine F-H (Table 4-1) and

7,8,10-trimethyl isoalloxazine (lumiflavin) (Table 4-2) with the latter being a model for RFT. Just like RFT lumiflavin has two methyl groups in positions 7 and 8. F-H misses these groups. The difference in the signs of the calculated atomic spin densities that determine the detected Photo-CIDNP pattern can be seen from the comparison of Table 4-1 and Table 4-2. In particular the spin densities of C(6)-H, C(7)-H or C(7 α)-H₃, C(8)-H or C(8 α)-H₃ and C(9)-H are of importance for the interpretation of the detected ¹H Photo-CIDNP polarization patterns. For the 10-propyl isoalloxazine F-H the calculations show a negative sign for C(6)-H, a positive sign for C(7)-H, a negative sign for C(8)-H and again a positive sign for C(9)-H. This sign pattern is in accordance with the observed Photo-CIDNP polarization pattern for F-H showing alternating phases from C(6)-H to C(9)-H (Figure 4-8 and Figure 4-9). For lumiflavin the calculations yield spin densities with negative signs for C(6)-H and C(7 α)-H₃ and spin densities with positive signs for C(8 α)-H₃ and C(9)-H. Also these sign patterns are in accordance with experimentally detected Photo-CIDNP patterns of RFT radicals showing the same Photo-CIDNP phases for protons C(6)-H and C(7 α)-H₃ and the opposite phase for C(8 α)-H₃ and C(9)-H. It is obvious from the calculations presented in Table 4-1 and Table 4-2 that the signs of the spin densities at the aromatic protons C(6)-H and C(9)-H are the same for 10-propyl isoalloxazine F-H and 7,8,10-trimethyl isoalloxazine. This shows that the corresponding hyperfine coupling constants of the corresponding nuclei to the radical electrons have the same signs. Consequently, the Photo-CIDNP phases of the corresponding proton resonances should also be equal.

4.3.5.2 Atomic Spin Densities of Substrate Radicals

Next the Mulliken atomic spin densities of the methoxybenzyl alcohol (MBA) cationic and neutral radical were calculated. The results are shown in Table 4-3. In contrast to the situation found for the different flavin radicals here the cation and the neutral radical show different signs of the spin density at various different nuclei. From the calculations it can be expected that the different radicals can even be distinguished by means of ¹H Photo-CIDNP spectroscopy for example by the ¹H Photo-CIDNP polarization phases of C(4)-H.

So far a Photo-CIDNP effect in the MBA ¹H resonances was only detected experimentally for the MBA OH group. This Photo-CIDNP polarization can be due to chemical exchange of the Photo-CIDNP polarized RFT N(5)-H to the MBA OH. The flavin Photo-CIDNP studies were always conducted with solutions of 2 mM RFT and 20 mM MBA. The missing Photo-CIDNP effects in the alcohol/aldehyde resonances are most likely due to the excess of MBA and the associated small amount of Photo-CIDNP

polarized MBA. It is very likely that at lower MBA/RFT ratios also the transient MBA radicals can be detected and characterized by means of Photo-CIDNP spectroscopy.

Table 4-1 Mulliken atomic spin densities of the F-H biradical, the F-H anion and the neutral F-H radical with the corresponding total charges and spin multiplicities from DFT calculations. Atomic spin densities of opposite signs are highlighted in different colors (negative: black, positive: blue).

		F-H biradical	F-H anion radical	F-H neutral radical
total charge		0	-1	0
spin multiplicity		3	2	2
position	nucleus			
1	N	0.428338	0.010239	0.038594
2	C	-0.047472	0.011987	-0.007794
	O	0.179715	0.039268	0.054225
3	H	-0.000595	-0.000322	-0.001284
	N	-0.013774	-0.005096	0.012479
4	C	-0.015514	0.027954	0.000888
	O	0.115575	0.063905	0.081144
4a	C	0.282958	0.124387	0.340714
5	H			-0.011999
	N	0.327254	0.340021	0.256628
5a	C	0.075763	-0.068002	-0.030288
6	H	-0.005311	-0.008809	-0.00387
	C	0.080259	0.162497	0.06915
7	H	-0.003731	0.003291	0.00087
	C	0.066664	-0.068128	-0.021526
8	H	-0.011408	-0.010542	-0.005004
	C	0.19494	0.172042	0.087145
9	H	0.000543	0.000935	0.000893
	C	-0.036612	-0.02745	-0.025653
9a	C	0.170875	0.081781	0.05816
10	N	0.248889	0.099395	0.117876
10a	C	-0.045505	0.044426	-0.018085
11	H	0.006937	0.001066	0.001162
	H	0.002033	0.003709	0.003181
	C	-0.015825	-0.004381	-0.006224
12	H	-0.000601	-0.000361	-0.000399
	H	-0.000928	-0.000263	-0.000212
	C	0.0149	0.005679	0.008261
13	H	0.000603	0.000129	0.000255
	H	-0.000007	-0.000024	0.000053
	H	0.000081	0.000112	-0.000027
	C	0.000955	0.000555	0.000687
total spin density		1.999999	1.000000	1.000000

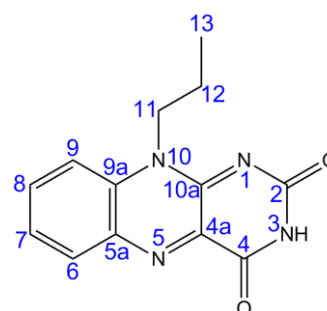


Table 4-2 Mulliken atomic spin densities of the lumiflavin biradical, the lumiflavin anion radical and the neutral lumiflavin radical with the corresponding total charges and spin multiplicities from DFT calculations. Atomic spin densities of opposite signs are highlighted in different colors (negative: black, positive: blue).

		Flavin biradical	Flavin anion	Flavin neutral
total charge		0	-1	0
spin multiplicity		3	2	2
position	nucleus			
1	N	0.396637	0.0083	0.033988
2	C	-0.042751	0.011539	-0.007143
	O	0.170149	0.037183	0.050923
3	H	-0.000591	-0.000336	-0.001274
	N	-0.013448	-0.004585	0.012674
4	C	-0.014641	0.028147	0.002047
	O	0.115204	0.061723	0.077301
4a	C	0.287173	0.120356	0.329556
5	H			-0.012234
	N	0.320897	0.342409	0.262752
5a	C	0.087908	-0.066203	-0.0262
6	H	-0.004718	-0.008718	-0.003637
	C	0.059729	0.154258	0.062755
7	C	0.094167	-0.061512	-0.016955
7a	H	-0.000294	-0.002393	-0.000588
	H	0.005852	-0.000329	-0.000147
	H	0.005852	-0.002387	-0.00059
	C	-0.00496	0.004226	0.001088
8	C	0.21353	0.172082	0.094363
8a	H	0.010172	0.007556	0.004208
	H	0.010172	0.00762	0.004191
	H	0.000059	0.000248	0.000082
	C	-0.015134	-0.014082	-0.006754
9	H	0.001621	0.001315	0.001243
	C	-0.059759	-0.033188	-0.03365
9a	C	0.185024	0.085804	0.063736
10	N	0.227527	0.099052	0.117982
10a	C	-0.042488	0.045063	-0.016425
11	H	0.012477	0.008008	0.008196
	H	0.012477	-0.000055	0.008234
	H	-0.00095	0.008028	-0.000079
	C	-0.016894	-0.00913	-0.009642
total spin density		1.999999	0.999999	1.000001

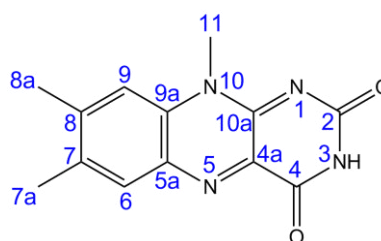
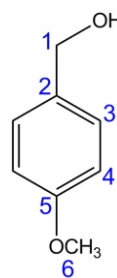


Table 4-3 Mulliken atomic spin densities of the methoxybenzyl alcohol (MBA) cationic radical and the MBA neutral radical with the corresponding total charges and spin multiplicities from DFT calculations. Atomic spin densities of opposite signs are highlighted in different colors (negative: black, positive: blue).

		MBA cation radical	MBA neutral radical
spin multiplicity		1	0
total charge		2	2
position	nucleus		
OH	O	0.016666	0.094623
	H	-0.000858	-0.003183
1	H	0.034843	
	H	0.034874	-0.032363
	C	-0.014041	0.622141
2	C	0.350382	-0.119385
3	H	0.001601	-0.010858
	C	-0.065376	0.19727
	H	-0.0021	-0.012069
	C	0.020354	0.212744
4	H	-0.008616	0.00459
	C	0.157855	-0.099085
	H	-0.004602	0.004433
	C	0.073896	-0.101302
5	C	0.196508	0.204567
	O	0.198561	0.034614
6	H	-0.000101	-0.003144
	H	0.011606	0.003321
	H	0.01164	-0.000229
	C	-0.01309	0.003316
total spin density		1.000002	1.000001



4.3.6 Photo-CIDNP Polarizations - Kaptein's Sign Rules

The phases of the Photo-CIDNP signals and their relation to each other can, in terms of polarization phase, qualitatively be described by Kaptein's multiplicative sign rule^[12,40] which gives a positive sign for nuclei with absorptive Photo-CIDNP signal and a negative sign for nuclei showing emissive Photo-CIDNP signals:

$$I_i = \mu \varepsilon \Delta g A_i$$

$$\varepsilon = \begin{cases} - & \text{recombination or disproportionation products} \\ + & \text{escape products} \end{cases}$$

$$\mu = \begin{cases} - & \text{triplet precursor} \\ + & \text{singlet precursor} \end{cases}$$

The radical pair is formed from either a singlet or triplet precursor differentiated by the sign of μ . The radicals of the radical pair have a difference in g-factors of Δg which can be positive or negative. Each nucleus i of both radicals has a positive or negative hyperfine coupling constant A_i to the corresponding unpaired electron. The radicals of the radical pair end up in either escape product or recombination (disproportionation) products which is considered by the sign of ε . The resulting sign as the product of all four signs yields the phase of the Photo-CIDNP polarization with a positive sign indicating an absorptive Photo-CIDNP signal and a negative sign indicating an emissive Photo-CIDNP signal.^[12] More elaborated rules for the multiplet effect (different polarizations within one multiplet additionally depending on the spin-spin coupling J) exist but are not relevant for the present experiments due to the high magnetic field in which these experiments were conducted (14.1 T).^[12,17] However, it has been shown experimentally that the sign rule can be erroneous in some cases caused by the different nuclei in the radicals sharing hyperfine interactions with the same electron. Furthermore, at high fields the net polarizations turned out to show a field dependence.^[40] Another factor that alters Photo-CIDNP signals and can eventually even lead to altering Photo-CIDNP phases is cross polarization between the different nuclei experiencing Photo-CIDNP effects (chapter 3.6.6).^[2]

To gain further insight in the formation mechanism and the character of the observed Photo-CIDNP signals the detected Photo-CIDNP phases of the different investigated flavins and flavin species were studied in matters of Kaptein's sign rules. From these studies conclusions on the interplay of the precursor spin multiplicity, the intersystem crossing within the radical pair and the singlet and triplet exit channel were drawn. The nomenclature of the involved reaction steps is shown in Figure 4-10. A spin correlated radical pair is formed from an excited precursor RFT* in the singlet or the triplet state.

The electron spin correlated radical pair itself can undergo intersystem crossing (ISC). The dependence of this intersystem crossing on the nuclear spin state causes sorting of the nuclear spins and thus Photo-CIDNP polarizations. For energetic reasons the singlet radical pair tends to form recombination products (singlet exit channel) whereas the triplet radical pair yields the escape products (triplet exit channel).

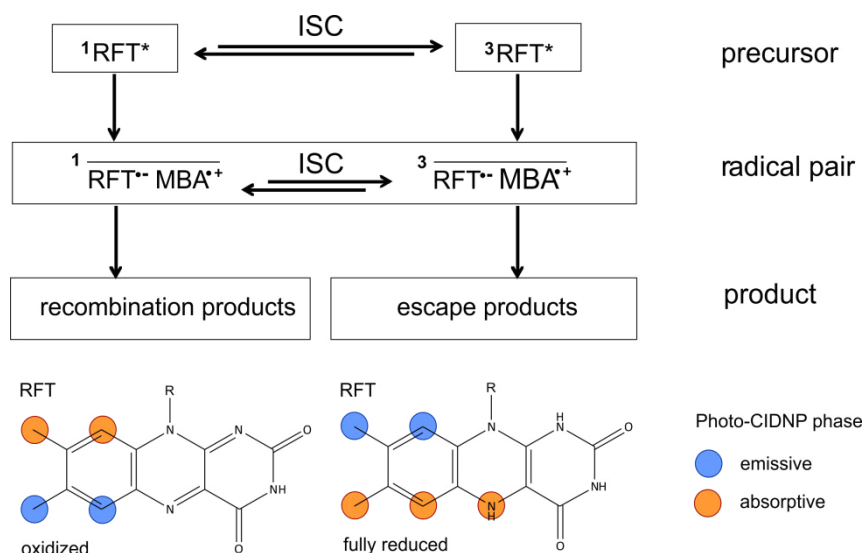


Figure 4-10 Scheme of the spin multiplicities of the chromophore RFT as the precursor of the formation of electron spin correlated radical pairs with the corresponding electron spin multiplicities. The escape product (fully reduced RFT) is formed from the triplet exit channel and the recombination product from the singlet exit channel (oxidized RFT) according to the radical pair mechanism Photo-CIDNP theory.^[2,17] The detected Photo-CIDNP polarizations in the ^1H NMR signal sets of the oxidized and the fully reduced RFT are represented by colored circles.

The Photo-CIDNP polarization phases were studied in matters of Kaptein's sign rules for RFT, the sterically hindered flavin **2b** and the heavy atom flavins F-Br and F-I together with the flavin F-H that serves as a reference for the heavy atom substituted flavins.

4.3.6.1 Riboflavin Tetraacetate

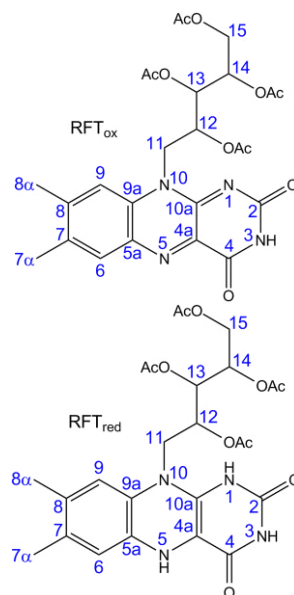
The overall signs Γ of the Photo-CIDNP polarization phases were determined experimentally, with an emissive phase being reflected in a negative sign and an absorptive signal in a positive sign. For example for the aromatic proton C(6)-H of the oxidized RFT emissive Photo-CIDNP polarization is observed. All other signs Γ for all protons exhibiting Photo-CIDNP polarizations are listed in Table 4-4 for the oxidized and the fully reduced form of RFT.

The Photo-CIDNP polarizations in the signal set of the oxidized RFT result from electron back transfer and the recombination of the radical pair. This results in a negative ϵ for Kaptein's sign rule. In contrast the reduced flavin species as the escape product of the triplet exit channel yields a positive ϵ (Table 4-4).

The signs of μ , ϵ and Δg are equal for the same ^1H signal set resulting from the same radical precursor. The only sign assumed in Kaptein's sign rule that varies with different nuclei within the same radical precursor is the sign of the hyperfine coupling constant of the respective nucleus with the unpaired radical electron. This sign is expressed by A . The comparison of the hyperfine coupling constants of numerous different isoalloxazine radicals listed in the extensive compendium Landolt-Börnstein on magnetic properties of free radicals determined by means of EPR spectroscopy^[41,42] shows that the signs of most hyperfine coupling constants depend on the substitutions of the flavins in the different possible positions. However, the sign of the hyperfine coupling constant of C(8)-H₃ is positive for all the listed semiquinone radicals irrespective of the substitution patterns for all riboflavin radicals. For this reason the sign of C(8)-H₃ was employed as a reference for the contribution of the sign of the hyperfine coupling constants to the Kaptein's sign rule with a positive sign for A of C(8)-H₃ in RFT (Table 4-4). The other signs of A of RFT were supplemented relating to the overall sign Γ . For isoalloxazine radical without methyl substitution in positions 7 and 8 no consistent signs of the hyperfine coupling constants were found for any nucleus.

Table 4-4 Photo-CIDNP recombination type and escape type polarization phases determined experimentally in the NMR signal sets of the oxidized and fully reduced RFT. The signs show the relation between the Photo-CIDNP phase Γ , the precursor electron spin multiplicity μ , the exit channel ϵ , the g-factor difference Δg and the hyperfine coupling constant A according to Kaptein's sign rule.^[12]

	RFT _{ox}					RFT _{red}				
	Γ	μ	ϵ	Δg	A	Γ	μ	ϵ	Δg	A
N(5)-H						+	+	+	-	-
C(6)-H	-	+	-	-	-	+	+	+	-	-
C(7 α)-H ₃	-	+	-	-	-	+	+	+	-	-
C(8 α)-H ₃	+	+	-	-	+	-	+	+	-	+
C(9)-H	+	+	-	-	+	-	+	+	-	+
C(11)-H ₂	+	+	-	-	+	-	+	+	-	+



For the signs for A and ϵ to yield an overall sign Γ it is obvious from Table 4-4 that μ and Δg must have opposite signs. This means if the difference in g-factors between the RFT and the MBA radical $\Delta g = g_{\text{RFT}} - g_{\text{MBA}}$ is negative the sign of μ is positive and thus the

radical pair responsible for the observed Photo-CIDNP polarizations is formed from the singlet precursor $^1\text{RFT}^*$. On the other hand, if this radical pair is formed from the triplet precursor $^3\text{RFT}^*$ (μ negative) the g-factor of the RFT radical is bigger than the one of the MBA radical.

From probability and lifetime considerations it seems likely that the radical pairs causing the Photo-CIDNP polarizations are formed from $^3\text{RFT}^*$ as the lifetime of this radical pair in the triplet state is longer than the one of the radical pair in the singlet state.^[13] The radicals that do not perform a second electron oxidation or reduction before intersystem crossing within the radical pair recombine by back electron transfer and end up as recombination products. A triplet precursor would mean a negative sign μ for Kaptein's sign rule and thus a positive Δg .

4.3.6.2 Sterically Demanding Flavin 2b

Like for RFT the overall signs Γ of the Photo-CIDNP polarization phases of flavin **2b** again were determined experimentally, with an emissive phase being reflected in a negative sign and an absorptive signal in a positive sign. The signs Γ for all protons of the sterically demanding flavin **2b** exhibiting Photo-CIDNP polarizations are listed in Table 4-5. The corresponding protons of the oxidized and the fully reduced form of RFT show opposite signs.

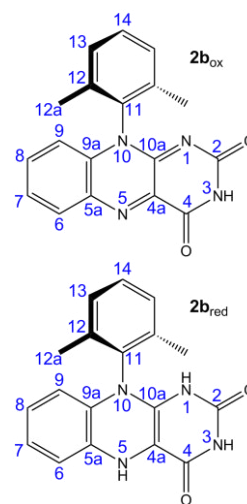
The Photo-CIDNP polarizations detected in the ^1H NMR signal set of the oxidized flavins result from the singlet exit channel and those detected in the signal set of the fully reduced flavin from the triplet channel. This results in a negative sign for ϵ for Photo-CIDNP polarizations detected in the signal set of the oxidized flavin **2b**. Correspondingly, ϵ is positive for all Photo-CIDNP polarizations detected in the ^1H NMR signal sets of the fully reduced flavin **2b**.

The signs of the hyperfine coupling constants were determined by the calculations described in chapter 4.3.5.1. They yield positive signs for the protons C(7)-H and C(9)-H and negative signs for the protons C(6)-H and C(8)-H. The signs of the hyperfine coupling constants of the protons in the flavin side chain that show Photo-CIDNP polarizations were supplemented according to the signs determined by the calculations. Both the CIDNP-polarizations detected in the ^1H NMR signal set of the oxidized and of the fully reduced flavin **2b** result from the flavin radical within the same MBA-flavin radical pair. Thus the signs A are equal for both the oxidized and the fully reduced flavin **2b**.

For the signs for A and ϵ to yield an overall sign Γ it is obvious from Table 4-5 that μ and Δg must have opposite signs. This means if the difference in g-factors between the flavin and the MBA radical $\Delta g = g_{\text{flavin}} - g_{\text{MBA}}$ is positive the sign of μ has to be negative and thus the radical pair responsible for the observed Photo-CIDNP polarizations is formed from the triplet precursor. On the other hand, if this radical pair is formed from the singlet precursor (μ positive) the g-factor of the MBA radical is bigger than the one of the flavin radical.

Table 4-5 Photo-CIDNP recombination type and escape type polarization phases determined experimentally in the NMR signal sets of the oxidized and fully reduced sterically demanding flavin **2b**. The signs show the relation between the Photo-CIDNP phase Γ , the precursor electron spin multiplicity μ , the exit channel ϵ , the g-factor difference Δg and the hyperfine coupling constant A according to Kaptein's sign rule.^[12]

	2b_{ox}					2b_{red}				
	Γ	μ	ϵ	Δg	A	Γ	μ	ϵ	Δg	A
C(6)-H	-	+	-	-	-	+	+	+	-	-
C(7)-H	+	+	-	-	+	-	+	+	-	+
C(8)-H	-	+	-	-	-	+	+	+	-	-
C(9)-H	+	+	-	-	+	-	+	+	-	+
C(13)-H	+	+	-	-	+	-	+	+	-	+
C(12a)-H ₃	+	+	-	-	+	-	+	+	-	+



This is in accordance with the observations made for RFT in chapter 4.3.2. For both the sterically demanding flavin **2b** and RFT μ and Δg have opposite signs. The first possibility is that both flavins **2b** and RFT have the same sign of Δg and the corresponding radicals are formed from the excited RFT and flavin **2b** with the same spin multiplicity. Another conceivable correlation is that the g-factors of flavin **2b** and RFT differ resulting in different signs Δg and that thus the radical pair is formed from excited flavin precursors with different spin multiplicities.

4.3.6.3 Heavy Atom Flavins F-H, F-Br and F-I

Next the heavy atom flavins F-Br and F-I were studied together with F-H as a reference. For these three flavins no signal set for the fully reduced form was detected.

Again the overall signs Γ of the Photo-CIDNP polarization phases were determined experimentally. Emissive phases are reflected in negative signs, absorptive signals in positive signs. The signs Γ for all protons exhibiting Photo-CIDNP polarizations are listed in Table 4-6.

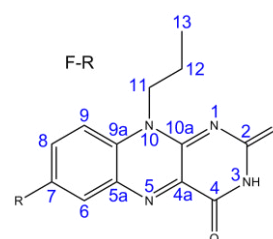
As no ^1H NMR signal set was detected for the fully reduced flavins F-H, F-Br and F-I only the Photo-CIDNP polarizations detected in the signal set of the corresponding oxidized forms were studied. The Photo-CIDNP polarizations detected in the corresponding signal sets of the oxidized flavin species result from recombination of the radical pair. Therefore the sign ε is negative.

Again the signs of the hyperfine coupling constants were determined by the calculations described in chapter 4.3.5.1. They yield positive signs for the protons C(7)-H and C(9)-H and negative signs for the protons C(6)-H and C(8)-H. The calculations of the atomic spin densities were only performed for flavin F-H (Table 4-6) due to software internal constraints.

The difference in g-value of the RFT and the MBA radical is reflected in $\Delta g = g_{\text{flavin}} - g_{\text{MBA}}$. Due to the heavy atom in the flavins F-Br and F-I (Table 4-6) and the associated high spin-orbit coupling the g-value of the corresponding radicals is higher than the one of methoxybenzyl alcohol yielding a positive value for Δg .^[20,43]

Table 4-6 Photo-CIDNP recombination type polarization phases determined experimentally in the NMR signal sets of the oxidized flavin derivatives F-H, F-Br and F-I. The signs show the relation between the Photo-CIDNP phase Γ , the precursor electron spin multiplicity μ , the exit channel ε , the g-factor difference Δg and the hyperfine coupling constant A according to Kaptein's sign rule.^[12]

	F-H					F-Br / F-I				
	Γ	μ	ε	Δg	A	Γ	μ	ε	Δg	A
C(6)-H	-	+	-	-	-	+	+	-	+	-
C(7)-H	+	+	-	-	+					
C(8)-H	-	+	-	-	-	+	+	-	+	-
C(9)-H	+	+	-	-	+	-	+	-	+	+



Overall, for flavin F-H the signs of Γ , ε and A are known. From Kaptein's sign rule it can be derived that the signs of μ and Δg have to be opposite. For the heavy atom flavins F-Br and F-I the signs of Γ , ε and Δg are known. According to Kaptein's sign rule the correlation between the signs of μ and A were determined and are listed in Table 4-6.

Remarkably, the Photo-CIDNP pattern of F-H is the inverted pattern relative to the patterns of F-Br and F-I. Possible reasons for these observations can be derived from the sign compositions in Table 4-6. The changes can be caused by the change of the g-value of flavin due to the weaker spin-orbit coupling with the missing heavy atom. For F-H thus the g-value of the flavin is smaller than that of MBA resulting in a negative value for Δg and inverted Photo-CIDNP phases of all ^1H resonances. An inversion of the Photo-CIDNP phases of adenosine, inosine and 1-methylguanosine after replacing riboflavin by a 7-methyl-8-bromo-10-(1-D-ribityl)isoalloxazine brominated riboflavin was attributed to the different g-values of the different flavin radicals.^[2,44] A second reason for the inversion of the Photo-CIDNP pattern upon heavy atom substitution suggested by the observations listed in Table 4-6 is a change of the electron spin density of the flavin radical and the resulting change of hyperfine coupling constants caused by the heavy atom substitution. Finally, the inversion of the Photo-CIDNP polarization pattern can also be explained by the change of the precursor multiplicity. The enhanced spin-orbit coupling caused by the heavy atom effect results in an increased intersystem crossing rate. The increased intersystem crossing rate can vary the contributions of the intersystem crossing of the excited precursor and the intersystem crossing within the electron spin correlated radical pair. These different contributions thus can alter the Photo-CIDNP polarizations (Figure 4-2).

4.4 Conclusion and Outlook

Most of the studies of Photo-CIDNP effects using flavins employ flavins only as a photosensitizer and focus on the Photo-CIDNP polarizations of its reaction partner. Previous studies with free flavins in solution have only marginally or not at all dealt with the Photo-CIDNP polarizations of flavins themselves. This is to a great part due to the fact that free flavins in water show only very weak or no Photo-CIDNP polarizations.^[2] It is shown that the vanishing Photo-CIDNP effects are caused by the solvent and that the change of the solvent from water to acetonitrile reveals clear Photo-CIDNP polarizations of free flavins. Comprehensive studies of the Photo-CIDNP effects in flavins themselves are presented. The Photo-CIDNP patterns of flavins were studied in detail with focus on the Photo-CIDNP patterns for both the singlet and triplet exit channel and the effect of different substituents at the isoalloxazine moiety.

The flavin Photo-CIDNP patterns resulting from the singlet and the triplet pathway were separated and elucidated. The influence of the methylation in positions 7 and 8 was studied by comparing the Photo-CIDNP polarizations of RFT with the sterically demanding flavin **2b** and flavin F-H. With flavin **2b** also the influence of the sterical demand of the flavin on its polarization pattern was studied. Finally the heavy atom substituted flavins F-Br and F-I were studied and the effect of heavy atom substitution on the Photo-CIDNP patterns was elucidated by comparing the heavy atom flavins to a reference flavin F-H. Spectroscopic and mechanistic implications of substitutions with methyl groups and heavy atoms enhancing spin-orbit coupling were discussed in terms of Kaptein's sign rule and supported by DFT calculations. The substitution of the isoalloxazine moiety by methyl groups in position 7 and 8 does not have an effect on the associated Photo-CIDNP patterns arising from the singlet and triplet exit channel. This suggests that these substitutions do not have a major impact on the overall reaction mechanism. In particular the substitutions are not expected to change the precursor multiplicity or the g-factor difference between the radicals of the primary radical pair. In contrast the substitution at the isoalloxazine ring system by a heavy atom inverts the Photo-CIDNP patterns. This can be due to a change of the g-factor of the flavin radical by the heavy atom flavins, modified hyperfine coupling constants or changing the multiplicity of the radical pair precursor. DFT calculations for the heavy atom substituted flavins seem very promising to elucidate if the inversion of the Photo-CIDNP pattern upon the substitution by a heavy atom is caused by changing hyperfine coupling constants or due to the variation of the contributions of the singlet and triplet exit channel to the overall polarization pattern. Calculations of the g-factors of the different flavin and

alcohol radicals could be used to determine the g-factor difference between the radicals in the radical pair $\Delta g = g_{\text{RFT}} - g_{\text{MBA}}$. By that all the other signs contributing to Kaptein's sign rule could be determined and the influence of the substitutions on the precursor multiplicity can be elucidated.

4.5 Additional Experimental Findings

4.5.1 Heavy Atom Flavins - Quantum Yields and Chemical Conversions

The quantum yields for the oxidation of methoxybenzyl alcohol catalyzed by the new heavy atom flavins were measured and compared to the quantum yield of RFT. For RFT the quantum yield was measured to be 0.5 %, for the propyl side chain flavin with hydrogen in position 7 2.0 %, for the bromine substituted one 3.1 % and for the iodine substituted one 2.0 %.^[35,45] In general the flavins with the propyl side chain show higher product quantum yields than RFT. Among these flavins the bromine substituted one is the most effective. The iodine one with the same product quantum yield as the flavin without heavy atom shows that there is no correlation between the introduction of a heavy atom and the achieved product quantum yield. The heavy atom effect enhances spin-orbit coupling and thus the probability for intersystem crossing.^[31,33,34] However, not only the intersystem crossing from the singlet to the reactive triplet state is enhanced but also intersystem crossing in the opposite direction. In diffusion controlled reactions like the photooxidation of benzyl alcohols to the corresponding aldehydes catalyzed by flavins^[13] a too high intersystem crossing rate can have a negative effect on the overall product quantum yield.^[35]

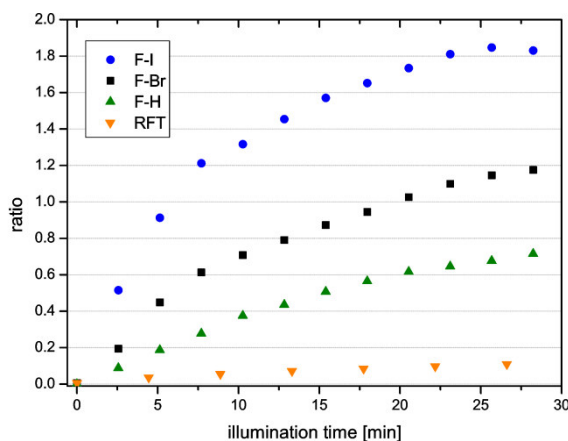


Figure 4-11 Reaction profile of the formation of methoxybenzyl aldehyde from 20 mM methoxybenzyl alcohol (not shown) catalyzed by different flavins as photocatalysts (2 mM riboflavin tetraacetate RFT, 2 mM F-H, 2 mM F-Br and 2 mM F-I) in CD₃CN. The amount of formed aldehyde was referenced to the initial amount of flavin (2mM).

To investigate the influence of the heavy atom substitution on the product formation the reaction of 20 mM methoxybenzyl alcohol to the corresponding aldehyde catalyzed by 2 mM of flavin was studied. For this purpose four samples with the different flavin derivatives RFT, F-H, F-Br and F-I were prepared and the formation of the aldehyde was monitored by rows of ¹H spectra during *in situ* illumination of the different samples. The observed aldehyde signal at 9.86 ppm is not affected by Photo-CIDNP polarization under

the applied conditions and was thus used as a monitor for the aldehyde formation. Figure 4-11 shows the reaction profile of the aldehyde formation catalyzed by the different flavin derivatives. It is obvious from the kinetics that the use of F-H instead of RFT significantly accelerates the product formation. A further comparison between the product formations catalyzed by F-H, F-Br and F-I reveals that with increasing atomic number in position 7 also the product formation rate increases.

The flavin derivative F-Br is not the best among the tested flavins as it could be expected from the quantum yield measurements that reported F-Br to have a higher quantum yield than F-H and F-I. The heavy atom flavins F-Br and especially the heavy atom flavin F-I showed fast decomposition compared to RFT. This suggests that the energy absorbed by the different molecules is partially wasted for decomposition of the photocatalyst.

4.5.2 Temperature Dependent Photo-CIDNP Polarizations

In order to minimize chemical exchange and thus make the signals of chemically exchanging protons sharp the reaction was conducted at lower temperatures (CD_3CN : 250 K, $\text{CD}_3\text{CN}/\text{D}_2\text{O}$ (1:1): 280 K). One unanticipated result to emerge from these studies at different temperatures is that surprisingly with temperature some Photo-CIDNP phases changed significantly. The temperature dependence of the Photo-CIDNP polarizations is shown in Figure 4-12 for RFT in the oxidized and fully reduced form corresponding to the singlet and triplet exit channel respectively at 250 K and 300 K. As described before the Photo-CIDNP polarization phases detected in the RFT ^1H resonances of the oxidized RFT and the fully reduced RFT at 300 K complement each other in terms of the signs of polarization. This is not particularly surprising keeping in mind that the creation of Photo-CIDNP polarization results from sorting of nuclear spins. So for each polarization caused by nuclear spin sorting there must be a complementary polarization of nuclear spins of the opposite phase sorted in the product of the other reaction path (singlet exit channel / triplet exit channel). The situation changes drastically when the sample is cooled down to 250 K (Figure 4-12 B). The polarization pattern corresponding to the singlet exit channel detected in the ^1H signal set of the oxidized flavin does not change with lowering the temperature to 250 K. However, the comparison of the Photo-CIDNP polarization patterns at different temperatures shows that the pattern of the fully reduced RFT changes drastically. Surprisingly, at 250 K all proton resonances carrying Photo-CIDNP polarizations (C(6)-H, C(7 α)-H₃, C(8 α)-H₃ and C(9)-H) show the same polarization phases and thus do not longer correspond to the polarization pattern detected in the respective signal set for the oxidized RFT. This means that at 300 K the Photo-CIDNP polarizations of the

corresponding nuclei in the oxidized and reduced form of RFT complement each other, i.e. for every emissive Photo-CIDNP signal there is a corresponding absorptive Photo-CIDNP signal of the corresponding nucleus. However, at 250 K the Photo-CIDNP spectra do not complement each other any longer.

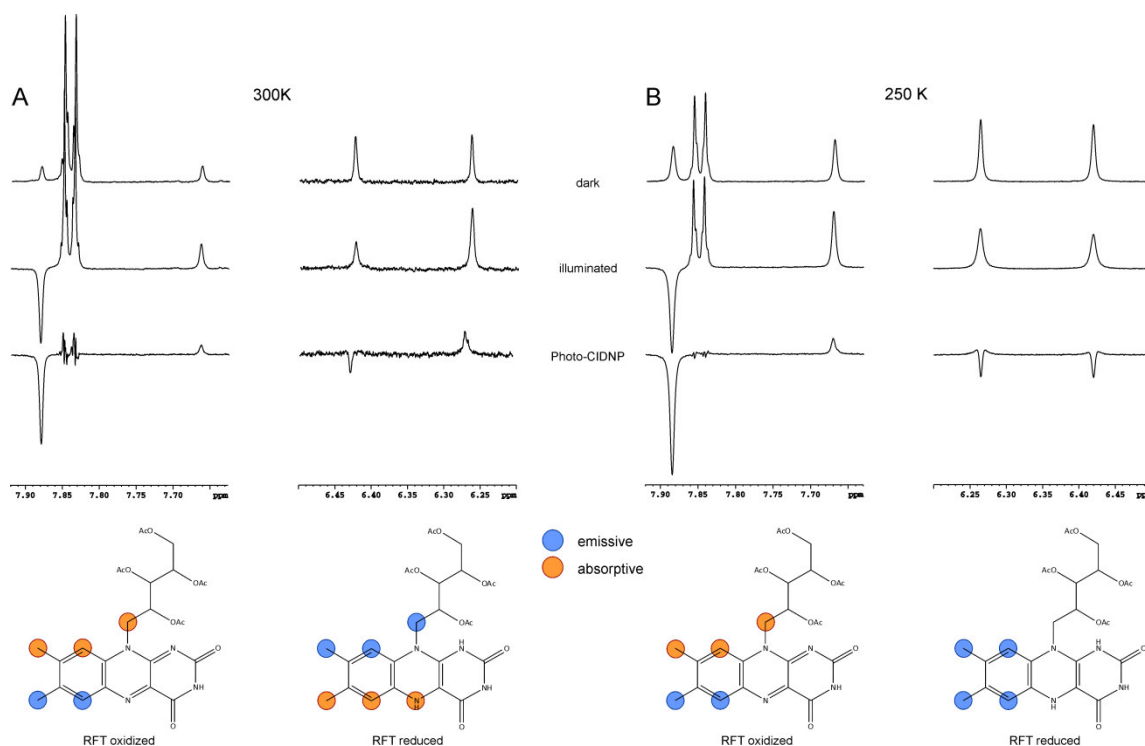


Figure 4-12 ^1H spectra showing exemplarily the signals of the aromatic proton resonances of the oxidized and reduced flavin of the dark, the illuminated sample and the resulting Photo-CIDNP spectra. The circles in the molecule structures depict the resulting Photo-CIDNP polarization phases of the RFT protons at 300 K and at 250 K. Blue circles depict emissive ^1H Photo-CIDNP signals, orange circles absorptive ^1H Photo-CIDNP signals.

Temperature dependent changes of Photo-CIDNP phases have been reported by some groups. Grimme *et al.* reported on an inversion of the Photo-CIDNP polarization signs with varying temperatures in the photolysis of (N-methylanilino)acetone. The inversion of the Photo-CIDNP phases was attributed to the temperature dependent domination of different precursor spin multiplicities.^[46] However, in this study all phases detected in the geminate recombination products and the escape products exhibited phase inversion. Another temperature dependence of Photo-CIDNP polarizations after illumination of cyclopent-2-enyl methyl ketones was reported by Henne *et al.*^[47]

A modification of the initial Photo-CIDNP polarization phases generated by nuclear spin sorting in the electron spin correlated radical pair by means of cross polarization^[2,48,49] can be excluded because cross polarization can be expected to take effect on both the polarizations in the oxidized flavin species and the reduced flavin species in the same way. This means that for cross polarization altering the polarization patterns both

patterns of the oxidized and the fully reduced RFT would be altered in the same way so that the patterns would again complement each other. The surprising dependence of the polarization patterns of the fully reduced RFT on the temperature thus has to be considered in terms of a changing reaction mechanism such as a radical pair substitution involving different flavin radicals or the competition between disproportionation and two-electron reduction of the flavin. These different radicals with different hyperfine coupling constants impose different contributions to the overall Photo-CIDNP polarization. To elucidate the cause for the observed temperature dependence time resolved Photo-CIDNP studies or variations of the photocatalyst concentrations seems most promising.

4.6 Experimental Details

The NMR spectra were measured with solutions of 2 mM of the respective flavin and 20 mM methoxybenzyl alcohol (MBA) in CD₃CN or CD₃CN/D₂O (1:1). To minimize the Photo-CIDNP relaxation and to separate the singlet from the triplet channel the sample was deoxygenated by purging the solution with argon for 1 hour as described in literature.^[2] Subsequently the samples were transferred under argon atmosphere into a NMR tube and sealed airtight. NMR spectra were recorded on a Bruker Avance 600 spectrometer with a 5 mm broadband triple resonance z-gradient probe. The temperature of 300 K, 280 K and 250 K was controlled by a Bruker BVTE 3000 unit. Alternatingly measurements of ¹H spectra with and without illumination were conducted. *In situ* illumination of the samples was realized with a LED based illumination device.^[18] All light spectra are recorded with continuous illumination of the sample over the whole ¹H pulse sequence. Spectra of the illuminated samples were subtracted from the ones recorded without illuminating the sample to yield the Photo-CIDNP spectra. As the appearance of the Photo-CIDNP polarizations in terms of polarization phases does not change during illumination spectra with the highest Photo-CIDNP intensities are displayed. NMR data were processed with Bruker TOPSPIN 3.0. As a light source a Cree XP-E high power LED with a center wavelength of 455 nm and 500 mW optical output power operated at a current of 1 A was used, according to the absorption maximum of RFT.^[13] The kinetics were derived from the integrals of the corresponding signals referenced to a signal in the first spectrum. In the case of F-H a small amount of aldehyde was formed before starting *in situ* illumination of the sample. For comparability of the kinetics the amount of aldehyde already formed before illumination was subtracted from all following signals. All assignments were made by a complete standard set of 1D and 2D NMR spectra consisting of ¹H, ¹³C, ¹H,¹H-COSY, ¹H,¹H-NOESY, ¹H,¹³C-HSQC and ¹H,¹³C-HMBC. An exception is the assignment of the fully reduced riboflavin tetraacetate in CD₃CN/D₂O (1:1). The line broadening inhibits the assignment by 2D NMR and the proton resonances were assigned in analogy to the fully reduced riboflavin tetraacetate in CD₃CN. With the proton resonances at 1.93 ppm and 2.09 ppm corresponding to the methyl groups in positions 7 and 8 (2.03 ppm and 2.06 ppm for pure CD₃CN) and the signals at 6.30 ppm and 6.45 ppm corresponding to the aromatic protons C(6)-H and C(9)-H (6.28 ppm and 6.43 ppm for pure CD₃CN). The chemical shifts were referenced to the ¹H chemical shift of tetramethylsilane (TMS) of 0.00 ppm.

Density-functional (DFT) calculations were performed with the program package Gaussian 09 and carried out at the LRZ Linux cluster at the Leibniz Supercomputing

Centre in Munich. Geometry optimizations of the corresponding molecules were conducted with the hybrid functional B3LYP and the 6-31G(d) basis set. Calculations of the Mullikan spin densities were performed with the hybrid functional B3LYP and the basis set EPR-II.

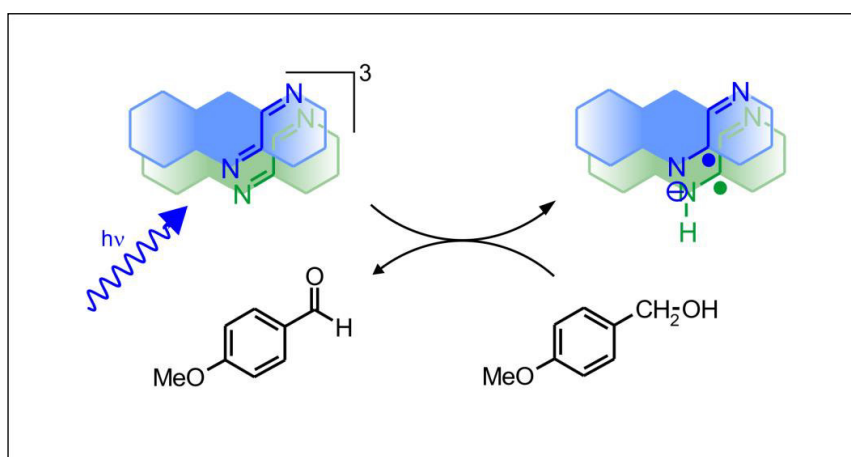
4.7 References

- [1] M. Goez, in *Adv. Photochem.* (Eds.: D. Neckers, D. Volmann, G. Büнау), Wiley New York, **1997**.
- [2] P. J. Hore, *Photo-CIDNP of Biopolymers*, Pergamon Press, Oxford, **1993**.
- [3] H. Hayashi, *Introduction to Dynamic Spin Chemistry*, World Scientific Publishing, **2004**.
- [4] L. Kuhn, in *Top. Curr. Chem.*, Springer Berlin Heidelberg, **2013**, pp. 1–72.
- [5] N. J. Turro, V. Ramamurthy, J. C. Scaiano, *Modern Molecular Photochemistry of Organic Molecules*, University Science Books, **2010**.
- [6] M. Goez, in *Adv. Photochem.*, John Wiley & Sons, **2007**, pp. 63–163.
- [7] R. Miura, *Chem. Rec.* **2001**, *1*, 183–194.
- [8] A. M. Edwards, in *Flavins Photochem. Photobiol.*, The Royal Society Of Chemistry, **2006**, pp. 1–11.
- [9] V. Massey, *Biochem. Soc. Trans.* **2000**, *28*, 283–296.
- [10] M. W. Fraaije, A. Mattevi, *Trends Biochem. Sci.* **2000**, *25*, 126–132.
- [11] S. Ghisla, V. Massey, *Eur. J. Biochem.* **1989**, *181*, 1–17.
- [12] R. Kaptein, *J. Chem. Soc. D* **1971**, *0*, 732–733.
- [13] U. Megerle, M. Wenninger, R.-J. Kutta, R. Lechner, B. König, B. Dick, E. Riedle, *Phys. Chem. Chem. Phys.* **2011**, *13*, 8869–8880.
- [14] J. Svoboda, H. Schmaderer, B. König, *Chem. – A Eur. J.* **2008**, *14*, 1854–1865.
- [15] J. Daďová, S. Kümmel, C. Feldmeier, J. Cibulková, R. Pažout, J. Maixner, R. M. Gschwind, B. König, R. Cibulka, *Chem. – A Eur. J.* **2013**, *19*, 1066–1075.
- [16] H. Schmaderer, P. Hilgers, R. Lechner, B. König, *Adv. Synth. Catal.* **2009**, *351*, 163–174.
- [17] M. Goez, in *Annu. Reports NMR Spectrosc.* (Ed.: A.W. Graham), Academic Press, **2009**, pp. 77–147.
- [18] C. Feldmeier, H. Bartling, E. Riedle, R. M. Gschwind, *J. Magn. Reson.* **2013**, *232*, 39–44.
- [19] M. Goez, G. Eckert, U. Müller, *J. Phys. Chem. A* **1999**, *103*, 5714–5721.
- [20] G. Eckert, M. Goez, B. Maiwald, U. Müller, *Berichte der Bunsen Gesellschaft* **1996**, *100*, 1191–1198.

- [21] I. R. Gould, R. H. Young, R. E. Moody, S. Farid, *J. Phys. Chem.* **1991**, *95*, 2068–2080.
- [22] I. R. Gould, D. Ege, J. E. Moser, S. Farid, *J. Am. Chem. Soc.* **1990**, *112*, 4290–4301.
- [23] C. Reichardt, T. Welton, *Solvents and Solvent Effects in Organic Chemistry*, Wiley-VCH Verlag, **2010**.
- [24] R. Kaptein, K. Dijkstra, F. Müller, C. G. van Schagen, A. J. W. G. Visser, *J. Magn. Reson.* **1978**, *171*.
- [25] P. J. Hore, E. R. P. Zuiderweg, R. Kaptein, K. Dijkstra, *Chem. Phys. Lett.* **1981**, *83*, 376–383.
- [26] M. N. Berberan Santos, *PhysChemComm* **2000**, *3*, 18–23.
- [27] M. Rae, F. Perez-Balderas, C. Baleizão, A. Fedorov, J. A. S. Cavaleiro, A. C. Tomé, M. N. Berberan-Santos, *J. Phys. Chem. B* **2006**, *110*, 12809–12814.
- [28] R. H. Hofeldt, R. Sarai, S. H. Lin, *J. Chem. Phys.* **1970**, *53*, 4512 – 4518.
- [29] A. C. Neto, L. C. Ducati, R. Rittner, C. F. Tormena, R. H. Contreras, G. Frenking, *J. Chem. Theory Comput.* **2009**, *5*, 2222–2228.
- [30] M. Kaupp, O. L. Malkina, V. G. Malkin, P. Pyykkö, *Chem. – A Eur. J.* **1998**, *4*, 118–126.
- [31] N. J. Turro, V. Ramamurthy, J. Scaiano, *Modern Molecular Photochemistry of Organic Molecules*, Palgrave Macmillan, **2010**.
- [32] Y. Nomura, Y. Takeuchi, N. Nakagawa, *Tetrahedron Lett.* **1969**, *10*, 639–642.
- [33] J. W. Verhoeven, *Pure Appl. Chem* **1996**, *68*, 2223–2286.
- [34] J. B. Birks, *Photophysics of Aromatic Molecules*, John Wiley & Sons, **1970**.
- [35] S. Kümmel, *Chemical Photocatalysis with Flavins - New Applications and Catalyst Improvement*, University of Regensburg, **2013**.
- [36] O. B. Morozova, K. L. Ivanov, A. S. Kiryutin, R. Z. Sagdeev, T. Kochling, H. M. Vieth, A. V Yurkovskaya, *Phys. Chem. Chem. Phys.* **2011**, *13*, 6619–6627.
- [37] R. G. Brereton, J. K. M. Sanders, *Org. Magn. Reson.* **1982**, *19*, 150–152.
- [38] A. S. Kiryutin, O. B. Morozova, L. T. Kuhn, A. V Yurkovskaya, P. J. Hore, *J. Phys. Chem. B* **2007**, *111*, 11221–11227.
- [39] G. Richter, S. Weber, W. Römisch, A. Bacher, M. Fischer, W. Eisenreich, *J. Am. Chem. Soc.* **2005**, *127*, 17245–17252.
- [40] P. J. Hore, S. Stob, J. Kemmink, R. Kaptein, *Chem. Phys. Lett.* **1983**, *98*, 409–413.

- [41] A. Berndt, F. A. Neugebauer, *Landolt-Börnstein - Numerical Data and Functional Relationships in Science and Technology II/17c Magnetic Properties of Free Radicals, Conjugated Carbon-Centered and Nitrogen Radicals*, Springer, **1987**.
- [42] O. Madelung, Ed., *Landolt-Börnstein - Numerical Data and Functional Relationships in Science and Technology II/17h Magnetic Properties of Free Radicals*, Springer, **1985**.
- [43] L. T. Muus, P. W. Atkins, K. A. McLauchlan, J. B. Pederson, *Nachrichten aus Chemie, Tech. und Lab.* **1977**.
- [44] E. F. McCord, K. M. Morden, A. Pardi, I. Tinoco, S. G. Boxer, *Biochemistry* **1984**, *23*, 1926–1934.
- [45] R. J. Kutta, B. Dick, Blitzlichtphotolyse - Untersuchung zu LOV-Domänen und photochromen Systemen, University of Regensburg, **2012**.
- [46] S. Grimme, H. Dreeskamp, *J. Photochem. Photobiol. A Chem.* **1992**, *65*, 371–382.
- [47] A. Henne, N. P. Y. Siew, K. Schaffner, *Helv. Chim. Acta* **1979**, *62*, 1952–1965.
- [48] F. J. J. De Kanter, R. Kaptein, *Chem. Phys. Lett.* **1979**, *62*, 421–426.
- [49] G. L. Closs, M. S. Czeropski, *Chem. Phys. Lett.* **1977**, *45*, 115–116.

5 Solvent Stabilized Radical Intermediates in Flavin Catalyzed Reactions: One- vs. Two-Electron Oxidations



The sample preparation and the NMR measurements of the fully deoxygenated CD₃CN/D₂O sample (Figure 5-2 C and Figure 5-6 B) were done by Hanna Bartling.

Christian Feldmeier, Ruth M. Gschwind

5.1 Abstract

The importance of flavin as a cofactor is to a great extent due to its ability to act as both a one- or two-electron mediator, with the role as an one-electron mediator being associated with the protein being able to stabilize the semiquinone radical. In this study it is shown that the stabilization of the semiquinone radical and the associated role of the flavin to act as a one-electron oxidation agent are also possible in solution and can be tuned by variation of the solvent. This is shown by a combination of NMR, UV/Vis and Photo-CIDNP spectroscopy on flavin catalyzed photooxidations of benzyl alcohols as a model system. Whereas for acetonitrile no stabilization of the flavin radical intermediate is observed the addition of water stabilizes the semiquinone radical and makes it act as a resting state after one-electron reduction of the substrate. In contrast, on the substrate side no radical is stabilized and the substrate is oxidized by two electrons. The stabilization of the radical is associated with enhanced chemical exchange between the three different oxidation states. Therefore the stabilization of the radical intermediate by water is proposed to be the reason for the strong solvent dependence of the efficiency of flavin catalyzed photooxidations.

5.2 Introduction

Flavins are extraordinarily versatile cofactors that are able to catalyze a huge variety of different biochemical reactions in various proteins. They exist mostly in the form of flavin mononucleotide (FMN) or flavin adenine dinucleotide (FAD). What sets flavin apart from other cofactors is its unique capacity to act both as a one-electron and two-electron mediator in redox reactions.^[1-5] This important property enables them to mediate between two-electron oxidations of organic substrates and the respiratory chain with one-electron transfers.^[3] Flavoenzymes have been classified by their substrates or by the kind of reactions they catalyze.^[3,6] An alternative classification of flavoenzymes by Miura is based on the number of electron transfers in both the reductive and the oxidative part of the reaction. Thereby, the flavoenzymes are grouped into the class 2/1 for a two-electron transfer in the reductive half of the reaction and an one-electron transfer in the oxidative part, and classes 1/1 and 2/2 for one-electron or respectively two-electron transfers on both sides of the reaction.^[1] The function of the flavin depends strongly on the protein and its interactions with the flavin cofactor. The role of the flavin to act either as a one-electron or a two-electron mediator is associated with the ability of the protein to stabilize the semiquinone radical with some proteins being able to stabilize almost 100 % of the radical.^[2,3,7]

Apart from its importance in biology flavin is increasingly gaining attention as a photocatalyst.^[5,8-12] Many derivatives of natural flavins have been synthesized and are employed as effective photocatalysts for the oxidation of various substrates among others for phenols,^[13] indols,^[14] glucose,^[15] dopamine,^[16] benzyl methyl ethers,^[10] benzyl amines,^[17] benzyl alcohols^[10] or methylbenzenes.^[16] Much is known about the enzymatic catalysis by flavins as cofactors in proteins, but there has been little discussion about flavin mechanisms as a chemical photocatalyst in solution. Especially the interactions of flavin with the solvent molecules and the consequences of these interactions for the overall reaction mechanism have not been addressed so far. In particular nothing about the influence of the surroundings being the solvent in synthetic chemistry on the ability of the flavin catalyst to act as a one-electron or two-electron mediator has been reported so far to the best of our knowledge.

Here we present a combined NMR, UV/Vis and Photo-CIDNP spectroscopic mechanistic study that demonstrates on the model system of the riboflavin tetraacetate catalyzed photooxidation of methoxybenzyl alcohol to the corresponding aldehyde that also in synthetic applications flavin can act as a one-electron oxidizing agent due to the stabilization of the flavin radical.

5.3 Results and Discussion

5.3.1 Model System

To investigate the influence of the solvent on the flavin reduction state the flavin catalyzed photooxidation of benzyl alcohols^[8,10–12,18] to the corresponding aldehydes was chosen as a model reaction (Figure 5-1). In the overall reaction two electrons are transferred from methoxybenzyl alcohol (MBA) to riboflavin tetraacetate (RFT) after excitation of the photocatalyst by blue light leading to the formation of methoxybenzyl aldehyde and the reduced RFT. Subsequently RFT is reoxidized by oxygen yielding H₂O₂ as a second reaction product and closing the catalytic cycle. To study exclusively the reductive side of the cycle and to be able to detect and characterize its reaction intermediates all reactions were performed under anaerobic conditions to prevent the reduced flavin from reoxidizing. In this way different reduced flavin species were stabilized and characterized by a combination of NMR and UV/Vis spectroscopy and the stoichiometry of the product and the reduced flavin species was monitored over the reaction time.

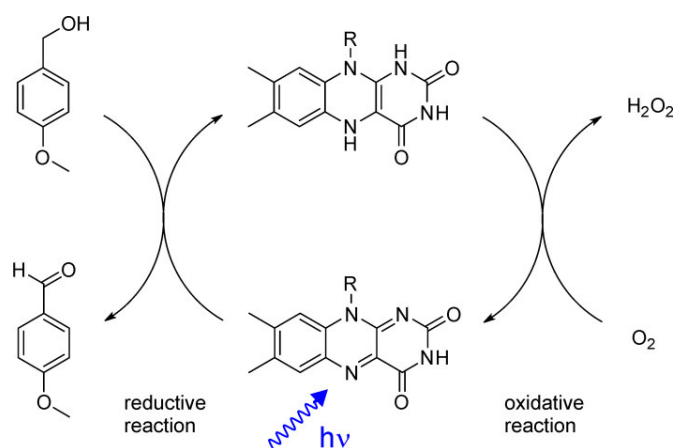


Figure 5-1 Reaction scheme of the model system. Flavin is excited by blue light ($\lambda = 455$ nm) and oxidizes methoxybenzyl alcohol to the corresponding aldehyde. The photocatalyst is reoxidized by oxygen under production of hydrogen peroxide. To study only the reductive side and intermediates of the cycle the experiments were conducted under anaerobic conditions. In this way the reduced flavin species is stabilized and at the same time the exact stoichiometry of the product and reduced flavin formation could be determined.

Three redox states of flavin isoalloxazine can be stabilized. It can appear in the oxidized state (quinone), in the one-electron reduced state (semiquinone) or in the fully two-electron reduced state (hydroquinone). All redox states can appear in the cationic, neutral or anionic form.^[1,2,19] The quinone and the hydroquinone are diamagnetic and accessible by NMR spectroscopy.^[20–23] In contrast the semiquinone as a paramagnetic radical is not directly accessible NMR but by means of Photo-CIDNP,^[24] EPR^[25] and UV/Vis spectroscopy.^[18,26]

To elucidate the influence of the surroundings of the flavins on the flavin oxidation state and the associated role of flavin as a one- or two-electron acceptor in the photooxidations the studies were conducted with different solvents (pure CD₃CN and CD₃CN/D₂O (1:1) mixture). It is known from synthetic applications that in comparison to the situation in pure CD₃CN the addition of D₂O causes a strong acceleration of the product formation.^[11,12,18,27]

5.3.2 Reduced Flavin Species - Characterization and Stabilization

5.3.2.1 NMR

First it was studied which form of the reduced flavin (semiquinone or hydroquinone) is stabilized in the different solvents pure CD₃CN and CD₃CN/D₂O (1:1) mixture. The interruption of catalytic cycles by omitting substrates or using substrates of poor reactivity has proven to be a successful strategy for the stabilization and NMR detection of otherwise inaccessible elusive intermediates like Cu(I) and Cu(III) intermediates^[28–30] or the enamine intermediate.^[31] In the case of flavin the catalytic cycle was interrupted by excluding oxygen from the reaction mixture and thus preventing the reduced flavin from reoxidizing. As a result the reduced flavin species could be accumulated and characterized spectroscopically. The reaction was conducted directly inside the NMR spectrometer by illuminating the NMR sample inside the NMR tube by a LED based illumination device.^[32] In this way photochemical reactions can be run directly inside the spectrometer under synthetic conditions. Figure 5-2 B shows ¹H spectra of the reaction mixture of 2 mM riboflavin tetraacetate (RFT) and 20 mM methoxybenzyl alcohol (MBA) in deoxygenated CD₃CN before illumination, and exemplarily ¹H spectra of the reaction mixture after 1 h of illumination and after 2 h of illumination. The ¹H spectra were all recorded of dark samples so that the signal intensities are not affected by additional Photo-CIDNP polarizations.^[24,33] With ongoing illumination a new signal set for the product methoxybenzyl aldehyde appears (black). While the signals of the oxidized flavin (blue) decrease during the reaction a complete new signal set (green) appears. This diamagnetic species was assigned to the fully two-electron reduced flavin by a complete set of 1D and 2D NMR spectra consisting of ¹H, ¹³C, ¹H,¹H-COSY, ¹H,¹H-NOESY, ¹H,¹³C-HSQC and ¹H,¹³C-HMBC (data not shown). The signal set of the fully reduced flavin is conserved if the light is switched off. The addition of oxygen to the reaction mixture leads to immediate reoxidation of the flavin making the signal set of the fully reduced flavin disappear and the signal set of the oxidized flavin reappear. The one-electron reduced flavin semiquinone radical is short lived, transient and paramagnetic and thus not detectable directly by means of NMR. Its lifetime is too short

to have a noticeable effect on the NMR line width by acting as an additional relaxation source (Figure 5-2 B). It is however evident as a transient intermediate from Photo-CIDNP measurements (Figure 5-2 D). Photo-CIDNP spectra were yielded from the difference of subsequently recorded ^1H spectra of the illuminated and the dark sample. Nuclear spin selective intersystem crossing in radical pairs of photochemical reactions together with electron spin multiplicity dependent reaction pathways result in a sorting of nuclear spins and thus in anomalous signal intensities in the NMR spectra of the illuminated samples. By these additional Photo-CIDNP polarizations transient paramagnetic radical intermediates are detected in their diamagnetic products by means of NMR.^[24,33–36] The Photo-CIDNP polarization phases (emissive or absorptive) detected in the signal sets for the oxidized and the fully reduced RFT are depicted in Figure 5-2 D. The reaction is initiated by an electron transfer from MBA to RFT.^[18] The spin correlated radical pair in the singlet state recombines and results in the Photo-CIDNP effects in the signal set of the oxidized flavin the product from back electron transfer after formation of the spin correlated initial radical pair. The radical pair in the triplet state yields the product of the reaction and causes the Photo-CIDNP polarizations in the signal set of the fully reduced RFT (compare chapter 4.3.2).

If the reaction is performed in deoxygenized $\text{CD}_3\text{CN}/\text{D}_2\text{O}$ (1:1) mixture the situation and the character of the reduced flavin species changes drastically (Figure 5-2 C). After starting the illumination the signals of the oxidized flavin rapidly decrease and broaden. The broadening of signals caused by the illumination only affects the signals of the flavin but neither the ones of the alcohol, the aldehyde or the solvents. Figure 5-2 C shows ^1H spectra before illumination, after 1 h of illumination and after 2 h of illumination. Before illumination all signals are sharp, after 1 h of illumination the signals of the oxidized flavins got broad and decreased, a new sharp signal set for the product methoxybenzyl aldehyde appeared. Additionally new broadened signals of the fully reduced flavin species appear. Figure 5-2 C shows the aromatic protons C(6)-H and C(9)-H exemplarily for the new broadened signal set of the fully reduced flavin. The broadening of the signals of the oxidized flavin is much more pronounced for the signals of the isoalloxazine ring system where the electron density of the unpaired electron of the flavin semiquinone radical is distributed. The signals of the flavin side chain show less line broadening with increasing distance from the isoalloxazine ring system (see supporting information). With continued illumination the lines continue to flatten. After turning off the light the product formation stops immediately and the broadened lines remain broad. Without any changes in conditions they remain broad for hours. Addition of oxygen and shaking the mixture makes the flavin signals recover again to sharp lines

(see supporting information). In contrast to pure CD_3CN as the solvent no Photo-CIDNP polarizations are detected when the reaction is conducted in deoxygenated $\text{CD}_3\text{CN}/\text{D}_2\text{O}$ (1:1) mixture.

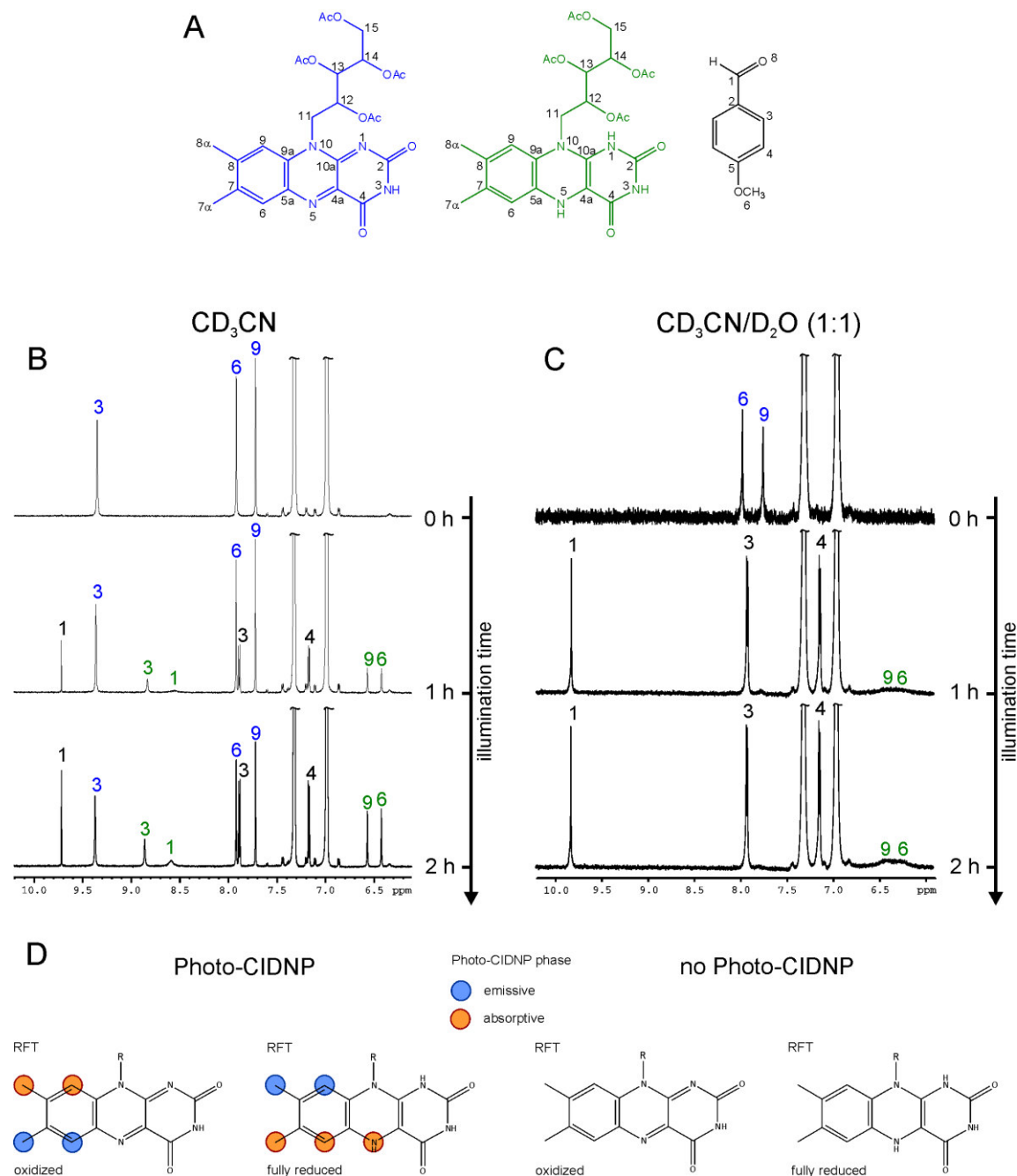


Figure 5-2 ^1H NMR spectra recorded in the course of the formation of methoxy benzyl aldehyde (black) from 20 mM methoxybenzyl alcohol (not shown) catalyzed by 2 mM riboflavin tetraacetate (oxidized RFT: blue, fully reduced RFT: green) in deoxygenated CD_3CN (B) and $\text{CD}_3\text{CN}/\text{D}_2\text{O}$ (1:1) (C). D) shows the Photo-CIDNP polarizations detected in the oxidized and fully reduced flavin species. A) shows the labeling of the flavin species and the product of the reaction. The spectra of the solution in CD_3CN were recorded at 250 K, the spectra of the solution in $\text{CD}_3\text{CN}/\text{D}_2\text{O}$ (1:1) at 280 K to minimize chemical exchange.

The missing Photo-CIDNP effect in the ^1H signal set of the fully reduced flavin after the addition of water can be explained by disproportionation of the flavin radicals to their

diamagnetic counterparts and degenerated exchange cancelation of Photo-CIDNP polarizations.^[24,37,38] Disproportionation of the semiquinone radicals makes 50 % of the Photo-CIDNP sorted nuclear spins end up as recombination products (oxidized flavin) and thus reduces Photo-CIDNP polarizations. The broadened NMR resonances of the oxidized and fully reduced flavin that get sharper at lower temperatures (data not shown) suggest facilitated exchange between the different RFT redox states. This exchange mixes the nuclear spins that were sorted by nuclear spin dependent intersystem crossing at the stage of the electron spin correlated RFT/MBA radical pair. Thus the nuclear spin sorting is undone and the Photo-CIDNP polarizations in the diamagnetic products are deleted. A third factor likely to contribute to the Photo-CIDNP cancelation upon the addition of water to the reaction mixture is the faster separation of the initial ionic radical pair associated with the high polarity of water. The back electron transfer is hampered by the solvent separated radical pair and thus the sorting of nuclear spins by the Photo-CIDNP effect in the recombination product (oxidized RFT) diminished.

The observations of the flavin line-broadening are in accordance with a line broadening of the ¹H and ¹³C NMR resonances of flavin mononucleotide (FMN) ring systems in deoxygenated solution that was described for other systems and attributed to the formation of the semiquinone radical.^[39,40]

5.3.2.2 UV/Vis

UV/Vis measurements were conducted to show that the observed line broadening after the addition of water is caused by the semiquinone radical. UV/Vis spectroscopy has proven effective and has gained widespread recognition for the detection and characterization of radicals in general and in particular for flavin semiquinone radicals.^[18,26]

Compared to the absorption spectrum of the oxidized flavin with the characteristic well-resolved absorption bands located at about 450 nm ($S_0 \rightarrow S_1$ transition) and at about 360 nm ($S_0 \rightarrow S_2$ transition) the absorption spectra of the semiquinone radicals are characterized by an additional spectral feature at about 580 nm.^[18,26] The full reduction of flavin is usually associated with bleaching of the sample and disappearing of the well-resolved absorption bands. The corresponding UV/Vis spectra have rather structureless and atypical absorption in the near UV and visible range strongly changing with conditions most probably caused by the butterfly-bending conformational changes.^[41,42]

The characteristic absorption bands of the flavin semiquinone radical in UV/Vis spectroscopy^[18,26] were employed to characterize the radical and to study the influence of the solvents and concentrations of both RFT and MBA on the stabilization of the semiquinone radical.

First a sample of 2 mM RFT and 20 mM MBA solved in deoxygenated CD₃CN/D₂O (1:1) was prepared to provide direct comparability of the UV/Vis measurements with the NMR measurements described before and to elucidate by means of UV/Vis spectroscopy if the broadened NMR signals are caused by the formation of a stable semiquinone radical. Figure 5-3 shows the UV/Vis spectra of the reaction mixture after different illumination times with 455 nm light. Figure 5-3 A shows the spectra with the characteristic absorption bands of RFT in the oxidized ground state. With increasing illumination time the intensity of the two absorption bands decreases and their ratio to each other changes indicating the formation of additional flavin species. The close up view in Figure 5-3 B shows that upon irradiation of the sample a new optical feature appears at a wavelength of about 580 nm. The new absorption correlates with the species associated spectra for the semiquinone radicals reported by Megerle *et al.*^[18] and Sakai *et al.*^[26] This confirms that the broadened lines observed in ¹H NMR spectra are caused by the stabilization of the semiquinone radical.

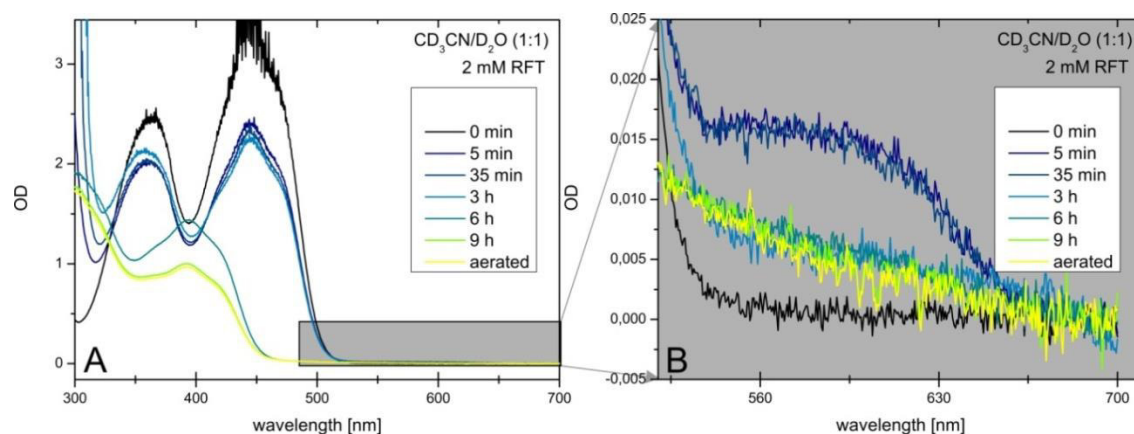


Figure 5-3 UV/Vis spectra of a degassed solution of 2 mM riboflavin tetraacetate (RFT) and 20 mM of methoxy benzyl alcohol (MBA) in CD₃CN/D₂O (1:1) before illumination and after 5 min, 35 min, 3 h, 6 h and 9 h of continuous illumination, after nine hours of illumination the samples were aerated (yellow spectrum). B) shows a close up of the absorption of the flavin in the range of 300 nm up to 700 nm, the range of the characteristic absorption band of the flavin semiquinone radical.

With the UV/Vis spectroscopic evidence for the stabilization of the semiquinone radical at hand, conditions likely to influence this stabilization were changed to elucidate which factors influence the semiquinone stabilization. The NMR data show the broadening of the signals only for the case of the solvent mixture CD₃CN/D₂O (1:1) and not for pure CD₃CN which suggests that the addition of D₂O to the reaction mixture is responsible for

the stable radical. In this context the disaggregation of RFT aggregates upon change of the solvent from CD_3CN to D_2O (CD_3CN : RFT trimers; D_2O : RFT monomers) shown by ^1H -DOSY NMR studies^[8] (chapter 2) can be expected to play an important role. For these reasons the influence of the solvent on the stabilization of the semiquinone radical was studied by means of UV/Vis spectroscopy. To determine whether and to what extent the solvent influences the stabilization a deoxygenated solution of 2 mM RFT and 20 mM MBA in CD_3CN was prepared and illuminated with 455 nm light over illumination periods of different lengths and UV/Vis spectra were taken after each illumination period. The spectra are shown in Figure 5-4. In the case of pure CD_3CN the oxidized flavin is directly reduced to the fully reduced form without the semiquinone radical being stabilized and detectable by means of NMR. In comparison to $\text{CD}_3\text{CN}/\text{D}_2\text{O}$ (1:1) the reaction proceeds much slower as known from synthetic studies.^[11,12] The observation that no semiquinone radical is stabilized if the reaction is performed in pure CD_3CN correlates with the NMR studies of the reaction in the two different solvents. In the case of pure CD_3CN the ^1H resonances of the oxidized and the fully reduced flavin species appear as sharp signals indicating no stabilization of the radical. The ^1H spectra of the $\text{CD}_3\text{CN}/\text{D}_2\text{O}$ (1:1) reaction mixture in contrast show strongly broadened ^1H flavin resonances most probably caused by semiquinone stabilization and the associated facilitated exchange of the three redox states of flavin reflected in the NMR line broadening.

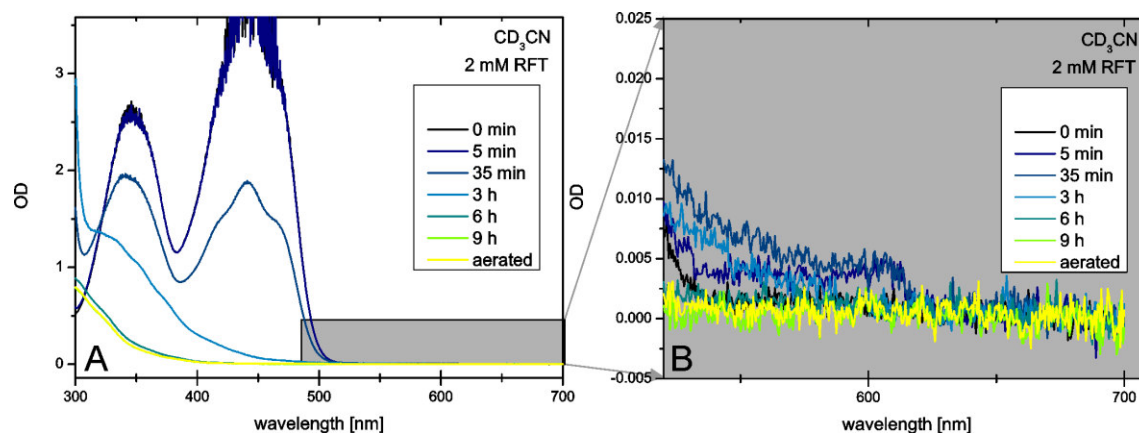


Figure 5-4 UV/Vis spectra of a degassed solution of 2 mM riboflavin tetraacetate (RFT) and 20 mM of methoxy benzyl alcohol (MBA) in CD_3CN before illumination and after 5 min, 35 min, 3 h, 6 h and 9 h of continuous illumination, after nine hours of illumination the samples were aerated (yellow spectrum). B) shows a close up of the absorption of the flavin in the range of 300 nm up to 700 nm, the range of the characteristic absorption band of the flavin semiquinone radical.

Overall, the UV/Vis experiments reveal that the line broadening observed in the ^1H NMR flavin resonances is caused by the stabilization of the semiquinone radical. Moreover the experiments reveal that water in the $\text{CD}_3\text{CN}/\text{D}_2\text{O}$ (1:1) mixture is necessary to stabilize the semiquinone radical. In pure CD_3CN the oxidized RFT is directly reduced to the fully

reduced species without stabilization of the semiquinone radical intermediate observable on the NMR time scale. The oxidized and the fully reduced flavin are known to be in equilibrium with a certain amount of semiquinone radical in pure water solution.^[3,19,43] As the stabilization of the radical has to be caused by its surroundings it could be speculated that the solvent dependent self-aggregation of RFT^[8] with aggregation numbers of 1.0 for D₂O, 1.7 for CD₃CN/D₂O (1:1) and 3.0 for CD₃CN plays an important role in the observed radical stabilization with the self-aggregation inhibiting the stabilization.

Next the influence of the ratio of concentrations of MBA and RFT on the semiquinone stabilization in CD₃CN/D₂O (1:1) deoxygenated solution was addressed to elucidate if and to what extent RFT and MBA are involved in the radical stabilization. For that different samples were illuminated for 1 min, 5 min and 30 min and the UV/Vis spectra were recorded after these illumination periods. To test if intra- or intermolecular processes between flavins themselves^[39] or photoejections of electrons from the flavins^[44] cause the formation of the semiquinone radical a sample without MBA, just containing 2 mM of RFT was prepared and the UV/Vis spectra were recorded after the described illumination periods. Figure 5-5 A shows the corresponding UV/Vis spectra. The spectra show the formation of the semiquinone radical by the characteristic absorption band at 600 nm. The radical is detected after 5 min of irradiation and becomes more pronounced after 30 min illumination. After aeration of the sample it disappears due to the reoxidation of the reduced flavin by oxygen. Surprisingly even without MBA as an electron donor a small amount of the stable semiquinone radical is formed. To study the influence of MBA on the radical formation the measurement was conducted using a sample of the same RFT concentration but with 400 μ M MBA as an electron donor. The UV/Vis spectra (Figure 5-5 B) show no significant increase in amount of formed semiquinone compared to the case that only RFT is present in the solution (Figure 5-5 A). This suggests that also with a small amount of MBA the major sources for the radical formation are intra- or intermolecular processes between flavins themselves. Finally a sample with increased amount of 20 mM MBA and unchanged RFT concentration of 2 mM was tested according to the concentrations used in synthesis.^[8-12,45] Figure 5-5 C shows a close up of the spectra of the 2 mM RFT and 20 mM MBA solution. The radical is already formed after 1 min of irradiation and becomes more pronounced after 5 min and 30 min illumination. After aeration of the sample it disappears due to the reoxidation of the reduced flavin by oxygen. Compared to the cases of only 2 mM RFT or of 2 mM RFT and 400 μ M MBA the increased amount of MBA causes the formation and stabilization of more semiquinone radical. This reveals

that a significant amount of semiquinone radical is only formed and stabilized when both RFT and MBA are present in sufficient concentrations. The RFT concentration has to be high because the semiquinone radical is formed from the flavin in the oxidized ground state. MBA acts as an electron donor for the radical formation. This shows that the formation of the semiquinone radical results from the intermolecular electron transfer from MBA to RFT also observed by Megerle *et al.*^[18] Therefore it can be concluded that the stabilized radical observed at 2 mM RFT and 20 mM MBA is predominantly formed by intermolecular electron transfer from MBA to RFT and that intramolecular processes within the RFT molecule or intermolecular processes between flavins play just a minor role. Overall, the experiments with different RFT and MBA ratios showed that both RFT and MBA are necessary in significant amounts to stabilize the semiquinone radical and that the stabilized semiquinone radical predominantly results from the oxidation of MBA by RFT.

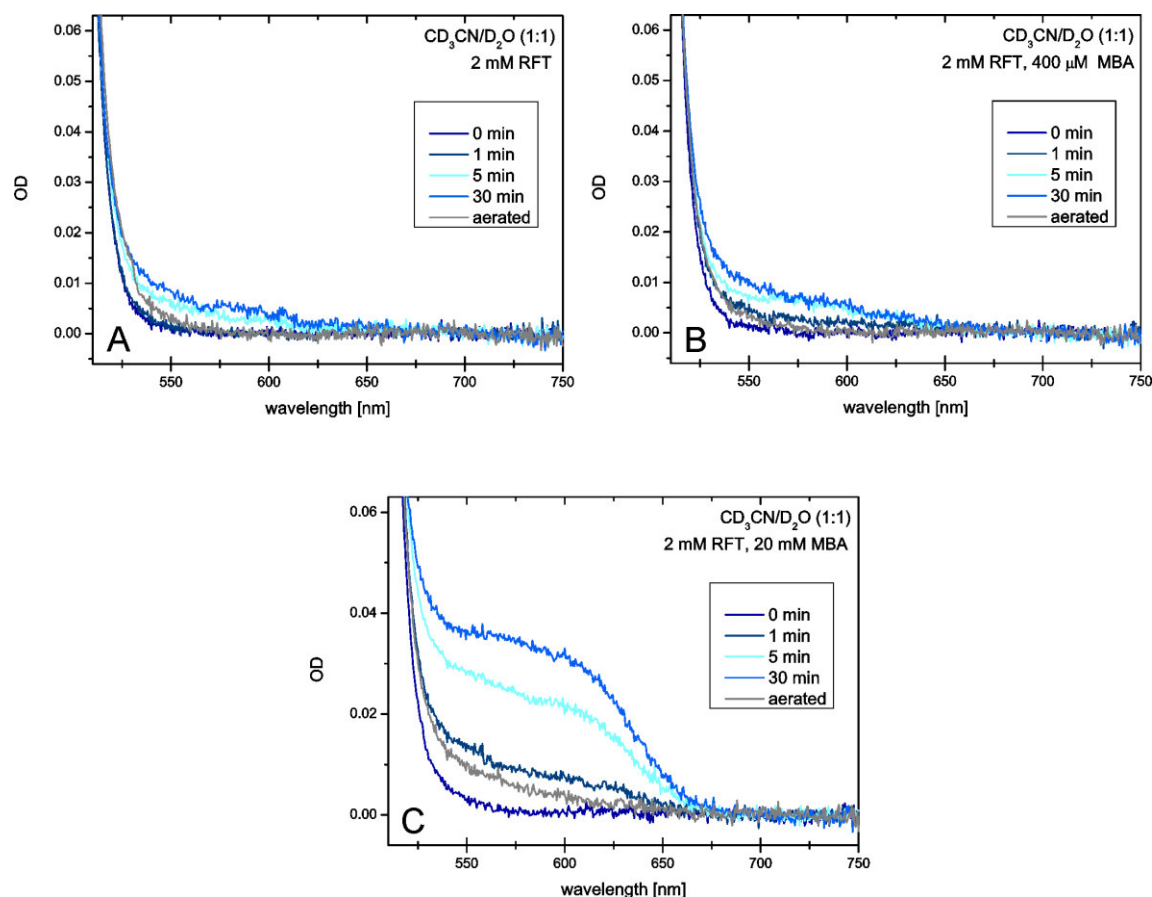


Figure 5-5 UV/Vis spectra of deoxygenated reaction mixture of riboflavin tetraacetate (RFT) and methoxybenzyl alcohols (MBA) of different concentrations in $\text{CD}_3\text{CN}/\text{D}_2\text{O}$ (1:1) before and after 1 min, 5 min and 30 min of continuous illumination and after subsequent aeration of the solution (grey spectra): A) only 2 mM RFT without MBA, B) low MBA concentration (2 mM RFT and 400 μM MBA), C) standard concentration used for NMR studies (2 mM RFT and 20 mM MBA).

5.3.3 Kinetics

To get reaction profiles and thus to draw conclusions on the reaction mechanism and the interplay of the involved species from their relative stoichiometry a row of ^1H spectra was taken during the reaction of methoxybenzyl alcohol to the corresponding aldehyde. The spectra were all taken of the dark sample between illumination periods to prevent unwanted additional polarization caused by Photo-CIDNP effects. To elucidate the influence of the solvent on the mechanism the kinetics of the reaction in pure CD_3CN and of the reaction in $\text{CD}_3\text{CN}/\text{D}_2\text{O}$ (1:1) mixture were studied and compared.

Figure 5-6 A shows the reaction profile as signal intensities of the ^1H spectra in the course of 4 h of illumination when the reaction takes place in deoxygenated pure CD_3CN . It is obvious from the reaction profiles that upon illumination the oxidized form of the flavin is reduced to the fully reduced flavin. The lack of oxygen prevents reoxidation and the fully reduced form of the flavin (green) increases at a rate corresponding to the decrease of oxidized flavin. The flavin semiquinone radical is only observed as a transient intermediate in corresponding Photo-CIDNP spectra (Figure 5-2 D) but has a lifetime beyond the NMR time scale and thus does not affect the NMR spectra or the associated kinetics. Notably the comparison of the time profiles of RFT_{ox} and RFT_{red} shows that on the NMR time scale RFT is directly reduced to the fully reduced RFT_{red} without the semiquinone radical altering the kinetics. Methoxybenzyl aldehyde is initially formed at the same rate as the reduced flavin showing the need of one molecule of RFT for the oxidation of one molecule of MBA.

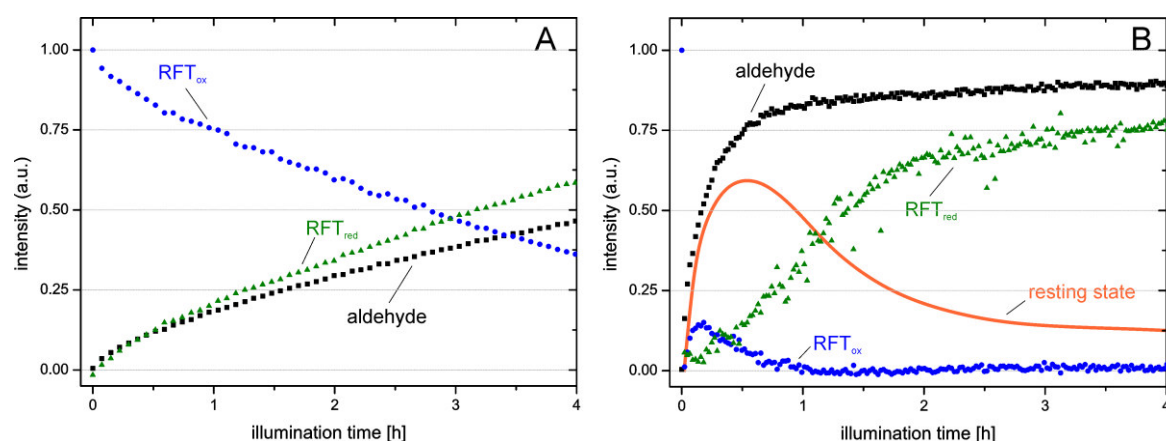


Figure 5-6 Reaction profile from a row of ^1H spectra recorded in the course of the formation of methoxybenzyl aldehyde (black) from methoxybenzyl alcohol (not shown) catalyzed by riboflavin tetraacetate (oxidized RFT_{ox} : blue, fully reduced RFT_{red} : green) in deoxygenated CD_3CN (A) and $\text{CD}_3\text{CN}/\text{D}_2\text{O}$ (1:1) (B). The kinetics were derived from the integrals of the ^1H signals C(6)-H and C(9)-H (fully reduced flavin RFT_{red} and oxidized flavin RFT_{ox}) and from the C(1)-H proton of the aldehyde (compare Figure 5-2 C). The resting state estimated from the difference of the aldehyde and RFT_{red} kinetics is outlined in red.

The solvent effect of D_2O on the reaction mechanism was studied by conducting the same experiment in $\text{CD}_3\text{CN}/\text{D}_2\text{O}$ (1:1) mixture. The reaction profile changes significantly

after the addition of water to the reaction mixture ($\text{CD}_3\text{CN}/\text{D}_2\text{O}$ (1:1)). The kinetics of the NMR signals of the oxidized flavin, the fully reduced flavin and the product methoxybenzyl aldehyde are shown in Figure 5-6 B. Compared to the situation in pure CD_3CN the addition of D_2O causes a strong acceleration of the product formation as known from synthetic applications.^[11,12,18,27] After only 10 min half of the possible product is formed, whereas in the case of pure CD_3CN as the solvent it takes about 4 h to achieve the same conversion. However, the most striking changes in the reaction profile after the addition of D_2O are the changes concerning the relative stoichiometries of the oxidized and fully reduced flavin and the product formation. Figure 5-6 B compares the reaction profiles of these species. Right at the beginning of illumination the concentration of the oxidized flavin species (blue) drops and reappears in a small amount to decrease gradually again. The fast decrease at the beginning is caused by the high radical formation at the beginning of the reaction leading to broadened lines. More surprisingly the reduced flavin species with only slightly broadened resonances compared to the signals of the oxidized flavin appears right from the start of illumination but with an apparent delay relative to the product formation. Both the reduced flavin species and the methoxybenzyl aldehyde approach a saturation concentration with prolonged illumination time corresponding to one catalytic cycle of a two-electron reduction of the flavin and a two-electron oxidation of the alcohol. However, the delay of the formation of the fully reduced flavin species behind the product formation demands a resting state to be involved in the mechanism. The broadening of the oxidized flavin NMR signals and the detection of a stable flavin radical by means of UV/Vis spectroscopy strongly suggests the flavin radical to serve as this resting state.

The amount of radical after 5 min of illumination was estimated from the characteristic semiquinone UV/Vis absorption band (Figure 5-3) and the species associated spectra^[18] of the anion and the neutral flavin semiquinone for the cases that only the anion radical is stabilized and for the case that only the neutral radical is stabilized. For the anion radical $\text{RFT}^{\cdot-}$ the estimation gives an amount of 0.775 mM of stabilized radical which would correspond to 39 % of the overall flavin concentration. For the neutral radical RFT-H^{\cdot} the estimation gives an amount of 0.019 mM of stabilized radical which would correspond to 1 % of the overall flavin concentration (for details about the estimation see supporting information). From the amount of flavin radical necessary to explain the gap between the oxidized and reduced flavin concentration and the delay of the formation of the fully reduced flavin behind the aldehyde formation (Figure 5-6) it can be concluded that the stabilized semiquinone radical appears mainly in the anionic form.

The oxidized flavin species reappears with the typical behavior of an intermediate. However, it is not the rate determining intermediate because the maximum of its intensity does not correlate with the maximal slope in product formation. This shows that it is a downstream intermediate to aldehyde formation. The reappearing of the signal set of the oxidized RFT is accompanied with a downfield shift of the C(9)-H resonance of about 0.2 ppm. The chemical shift change can be explained by the formation of mixed dimers consisting of one oxidized and one fully reduced RFT molecule as products of disproportionation of the two semiquinone radicals. The same chemical shift changes are observed if the reaction is conducted in pure CD₃CN with the C(9)-H resonance shifting downfield in the course of the reaction.

The stabilization of the flavin radical intermediate and the concurrent immediate oxidation of the alcohol to the aldehyde without the stabilization of a radical intermediate clearly show that a second flavin is necessary for the full oxidation of the alcohol. This is strongly supported by the kinetics of the reaction in CD₃CN/D₂O (1:1) mixture that show that the fully reduced flavin is formed with a delay behind the product formation demanding for a resting state not detectable by NMR. This shows that RFT acts as a one-electron oxidation agent for the oxidation of MBA. MBA is instantaneously oxidized without a radical resting state observable by broadened NMR signals. This reveals that the second electron of the MBA has to be transferred to a second flavin.

5.3.4 Mechanistic Proposal

From all the observations made by means of NMR spectroscopy, *in situ* NMR kinetics and UV/Vis spectroscopy a new mechanism for the flavin catalyzed photooxidation of methoxybenzyl alcohol to the corresponding aldehyde in deoxygenated CD₃CN/D₂O (1:1) mixture is proposed based on flavin acting as an one-electron oxidizing agent and the dimerization of RFT in CD₃CN/D₂O (1:1). The reaction scheme for this mechanism is shown in Figure 5-7. The stabilization of the flavin radical intermediate and the concurrent immediate oxidation of the alcohol to the aldehyde without the stabilization of a radical intermediate clearly show that a second flavin is necessary for the full oxidation of the alcohol. Two electron transfers from the alcohol to two different flavins yield the aldehyde and two flavin radicals. Water stabilizes the radicals which subsequently most probably disproportionate to yield the fully reduced and the oxidized flavin species in a mixed dimer. The chemical exchange between the semiquinone radicals and the oxidized and fully reduced states of RFT enabled by disproportionation and comproportionation reactions between the corresponding RFT oxidation states stabilizes the semiquinone radical and makes it a resting state for the photooxidation.

The exchange of mixed dimers and dimers consisting of either two oxidized flavins or two fully reduced flavins closes the cycle.

Overall, the experimental data provide clear evidence for flavin acting as a one-electron oxidizing agent due to the stabilization of the flavin radical in the presence of water in the solution, i.e. when the reaction is performed in $\text{CD}_3\text{CN}/\text{D}_2\text{O}$ (1:1) mixture. If no water is present in the solution and the photooxidation is performed in pure CD_3CN the stabilization of the semiquinone radical is not observed and from the corresponding kinetics it is obvious that it does not act as a resting state for the photooxidation. The less polar solvent acetonitrile does not stabilize the semiquinone radical and enhance chemical exchange between the three different flavin oxidation states. The reduction of the semiquinone by a second electron from MBA or disproportionation with a second semiquinone radical is energetically favored and no stable semiquinone radical is observed for the case of CD_3CN .

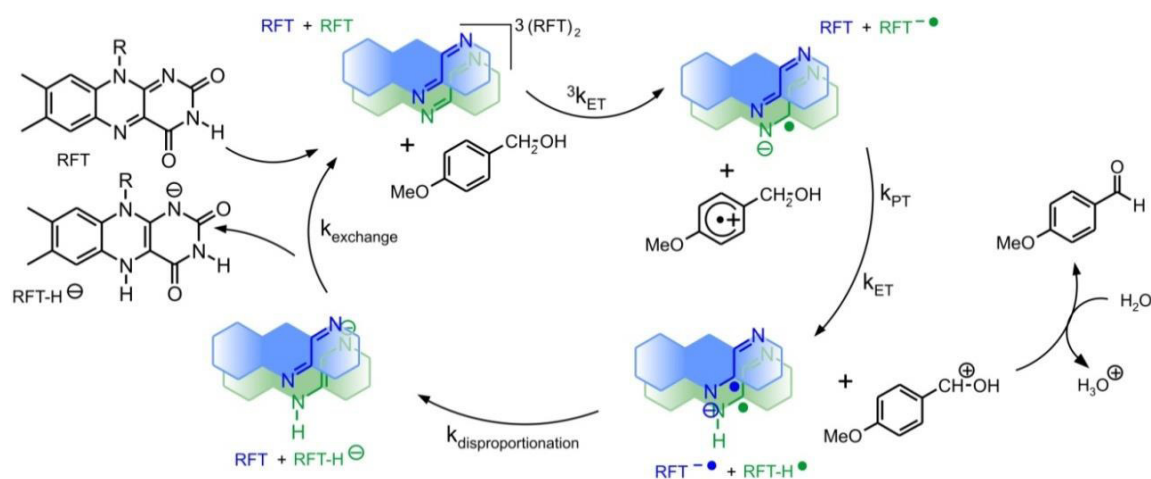


Figure 5-7 Scheme of the photooxidation by two one-electron transfers to the flavins. Two flavins are reduced by one electron each to the semiquinone radical to oxidize one benzyl alcohol to the corresponding aldehyde. The semiquinone radicals disproportionate to yield the fully reduced and the oxidized flavin.

5.3.5 Reoxidation of Flavin

All previous experiments were conducted under exclusion of oxygen to stabilize and investigate the reduced flavin species and because the reoxidation of the reduced flavin species by oxygen is known to be quite complex involving the semiquinone radical and the superoxide anion as transient intermediates.^[3,46,47] Next the oxidative side of the reaction was included to test if the results gained for the deoxygenized reaction are also valid and transferable to the situation in synthesis where for reoxidation of the photocatalyst oxygen is present in the solution. For this the reaction of 2 mM RFT and 20 mM MBA in $\text{CD}_3\text{CN}/\text{D}_2\text{O}$ (1:1) mixture was monitored again by a row of ^1H NMR

spectra. Now, the experiments were not performed under anaerobic conditions but some residual oxygen was left in the reaction mixture. From the stoichiometry of the reduced flavin and the product (Figure 5-8 A) the initial oxygen concentration was estimated to be about 2 mM.

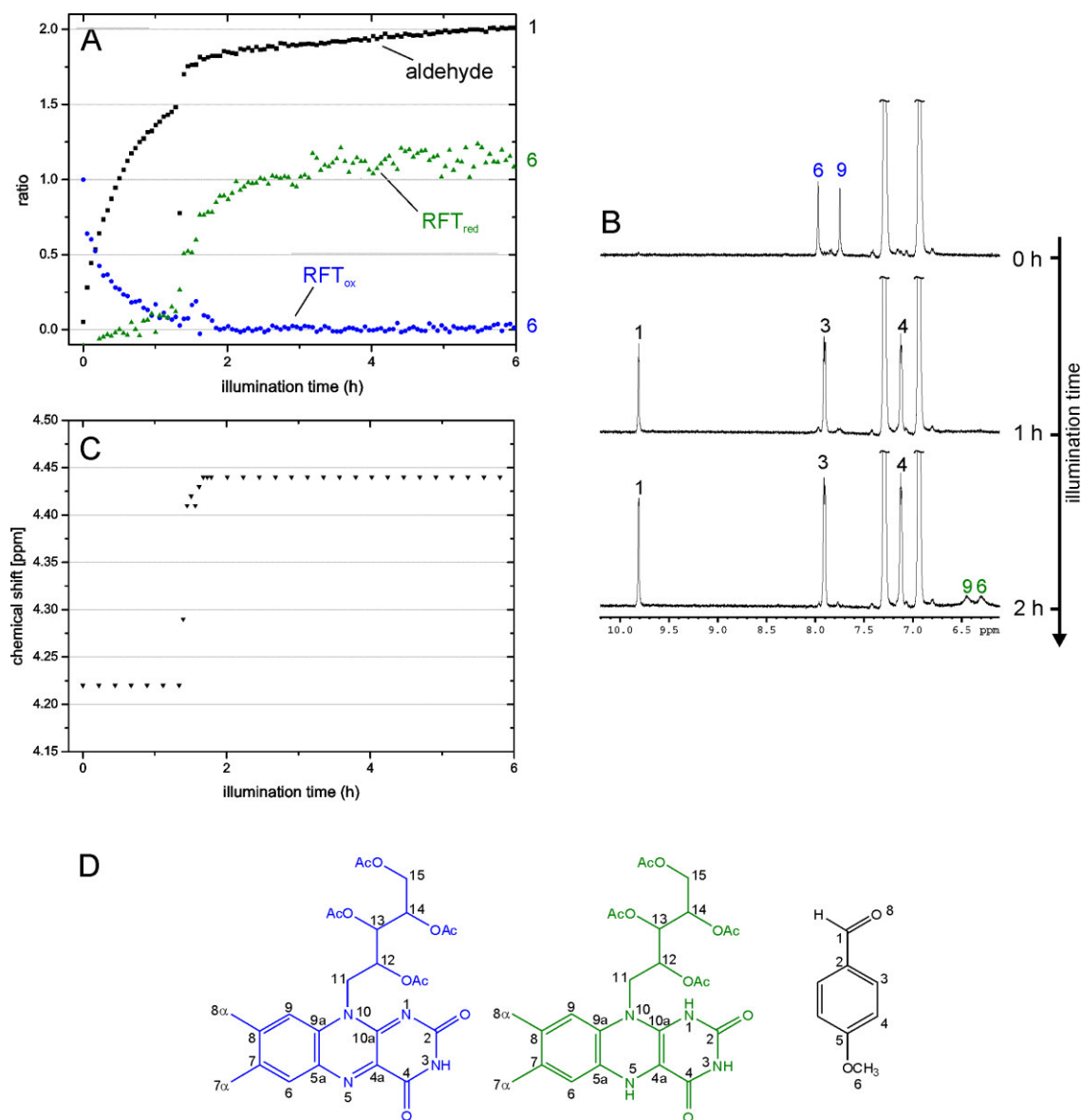


Figure 5-8 Formation of methoxybenzyl aldehyde (black) from 20 mM methoxybenzyl alcohol (not shown) catalyzed by 2 mM riboflavin tetraacetate (oxidized RFT_{ox}: blue, fully reduced RFT_{red}: green) in CD₃CN/D₂O (1:1) in the presence of ~2 mM oxygen. A) reaction profile of RFT_{ox}, RFT_{red} and methoxybenzyl aldehyde referenced to the amount of the oxidized RFT in the beginning (1.0) B) exemplary fractions of ¹H spectra before, after 1 h and after 2 h of continuous illumination, C) change of the H₂O ¹H chemical shift during illumination D) structures of the oxidized and fully reduced flavin species and methoxybenzyl aldehyde.

The kinetics of the NMR signals of the oxidized flavin, the fully reduced flavin and the product methoxybenzyl aldehyde are shown in Figure 5-8 A. Figure 5-8 B shows exemplary ¹H spectra before illumination, after 1 h and after 2 h of illumination. Just like in the kinetics observed for the case of complete deoxygenation (compare chapter 5.3.3)

the amount of aldehyde shows a steep increase right from the beginning of the photooxidation. The signals of the oxidized flavin decrease quickly due to line broadening. Compared to the oxidation conducted under anaerobic conditions, however, this happens at a slower rate due to the concurrent reoxidation of the reduced flavin species by oxygen. In contrast to the situation of full deoxygenation the signals of the fully reduced flavin now start to appear not right from the beginning but after a delay of about 1.5 h. When no more product can be formed and the amount of fully reduced flavin approaches the initial amount of oxidized flavin the stoichiometry of the aldehyde and the reduced flavin is about 2:1. This means that the catalytic cycle performed one turnover before it was interrupted by the lack of oxygen as oxidizing agent and thus that about 2 mM of oxygen was consumed for reoxidation.

The most striking observation from Figure 5-8 A arises from the correlation between the reaction profiles of the fully reduced flavin species and the reaction profile of the oxidized form of flavin. Interestingly, the oxidized flavin signals begin to broaden and decrease right from the beginning of the reaction, even though not all oxygen is consumed. However, the fully reduced flavin species does not appear right from the beginning of the reaction but after some delay when all oxygen is consumed. This shows that the stabilization of the semiquinone radical is not directly related to the prohibition of reoxidation by exclusion of oxygen. The semiquinone radical is stabilized from the beginning of the reaction even when oxygen is still available for reoxidation. The fully reduced flavin species starts to appear much later when all oxygen has been consumed. This shows that the flavin is reoxidized by oxygen from the fully reduced form and not from the semiquinone radical. Otherwise the semiquinone radical could not be stabilized right from the beginning of the reaction. The fast appearance of the fully reduced flavin after a delay of about 1.5 h confirms these observations. The appearance of the ^1H NMR signal set for the fully reduced flavin species correlates with a sudden chemical shift change of the H_2O ^1H signal (Figure 5-8 C). The change in chemical shift of H_2O is most probably caused by the additional interaction of H_2O with NH protons of the fully reduced flavin species that is formed. When oxygen is left in the reaction mixture the fully reduced flavin species is instantly reoxidized by oxygen and thus not observable on the NMR time scale, when all oxygen is consumed the fully reduced flavin accumulates rapidly and becomes visible as a signal set in the ^1H NMR spectra. The semiquinone radical has to disproportionate or to experience a second electron transfer to yield the fully reduced flavin species which then is reoxidized by oxygen. The disproportionation or second electron transfer step has to be comparatively slow so that the semiquinone radical is stabilized and observable by the broadened NMR signals even if not all oxygen is

consumed. Overall, the investigations of the reaction with residual oxygen show that also before consumption of oxygen the semiquinone radical is stabilized and the observations and conclusions made from deoxygenated samples also hold true for conditions in synthesis where oxygen is used for reoxidation of the reduced flavin.

5.4 Conclusion and Outlook

Despite the huge importance of the stabilization of the flavin semiquinone radical for the function of flavin cofactors as one-electron mediators no evidence for this concept for reactions in solution has been reported so far. In this work we investigated the flavin catalyzed photooxidation of methoxybenzyl alcohol as a model reaction by combination of NMR, UV/Vis and Photo-CIDNP spectroscopy to have access both to the paramagnetic radical species and the diamagnetic species involved in the reaction. When the reaction is performed in pure CD_3CN the oxidized flavin is reduced by two electrons to the fully reduced flavin species without the stabilization of any radical intermediate species. Both the signal set of the oxidized and the fully reduced flavin appear as sharp signals in the ^1H NMR spectrum. The transient radical intermediates are only detected in Photo-CIDNP polarizations as transient intermediates.

If water is present as the solvent the flavin semiquinone radical is stabilized and in exchange with both the oxidized and the fully reduced flavin species. The high polarity of water facilitates the formation of charge separated species as the initial ionic radical pair. As a protic solvent it facilitates the protonation and deprotonation of the radical species. These two properties thus lead to the exchange of the three flavin oxidation states (quinone, semiquinone, hydroquinone) observed by the broadened ^1H signals. The stabilization of the flavin radical intermediate and the concurrent immediate oxidation of the alcohol to the aldehyde without the stabilization of a radical intermediate clearly show that a second flavin is necessary for the full oxidation of the alcohol. Flavin acts as a one-electron oxidizing agent for the substrate. The one-electron reduced flavin then undergoes disproportionation with a second flavin radical yielding the oxidized and the fully reduced flavin or accepts a second electron from the substrate. The second reduction of the flavin however happens at a slower rate than the first reduction.

The stabilization of the semiquinone radical makes it act as a resting state in the reaction and makes flavin a one-electron oxidizing agent for the photooxidation. The stabilization has to be caused by the surroundings of the radical. In this context the solvents CD_3CN and D_2O as well as the substrate and the photocatalyst itself have to be considered. Without doubt the stabilization is caused by the solvent water. It facilitates transitions between the three different oxidation states of flavin and thus chemical exchange leading to an equilibrium between the three oxidation states and thus to the stabilization of the flavin radical. It was reported by Müller *et al.*^[48] that flavin radicals can be stabilized by formation of π -complexes. The self-aggregation of RFT^[8] can be excluded as a reason for the radical stabilization as it shows an opposing trend with RFT trimers in CD_3CN and

RFT monomers in D₂O. Apart from water as the obvious primary reason for the radical stabilization another likely reason is the complex formation of RFT with the MBA described in chapter 2.7.2.

The addition of D₂O causes a strong acceleration of the product formation compared to the case that the reaction is performed in pure CD₃CN.^[11,12,18,27] This correlates with the disaggregation of flavins with the addition of water. It was reported that sterically demanding less self-aggregating flavins show higher efficiency for the studied photooxidation.^[8] The disaggregation thus in general seems to have a huge positive effect on the reaction efficiency. The disaggregation caused by D₂O with changing the solvent from pure CD₃CN to CD₃CN/D₂O (1:1) mixture goes along with increased stabilization of the flavin radical and the facilitated conversion between the different flavin oxidation states. From this observation the question arises which role the flavin self-aggregation plays for the stabilization of the semiquinone radical. A very promising approach to address this question is to study the grade of radical stabilization in dependence of the CD₃CN/D₂O ratio.

In general the stabilization of the semiquinone radical and the facilitated conversion between the three flavin redox states has a positive effect on the reaction efficiency. Therefore a very promising approach to improve the performance of flavin photocatalysts is to stabilize the semiquinone radical. It is well known that semiquinone radicals can be stabilized by π -complexes^[19] or arylations in position 5.^[48]

This research has thrown up many questions in need for further investigation. A deeper insight in the semiquinone stabilization mechanism can be achieved by varying experimental conditions. The study of the reaction in CD₃CN/D₂O mixture with increased D₂O amount can confirm that the stabilization of the semiquinone radical is caused by water. The amount of water can be increased to an extent that just enough CD₃CN is left to solve all RFT. The study of other flavins as photocatalysts is a very promising approach to elucidate the steric factors influencing the stabilization of the semiquinone radical. In particular the study of the photooxidation catalyzed by sterically demanding flavins with an orthogonal aryl ring in position 10 hindering π - π stacking (chapter 2) could give information on the contribution of flavin self-aggregation or flavin-substrate aggregation on the stabilization mechanism. Furthermore experiments with other solvents than CD₃CN and D₂O can give clues which intermolecular interactions and solvent properties are responsible for the stabilization of the semiquinone radical. The estimated kinetics for the semiquinone radical in Figure 5-6 B could be measured directly and included as experimental data in Figure 5-6. A very promising approach for this is to

measure UV/Vis spectra of a NMR sample. For this the NMR tube containing the sample is placed inside a UV/Vis cuvette and the NMR tube glass is index matched with an appropriate liquid inside the UV/Vis cuvette so that the NMR tube becomes invisible for UV/Vis spectroscopy. In this way parallel kinetics of both the diamagnetic species detected by NMR and the paramagnetic radical detected by UV/Vis spectroscopy can be performed. The combined radical and non-radical kinetics can be expected to yield valuable information about the interplay of the different species and about the role of the semiquinone radical serving as a resting state.

In general the presented study and the further investigation of the presented model system can be expected to yield valuable information about the stabilization mechanism and the intermolecular interactions causing the stabilization of the radical. From the observation that the semiquinone radical is stabilized by water but not by acetonitrile it could be speculated that hydrogen bonds are responsible for the stabilization. The investigation of the radical stabilization of flavins methylated in position 3 could give further insight in the role of hydrogen bonds for the radical stabilization.

Overall, it was shown that the tuning of the flavin semiquinone radical stabilization by intermolecular interactions with its surroundings, a concept well known from flavin proteins, can be mimicked by flavins in free solution by variation of the solvent. The flavin catalyzed photooxidation of benzyl alcohols thus provides a valuable small molecule model system for studying the intermolecular interactions responsible for the semiquinone stabilization in proteins and the regulation between one- and two-electron transfers.

Figure 5-9 shows an overview of the ^1H and ^{13}C chemical shift assignment of the oxidized and the fully reduced riboflavin tetraacetate, methoxybenzyl alcohol and methoxybenzyl aldehyde solved in pure CD_3CN and in a mixture of $\text{CD}_3\text{CN}/\text{D}_2\text{O}$ (1:1).

5.6 Additional Experimental Findings

5.6.1 EPR Spectra of the Semiquinone Radical

Further evidence that the broadened lines in the NMR spectra of the illuminated reaction mixture in $\text{CD}_3\text{CN}/\text{D}_2\text{O}$ (1:1) are caused by a radical and not by other effects associated with NMR line broadening is provided by EPR spectroscopic studies. EPR has proven effective and has gained widespread recognition for the detection and characterization of radicals in general and in particular for flavin semiquinone radicals.^[25,49]

EPR spectra of the deoxygenated reaction mixture of 2 mM RFT and 20 mM MBA in $\text{CD}_3\text{CN}/\text{D}_2\text{O}$ (1:1) were taken after 20 min illumination with 455 nm light. After this illumination period the signals of the oxidized flavin in the corresponding ^1H NMR spectrum disappeared due to line broadening. Figure 5-10 A shows the EPR spectrum at room temperature, the spectrum in Figure 5-10 B was measured after cooling the same sample down to the temperature of liquid nitrogen. The spectra provide clear evidence for a stable radical, at lower temperature the characteristic g anisotropies of the radical appear.

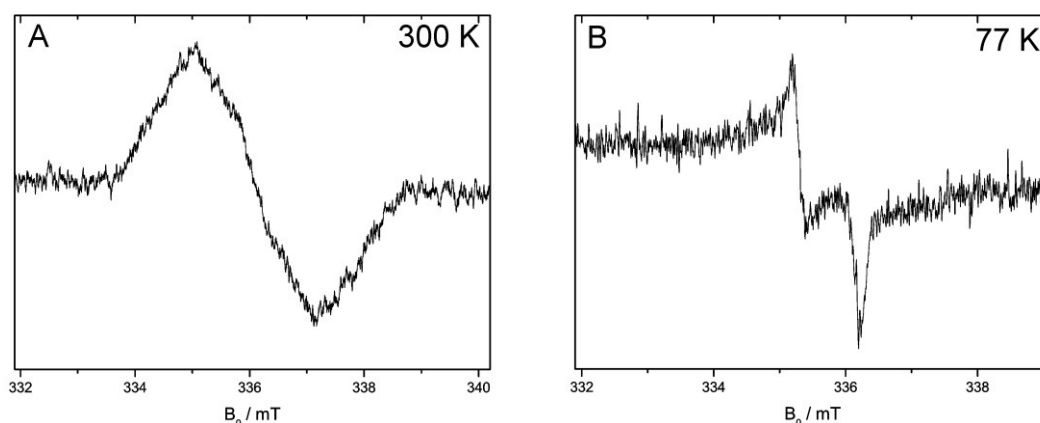


Figure 5-10 Continuous wave EPR spectra of the stable semiquinone radical in degassed $\text{CD}_3\text{CN}/\text{D}_2\text{O}$ (1:1) mixture after 20 min of illumination with 455 nm light at A) room temperature 300 K and B) at 77 K.

From the EPR spectra the g-factor of the radical was determined to be 2.1281 for 77 K. This value strongly deviates from usual g-factors of flavin semiquinone reported in literature of 2.0034.^[25] This huge deviation is most probably due to the bad or missing calibration of the EPR spectrometer used at a trial at a spectrometer demonstration. Other tested samples with semiquinone radicals stabilized in proteins showed the same strong deviation of the g-factors from literature reported values. Owing to this the g-factor determined from the EPR spectrum cannot be employed for further characterization of the detected radical.

However, the EPR spectra confirm that the broadened lines in the NMR spectra are caused by a stable radical. The fact that only RFT ^1H NMR signals are affected by the broadening is a strong indicator for the flavin semiquinone radical as the stabilized radical species. However, for further characterization of the radical more sophisticated and time consuming EPR techniques have to be employed.^[25]

5.6.2 Spin Density Dependent Line Broadening

A further indicator for the stable radical as the cause for line broadening is the dependence of the broadening on the distance from the radical center. The broadening is expected to be proportional to the square of the hyperfine coupling constants of the exchanging radical at fast exchange.^[50,51] The technique of paramagnetic relaxation enhancement (PRE) utilizes this dependence to determine distances longer than those accessible by NOE from the line broadening which depends on the distance from a stable paramagnetic center.^[52-54] For this reason the correlation between the line broadening and the electron spin density of the unpaired radical electron reflected in the Photo-CIDNP spectra in chapter 4 was studied. Figure 5-11 shows a selection of ^1H spectra taken during the illumination (455 nm light) of a sample of 2 mM RFT and 20 mM MBA in $\text{CD}_3\text{CN}/\text{D}_2\text{O}$ (1:1) that was not deoxygenated but sealed airtight. The first spectrum was taken just before starting the illumination and shows only sharp signals for all proton resonances. The following ^1H spectra show that there is a gradual broadening of the RFT resonances with increasing illumination time. The broadening is exclusively detected for the RFT resonances, neither the substrate, the product or the solvent signals are affected. A line broadening of the ^1H and ^{13}C NMR resonances of flavin mononucleotide (FMN) ring systems in deoxygenated solution was described before^[39] and attributed to the formation of the semiquinone radical. A closer look at the broadening of the RFT resonances reveals that they are not broadened equally. A comparison of the RFT signals C(6)-H, C(9)-H, C(11)-H₂, C(12)-H, C(13)-H and C(14)-H shows that the broadening of the signal is more prominent with shorter distance of the corresponding proton from the isoalloxazine ring system. This is especially apparent from the signals C(12)-H, C(13)-H and C(14)-H that show a very clear dependence of the broadening on the distance from the isoalloxazine ring system. As the semiquinone radical is stabilized under the conditions of this experiment ($\text{CD}_3\text{CN}/\text{D}_2\text{O}$ (1:1) solution, consumption of oxygen) the unpaired electron of the semiquinone radical acts as an additional relaxation source for the nuclear spins and thus enhances their relaxation and shortens their relaxation time T_2 . The line broadening of the observed NMR signals is correlated to the unpaired electron spin density mediated by the hyperfine interaction.

The spin density of the unpaired electron of the semiquinone radical is reflected in the Photo-CIDNP patterns detected if the reaction is performed in CD_3CN . The Photo-CIDNP polarizations are observed for the proton resonances of the isoalloxazine moiety, the protons of the RFT side chain do not show Photo-CIDNP effects (except C(11)- H_2) (compare chapter 4.3.2). This is in accordance with the observations regarding the line broadening of ^1H NMR signals due to the stabilization of the semiquinone radical where also resonances of protons attached to the isoalloxazine ring system exhibit the most pronounced line broadening and resonances of protons in the side chain show decreasing line broadening with larger distance from the isoalloxazine ring system.

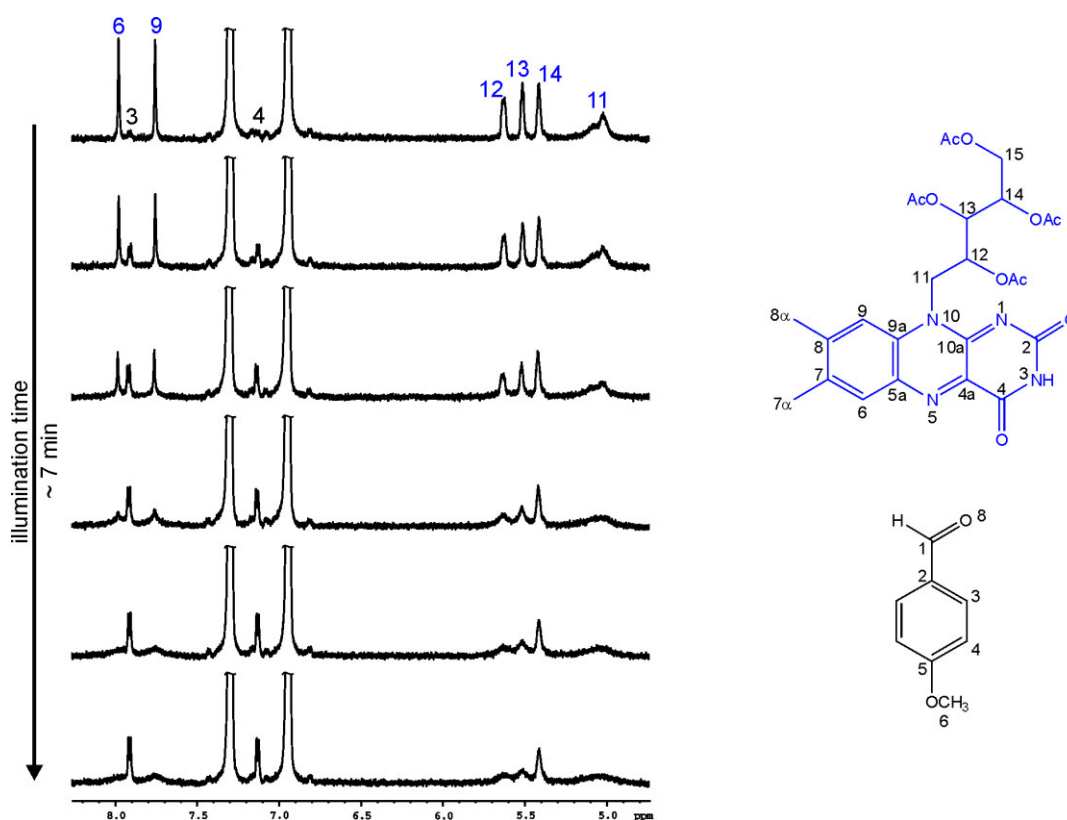


Figure 5-11 Row of ^1H spectra taken during illumination of a sample of 2 mM RFT and 20 mM MBA in $\text{CD}_3\text{CN}/\text{D}_2\text{O}$ (1:1) sealed airtight. The first spectrum was recorded before starting illumination. The methoxybenzyl aldehyde shows sharp signals whereas the RFT signals broaden with increasing illumination time.

5.6.3 Semiquinone Radical Stability

As described before, the illumination of samples of 2 mM RFT and 20 mM MBA in deoxygenated $\text{CD}_3\text{CN}/\text{D}_2\text{O}$ (1:1) mixture causes broadened flavin signals in the ^1H NMR spectra. The broadening is caused by the formation of a stable semiquinone radical. In order to determine the grade of stabilization in terms of the semiquinone lifetime a sample of 2 mM RFT and 20 mM MBA in deoxygenated $\text{CD}_3\text{CN}/\text{D}_2\text{O}$ (1:1) mixture was illuminated with 455 nm light inside the spectrometer^[32] until a sufficient amount of

semiquinone radicals was formed and the flavin signals exhibited respective broadening. Afterwards the light was switched off and a row of ^1H spectra was recorded. Figure 5-12 A shows the aromatic region of these ^1H spectra.

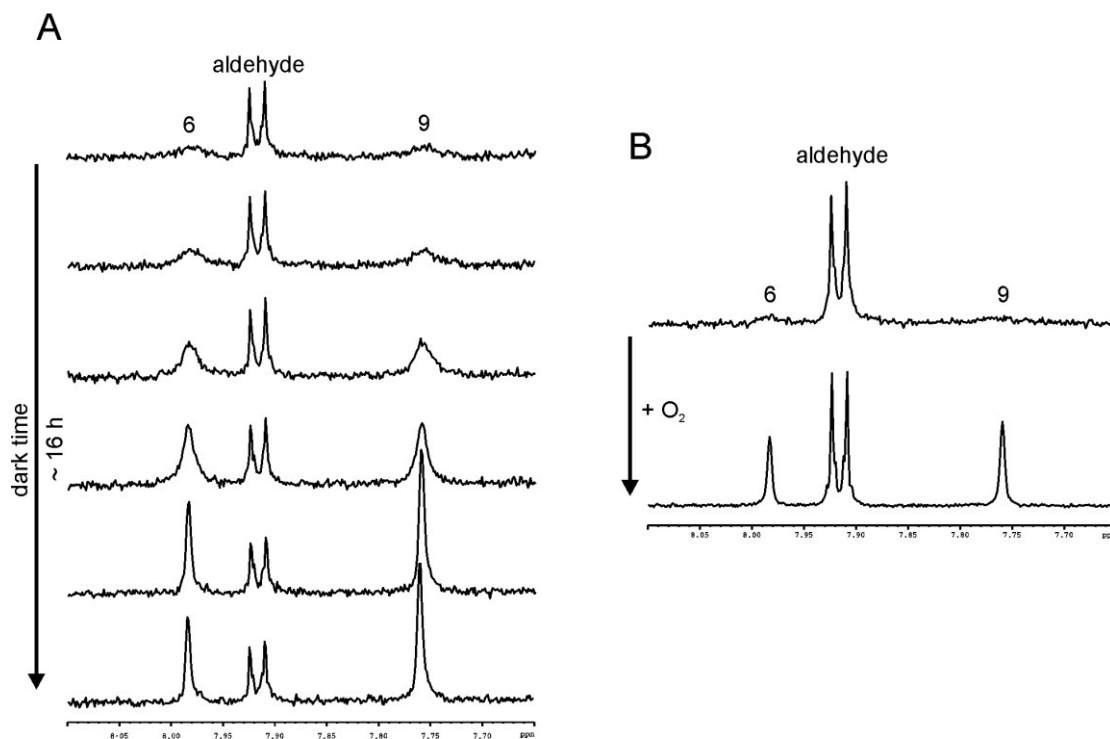


Figure 5-12 A) Reappearance of the broadened RFT signals in the dark over a time interval of ~ 16 h. B) Reappearance of the broadened RFT signals after aerating the sample.

In the first spectrum recorded directly after the sample was illuminated the aromatic flavin resonances C(6)-H and C(9)-H show a clear broadening caused by the semiquinone radicals acting as an additional relaxation source shortening T_2 . The signals of the aldehyde, the alcohol and the solvents (not shown) are not affected by the broadening. The following spectra show the behavior of the spectrum during 16 h of darkness. The broadened signals reappear when the sample is left in the dark. However, the observation that even after hours in the dark the RFT signals are considerably broadened suggests that the semiquinone is stable for hours. During all the time only the broadened flavin signals recover. The signals of MBA, the aldehyde and none of the other signals show any changes during the recovery of the RFT lines. This strongly suggests that the flavin semiquinone or the fully reduced flavin is reoxidized by entering oxygen resulting in the formation of H_2O_2 . H_2O_2 would be deuterated and in fast exchange with D_2O and thus not observable for ^1H NMR spectroscopy. The reoxidation of the reduced flavin is thus the only dark reaction observable on the NMR time scale.

The observation that the broadened NMR resonances, the EPR radical spectrum and characteristic absorption band of the semiquinone radical in UV/Vis-spectra are only

observed if the samples were degased before illumination or after consumption of oxygen and spectroscopic investigations suggests that the exclusion of oxygen hinders reoxidation of the reduced flavin and stabilizes the semiquinone radical. In that case the broadened lines should recover after aerating the samples. To test this a sample of 2 mM RFT and 20 mM MBA in deoxygenated CD₃CN/D₂O (1:1) mixture was illuminated with 455 nm light inside the spectrometer^[32] until a sufficient amount of semiquinone radical was formed and the flavin signals exhibited respective broadening. The sample was left in the dark and a ¹H spectrum of the mixture with the broadened RFT signals was recorded. After that oxygen was added to the solution and a second ¹H spectrum was recorded. Figure 5-12 B shows the ¹H spectra before and after the addition of oxygen. It is apparent from the spectra that the addition of O₂ causes the reoxidation of the reduced flavin and thus the reappearance of the sharp resonances of the oxidized flavins. The addition of oxygen only causes the recovery of the sharp signal set of the oxidized flavin but no other changes in signal intensities or signal forms.

5.6.4 Oxidative Side of the Catalytic Cycle - Oxygen Concentration

The influence of oxygen on the reaction was studied by monitoring the events in reaction mixtures of 2 mM RFT and 20 mM MBA in CD₃CN at different oxygen concentrations by a row of ¹H spectra during *in situ* illumination of the NMR sample.^[32] For this purpose three different samples were prepared from the same stock solution. One sample was taken from the stock solution without changing the O₂ concentration (medium O₂ concentration), one sample was taken from the stock solution and purged with O₂ (high O₂ concentration) and another sample taken from the stock solution was purged with argon to reduce the O₂ concentration (low oxygen concentration).

First, the influence of the O₂ concentration on the formation of the reaction product methoxybenzyl alcohol was studied. Figure 5-13 A shows the kinetics of the aldehyde proton signal intensity exemplarily for the product formation in dependence of the oxygen concentration. At higher oxygen concentration the product formation lasts longer because the reduced flavin can instantly be reoxidized by oxygen and thus can again act as an oxidizing agent. At lower oxygen concentrations all oxygen is converted to H₂O₂ and thus no longer available to reoxidize the flavin. The interrupted catalytic circle stops the product formation. An unanticipated finding in this context is that the reactions at lower oxygen concentrations proceed faster than those of higher oxygen content at the beginning of the reaction. A very probable explanation for this observation is that oxygen quenches the excited triplet state of RFT.^[55] It was shown in a study by Megerle *et al.*^[18] that RFT in the triplet state is the precursor for the productive pathway of the product

formation. With higher oxygen content the probability for the triplet state to be quenched is increased and thus the probability for the productive pathway decreased. At high oxygen content at the one hand the reduced flavin is reoxidized easily promoting the reaction rate. On the other hand the productive triplet state is quenched by oxygen hindering the product formation. So the reaction rate is maximized not at maximal or minimal oxygen content but at an intermediate value.

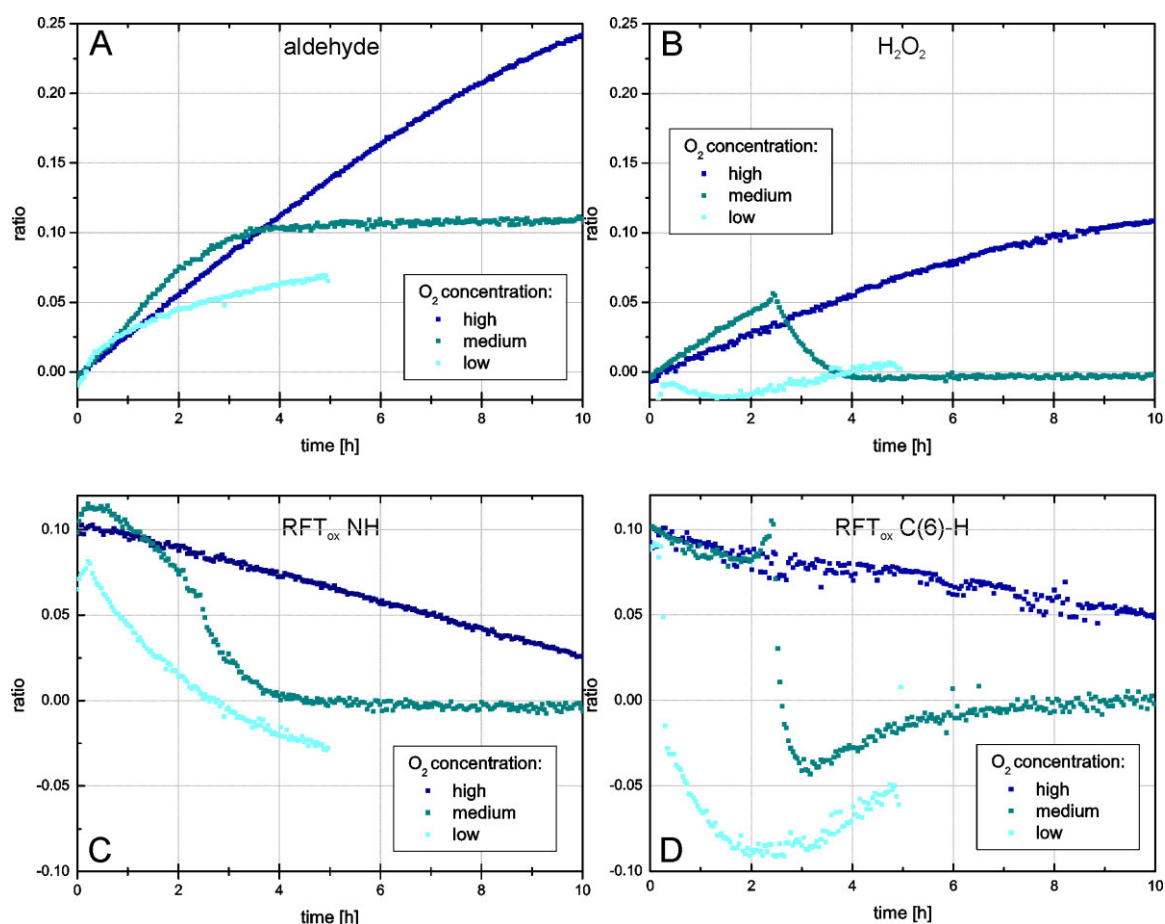


Figure 5-13 Comparison of kinetics of reactions of 2 mM RFT and 20 mM MBA in CD_3CN at different initial concentrations of oxygen. A) shows the kinetics of the product methoxybenzyl aldehyde, B) the kinetics of H_2O_2 , C) kinetics of the oxidized RFT NH signal and D) the kinetics of the flavin aromatic proton C(6)-H of the oxidized RFT. All kinetics are referenced to the initial amount of substrate of 1.0.

It is conceivable that additionally to O_2 the produced H_2O_2 can also act as an oxidizing agent for the reduced flavin species. For this reason next the reaction profile of H_2O_2 the second reaction product of the catalysis was studied by monitoring the ^1H NMR H_2O_2 resonance at a chemical shift of 8.60 ppm during *in situ* illumination at the three different oxygen concentrations. The addition of small amounts of H_2O_2 as an oxidizing agent for the reoxidation of reduced flavins in protein Photo-CIDNP studies was suggested by Maeda *et al.*^[56] The comparison of the H_2O_2 kinetics at low, medium and high oxygen content are shown in Figure 5-13 B. At high oxygen content H_2O_2 is formed at a lower rate than the first product of the reaction, methoxybenzyl aldehyde. Due to the high

oxygen content at the beginning of the reaction even after 10 h of illumination no saturation of the amount of H_2O_2 is reached. At medium oxygen concentration H_2O_2 is also formed at a lower rate than the product methoxybenzyl aldehyde until it reaches a maximum after which the H_2O_2 concentration drops. While from the comparison of the kinetics of the aldehyde and the H_2O_2 formation at high oxygen contents (Figure 5-13 A and B) a stoichiometry of aldehyde to H_2O_2 of 2:1 could be assumed. The comparison of the same kinetics at medium oxygen content reveals that there is no direct correlation between the formation of the aldehyde and H_2O_2 . The observation that the amount of H_2O_2 does not stay constant after full consumption of oxygen but decreases suggests that at the same time H_2O_2 is formed a second mechanism in the reaction causes the decomposition of H_2O_2 . This also explains the different and surprising stoichiometries of H_2O_2 and aldehyde at different O_2 contents. These observations are discussed in more detail in chapter 5.6.5.

Next the dependence of the kinetics of the oxidized flavin on the oxygen content was studied. For this the kinetics of the N(3)-H proton were recorded exemplarily for the kinetics of the oxidized flavin species by rows of ^1H spectra (Figure 5-13 C). The decrease of the signals of the oxidized flavin species is lower at higher oxygen content. When the oxygen is consumed the fully reduced (hydroquinone) form of the flavin is stabilized and the amount of oxidized flavin decreases. Additionally, decomposition of flavin contributes to the decrease in oxidized flavin content. However, it can be concluded from the small amount and intensity of new not assignable signals that this contribution is rather small.

Finally, the kinetics of the aromatic RFT proton C(6)-H were studied exemplarily to investigate the appearance of the Photo-CIDNP effect in the course of the reaction (compare chapter 4). For these investigations only the C(6)-H signal of the oxidized RFT and not the one of the fully reduced RFT was considered as the latter is only detectable after the complete consumption of oxygen. Diamagnetic products detected by ^1H NMR carry the characteristic singlet or triplet radical pair precursor Photo-CIDNP pattern. The overall pattern changes in the course of the reaction due to changing contributions of singlet and triplet pathways. In experiments described in chapter 4.3.2 it was found that the productive triplet channel of the reaction leads to an absorptive CIDNP signal for proton C(6)-H and the singlet channel as the loss channel yields an emissive Photo-CIDNP signal detected in the signals of the reduced and the oxidized flavin species respectively. Figure 5-13 D illustrates the influence of the oxygen content on the Photo-CIDNP polarization detected in the course of the reaction. The samples were illuminated

during all the measurements. Reference measurements showed that all deviations from standard kinetics are due to additional Photo-CIDNP polarizations. At high oxygen concentrations a small steady decrease of the aromatic RFT C(6)-H proton signal is detected due to decomposition of the catalyst. At high oxygen concentrations no CIDNP-polarizations of the proton resonance are detected. A Photo-CIDNP cancelation mechanism results from the fact that in cyclic reactions geminate type and escape type Photo-CIDNP polarizations end up in the same diamagnetic product and thus nuclear spin sorting is undone.^[57] This is caused by the instantaneous reoxidation of the reduced flavin resulting in the detection of both the product of the singlet exit channel and the product of the triplet exit channel in the oxidized flavin. This undoes the spin sorting by the Photo-CIDNP effect. A further factor diminishing Photo-CIDNP effects is the quenching of the Photo-CIDNP polarization by oxygen.^[24] At low oxygen content the quenching is prevented and a strong emissive Photo-CIDNP effect evolving at an early stage of the reaction is detected. These emissive signals correspond to the loss singlet pathway in which an electron transfer from the substrate to the flavin is followed by a fast electron back transfer yielding the oxidized flavin. The most interesting findings in this context are revealed by the data of the measurements at medium oxygen concentrations. At the beginning of the reaction when some oxygen is left in the solution no Photo-CIDNP polarization is detected. Right before all oxygen has been consumed an increase of the signal intensity is detected caused by an absorptive Photo-CIDNP polarization. After reaching a maximum the signal intensity drops and even gets negative due to emissive Photo-CIDNP polarization. The emissive Photo-CIDNP polarization corresponding to the singlet loss channel is observed after the oxygen is completely consumed and the reduced flavin species is stabilized. By this the oxidized flavin as the recombination product of the singlet channel and the reduced flavin as the product of the productive triplet channel are separated and detected in two different signal sets. The full Photo-CIDNP polarization becomes visible in an emissive signal corresponding to the singlet loss channel of the reaction. However, even without the stabilization of the fully reduced flavin an absorptive CIDNP-polarization is detected before the fast change to the emissive Photo-CIDNP signal. The absorptive signal is associated with the productive triplet channel and detected in the signal set of the fully reduced flavin (compare chapter 4.3.1). A conceivable explanation for the observation of this signal is the variation of the different lifetimes of different involved species and the modulated relaxation of the Photo-CIDNP polarizations in the presence of oxygen.

5.6.5 H₂O₂ as the Second Reaction Product

5.6.5.1 Role of H₂O₂ for the Reaction Mechanism

In the studied reaction methoxybenzyl alcohol is oxidized by flavin as the photocatalyst. Subsequently the reduced flavin is reoxidized by O₂ yielding H₂O₂ as a second reaction product. H₂O₂ can decompose to H₂O and O₂. This process can be catalyzed by transition metal catalysts or in biological systems by the enzyme catalase.^[58] To study the oxidative side of the reaction it is essential to include the role of H₂O₂ as it is conceivable that it is not only the second product of the reaction but interferes with the reaction and takes part in it. It was described above that the amount of H₂O₂ increases at a smaller rate as the aldehyde forms until all oxygen is consumed. Surprisingly, the amount of H₂O₂ does not stay constant after the full consumption of oxygen but decreases (compare chapter 5.6.4) whereas the H₂O signal increases suggesting that H₂O is formed from H₂O₂ (data not shown).

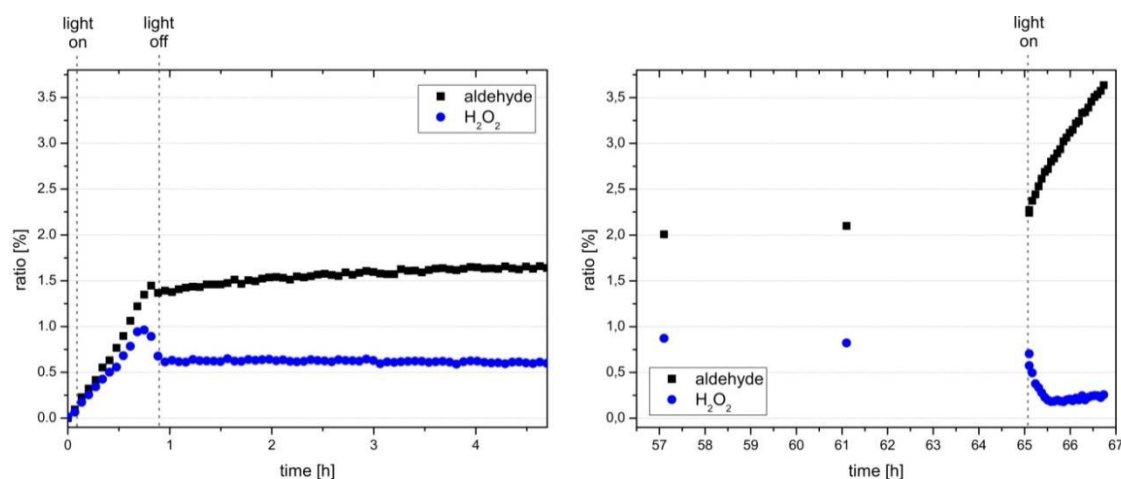
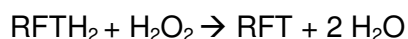


Figure 5-14 Reaction profiles from rows of ¹H spectra of the RFT catalyzed photooxidation of methoxybenzyl alcohols to the corresponding aldehydes at periods of illumination (starting with "light on") and periods without illumination (starting with "light off"). A) Kinetics of the aldehyde and H₂O₂ the first 4.5h, B) Kinetics of the same signals about 50 h later and with continued illumination. The kinetics are referenced to the initial amount of substrate (100 %).

To test the influence of the light on the decomposition of H₂O₂ the reaction of methoxybenzyl alcohol to the corresponding aldehyde catalyzed by RFT was monitored by a row of ¹H spectra and *in situ* illumination.^[32] The reaction mixture was prepared with some residual oxygen in the solution to enable the formation of H₂O₂. The NMR tube was sealed airtight so that the reaction could be studied under anaerobic conditions after all oxygen was converted to H₂O₂. After H₂O₂ had reached its maximal concentration the photocatalytic reaction was stopped by switching off the light and the behavior of the two products methoxybenzyl aldehyde and H₂O₂ was monitored while the sample was left in the dark. Later the sample was illuminated again and the online monitoring of the

reaction products was continued. Figure 5-14 shows the corresponding reaction profiles. With starting the illumination the two products methoxybenzyl aldehyde and H_2O_2 start to form (Figure 5-14 A). The amount of H_2O_2 shows a similar increase as the amount of the aldehyde. This is due to additional polarization of the H_2O_2 ^1H resonances caused by absorptive Photo-CIDNP polarization of protons exchanged chemically from the fully reduced flavin N(5)-H proton. After the light is switched off the deviation between the aldehyde and H_2O_2 amounts increases confirming the assumption that Photo-CIDNP effects are responsible for the parallel formation of H_2O_2 and the aldehyde. The formation of the aldehyde immediately stops after switching off the light. When the sample is left in the dark the concentrations of both H_2O_2 and the aldehyde stay the same, even after more than 60 h only minor changes are observed (Figure 5-14 B). When the light is switched on again the product formation continues at a lower rate than before consumption of oxygen whereas the H_2O_2 concentration drops. Interestingly, the H_2O_2 concentration stays constant for days, only when the sample is illuminated it decreases. At the same time the products continue to form at a lower rate than before oxygen was consumed. This shows that the decomposition of H_2O_2 is triggered by light. These observations strongly suggest that H_2O_2 is further reduced photocatalytically to H_2O and itself acts as an oxidizing agent for the reoxidation of the fully reduced flavin and the fully reduced flavin has to be excited by light for the reduction of H_2O_2 to H_2O . A probable mechanism is:



This explains the observation that H_2O_2 is formed in lower amounts than methoxybenzyl alcohol. When the reduced flavin species is both reoxidized by O_2 and H_2O_2 , H_2O_2 is formed and consumed at the same time and thus shows kinetics associated with an intermediate. After all oxygen is consumed the formation of H_2O_2 is prohibited and the ongoing decomposition of H_2O_2 to H_2O results in the vanishing H_2O_2 signal.

To confirm this proposed mechanism it is indispensable to correlate the decrease of the H_2O_2 signal with the increase of the H_2O signal. The determination of the T_1 relaxation times showed that a quantitative comparison of the signal intensities is quite prone to errors due to the long T_1 relaxation times of protons in degassed solvents. In particular the strong T_1 changes associated with the consumption of oxygen are likely to cause severe deviations. For this purpose ^1H NMR kinetic studies with long relaxation delays D_1 have to be conducted. Additionally, alternating ^1H spectra of illuminated and dark spectra of which only the dark ones are taken into account for the kinetics would inhibit distortions of the signal intensities by additional Photo-CIDNP polarizations.

5.6.5.2 Assignment of H₂O₂

In ¹H NMR spectra hydrogen peroxide is expected to have a relatively broad signal with a strongly changing chemical shift dependent on the number and nature of other mobile protons and the resulting exchange.^[59] This makes the H₂O₂ signal easy to confuse with the N-H signals of the oxidized and fully reduced flavin species. The H₂O₂ was distinguished from the other similar signals in three different ways.

¹H-DOSY NMR measurements^[60,61] were performed in order to determine the sizes of the different molecules in the reaction mixture. In CD₃CN solution at room temperature the signal of H₂O₂ delivered a diffusion coefficient lying between the diffusion coefficient of H₂O and the one of acetonitrile (Table 5-1). The diffusion coefficients of the flavin species and the alcohol and aldehyde are much lower so that the H₂O₂ signal can easily be distinguished by means of ¹H DOSY NMR measurements. In this way the signal of H₂O₂ was assigned to the proton resonance at 8.60 ppm. However, the chemical shift strongly depends on the amount of water and fully reduced flavin in the reaction mixture.

Table 5-1 ¹H chemical shifts and diffusion coefficients of H₂O, H₂O₂ and CH₃CN in CD₃CN.

	H ₂ O	H ₂ O ₂	CH ₃ CN
¹ H chemical shift [ppm]	2.13	8.60	1.94
diffusion coefficient [m ² s ⁻¹]	6.57	6.06	5.08

To confirm the assignment, H₂O₂ 30 % in water was titrated to the mixture. An enhancement of the signal at 8.60 ppm confirmed the assignment of this signal to H₂O₂.

A further confirmation for the assignment of the signal can be drawn from the kinetics of the reaction in a not perfectly deoxygenated sample. The H₂O₂ signal increases until all oxygen is consumed. Only after all oxygen is consumed the signals of the fully reduced flavin start to rise and the signals of the oxidized flavin decrease.

5.6.6 Protonation of the Flavin Species

Three redox states of flavin isoalloxazine can be stabilized. It can exist in the oxidized (quinone) state, in the one-electron reduced (semiquinone) state or in the fully two-electron reduced (hydroquinone) state. All of the three different redox states can appear in the anionic, the cationic or the neutral form. Considering all oxidation and protonation states in total 9 different forms of appearances of the isoalloxazine are possible.^[1,2,7,19,62] The different states are shown in Figure 5-15 with their associated pK values.

The protonation of the different involved redox states has a huge impact on the overall reaction mechanism, e.g. the protonation of N(1)-H in the fully reduced flavin has a strong impact on its reactivity with oxygen.^[62] Therefore the protonation state of the flavins in the different redox states was studied by means of NMR (diamagnetic quinone and hydroquinone) and UV/Vis spectroscopy and Photo-CIDNP spectroscopy (paramagnetic semiquinone). The ionization equilibrium is dependent on the solvents acidity/basicity, its relative permittivity and solvation ability.^[63] For this reason the ionization was studied for flavin solved in pure CD₃CN and in CD₃CN/D₂O (1:1) mixture. The different solvents change the reactivities of the involved species drastically. For all the studies on the ionization states of the different oxidation states riboflavin tetraacetate (RFT) was chosen as a model system due to its importance in synthetic chemistry and for comparability with the other experiments described in this chapter 5.

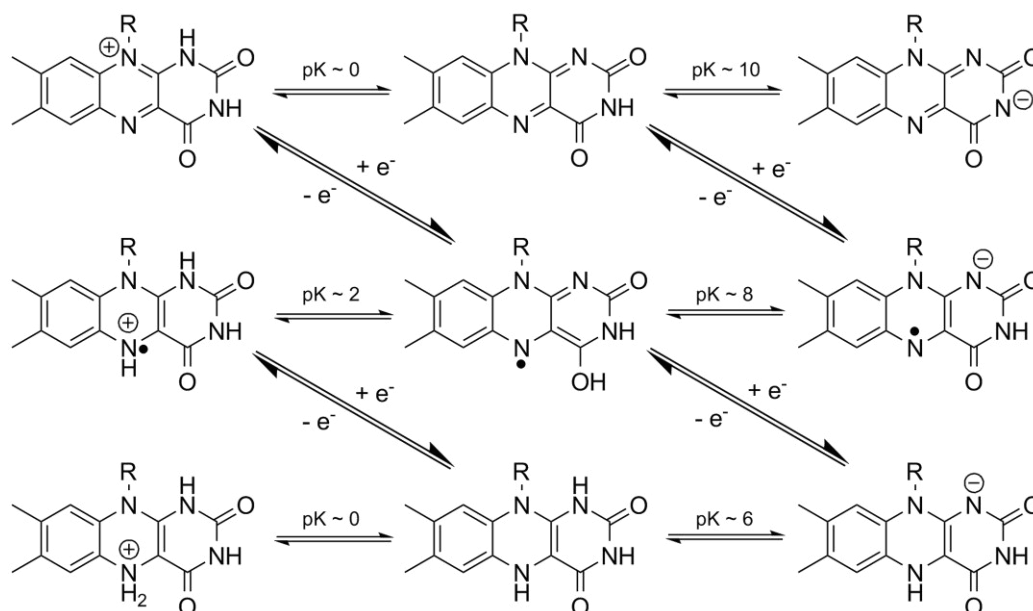


Figure 5-15 The different oxidation states of flavin and the corresponding ionization states with the associated pK values (according to Edwards^[2] and Heelis^[47]). Top: oxidized flavin (quinone), middle: one-electron reduced flavin (semiquinone), bottom: two-electron reduced flavin (hydroquinone). Left: protonated forms, middle: neutral forms, right: deprotonated forms.

5.6.6.1 Oxidized Flavin - Quinone

First the protonation of the oxidized state was studied by means of NMR. Before illumination RFT appears as a signal set of sharp signals both in pure CD₃CN and CD₃CN/D₂O (1:1) mixture. The assignment of the ¹H and ¹³C chemical shift is straightforward and accomplished by a standard set of 1D and 2D NMR spectra consisting of ¹H, ¹³C, ¹H,¹H-COSY, ¹H,¹H-NOESY, ¹H,¹³C-HSQC and ¹H,¹³C-HMBC. The assignments are summarized in Figure 5-9. In the ¹H spectra only one single NH proton resonance with integral 1 is detected at 9.25 ppm and readily assigned to the RFT

N(3)-H by ^1H , ^{13}C -HMBC and ^1H -DOSY spectra. This clearly shows that the oxidized flavin is present in the neutral form in CD_3CN .

In $\text{CD}_3\text{CN}/\text{D}_2\text{O}$ (1:1) where a stabilization of charged species seems more likely due to the polarity and proticity of D_2O , the NH protons are not accessible by means of NMR due to their chemical exchange with D_2O . However, the similarity of all the ^1H chemical shifts of the isoalloxazine ring system in CD_3CN and $\text{CD}_3\text{CN}/\text{D}_2\text{O}$ (1:1) strongly suggest that also under these conditions the oxidized flavin appears in the neutral form (compare Figure 5-9) as any charge in the isoalloxazine ring system would inherently shift the electron density and thus change chemical shifts, especially for the neighboring carbon ^{13}C resonances.

5.6.6.2 One-Electron Reduced Flavin - Semiquinone

The semiquinone radical as a paramagnetic species is not directly accessible by means of NMR spectroscopy. However, in pure CD_3CN the semiquinone leaves Photo-CIDNP patterns in the ^1H spectra of their diamagnetic products. This polarization pattern is different for the case that the semiquinone is neutral or anionic as described by Richter *et al.*^[64] This allows for distinction of the two species by the phases of the Photo-CIDNP polarizations. The rate determining step, the anion or the neutral radical, provides the largest contribution to the overall Photo-CIDNP pattern detected in the products of the singlet and triplet exit channel (oxidized flavin and fully reduced flavin respectively). Therefore, this rate determining step can be characterized by the phases of the Photo-CIDNP pattern. However, calculations of unpaired electron spin density of the flavin anion radical and the flavin neutral radical performed by Richter *et al.*^[64] showed that the spin densities of these two radicals only show a difference in sign for carbon C(10a). Own calculations showed that the spin densities at the flavin protons for both cases do not differ in sign (compare chapter 4.3.5.1). Thus the distinction between the neutral and anionic flavin radical is only possible by ^{13}C Photo-CIDNP studies. However, the small natural abundance makes them more difficult to detect and the assignment of the quaternary ^{13}C in the isoalloxazine moiety is challenging. Therefore, ^{13}C Photo-CIDNP studies with flavins labeled with ^{13}C at position 10a are most promising as the anion flavin radical and the neutral flavin radical differ in the phase of the Photo-CIDNP polarization of C(10a). Studies to distinguish between the anion and the neutral radical by Photo-CIDNP spectroscopy with unlabeled RFT failed due to the low signal to noise ratio. The signal to noise ratio, however can be enhanced by using the cryo probe. Under continuous illumination the Photo-CIDNP effect in RFT can be observed for several

hours making Photo-CIDNP investigations with a more sensitive cryo probe and unlabeled RFT a promising alternative to studies with ^{13}C labeled flavins.

When the reaction is performed in the $\text{CD}_3\text{CN}/\text{D}_2\text{O}$ (1:1) mixture no Photo-CIDNP effects are detected due to exchange cancelation of Photo-CIDNP polarization. However, in this case the semiquinone radical is stabilized (compare chapter 5.3.2). Compared to the absorption spectrum of the oxidized flavin with the characteristic absorption bands located at about 450 nm ($\text{S}_0 \rightarrow \text{S}_1$ transition) and at about 360 nm ($\text{S}_0 \rightarrow \text{S}_2$ transition) the absorption spectra of the semiquinone radical are characterized by an additional spectral feature at about 580 nm. The absorption spectra of the neutral and the anionic flavin radical vary in the relative ratios of the three absorption bands.^[18,26] Owing to that, UV/Vis spectroscopy can be used for the distinction between the anionic and the neutral flavin radical. However, from stationary UV/Vis spectroscopy no further characterization of the protonation of the semiquinone radical is possible. The anion semiquinone radical and the neutral semiquinone radical both show absorption at about 580 nm. The other two absorption bands at 450 nm and 360 nm or their ratio to the band at 580 nm cannot be used for the estimation as four different flavin species contribute to these absorptions (oxidized flavin, anion semiquinone, neutral semiquinone, fully reduced flavin).^[18,26,41] To get reliable evidence for the ionization state of the stabilized radical it is inevitable to perform transient absorption measurements under anaerobic conditions to prevent the reoxidation of the reduced flavin species. A global fit of the temporal change in the absorption spectra can give further evidence for the character of the stabilized radical. It was reported by Jan-Roger Kutta performing transient absorption measurements on the photooxidation of MBA catalyzed by flavin in deoxygenated $\text{CD}_3\text{CN}/\text{D}_2\text{O}$ (1:1) solution that within the measurement time frame the flavin radical anion was not protonated.^[65] Extending the measurement time frame could show if the stabilized radical observed by NMR spectroscopy, EPR spectroscopy and stationary UV/Vis spectroscopy is still the radical anion or the protonated neutral radical.

5.6.6.3 Two-Electron Reduced Flavin - Hydroquinone

The ionization state of the fully reduced flavin (hydroquinone) has a huge impact on its chemical properties and reactivity, e.g. the ionization of the N(1)-H strongly changes the chemical properties of the fully reduced flavin, in particular its reactivity with oxygen.^[62] For this reason the ionization of the fully reduced RFT was studied under the reaction conditions in CD_3CN . The two-electron fully reduced form of RFT as a diamagnetic species can again be accessed directly by means of NMR. The fully reduced species was generated *in situ* by illuminating the reaction mixture inside the spectrometer.

Deoxygenation of the reaction mixture prevents reoxidation of the reduced form and thus stabilizes the hydroquinone. In pure CD_3CN a new signal set consisting of sharp lines is detected for the fully reduced flavin. The assignment of all ^1H chemical shifts except the N-H is straightforward and done by a standard set of 1D and 2D NMR spectra consisting of ^1H , ^{13}C , $^1\text{H}, ^1\text{H}$ -COSY, $^1\text{H}, ^1\text{H}$ -NOESY, $^1\text{H}, ^{13}\text{C}$ -HSQC and $^1\text{H}, ^{13}\text{C}$ -HMBC spectra. The assignment is shown in Figure 5-9. Strong changes of the chemical shifts of the reduced form compared to the oxidized form are detected. The reduction of flavins causes a notable upfield shift of the isoalloxazine NMR resonances as it was reported for all ^{13}C resonances except C(5a), C(9) and C(10a).^[20,22,66] The resonances of the side chain are not affected by this shift. The two electron reduced flavin (hydroquinone) is not coplanar but exhibits bending about the N(5)-N(10) axis of the molecule^[20,21,42,67] with N(5) changing from sp^2 hybridization to sp^3 hybridization.^[62] Various of this so called “butterfly wing” conformations have been investigated with different dihedral angles ranging from 9° to 36° depending on the N(5) substituents. For hydrogen in position 5 the angle measures 21° .^[21]

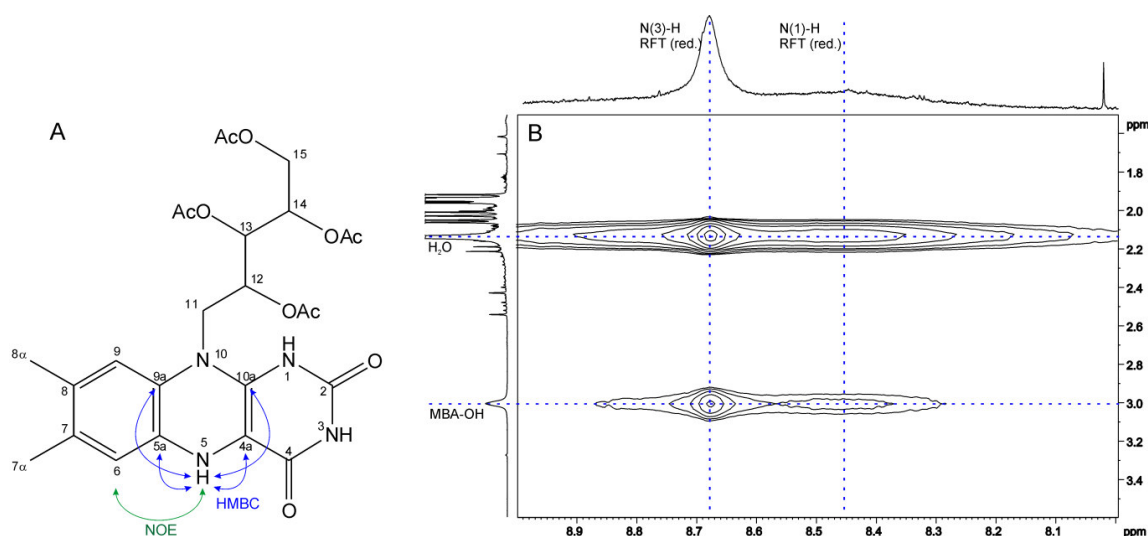


Figure 5-16 Ionization state of the fully reduced RFT A) scheme of the fully reduced flavin N-H assignment by $^1\text{H}, ^1\text{H}$ -NOESY and $^1\text{H}, ^{13}\text{C}$ -HMBC B) Section of the $^1\text{H}, ^1\text{H}$ -NOESY spectrum showing exchange peaks of N(3)-H and the N(1)-H of the fully reduced flavin to H_2O and the MBA-OH group.

For ionization the functions N(3), N(5) and N(1) have to be considered.^[62] N(3)-H is readily assigned to the broad proton resonance at 8.64 ppm (Figure 5-9). For N(5)-H a proton signal of integral 1 (relative to the reduced flavin molecule) is detected at 5.01 ppm and assigned by means of $^1\text{H}, ^{13}\text{C}$ -HMBC and ^1H -DOSY experiments and the NOE contact to C(6)-H (Figure 5-16 A). A double protonation of N(5) can be ruled out by the signal integral. For N(1)-H no clear signal is detected in the ^1H spectra. However, all assigned N-H resonances of both the quinone and the hydroquinone, the MBA-OH group and the signal of H_2O show strong and broad exchange cross peaks to a chemical shift

of 8.68 ppm in the ^1H , ^1H -NOESY spectrum (mixing time 350 ms) (Figure 5-16 B). From the broadness of the exchange peak and the characteristic chemical shift it is very probable that the N(1)-H proton resonance of the fully reduced RFT appears at a ^1H chemical shift of 8.68 ppm. The strong broadening of the resonance is most probably caused by strong exchange and partial deprotonation corresponding to an in N(1) only partially protonated fully reduced flavin species. The N(5)-H signal is the sharpest among the N-H resonances with a line width of 4 Hz, followed by N(3)-H with 24 Hz and N(1)-H with 337 Hz. The line widths correlate with the pK_a values^[23] for the fully reduced flavin of $\text{pK}_a = 6.8$ for N(1)-H, $\text{pK}_a = 14$ for N(3)-H and $\text{pK}_a > 20$ for N(5)-H and reflect the relative acidity of the different flavin N-H.

For the case of $\text{CD}_3\text{CN}/\text{D}_2\text{O}$ (1:1) mixture no information about the nature of the reduced flavins can be gained from NMR spectroscopy due to the chemical exchange of the crucial N-H protons with D_2O . The ^1H chemical shift assignments of protons C(8 α)-H₃, C(7 α)-H₃, C(6)-H and C(9)-H that show very similar values as the corresponding chemical shifts in CD_3CN cannot be used as an indicator for ionization of the fully reduced RFT in $\text{CD}_3\text{CN}/\text{D}_2\text{O}$ (1:1) due to large distance from the protonation sites of the isoalloxazine ring system. From the polarity of D_2O it can be expected that in the $\text{CD}_3\text{CN}/\text{D}_2\text{O}$ (1:1) mixture ionic species are stabilized better than in CD_3CN , and that the addition of water may change the protonation state of the fully reduced flavin.

5.6.7 Amount of Semiquinone Radical

By means of UV/Vis spectroscopy a stabilized semiquinone radical was detected. To estimate the amount of the stabilized radical after 5 min of continuous illumination the characteristic absorption band of the semiquinone radicals at about 580 nm was employed.

Table 5-2 Extinction coefficients ϵ of the oxidized form of RFT, the one-electron reduced flavin anion and flavin neutral radical at 360 nm, 450 nm and 580 nm according to Megerle *et al.*^[18]

	ϵ [$10^3 \text{ L M}^{-1} \text{ cm}^{-1}$]		
	360 nm	450 nm	580 nm
RFT _{ox}	8.5	12.5	0
RFT ^{•-}	22	8.5	0.1
RFT-H [•]	13.5	8.5	4.0

Table 5-2 shows the extinction coefficients from the species associated spectra^[18] of the oxidized riboflavin tetraacetate RFT_{ox}, the corresponding anion radical RFT^{•-} and the neutral radical RFT-H[•] for three selected wavelengths (360 nm, 450 nm and 580nm). The

characteristic absorption band of the flavin semiquinone radical is represented by the absorption at 580 nm, the absorptions at 360 nm and 450 nm represent the other absorption bands of RFT. With also the UV/Vis spectra of fully reduced flavins showing absorptions for wavelengths shorter than 550 nm,^[41] in total all four flavin species can contribute to the overall spectrum of the reaction mixture after 5 min of illumination (Figure 5-17) in the spectral range below 550 nm. As a consequence a simple estimation by a linear combination of the absorption spectra of the single RFT species is not possible due to the under-determined system. However, in the spectral range above 550 nm only the semiquinone radicals (anion and neutral) show absorption,^[18,26] the corresponding spectra of the oxidized and the reduced flavins do not have spectral features in this range.^[18,26,41]

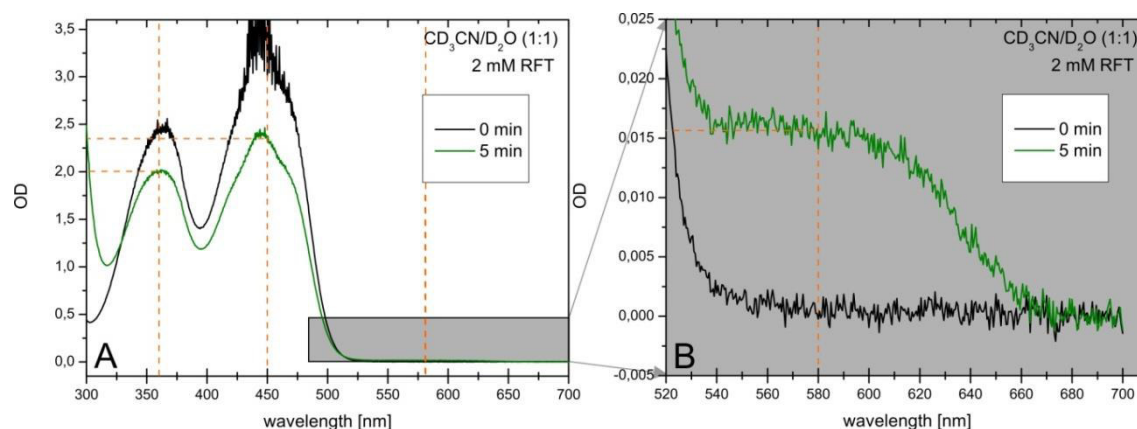


Figure 5-17 UV/Vis spectra of a deoxygenated reaction mixtures of 20 mM MBA and 2 mM RFT as a photocatalyst in $\text{CD}_3\text{CN}/\text{D}_2\text{O}$ (1:1) mixture. UV/Vis spectra were taken before illumination and after 5 min of continuous illumination.

From the optical density of the absorption band at 580 nm (Figure 5-17) the amount of semiquinone radical can be estimated for the cases that 100 % of the detected semiquinone radical is protonated or that 100 % of the detected semiquinone radical is deprotonated (anionic or neutral radical). The Beer–Lambert law^[68] gives the concentration of the radical species c from the optical density OD and the extinction coefficient ϵ of the corresponding radical at 580 nm and the path length d .

$$c = \frac{OD}{\epsilon d}$$

The optical density of 0.016 at a wavelength of 580 nm (from Figure 5-17), an optical path length of 2.00 mm and an extinction coefficient of $0.1 \cdot 10^3 \text{ L mol}^{-1} \text{ cm}^{-1}$ for the anion flavin radical and an extinction coefficient of $4.0 \cdot 10^3 \text{ L mol}^{-1} \text{ cm}^{-1}$ for the neutral flavin radical are used to estimate the amount of radical stabilized in the reaction mixture after 5 min of illumination. For the anion radical RFT^- the estimation gives an amount of

0.775 mM of stabilized radical which would correspond to 39 % of the overall flavin concentration. For the neutral radical RFT-H[•] the estimation gives an amount of 0.019 mM of stabilized radical which would correspond to 1 % of the overall flavin concentration.

For a further characterization the other absorption bands of the flavin species have to be included in the considerations. However, due to the limited validity of the Beer–Lambert law for low concentrations and due to the fact that the fully reduced flavin species also has optical features at the corresponding wavelength ranges^[41] and the system thus would be under-determined these absorption bands cannot be employed for the evaluation of the data. Further information about the stabilization of the radicals and about the protonation of the stabilized radical could be gained from transient absorption measurements under exclusion of oxygen.

5.7 Experimental Details

For the measurements in CD₃CN and in CD₃CN/D₂O (1:1) 0.5 ml solutions of 2 mM riboflavin tetraacetate (RFT) and 20 mM methoxybenzyl alcohol (MBA) were prepared in amberized Rototec-Spintec 5 mm NMR-Tube 7 inch 535-PP-7 to protect the samples from unwanted exposition to light. The samples were prepared and deoxygenated in a Schlenk flask by means of Freeze-Pump-Thaw cycling and transferred under argon atmosphere to the NMR tube which was sealed airtight after insertion of a transparent inlet. The samples with residual oxygen were purged with argon for 1 h and sealed after insertion of a transparent inlet to prevent oxygen from entering. For the illumination of the samples a Cree XP-E high power LED with a center wavelength of 455 nm and 500 mW optical output power was used. The LED was used together with a setup consisting of an optical fiber to guide the light directly into the sample and a transistor circuit operated by the spectrometer to switch the LED automatically.^[32] In order to ensure that the NMR signal intensities are not distorted by unwanted additional Photo-CIDNP polarizations ¹H spectra were recorded alternatingly with and without illumination. Starting with a ¹H spectrum of the not illuminated spectrum a row of ¹H spectra was taken and the light was switched on and off between two consecutive ¹H spectra. For the reaction profiles only the dark spectra were used. The kinetics were derived from the integrals of the corresponding signals referenced to a signal in the first spectrum. NMR spectra were recorded on a Bruker Avance 600 spectrometer with a 5 mm broadband triple resonance z-gradient probe. Constant temperatures were controlled by a Bruker BVTE 3000 unit. The 2D spectra for the assignments were partially recorded at a BRUKER Avance III 600 (600.25 MHz) spectrometer with a TCI z-gradient cryoprobe. The spectra were processed, evaluated and plotted with Bruker Topspin 3.2. All assignments were made by a complete standard set of 1D and 2D NMR spectra consisting of ¹H, ¹³C, ¹H,¹H-COSY, ¹H,¹H-NOESY, ¹H,¹³C-HSQC and ¹H,¹³C-HMBC. An exception is the assignment of the fully reduced riboflavin tetraacetate in CD₃CN/D₂O (1:1). The line broadening inhibits the assignment by 2D NMR and the proton resonances were assigned in analogy to the fully reduced riboflavin tetraacetate in CD₃CN. With the proton resonances at 1.93 ppm and 2.09 ppm corresponding to the methy groups in positions 7 and 8 (2.03 ppm and 2.06 ppm for pure CD₃CN) and the signals at 6.30 ppm and 6.45 ppm corresponding to the aromatic protons C(6)-H and C(9)-H (6.28 ppm and 6.43 ppm for pure CD₃CN). The chemical shifts were referenced to the ¹H chemical shift of tetramethylsilane (TMS) of 0.00 ppm.

Different samples of the concentrations used in NMR and synthesis ($c_{\text{RFT}} = 2 \text{ mM}$; $c_{\text{MBA}} = 20 \text{ mM}$) and the concentrations used for UV/Vis spectroscopy ($c_{\text{RFT}} = 40 \text{ }\mu\text{M}$; $c_{\text{MBA}} = 400 \text{ }\mu\text{M}$) were prepared each in pure CD_3CN and in $\text{CD}_3\text{CN}/\text{D}_2\text{O}$ (1:1) mixture. The samples were prepared in HELLMA 110-QS 2.00 mm cuvettes and purged with Argon for 30 min to exclude oxygen, then closed airtight and sealed with parafilm. The spectra were measured at a Perkin-Elmer Lambda 9a spectrometer with a modified cuvette holder. Temperature was thermostated at 20°C . The small thickness of 2.00 mm of the cuvette keeps the light path in the UV/Vis measurement small so that even the relative high concentrations used for NMR can be measured by UV/Vis spectroscopy. The samples were illuminated outside the spectrometer all arranged in a distance of about 1 cm from a Cree XP-E high power LED with a center wavelength of 455 nm and 500mW optical output power operated at a current of 700 mA.

The EPR samples were prepared in the same manner as the NMR samples for direct comparability. 2 mM RFT and 20 mM MBA were dissolved in $\text{CD}_3\text{CN}/\text{D}_2\text{O}$ (1:1) mixture in a NMR tube and purged with argon for 1 h. Then a part of the sample was transferred to 50 μl glass capillaries and sealed airtight with vinyl under protective argon atmosphere. The samples subsequently were illuminated for 15 min with a Cree XP-E high power LED with a center wavelength of 455 nm and 500 mW optical output according to the absorption maximum of RFT in $\text{CD}_3\text{CN}/\text{D}_2\text{O}$ (1:1). After immediate transfer of the samples to the spectrometer the EPR spectra were recorded on an X-band benchtop Magnettech MiniScope MS400 equipped with a fixed temperature dewar filled with liquid nitrogen for the measurement at 77 K at a microwave frequency of 10 GHz. The spectra were processed, interpreted and plotted with the Magnettech software Analysis 2.02 and Multiplot 2.26.

The instantaneous appearance of the ^1H NMR signal set of the fully reduced flavin right from the beginning of the photooxidation is employed as an indicator for the complete deoxygenation of the reaction solution as the reduced species can only be stabilized when oxygen is excluded. With residual oxygen in the reaction mixture the fully reduced flavin forms with a delay after the product.

H_2O_2 as the second product from the reoxidation of the reduced flavin appears in the ^1H spectra at a chemical shift of 8.60 ppm (compare chapter 5.6.5). The absence of the H_2O_2 resonance thus provides a second evidence for the complete deoxygenation. The amount of residual oxygen can be estimated from the maximal amount of formed H_2O_2 . If D_2O is present in the solution, however, H_2O_2 cannot be employed as an indicator for the grade of deoxygenation as it is deuterated by chemical exchange.

The stoichiometry of the reduced flavin and the aldehyde at the end of the reaction provides a third indicator for the grade of deoxygenation of the reaction mixture. In the case of complete deoxygenation both the signal intensity of the fully reduced flavin and the aldehyde approximate the same value in the course of illumination. With residual oxygen more product than reduced flavin is formed due to the delayed interruption of the catalytic cycle. The amount of residual oxygen can be estimated from the stoichiometry of the fully reduced flavin and the product.

The persistent broadening of the ^1H NMR signals of the oxidized flavin in $\text{CD}_3\text{CN}/\text{D}_2\text{O}$ (1:1) mixture cannot be employed as an indicator for deoxygenation or full consumption of oxygen as measurements described in chapter 5.3.5 showed that the lines begin to broaden before complete consumption of oxygen.

5.8 References

- [1] R. Miura, *Chem. Rec.* **2001**, *1*, 183–194.
- [2] A. M. Edwards, in *Flavins Photochem. Photobiol.*, The Royal Society Of Chemistry, **2006**, pp. 1–11.
- [3] V. Massey, *Biochem. Soc. Trans.* **2000**, *28*, 283–296.
- [4] M. W. Fraaije, A. Mattevi, *Trends Biochem. Sci.* **2000**, *25*, 126–132.
- [5] G. de Gonzalo, M. W. Fraaije, *ChemCatChem* **2013**, *5*, 403–415.
- [6] V. Massey, P. Hemmerich, *Biochem. Soc. Trans.* **1980**, *8*, 246–257.
- [7] S. Ghisla, V. Massey, *Biochem. J.* **1986**, *239*, 1–12.
- [8] J. Dađová, S. Kümmel, C. Feldmeier, J. Cibulková, R. Pažout, J. Maixner, R. M. Gschwind, B. König, R. Cibulka, *Chem. – A Eur. J.* **2013**, *19*, 1066–1075.
- [9] B. König, S. Kümmel, R. Cibulka, in *Chem. Photocatal.* (Ed.: B. König), De Gruyter, **2013**, pp. 45–66.
- [10] R. Lechner, S. Kümmel, B. König, *Photochem. Photobiol. Sci.* **2010**, *9*, 1367–1377.
- [11] J. Svoboda, H. Schmaderer, B. König, *Chem. – A Eur. J.* **2008**, *14*, 1854–1865.
- [12] H. Schmaderer, P. Hilgers, R. Lechner, B. König, *Adv. Synth. Catal.* **2009**, *351*, 163–174.
- [13] K. Tatsumi, H. Ichikawa, S. Wada, *J. Contam. Hydrol.* **1992**, *9*, 207–219.
- [14] C. B. Martin, M.-L. Tsao, C. M. Hadad, M. S. Platz, *J. Am. Chem. Soc.* **2002**, *124*, 7226–7234.
- [15] E. Silva, A. M. Edwards, D. Pacheco, *J. Nutr. Biochem.* **1999**, *10*, 181–185.
- [16] W. A. Massad, Y. Barbieri, M. Romero, N. A. García, *Photochem. Photobiol.* **2008**, *84*, 1201–1208.
- [17] J. M. Kim, M. A. Bogdan, P. S. Mariano, *J. Am. Chem. Soc.* **1993**, *115*, 10591–10595.
- [18] U. Megerle, M. Wenninger, R.-J. Kutta, R. Lechner, B. König, B. Dick, E. Riedle, *Phys. Chem. Chem. Phys.* **2011**, *13*, 8869–8880.
- [19] F. Müller, *Free Radic. Biol. Med.* **1987**, *3*, 215–230.
- [20] K. Kawano, N. Ohishi, A. T. Suzuki, Y. Kyogoku, K. Yagi, *Biochemistry* **1978**, *17*, 3854–3859.

- [21] L. Tauscher, S. Ghisla, P. Hemmerich, *Helv. Chim. Acta* **1973**, *56*, 630–644.
- [22] C. G. Van Schagen, F. Müller, *Helv. Chim. Acta* **1978**, *61*, 3139–3142.
- [23] P. Macheroux, S. Ghisla, C. Sanner, H. Rüterjans, F. Müller, *BMC Biochem.* **2005**, *6*, 26.
- [24] P. J. Hore, *Photo-CIDNP of Biopolymers*, Pergamon Press, Oxford, **1993**.
- [25] E. Schleicher, S. Weber, in *EPR Spectrosc. Appl. Chem. Biol.* (Eds.: M. Drescher, G. Jeschke), **2012**, pp. 41–65.
- [26] M. Sakai, H. Takahashi, *J. Mol. Struct.* **1996**, *379*, 9–18.
- [27] R. Cibulka, R. Vasold, B. König, *Chem. – A Eur. J.* **2004**, *10*, 6223–6231.
- [28] T. Gärtner, N. Yoshikai, M. Neumeier, E. Nakamura, R. M. Gschwind, *Chem. Commun.* **2010**, *46*, 4625–4626.
- [29] K. Schober, H. Zhang, R. M. Gschwind, *J. Am. Chem. Soc.* **2008**, *130*, 12310–12317.
- [30] M. Neumeier, R. M. Gschwind, *J. Am. Chem. Soc.* **2014**, accepted.
- [31] M. B. Schmid, K. Zeitler, R. M. Gschwind, *Angew. Chemie Int. Ed.* **2010**, *49*, 4997–5003.
- [32] C. Feldmeier, H. Bartling, E. Riedle, R. M. Gschwind, *J. Magn. Reson.* **2013**, *232*, 39–44.
- [33] M. Goez, in *Adv. Photochem.*, John Wiley & Sons, **2007**, pp. 63–163.
- [34] M. Goez, in *Annu. Reports NMR Spectrosc.* (Ed.: A.W. Graham), Academic Press, **2009**, pp. 77–147.
- [35] M. Goez, *ChemInform* **2010**, *41*, 19.
- [36] M. Goez, in *Adv. Photochem.* (Eds.: D. Neckers, D. Volmann, G. Bünau), Wiley New York, **1997**.
- [37] P. J. Hore, E. R. P. Zuiderweg, R. Kaptein, K. Dijkstra, *Chem. Phys. Lett.* **1981**, *83*, 376–383.
- [38] R. Kaptein, K. Dijkstra, F. Müller, C. G. van Schagen, A. J. W. G. Visser, *J. Magn. Reson.* **1978**, *171*.
- [39] D. D. Macmurchie, R. J. Cushley, *Can. J. Chem.* **1978**, *56*, 1045–1051.
- [40] P. R. Andrews, M. D. Fenn, *Aust. J. Chem.* **1975**, *28*, 1609–1612.
- [41] S. Ghisla, V. Massey, J.-M. Lhoste, S. G. Mayhew, *Biochemistry* **1974**, *13*, 589–597.

- [42] P. Hemmerich, S. Ghisla, U. Hartmann, F. Müller, *First publ. Flavins Flavoproteins Proc. Third Int. Symp. Flavins Flavoproteins, Durham, North Carolina 1971*.
- [43] V. Massey, M. Stankovich, P. Hemmerich, *Biochemistry* **1978**, *17*, 1–8.
- [44] N. Getoff, S. Solar, *Sci.* **1978**, *201*, 616–618.
- [45] R. Lechner, B. König, *Synthesis* **2010**, *9*, 1712–1718.
- [46] V. Massey, *J. Biol. Chem.* **1994**, *269*, 22459–22462.
- [47] P. F. Heelis, *Chem. Soc. Rev.* **1982**, *11*, 15–39.
- [48] F. Müller, M. Brüstlein, P. Hemmerich, V. Massey, W. H. Walker, *Eur. J. Biochem.* **1972**, *25*, 573–580.
- [49] H. M. Swartz, J. R. Bolton, D. C. Borg, *Biological Applications of Electron Spin Resonance*, John Wiley & Sons, **1972**.
- [50] S. G. Boxer, G. L. Closs, *J. Am. Chem. Soc.* **1975**, *97*, 3268–3270.
- [51] R. G. Brereton, J. K. M. Sanders, *Org. Magn. Reson.* **1982**, *19*, 150–152.
- [52] I. Solomon, *Phys. Rev.* **1955**, *99*, 559–565.
- [53] J. L. Battiste, G. Wagner, *Biochemistry* **2000**, *39*, 5355–5365.
- [54] L. Banci, L. Bertini, C. Luchinat, *Nuclear and Electron Relaxation. The Magnetic Nucleus-Unpaired Electron Coupling in Solution*, VCH, **1991**.
- [55] P. J. Connolly, J. C. Hoch, *J. Magn. Reson.* **1991**, *95*.
- [56] K. Maeda, C. E. Lyon, J. J. Lopez, M. Cemazar, C. M. Dobson, P. J. Hore, *J. Biomol. NMR* **2000**, *16*, 235–244.
- [57] M. Goetz, *Chem. Phys.* **1990**, *147*, 143–154.
- [58] A. F. Holleman, E. Wiberg, *Lehrbuch Der Anorganischen Chemie*, De Gruyter, **1995**.
- [59] N. A. Stephenson, A. T. Bell, *Anal. Bioanal. Chem.* **2005**, *381*, 1289–1293.
- [60] D. Zuccaccia, A. Macchioni, *Organometallics* **2005**, *24*, 3476–3486.
- [61] A. Jerschow, N. Müller, *J. Magn. Reson.* **1997**, *125*, 372–375.
- [62] S. Ghisla, *Flavins Flavoproteins, Proc. 10th Internat. Symp.* **1991**, 27–32.
- [63] C. Reichardt, T. Welton, *Solvents and Solvent Effects in Organic Chemistry*, Wiley-VCH Verlag, **2010**.

- [64] G. Richter, S. Weber, W. Römisch, A. Bacher, M. Fischer, W. Eisenreich, *J. Am. Chem. Soc.* **2005**, *127*, 17245–17252.
- [65] R. J. Kutta, B. Dick, Blitzlichtphotolyse - Untersuchung Zu LOV-Domänen Und Photochromen Systemen, University of Regensburg, **2012**.
- [66] C. G. Van Schagen, F. Müller, *Helv. Chim. Acta* **1980**, *63*, 2187–2201.
- [67] J. D. Walsh, A.-F. Miller, *J. Mol. Struct.* **2003**, *623*, 185–195.
- [68] P. Atkins, J. de Paula, *Physical Chemistry, 9th Edition*, W. H. Freeman, **2009**.

6 Summary

Nature makes broad use of sunlight as an energy source for chemical conversions. In recent years the use of light as a driving force for chemical conversions has gained much attention in synthetic chemistry and the area of photocatalysis has seen rapid advances. These rapid developments in synthetic applications have heightened the need for comprehensive mechanistic pictures of the underlying mechanisms to enable a rational design of photocatalytic systems. Transient absorption spectroscopy has proven to be a very powerful technique for the study of photochemical reactions as it provides access to the transient excited intermediates of the absorbing chromophore. Not limited to light-absorbing molecules, NMR can provide additional information about structure, solvent effects, aggregations or chemical exchange. However, far too little attention has been paid to the application of NMR techniques for mechanistic investigations on photocatalytic reactions despite the manifold information accessible directly by means of NMR.

This thesis focuses on the application of NMR spectroscopic techniques for the investigation of photocatalytic reactions. The application of well-established modern NMR techniques to photocatalytic reactions was accomplished by the development of a device for *in situ* illumination of NMR samples. To obtain a comprehensive picture of the reaction mechanisms NMR spectroscopy was complemented by other spectroscopic techniques providing access to species inaccessible by NMR spectroscopy. Paramagnetic species were detected by means of UV/Vis and EPR spectroscopy along with the diamagnetic species detected by NMR spectroscopy. Moreover, Photo-CIDNP spectroscopy was employed as a further complementing technique to study the initial radical pair of the photocatalytic reactions. As a central model system for the investigation the flavin catalyzed photooxidation of benzyl alcohols was chosen for its general importance and the good spectroscopic properties of the system.

The importance of photocatalyst aggregations for its reactivity was shown by NMR aggregation studies in combination with synthetic approaches. It is shown how the photocatalyst aggregation, its photophysical properties and reactivity can be tuned by synthetically modifying the steric demand of the flavin side chain. By means of ¹H-DOSY solution NMR the solvent dependent self-aggregation of flavin photocatalysts was revealed. By combination of crystal structure analysis with DOSY aggregation studies the contributions of hydrogen bonds and π - π interactions for flavin self-aggregations were identified. The importance of photocatalyst self-aggregation for the quantum yields of the

catalyzed reactions is shown on the model system of the photooxidation of benzyl alcohols where the sterically demanding flavins show quantum yields higher by almost one order of magnitude. Additionally pre-associated flavin-substrate complexes are investigated by NMR-titration and ^1H -DOSY NMR. The insights in the intermolecular interaction modes of flavins in terms of self-aggregations and flavin-substrate aggregation are crucial for the future design of effective flavin photocatalysts and for the comprehension of the underlying reaction mechanisms.

In the framework of this thesis an LED based illumination device for the *in situ* illumination of NMR samples was developed in order to apply the whole variety of NMR techniques to the investigation of photochemical systems. Continuous or alternatively pulsed operation of the LEDs is realized with the help of a one-stage electronic circuit switched directly by the NMR spectrometer. Pulsed operation of the LEDs at high powers in low duty cycles provides exceptional high optical powers and makes the setup suitable even for single millisecond time resolved Photo-CIDNP spectroscopy. Continuous operation of the LEDs provides direct comparability with conditions in synthetic chemistry. The LEDs are efficiently coupled to an optical fiber guiding the light into the spectrometer without the need for additional optics. For a uniform and efficient illumination of the NMR sample over the full length of the receiver coil the tip of the optical fiber is roughened by sandblasting. The amount of light brought into the NMR sample is tremendously increased by the combination of the different techniques and makes LEDs an easy, versatile and handy light source for the *in situ* illumination of NMR samples. The presented LED based illumination device makes photo induced chemical processes accessible by means of NMR in a very easy to implement manner. It is thus expected to contribute essentially to the understanding and further development of all kinds of photo induced or controlled chemical processes. The scope of the presented illumination device goes far beyond illumination of NMR samples. Applications are conceivable in all areas where illumination in difficult to access confined spaces is needed.

The next part of this thesis deals with Photo-CIDNP effects of flavins generated by the nuclear spin dependent intersystem crossing within the electron spin correlated initial radical pair in the photooxidation of benzyl alcohols. Despite its huge importance as a photosensitizer for protein Photo-CIDNP studies and as a cofactor in enzymatic reactions no comprehensive investigation of Photo-CIDNP polarizations of free flavin in solution was presented so far. This is due to the small or vanishing Photo-CIDNP effect of flavins when water is used as a solvent for the investigations with proteins. It is shown that the change of the solvent to acetonitrile reveals the Photo-CIDNP polarizations in free flavins.

Comprehensive studies of Photo-CIDNP effects of flavins themselves are presented on the model system of the flavin catalyzed photooxidation of benzyl alcohols. The Photo-CIDNP patterns of flavin were studied in detail with focus on the Photo-CIDNP patterns for both the singlet and triplet exit channel and the effect of different substituents at the isoalloxazine moiety. Spectroscopic and mechanistic implications of substitutions with methyl groups and heavy atoms enhancing spin-orbit coupling are discussed in terms of Kaptein's sign rule and supported by DFT calculations. The characteristic recombination and escape type Photo-CIDNP polarizations determined for various flavins provide reference for Photo-CIDNP studies on flavins in proteins. As an external reference the characteristic polarization patterns can be expected to contribute essentially to the interpretation of Photo-CIDNP effects of flavins in proteins and to the comprehension of the underlying mechanism in terms of singlet and triplet radical pair mechanism.

By a combination of NMR, UV/Vis and Photo-CIDNP spectroscopy on the model system of flavin catalyzed photooxidation of benzyl alcohols the solvent dependent stabilization of the semiquinone radical is shown. The study reveals that the stabilization of the semiquinone radical, which is of utmost importance for the versatility of flavin as a cofactor, is also possible in solution and can be tuned by the solvent. The stabilization of the semiquinone causes flavin to act as a one-electron oxidizing agent for the model system as the substrate radical is not stabilized. Whereas for acetonitrile no stabilization of the flavin radical intermediate is observed the addition of water stabilizes the semiquinone radical and makes it act as a resting state after one-electron reduction of the substrate. The stabilization of the radical is associated with enhanced chemical exchange between the three different oxidation states. For this reason the stabilization of the radical intermediate by water is proposed to be the reason for the strong solvent dependence of the efficiency of flavin catalyzed photooxidation. For the first time it was shown that the tuning of the flavin semiquinone radical stabilization by intermolecular interactions with its surroundings, a concept well known from flavin proteins, can be mimicked by flavins in free solution by solvent variation. The flavin catalyzed photooxidation of benzyl alcohols thus provides a valuable small molecule model system for studying the intermolecular interactions responsible for the semiquinone stabilization in proteins and the regulation between one- and two-electron transfers.

Altogether, this thesis mainly deals with NMR, Photo-CIDNP and UV/Vis spectroscopic investigations of flavin catalyzed photooxidations of benzyl alcohols. The mechanistic studies provide valuable information for synthetic applications and the future design of flavin photocatalysts in terms of aggregation, solvent effects and stabilization of radical

intermediates. Methodically, a new LED based illumination device provides a valuable tool for *in situ* studies of all kinds of photochemical processes by means of NMR and is expected to contribute essentially to a broader understanding of photochemical processes. Furthermore, a set of characteristic flavin Photo-CIDNP patterns is presented that is expected to contribute essentially to the comprehension of Photo-CIDNP patterns detected in flavins in proteins. A methodical foundation for the study of the semiquinone stabilization in proteins by intermolecular interactions is laid by the proposal of a small molecule model system in which the stabilization can be tuned by solvent variation.

7 Zusammenfassung

Die Natur macht sich Sonnenlicht in vielfältiger Weise als Energiequelle für chemische Umsetzungen zunutze. In den vergangenen Jahren hat die Verwendung von Licht als treibende Kraft für chemische Reaktionen in der synthetischen Chemie zunehmend an Bedeutung gewonnen und auf dem Gebiet der Photokatalyse wurden zahlreiche Fortschritte erzielt. Diese rasanten Entwicklungen in synthetischen Anwendungen haben den Bedarf an umfangreichen mechanistischen Darstellungen der zugrundeliegenden Reaktions-mechanismen, die ein rationales Design von photokatalytischen Reaktionen ermöglichen, gesteigert. Transiente Absorptionsspektroskopie hat sich als sehr leistungsstarke Technik für Untersuchungen an photokatalytischen Systemen bewährt, da sie transiente angeregte Intermediate des absorbierenden Chromophors zugänglich macht. NMR als Technik, die nicht auf lichtabsorbierende Moleküle beschränkt ist, kann darüber hinaus Informationen zu Strukturen, Lösungsmittelleffekten, Aggregationen oder chemischem Austausch liefern. Trotz dieser vielfältigen Informationen, die durch NMR-Spektroskopie zugänglich sind, wurde der Anwendung von NMR-Techniken zur Untersuchung photokatalytischer Reaktionen bislang viel zu wenig Beachtung geschenkt.

Der Schwerpunkt dieser Arbeit liegt auf der Anwendung von NMR spektroskopischen Techniken auf Untersuchungen von photochemischen Reaktionen. Die Anwendbarkeit etablierter moderner NMR-Techniken auf photokatalytische Reaktionen wurde durch die Entwicklung eines Aufbaus zur *in situ* Beleuchtung von NMR-Proben möglich gemacht. Um umfangreiche Bilder der Reaktionsmechanismen zu erhalten wurde die NMR-Spektroskopie durch andere spektroskopische Techniken, die Zugang zu NMR-inaktiven Spezies ermöglichen, ergänzt. Paramagnetische Spezies wurden zusammen mit den durch NMR detektierten diamagnetischen Spezies mittels UV/Vis- und EPR-Spektroskopie nach-gewiesen. Darüber hinaus wurde Photo-CIDNP-Spektroskopie als weitere ergänzende Technik zur Untersuchung des anfänglichen Radikalpaars der photokatalytischen Reaktionen eingesetzt. Als zentrales Modellsystem wurde, aufgrund der allgemeinen Bedeutung und der guten spektroskopischen Eigenschaften dieses Systems, die Flavin katalysierte Photooxidation von Benzylalkoholen gewählt.

Die Bedeutung von Aggregationen von Photokatalysatoren für ihre Reaktivität wurde durch NMR-Aggregationsstudien in Kombination mit synthetischen Ansätzen nachgewiesen. Es wird gezeigt wie die Aggregation von Photokatalysatoren, ihre photophysikalischen Eigenschaften und ihre Reaktivität durch die synthetische Modifikation des sterischen Anspruchs der Flavin-Seitenkette beeinflusst werden kann.

Anhand von ^1H -DOSY NMR-Studien wurde die Solvens abhängige Selbstaggregation von Flavinen aufgedeckt. Durch Kombination von Kristallstrukturen und DOSY-Aggregationsstudien wurden die Beiträge von Wasserstoffbrücken und π - π Wechselwirkungen zur Flavin-Selbstaggregation identifiziert. Die Bedeutung von Selbstaggregationen von Photokatalysatoren für die Quantenausbeute der katalysierten Reaktionen wird am Modellsystem der Photooxidation von Benzylalkoholen gezeigt, in der sterisch anspruchsvolle Flavine eine um fast eine Größenordnung höhere Quantenausbeute zeigen. Zusätzlich wurden Flavin-Substrat-Komplexe durch NMR-Titrations und ^1H -DOSY NMR untersucht. Die Einsichten in die intermolekularen Wechselwirkungsarten im Hinblick auf Selbstaggregationen und Flavin-Substrat-Aggregationen sind entscheidend für das zukünftige Design von leistungsfähigen Flavin Photokatalysatoren und für das Verständnis der zugrundeliegenden Mechanismen.

Im Rahmen dieser Arbeit wurde ein LED basierter Aufbau für die Beleuchtung von NMR-Proben entwickelt um die ganze Bandbreite an unterschiedlichen NMR-Techniken zur Untersuchung von photokatalytischen Systemen nutzen zu können. Kontinuierlicher oder alternativ gepulster Betrieb der LEDs wird mit Hilfe eines einstufigen elektronischen Schaltkreises realisiert. Durch den gepulsten Betrieb der LEDs bei hohen Leistungen und niedrigen Tastraten werden ungewöhnlich hohe optische Leistungen erzielt, die den Aufbau selbst für Millisekunden aufgelöste Photo-CIDNP Spektroskopie einsetzbar machen. Kontinuierlicher Betrieb der LEDs ermöglicht direkte Vergleichbarkeit mit den Bedingungen in der synthetischen Chemie. Die LEDs sind effizient an einen Glasfaser gekoppelt, die das Licht in das Spektrometer leitet, ohne dass zusätzliche optische Komponenten erforderlich sind. Um eine gleichmäßige und effiziente Ausleuchtung der NMR Probe über die gesamte Länge der Empfängerspule zu gewährleisten wurde die Spitze der Glasfaser durch Sandstrahlbehandlung aufgeraut. Diese verschiedenen Techniken verstärken die Lichtmenge, die in die Probe gebracht wird, ungemein und machen LEDs zu einer einfachen, vielfältigen und praktischen Lichtquelle für die *in situ* Beleuchtung von NMR-Proben. Der dargestellte LED basierte Beleuchtungsaufbau macht photoinduzierte chemische Prozesse in einer einfach umzusetzenden Weise zugänglich. Es wird deshalb erwartet, dass er essentiell zum Verständnis und zur Weiterentwicklung von vielerlei photoinduzierten Prozessen beiträgt. Der Anwendungsbereich des dargestellten Beleuchtungsaufbaus geht dabei weit über die Beleuchtung von NMR-Proben hinaus. Anwendungen sind in jedem Bereich denkbar in dem Beleuchtung von begrenzten und schwer zugänglichen Orten nötig ist.

Ein weiterer Teil dieser Arbeit beschäftigt sich mit Photo-CIDNP Effekten von Flavinen die durch Kernspin abhängiges Intersystem Crossing innerhalb des Elektronenspin-korrelierten Radikalpaars bei der Photooxidation von Benzylalkoholen entstehen. Trotz der großen Bedeutung von Flavinen als Photosensitizer für Photo-CIDNP-Studien an Proteinen und als Kofaktor in enzymatischen Reaktionen wurde bisher keine umfassende Studie von Photo-CIDNP Polarisationen von freien Flavinen durchgeführt. Das ist auf die kleinen oder verschwindenden Photo-CIDNP-Effekte von Flavin zurückzuführen, wenn Wasser als Lösungsmittel verwendet wird. Es wird gezeigt, dass der Wechsel des Lösungsmittels von Wasser zu Acetonitril die Photo-CIDNP-Effekte von freiem Flavin zu erkennen gibt. Anhand des Modellsystems der Flavin katalysierten Photooxidationen von Benzylalkoholen werden die ersten umfassenden Studien zu Photo-CIDNP-Effekten von Flavinen selbst präsentiert. Die Photo-CIDNP-Muster von Flavinen wurden im Detail untersucht, wobei der Schwerpunkt auf den Photo-CIDNP-Mustern des Singlet und Triplet Exit Channels und dem Effekt von unterschiedlichen Substituenten am Isoalloxazin liegt. Spektroskopische und mechanistische Auswirkungen von Substitutionen durch Methylgruppen und durch Spin-Bahn-Kopplung verstärkende Schweratome werden im Hinblick auf die Vorzeichenregeln von Kaptein diskutiert und von DFT-Rechnungen gestützt. Die charakteristischen Recombination Type und Escape Type Photo-CIDNP-Polarisationen die für verschiedenartige Flavine bestimmt wurden stellen eine Referenz für Photo-CIDNP-Studien an Flavinen in Proteinen dar. Als externe Referenz dürften die charakteristischen Polarisationsmuster essentiell zur Interpretation von Photo-CIDNP-Effekten von Flavinen in Proteinen im Hinblick auf Singlet- und Triplet-Mechanismen und damit allgemein zum Verständnis der zugrundeliegenden Mechanismen beitragen.

Durch eine Kombination von NMR-, UV/Vis- und Photo-CIDNP-Spektroskopie angewendet auf das Modellsystem der Flavin-katalysierten Photooxidation von Benzylalkoholen wird eine solvensabhängige Stabilisierung des Semiquinon-Radikals gezeigt. Die Studie zeigt, dass die Stabilisierung des Semiquinon-Radikals, die von äußerster Wichtigkeit für die Vielseitigkeit von Flavin als Kofaktor in Proteinen ist, auch in Lösung möglich ist und dass sie durch das Lösungsmittel abgestimmt werden kann. Die Stabilisierung des Semiquinons zwingt Flavin in die Rolle eines Ein-Elektronen-Oxidationsmittels für das Modellsystem, da das Substratradikal nicht stabilisiert wird. Wohingegen für Acetonitril keine Stabilisierung das Flavin-Radikalintermediates beobachtet wird, stabilisiert die Zugabe von Wasser das Semiquinon-Radikal und verwandelt es in einen Resting-State nach der Ein-Elektronen-Oxidation des Substrates. Die Stabilisierung des Radikals ist verbunden mit verstärktem Austausch zwischen den

drei verschiedenen Oxidationszuständen. Aus diesem Grund wird die Stabilisierung des Radikalintermediates durch Wasser als Grund für die starke Lösungsmittelabhängigkeit der Effizienz von Flavin katalysierten Photooxidationen vorgeschlagen. Zum ersten Mal wurde gezeigt, dass die Variation der Flavin-Semiquinon-Radikalstabilisierung durch intermolekulare Wechselwirkungen mit der Umgebung, ein Konzept bekannt von Flavin-Proteinen, durch freies Flavin in Lösung bei Variation des Lösungsmittels nachgeahmt werden kann. Die Flavin katalysierte Photooxidation von Benzylalkoholen bietet daher ein wertvolles Modellsystem kleiner Moleküle zur Untersuchung der intermolekularen Wechselwirkungen, die für die Semiquinon-Stabilisierung in Proteinen und die Regulierung zwischen Ein- und Zwei-Elektronentransferen verantwortlich sind.

Insgesamt handelt diese Arbeit hauptsächlich von NMR, UV/Vis und Photo-CIDNP spektroskopischen Untersuchungen an Flavin katalysierten Photooxidationen von Benzylalkoholen. Die mechanistischen Studien liefern wertvolle Informationen für synthetische Anwendungen und das zukünftige Design von Flavin-Photokatalysatoren im Hinblick auf Aggregationen, Lösungsmittelleffekte und Stabilisierung von Radikalintermediaten. Methodisch bietet ein neuer LED basierter Beleuchtungsaufbau ein wertvolles Werkzeug für *in situ* Studien von vielerlei photochemischen Prozessen und dürfte essentiell zum breiteren Verständnis von photochemischen Reaktionen beitragen. Außerdem wird ein Satz von charakteristischen Photo-CIDNP-Mustern präsentiert der wesentlich zum Verständnis von Photo-CIDNP-Effekten in Flavin-Proteinen beitragen dürfte. Eine methodische Grundlage für Untersuchungen der Stabilisierung von Semiquinon-Radikalen in Proteinen durch intermolekulare Wechselwirkungen wurde durch den Vorschlag eines Modellsystems von kleinen Molekülen, bei dem die Stabilisierung durch Solvensvariation moduliert werden kann, gelegt.